

## ABSTRACT

Title of Dissertation: OYSTERS' INTEGRATION ON  
SUBMERGED BREAKWATERS AS  
NATURE-BASED SOLUTION FOR  
COASTAL PROTECTION WITHIN  
ESTUARINE ENVIRONMENTS

Iacopo Vona, Doctor of Philosophy, 2023

Dissertation directed by: Dr. William Nardin, UMCES

Rising sea levels and the increased frequency of extreme events put coastal communities at serious risk. Due to SLR, traditional solutions such as breakwaters (or gray/artificial structures) will become ineffective for wave attenuation and shoreline erosion control. Moreover, gray solutions do not consider the ecological aspects of the coast, and may negatively affect surrounding ecosystems. The “living shoreline” technique includes natural habitat features, such as oysters and/or vegetation into shoreline stabilization, to provide both protection and ecosystem services. Oysters create three-dimensional, complex reef structures that attenuate wave energy and increase sedimentation rates. If coupled with breakwaters, oysters may maintain breakwaters’ efficiency over time as they are expected to grow with SLR. However, guidance for the correct implementation of Natural and Nature Based Features (NNBF) for coastal protection is still unclear, and many authors within the literature have been repeatedly requested more insights.

In this thesis, we have therefore studied the coupling between oysters and breakwaters via field, modeling and laboratory experiments, in order to highlight the benevolent aspects of NNBF regarding coastal defense. Field results showed gray breakwaters allowed for shoreline protection (by reducing incoming wave energy) and increased sedimentation rates. However, SLR modeling scenarios showed a gradual reduction of wave attenuation over time, as well as increased sediment export from the coast. When oysters were included in the modeling, on the other hand, wave dampening and sediment retention were preserved through the time. Laboratory experiments showed oyster-reef breakwaters in emergent or near-emergent conditions produced higher drag coefficient compared to gray structures, resulting in greater dissipative features. Higher water levels simulated in our experiments produced less reliable results that will require further investigation. This thesis supports oysters for coastal protection, and emphasizes the positive aspects of NNBF regarding wave attenuation and sediment retention in the face of climate changes and SLR. However, challenges encountered during field studies underlined the importance of environmental and biogeochemical conditions (such as water level, aerial exposure, temperature and seasonality) for oyster reefs' establishment, growth and survivability. Future restoration plans involving oysters in coastal defense should definitely take these environmental and biogeochemical aspects into account, in order to properly protect the coast in the face of climate changes and SLR, while also providing many other useful ecosystem services for the environment. The coupling between oysters and breakwaters may represent a valuable and effective methodology to protect our coast over a changing climate and a rising sea, where optimal conditions for oysters' survivability occur and are maintained over time.

OYSTERS' INTEGRATION ON SUBMERGED BREAKWATERS AS NATURE-  
BASED SOLUTION FOR COASTAL PROTECTION WITHIN ESTUARINE  
ENVIRONMENTS

by

Iacopo Vona

Dissertation submitted to the Faculty of the Graduate School of the  
University of Maryland, College Park, in partial fulfillment  
of the requirements for the degree of  
[Doctor of Philosophy]  
[2023]

Advisory Committee:  
Professor William Nardin, Chair  
Professor Matthew W. Gray  
Professor Cindy Palinkas  
Professor Patricia Wiberg  
Professor Karen Prestegaard

© Copyright by  
[Iacopo Vona]  
[2023]

## Acknowledgements

Special thanks to my primary advisor, Dr. William Nardin, who inspired my work, giving me the opportunity to experience my PhD at the University of Maryland. Equally special thank goes to all of my committee members, Dr. Matt Gray, who inspired together with Dr. Nardin my PhD dissertation, Dr. Cindy Palinkas, Dr. Patricia Wiberg, and Dr. Karen Prestegaard.

All the people I have shared this journey with, are gratefully thank as well.

My girlfriend Ylenia supported me from Italy, and she came visiting me many times during these years. I thank her for always being close to me, and inspiring every single day of my life.

## Table of Contents

Acknowledgements.....	ii
Chapter 1: Introduction.....	1
1.1 Traditional adopted solutions for coastal protection.....	3
1.2 Oysters as nature-based solution for coastal protection.....	5
1.3 Objectives and research purposes .....	7
1.4 Anticipated results .....	10
1.5 References.....	12
Chapter 2: The impact of submerged breakwaters on sediment distribution along marsh boundaries .....	19
Abstract.....	19
2.1 Introduction.....	20
2.1.1 Laboratory experiments on breakwaters .....	22
2.1.2 Numerical modeling of breakwaters.....	23
2.1.3 Field studies on breakwaters .....	24
2.2 Material and Methods .....	26
2.2.1 Model description .....	26
2.3 Results.....	33
2.3.1 Hydrodynamic results .....	33
2.3.2 Morphodynamic results .....	37
2.4 Discussion.....	45
2.4.1 Model limitations.....	<b>Error! Bookmark not defined.</b>
2.5 Conclusions.....	48
2.6 References.....	50
Chapter 3: Oysters’ integration on submerged breakwaters: field and modeling simulations in the Choptank River (MD, US) .....	57
Abstract.....	57
3.1 Introduction.....	58
3.2 Study sites .....	62
3.2.1 Lake Cove .....	63
3.2.2 Bill Burton State Park .....	65
3.3 Material and Methods .....	66
3.3.1 Lake Cove .....	66
3.3.1.1 Field measurements .....	66
3.3.1.2 Numerical model.....	68
3.3.1.3 Model set-up .....	69
3.3.1.4 Modeling SLR and oysters’ growth.....	72
3.3.2 Bill Burton State Park .....	74
3.3.2.1 Field measurements .....	74
3.3.2.2 Numerical model.....	75
3.4 Results.....	78
3.4.1 Lake Cove – Field results .....	78
3.4.2 Lake Cove - Modeling results.....	82
3.4.2.1 Lake Cove – Model validation.....	82

3.4.2.2 Lake Cove – hydro and morphodynamic modeling results .....	85
3.4.3 Bill Burton State Park - Field results .....	95
3.4.4 Bill Burton - Hydro and morphodynamic modeling results .....	96
3.5 Discussion .....	99
3.5.1 Field observations .....	99
3.5.2 Numerical simulations .....	101
3.5.3 Coastal management indications and study limitations .....	104
3.6 Conclusions.....	107
3.7 Nomenclature.....	109
3.8 References.....	111
Chapter 4: Oysters’ integration on submerged breakwaters: a laboratory and numerical experiment with scaled-down oyster castles.....	119
Abstract.....	119
4.1 Introduction.....	121
4.2 Material and Methods .....	123
4.2.1 Laboratory experiments .....	123
4.2.2 Flow 3D model .....	126
4.3 Results.....	128
4.3.1 PIV results.....	128
4.3.1.1 Oyster-covered OCs vs gray OCs.....	130
4.3.1.2 The impact of different OCs geometries on flow hydrodynamic .....	136
4.3.1.3 Drag coefficient estimation based on the 1D momentum balance .....	142
4.3.1.4 Near bed TKE and Reynold stresses.....	144
4.3.2 Flow 3D results .....	145
4.4 Discussion.....	147
4.4.1 Oyster-covered OCs vs gray OCs .....	147
4.4.2 The impact of different OCs geometries on flow hydrodynamic .....	148
4.4.3 Drag coefficient .....	149
4.4.4 Implication for oyster restoration and coastal defense .....	150
4.4.5 Study limitation.....	152
4.5. Conclusions.....	153
4.6 References.....	154
Chapter 5: Conclusions .....	159
Appendices.....	161
A.1 Chapter 3 supporting information .....	161
A.2 Lessons learned from modeling experiments – Sediment exchange between saltmarshes and SAV .....	167
A.3 Flow 3D governing equations.....	169
A.4 Linear wave theory.....	173
A.4.1 Problem formulation .....	173
A.4.2 Solution for monochromatic waves .....	175
A.5 Sediment transport in open channels .....	177
A.5.1 Sediment properties .....	177
A.5.2 Initiation of motion and Suspension .....	179
A.5.3 Types of sediment transport and their quantification .....	180
A.6 Chapter 2 supplementary information.....	183

References..... 186

## Chapter 1: Introduction

Coastal environments are the most economically important and intensely used among all areas inhabited by humans (Post and Lundin, 1996; Kay and Alder, 2005). It has been estimated that around half of the world's population presently lives within 200 km of the coast, and this value is likely to double by 2025 (Creel, 2003; Kay and Alder, 2005). In the US, 50% of the population is confined within 50 miles of the shore and one-third of the gross national product is generated in the coastal zone (Marra et al., 2007). Due to their immense ecological, social and economic benefits, coastal regions are both widely regarded and protected. However, concern over the decline or loss of valuable coastal ecosystem services has been mounting over the past several decades due to growing threats to their long-term viability (e.g. human encroachment, habitat degradation, sea-level rise). Recent catastrophic events such as Hurricanes Katrina in 2005, Sandy in 2012, and Florence in 2018 have shown that coastal communities are at great risk of coastal inundation caused by storm surges and sea-level rise (Li et al., 2020). Many coastal zones throughout the world are also increasingly vulnerable to shoreline erosion (Post and Lundin, 1996; Creel, 2003; Kay and Alder, 2005; Board, 2007). A multitude of environmental factors and human activities, such as accelerated Sea Level Rise (SLR), enhanced storm activity, dam and levee construction, are thought to contribute to the shoreline retreat and the altered coastline configuration due to coastal development (Pilkey and Wright, 1988; Douglass and Pickel, 1999; Kennish, 2002).

To protect coastal regions, engineering interventions such as seawalls, breakwaters, or groynes, have historically been involved (Pilkey and Wright, 1988; Douglass and Pickel, 1999; Board, 2007). In the Chesapeake Bay (US), eight sub-estuaries are more than 50% armored, and twenty-three other sub-estuaries are between 30% and 50% armored, resulting in more than 1,609 km of armored shoreline (Patrick et al., 2016). However, these types of intervention are increasingly challenged by climate changes and their preservation may become unmaintainable (Temmerman et al., 2013). Breakwaters, for instance, attenuate wave energy and

promote deposition of sediments on the leeward side of the structure, but alone are not designed to provide habitat or other ecological functions aside from stabilizing the shoreline. Additionally, over time these structures will lose their effectiveness as the overlying-water depth increases due to SLR. Thus, over the years, scientists have begun to think about how to protect coastal communities and environments by ecosystem design and restoration, to offer a more sustainable, cost-effective and ecologically alternative to conventional coastal engineering. The Living Shoreline (LS) concept started to become more popular. The LS includes coastal ecology by incorporating natural habitat features into shoreline stabilization such as salt marshes and/or oysters. The approach aims to provide the same erosion-control functions of armored structures, while also maintaining the ecological benefits of nature-based solutions (Davis et al., 2015; Scyphers et al., 2015; Gittman et al., 2016a). Many recent studies on the use of vegetation and oysters in LS supported the importance and effectiveness of these nature-based solutions in providing ecosystem services and enhancing coastal resilience by reducing wave energy and facilitating sedimentation (Currin et al., 2010; Rodriguez et al., 2014; Manis et al., 2015; Ridge et al., 2015; Sutton-Grier et al., 2015; Palinkas et al., 2023; Safak et al., 2020).

Oysters are well recognized to have positive transformative effects on their environment and provide a wide variety of useful services for the environment (Coen et al., 2007). As an engineering species, oysters create three-dimensional complex reef structures that attenuate wave energy and increase sedimentation rates (Dame and Patten, 1981; Coen et al., 2007; Brandon et al., 2016). Many other studies have demonstrated the value of oysters for coastal protection (Rodriguez et al., 2014; Ridge et al., 2017; Wiberg et al., 2019, Hogan and Reidenbach, 2022), strengthening and promoting the use of these organisms in the safeguarding and protection of the coast.

**To enhance knowledge about coastal protection by ecosystem design and restoration, this dissertation examines the coupling of oysters and intertidal breakwaters in order to improve the effectiveness (more roughness and wave energy dissipation), ecological value and longevity of these gray structures in the face of SLR and climate change. Despite the many studies cited above regarding**

**the value of oysters for coastal protection, oyster integration with gray structures in order to create an effective hybrid infrastructure capable of self-maintaining in the face of SLR and climate change remains poorly understood.**

Natural and Nature-Based Features (NNBF) integration with existing grey infrastructure may enhance the current performance of the armoring (i.e. shoreline stabilization and soil accretion), extend its effectiveness into the future, and cost less to build and maintain, while also immediately improving the ecological value of these artificial structures (Sutton-Grier et al., 2018). Given the little information available on how to ‘green the gray’ infrastructure with oysters or other NNBF, more eco-engineering studies testing hybrid infrastructure, evaluating performances against SLR/climate change, and creating broad guidance for designs and siting of this technology have been repeatedly requested (e.g. Temmerman et al., 2013; Ferrario et al., 2014, Sutton-Grier et al., 2015, 2018). Without detailed studies and guidance, restoration efforts will likely be inefficient and lack full effectiveness for long-term coastal protection.

The following section gives an overview of traditional engineering structures used for coastal safety, followed by a summary of oysters and their involvement as nature-based solutions. The last paragraph illustrates purposes and objectives of the dissertation.

### *1.1 Traditional adopted solutions for coastal protection*

To provide protection to coastal communities from worldwide sea threats, traditional solutions consist of engineering structures that reduce wave energy and shoreline erosion. Such as structures are breakwaters, seawalls, jetties groynes or rip-raps, widely used to protect shorelines for years (USACE, 2002; Sutton-Grier et al., 2015; Schoonees et al., 2019).

Hard structures such as groins and breakwaters are built offshore to prevent and mitigate erosion (Hamm et al., 2002; Schoonees et al., 2019). Breakwaters are built parallel to the shore and designed to protect the coast and improve recreational conditions on the landward side of the structure (Pilarczyk and Zeidler, 1996). They are usually made of concrete, rocks, sandbags or geotextiles and are designed to

reduce wave energy at the shoreline. Part of the wave energy is dissipated by wave breaking or friction losses, part is reflected back to the sea, and part is transmitted through the porous structure or by overtopping (Pilarczyk, 2003). The restorative effect of the breakwaters provides protection against extreme events but also affects coastal morphodynamics. Changes in hydrodynamics induced by the presence of the structure (Mory and Hamm, 1997) alter gradients in sediment transport and thus cause morphological changes (Van Rijn, 2013). Decreasing current along the coast on the landward side of breakwaters can induce sediment deposition on the upstream side while increasing flow velocity as the current leaves the sheltered area can cause erosion downstream of the structure. Deposition is usually more pronounced in the middle of the structure (landward side) than on both sides, due to wave diffraction. Diffracted waves curve inwards in the sheltered area of the structure and decrease in height inside it (Hsu and Silvester, 1990). Variables, such as the number of structures, the distance between them (along the coast), their distance from the coast, the height of the structure's crest and the width of the surf zone, can induce different patterns of erosion and accretion (Suh and Dalrymple, 1987; Ranasinghe and Turner, 2006).

Breakwaters may be emerged or submerged. The greater the height of the crest with respect to the mean sea level, the greater wave energy reduction; however, higher structures increase wave reflection on the seaward side of the structure, which causes scouring and loss of intertidal areas (Douglass and Pickel, 1999; Winterwerp et al., 2013). Submerged breakwaters became popular because of their low visual impact, but the lack of understanding of their hydraulic behavior often resulted in erosion problems, as stated by Ranasinghe and Turner (2006) in a literature review. Coastal structures also affect currents dynamic, generating so-called rip-currents. A rip current is a localized current that flows away from the shoreline toward the open sea, due to gradients in water level along the shore caused by wave breaking. Rip-currents cause loss of sediment and represent a danger for recreational activities, if the flow velocities are high enough (Scott et al., 2016). In addition, flow contraction at the end of shore or between the gap of two breakwaters leads to flow acceleration and scour at the tip (Lillycrop and Hughes, 1993).

Other kind of structures such as groynes or jetties extend towards the sea perpendicular to the shoreline (USACE, 2002), made of rocks or concrete as well as breakwaters. They prevent, or slow down, the longshore sediment transport, resulting in accretion of sediment on the updrift side of the structure and erosion on the downdrift side (Van Rijn, 2013). Seawalls instead, are vertical waterproof structures parallel and attached to the coast designed to protect from overtopping and flooding, usually made of reinforced concrete. These structures fix the position of the shoreline, thereby preventing it from retreating landward. As seawalls form rigid barriers, they increase wave reflection which results in beach scouring on the seaward side of the structure. This makes seawalls to cause sediment loss and in turn structural instabilities (USACE, 2002). Similar to seawalls, rip-raps are built on the edge of the coast with rocks capable of providing a certain degree of permeability to the structure, essentially protecting against erosion.

None of these infrastructures provide ecosystem benefits and often have negative impact to coastal ecology (Sutton-Grier et al., 2015, 2018; Palinkas et al., 2023). Moreover, and more importantly, they cannot self-adapt to climate change and SLR, which will make the coast more vulnerable once these structures will no longer provide the expected protection. As sea level rises, defense purposes of coastal breakwaters will be inhibited since higher mean water level results in lower wave dampening. It is therefore appropriate to study NNBF for coastal protection capable of self-adapting to climate change without losing efficiency over time (Scyphers et al., 2015; Mamo et al., 2021; Saengsupavanich et al., 2022).

This dissertation focuses on incorporating oysters into breakwaters to provide coastal protection from waves while also providing co-benefits to the ecosystem.

## *1.2 Oysters as nature-based solution for coastal protection*

Oysters are a genus of bivalve mollusks found to live within the moderate salinity portion of coastal areas (5–3), where they seek refuge from predation, competition and disease (predominant in higher salinity areas, Chu et al., 1993; White et al., 1996; Fodrie et al., 2014; Johnson, 2014). Oysters and oyster reefs are among the

most threatened of marine habitats having suffered substantial declines globally over the past century (Kirby, 2004; Beck et al., 2011), primarily due to overfishing, hydrological changes, pollution, and disease (Winslow, 1887; Mackenzie, 2007; Powell et al., 2008; Wilberg et al., 2011). These losses have been quantified for the USA by Zu Ermgassen et al., (2012) in 64% decline in oyster extent and 88% loss of oyster biomass between the early 1900s and the early 2000s. Such measures underpin efforts to formulate estimates of the loss of a critical coastal ecosystem service such as water filtration.

Recent efforts have therefore been directed toward restoring oyster abundance across the world through restoration plans aimed to also improve and protect marine and coastal environments.

Oysters are capable of providing a wide variety of ecosystem services useful for the environment (Coen et al., 2007). Ecosystem services are defined as the benefits provided by natural systems to human and environmental health. They vary from basic provisions including food and water, to cultural and recreational benefits (MEA 2005), such as oyster biomass production and with each other protection, water filtration, carbon sequestration, ecosystem diversification and habitat provision, increasing biodiversity and productivity, improving fisheries and ecological communities (Coen et al., 2007; Grabowski and Peterson, 2007). From an engineering perspective, oysters are able to attenuate wave energy and increase sedimentation rates due to the three-dimensional structure they form once fully developed (Coen et al., 2007; Dame and Patten, 1981). In addition to physical interaction with overlying waters, unlike grey infrastructure, oyster reefs can self-repair after damage and respond to changing environmental conditions (Ferrario et al., 2014, Sutton-Grier et al., 2015). Furthermore, oyster reefs are expected to accrete at a similar pace to sea-level rise (Ridge et al., 2017; Rodriguez et al., 2014) and it is reasonable to expect that their ecosystem services, including shoreline stabilization, could also be sustainably maintained well into the future. Recent restoration projects have used “oyster castles” (OCs) to restore oyster population. OCs are concrete blocks that can interlock with each other and provide coastal protection. OCs have

proven successful at recruiting and retaining oysters, and promoting both vertical accretion and horizontal expansion of reef habitat (Theuerkauf et al., 2015).

Oysters as nature-based solutions have been extensively studied in the literature. They could provide wave attenuation, mitigate shoreline loss, facilitate fisheries, promote adjacent mudflat stability, and support marsh growth (Scyphers et al., 2011; Weaver et al., 2017; Chowdhury et al., 2019; Wiberg et al., 2019). Oyster reefs also increase hydrodynamic bottom roughness which in turn affects flow characteristics (Wright et al., 1990; Styles, 2015). However, tradeoffs between ecological and engineering needs are important to consider when employing oyster reefs for coastal defense (Hogan and Reidenbach, 2022). For oyster-based hybrid infrastructure to be most effective on a long-term basis, it is important that reefs are in areas that are vulnerable to SLR and locations that promote oyster-reef growth through regular recruitment. Then reef habitats create positive feedback for growth, as oyster larvae are gregarious settlers that actively recruit to oyster shells and thus promote reef accretion (Gutierrez et al., 2003; Scyphers et al., 2011). While vertical elevation has proven to have a positive effect on the success of oyster growth and recruitment (Bartol et al., 1999; Lenihan, 1999; Schulte et al., 2009), there are environmental tradeoffs. At higher elevations, oysters spend less time submerged and reduce their susceptibility to predation and sedimentation (Fodrie et al., 2014; Johnson and Smee, 2014; Lenihan, 1999). However, emergent time exposes oysters to greater stress through cold temperatures, desiccation, and lowered food supply which can affect growth and survivability (Johnson and Smee, 2014; Byers et al., 2015).

Environmental hydrodynamic conditions also affect oysters' establishment within coastal areas. Estuarine and coastal bays are characterized as low-energy environments, suitable for the settling and the establishment of new oyster population. Shorelines directly exposed to incoming wave heights, strong wind and longshore currents are definitely not suitable for oyster-based infrastructures.

### 1.3 Objectives and research purposes

The proposed research developed an integrated modeling system that links hydrodynamic and eco-geomorphological models to understand how adding oysters

to breakwaters affect wave attenuation and sediment transport around the structure under different SLR scenarios. This system was validated and compared with field data from Lake Cove along the Horn Point Laboratory – University of Maryland Center for Environmental Science (HPL - UMCES) Campus (MD, USA), where four breakwaters were constructed in the summer of 2019 in front of an eroding shoreline, and then coupled with oysters. The intent of the proposed work was to produce highly relevant and useful outcomes to managers in the Chesapeake Bay and beyond. The thesis answered the following questions:

1. What is the impact that breakwaters have in shallow coastal bays regarding shoreline protection? Can common structures for coastal protection in shallow coastal bays negatively impact solid transport and inhibit sediment supply for tidal marshes?
2. What is the morphodynamic impact of the 4 breakwaters we built in the Lake Cove? How effective are they in dampening waves with and without oysters?
3. Can the model made in Delft3D return the same results observed in the field? Can oysters' addition on breakwaters improve wave dampening and sediment retention over time?
4. What are the hydrodynamic differences between oyster-covered and gray breakwaters? Can oysters improve dissipative effects by increasing the Drag Coefficient?

Through the questions listed above, this research aimed to provide significant insights into the coupling between oysters and breakwaters, to offer coastal protection that may be more durable and resilient to climate change and SLR. To answer the questions of this research we applied field, laboratory, and modeling approaches.

Firstly, through an idealized model (made in Delft3D), the impact of breakwaters on the sediment supply for vegetated coastlines was analyzed. This model wanted to analyze the scenario where, although certainly able to prevent erosion and promote sedimentation, breakwaters may inhibit sediment transport to and within adjacent marsh platforms, starving them of sediment needed to keep up with SLR. This chapter was conceived as an introduction where we wanted to preliminarily study the

hydrodynamic and morphodynamic effect of a single breakwater and analyze which distance from the shoreline these structures should be placed in order to maximize coastal defense.

The study performed in the field aimed at measuring and quantifying wave dampening (for oyster-covered and gray breakwaters), as well as tracking bathymetry evolution over time to evaluate depositional/erosional patterns induced by the breakwaters. Two locations within the Choptank River were chosen as study sites, the Lake Cove within the Horn Point Laboratory - UMCES (Cambridge, MD) and the Bill Burton State Park in Cambridge (MD). In the first study site (Lake Cove), GPS surveys were conducted to monitor bathymetric changes induced by the presence of 4 man-made breakwaters, and wave data was recorded to quantify the effect of oysters on wave dampening. In the second study site (Bill Burton), bathymetric surveys were carried out to produce a Digital Elevation Model (DEM) in order to conduct numerical simulations (through Delft3D) on the response of three existing rocky-breakwaters with and without oysters to climate change and relative sea-level rise (RSLR) (in term of wave dampening and coastal protection).

Extensive field data has then been used to model the protective benefits of coupling breakwaters and oysters in the Lake Cove and Bill Burton, through Delft3D. After hydrodynamically (through water level and wave dampening data) and morphodynamically (through GPS bathymetric surveys) validating the Cove model, water level at 20, 50, and 100 years was projected, and the response of breakwaters with and without oysters to RSLR and climate changes was modeled under a combination of different scenarios (as well as for Bill Burton). The aim of the modeling was to assess how wave dampening and sediment transport was affected by breakwaters with and without oysters, under various scenarios of RSLR.

A key aspect of this research is the study of the roughness increase brought on by oyster addition on breakwaters. Such coupling should result in greater roughness over and around these structures and improve dissipative effects. In this regard, the current research aimed to provide a drag coefficient value for breakwaters with and without oysters. To study this phenomenon, we used optical laboratory techniques to study fluid flow around and over an object, the so-called Particle Image Velocimetry (PIV).

PIV allows to obtain instantaneous velocity fields which are then analyzed to trace hydrodynamic quantities such as vorticity, turbulent kinetic energy, turbulent dissipation, drag coefficient and so on. We run different experiments in order to analyze the impact of the water level, flow velocity and breakwater geometries, on flow characteristics. After ending PIV analysis, Computational Fluid Dynamic (CFD) software, Flow3D, was used to expand the research carried out in the laboratory, in order to support PIV results. Flow3D allows the numerical reconstruction of a laboratory flume, which was validated according to laboratory velocity data.

#### 1.4 Anticipated results

The current research has brought significant insights into the coupling between natural (oysters) and built (breakwaters) solutions for coastal protection.

Study results revealed breakwaters are important solutions for coastal defense, being able to reduce wave energy and protect the shoreline from erosion. However, they might negatively impact the sediment supply for coastal vegetation, starving tidal wetlands of sediment needed to keep up with SLR.

Modeling simulations showed a loss of protective benefits over time by gray breakwaters due to increase in sea level, except when coupled with oysters, capable of self-adapt and grow with SLR. Wave dampening drastically decreased over time, but remained significant only when oysters were included, as well as for the sediment budget of the shore.

Laboratory experiments revealed a higher drag coefficient (based on the 1D momentum balance) associated with emergent oyster-covered breakwaters, denoting a greater efficiency in reducing downstream flow momentum. However, fully submerged breakwaters showed a downstream momentum increase when covered by oysters, in both laboratory and CFD experiments, that will need further explanations.

Overall, the current dissertation highlights oysters' integration into coastal defense can offer new adaptive shoreline protection in the face of climate changes and SLR,

where optimal conditions for oysters' survivability occur and are maintained over time.

## 1.5 References

- Bartol, I.K., R. Mann, and M. Luckenbach. 1999. Growth and mortality of oysters (*Crassostrea virginica*) on constructed intertidal reefs: Effects of tidal height and substrate level. *Journal of Experimental Marine Biology and Ecology* 237: 157–184.
- Beck, M. W., Brumbaugh, R. D., Airoidi, L., Carranza, A., Coen, L. D., Crawford, C., ... & Guo, X. (2011). Oyster reefs at risk and recommendations for conservation, restoration, and management. *Bioscience*, 61(2), 107-116.
- Board, O.C.; National Research Council. Mitigating shore erosion along sheltered coasts; National Academic Press: 500 Fifth Street, N.W. Washington, DC 20001, USA, 2007.
- Brandon, C. M., Woodruff, J. D., Orton, P. M., & Donnelly, J. P. (2016). Evidence for elevated coastal vulnerability following large-scale historical oyster bed harvesting. *Earth surface processes and landforms*, 41(8), 1136-1143.
- Byers, J. E., Grabowski, J. H., Piehler, M. F., Hughes, A. R., Weiskel, H. W., Malek, J. C., & Kimbro, D. L. (2015). Geographic variation in intertidal oyster reef properties and the influence of tidal prism. *Limnology and Oceanography*, 60(3), 1051-1063.
- Chowdhury, M. S. N., Walles, B., Sharifuzzaman, S. M., Shahadat Hossain, M., Ysebaert, T., & Smaal, A. C. (2019). Oyster breakwater reefs promote adjacent mudflat stability and salt marsh growth in a monsoon dominated subtropical coast. *Scientific reports*, 9(1), 1-12.
- Chu, F.-L. E., La Peyre, J. F. & Burreson, C. S. *Perkinsus marinus* infection and potential defense-related activities in Eastern Oysters, *Crassostrea virginica*: salinity effects. *J. Invertebr. Pathol.* 62, 226–232 (1993).
- Coen, L. D., Brumbaugh, R. D., Bushek, D., Grizzle, R., Luckenbach, M. W., Posey, M. H., ... & Tolley, S. G. (2007). Ecosystem services related to oyster restoration. *Marine Ecology Progress Series*, 341, 303-307.
- Creel, L. *Ripple effects: Population and coastal regions*; Population Reference Bureau: 1875 Connecticut Ave., NW, Suite 520, Washington, DC 20009, USA, 2003; pp. 1-7.
- Currin, C. A., Chappell, W. S., and Deaton, A. (2010). “Developing alternative shoreline armoring strategies: the living shoreline approach in North Carolina,” in *Puget Sound Shorelines and the Impacts of Armoring-Proceedings of a State of the Science Workshop* (U.S. Geological Survey), 92–102.

- Dame, R. F., & Patten, B. C. (1981). Analysis of energy flows in an intertidal oyster reef. *Marine Ecology Progress Series*, 5(2), 115-124.
- Davis, J. L., Currin, C. A., O'Brien, C., Raffenburg, C., and Davis, A. (2015). Living shorelines: coastal resilience with a blue carbon benefit. *PLoS One* 10:e0142595. doi: 10.1371/journal.pone.0142595
- Douglass, S.L.; Pickel, B.H. The tide doesn't go out anymore - the effect of bulkheads on urban shorelines. *Shore and Beach*, 1999, 67, pp. 19-25.
- Ferrario, F., Beck, M. W., Storlazzi, C. D., Micheli, F., Shepard, C. C., & Airoidi, L. (2014). The effectiveness of coral reefs for coastal hazard risk reduction and adaptation. *Nature communications*, 5(1), 1-9.
- Fodrie, F. J. et al. Classic paradigms in a novel environment: inserting food web and productivity lessons from rocky shores and saltmarshes into biogenic reef restoration. *J. Appl. Ecol.* 51, 1314–1325 (2014).
- Gittman, R. K., Peterson, C. H., Currin, C. A., Fodrie, F. J., Piehler, M. F., and Bruno, J. F. (2016a). Living shorelines can enhance the nursery role of threatened estuarine habitats. *Ecol. Appl.* 26, 249–263 doi: 10.1890/14-0716
- Grabowski, J. H. & Peterson, C. H. Restoring oyster reefs to recover ecosystem services in *Ecosystem Engineers: Concepts, Theory and Applications*. (eds. Cuddington, K., Byers, J. E., Wilson, W. G. & Hastings, A.) Elsevier/Academic Press, Netherlands. *Ecosystem Engineers: Concepts, Theory and Application*. Netherlands, Elsevier/Academic Press. pp. 281–298 (2007).
- Gutiérrez, J. L., Jones, C. G., Strayer, D. L., & Iribarne, O. O. (2003). Mollusks as ecosystem engineers: the role of shell production in aquatic habitats. *Oikos*, 101(1), 79-90.
- Hamm, L., M. Capobianco, H. Dette, A. Lechuga, R. Spanhoff, and M.J. Stive. 2002. A summary of European experience with shore nourishment. *Coastal Engineering* 47 (2): 237–264. [https://doi.org/10.1016/S0378-3839\(02\)00127-8](https://doi.org/10.1016/S0378-3839(02)00127-8)
- Hogan, S., & Reidenbach, M. A. (2022). Quantifying Tradeoffs in Ecosystem Services Under Various Oyster Reef Restoration Designs. *Estuaries and Coasts*, 45(3), 677-690.
- Hsu, J.R.C., and R. Silvester. 1990. Accretion behind single offshore breakwater. *Journal of Waterway, Port, Coastal, and Ocean Engineering* 116 (3): 362–380. [https://doi.org/10.1061/\(ASCE\) 0733-950X\(1990\)116:3\(362\)](https://doi.org/10.1061/(ASCE) 0733-950X(1990)116:3(362)).
- Johnson, K. D. & Smee, D. L. Predators influence the tidal distribution of oysters (*Crassostrea virginica*). *Mar. Biol.* 161, 1557–1564 (2014).

- Kay, R; Alder, J. Coastal Planning and Management, 2nd ed.; Taylor & Francis: 270 Madison Ave, New York, NY 10016, USA, 2005.
- Kennish, M.J. Environmental threats and environmental future of estuaries. *Environmental Conservation*, 2002, 29, pp. 78–107.
- Kirby, M. X. Fishing down the coast: Historical expansion and collapse of oyster fisheries along continental margins. *Proc. Natl Acad. Sci. USA* 101, 13096–13099 (2004).
- Lenihan, H.S. 1999. Physical-biological coupling on oyster reefs: How habitat structure influences individual performance. *Ecological Monographs* 69: 251–275.
- Li, M., Zhang, F., Barnes, S., and Wang, X. (2020). Assessing storm surge impacts on coastal inundation due to climate change: case studies of Baltimore and Dorchester County in Maryland. *Nat. Hazards* 103, 2561–2588. doi: 10.1007/s11069-020-04096-4
- Lillicrop, W.J., and S.A. Hughes. 1993. Scour hole problems experienced by the Corps of Engineers; Data Presentation and Summary. CERC-93-2
- Mackenzie, C.L. 2007. Causes underlying the historical decline in eastern oyster (*Crassostrea virginica* Gmelin, 1791) landings. *Journal of Shellfish Research* 26: 927–938.
- Mamo, L.T., Coleman, M.A. and Kelaher, B.P., 2021. Ecological enhancement of breakwater upgrades: size and type of rocks used influence benthic communities. *Marine Ecology Progress Series*, 661, pp.71-82.
- Manis, J. E., Garvis, S. K., Jachec, S. M., and Walters, L. J. (2015). Wave attenuation experiments over living shorelines over time: a wave tank study to assess recreational boating pressures. *J. Coast. Conserv.* 19, 1–11. doi: 10.1007/s11852-014-0349-5
- Marra, J., Allen, T., Easterling, D., Fauver, S., Karl, T., Levinson, D., et al. (2007). An integrating architecture for coastal inundation and erosion program planning and product development. *Mar. Technol. Soc. J.* 41, 62–75. doi: 10.4031/002533207787442321
- Millennium ecosystem assessment, M. E. A. (2005). *Ecosystems and human well-being* (Vol. 5, pp. 563-563). Washington, DC: Island press.
- Morris, R. L., La Peyre, M. K., Webb, B. M., Marshall, D. A., Bilkovic, D. M., Cebrian, J., ... & Swearer, S. E. (2021). Large-scale variation in wave attenuation of oyster reef living shorelines and the influence of inundation duration. *Ecological Applications*, 31(6), e02382.

- Mory, M., and L. Hamm. 1997. Wave height, setup and currents around a detached breakwater submitted to regular or random wave forcing. *Coastal Engineering* 31 (1-4): 77–96. [https://doi.org/10.1016/S0378-3839\(96\)00053-1](https://doi.org/10.1016/S0378-3839(96)00053-1).
- Palinkas, C. M., and Lorie, S. (2018). “Promoting living shorelines for shoreline protection: understanding potential impacts to and ecosystem trade-offs with adjacent submersed aquatic vegetation (SAV),” Presented at the AGU Fall Meeting 2018
- Patrick, C. J., Weller, D. E., & Ryder, M. (2016). The relationship between shoreline armoring and adjacent submerged aquatic vegetation in Chesapeake Bay and nearby Atlantic coastal bays. *Estuaries and Coasts*, 39(1), 158-170.
- Pilarczyk, K.W., and R.B. Zeidler. 1996. Offshore breakwaters and shore evolution control. Rotterdam: Balkema ISBN: 90-5410-627-1.
- Pilarczyk, K.W. 2003. Design of low-crested (submerged) structures – An overview –. In 6th international conference on coastal and port engineering in developing countries, Colombo, Sri Lanka.
- Pilkey, O.H.; Wright, W. Seawalls versus Beaches. *Journal of Coastal Research*, 1988, special issue n° 4, pp. 41-64.
- Post, J.C.; Lundin, C.G. Guidelines for integrated coastal zone management; The World Bank: Headquarters, 1818 H Street, NW Washington, DC 20433, USA, 1996.
- Powell, E.N., K.A. Ashton-Alcox, J.N. Kraeuter, S.E. Ford, and D. Bushek. 2008. Long-term trends in oyster population dynamics in Delaware Bay: regime shifts and reponse to disease. *Journal of Shellfish Research* 27: 729–755.
- Ranasinghe, R., and I.L. Turner. 2006. Shoreline response to submerged structures: A review. *Coastal Engineering* 53 (1): 65–79. <https://doi.org/10.1016/j.coastaleng.2005.08.003>.
- Ridge, J. T., Rodriguez, A. B., Joel Fodrie, F., Lindquist, N. L., Brodeur, M. C., Coleman, S. E., Theuerkauf, E. J. (2015). Maximizing oyster-reef growth supports green infrastructure with accelerating sea-level rise. *Scientific Reports*, 5(1), 1-8.
- Ridge, J. T., Rodriguez, A. B., and Fodrie, F. J. (2017). Evidence of exceptional oyster-reef resilience to fluctuations in sea level. *Ecol. Evol.* 7, 10409–10420. doi: 10.1002/ece3.3473
- Rodriguez, A. B., Fodrie, F. J., Ridge, J. T., Lindquist, N. L., Theuerkauf, E. J., Coleman, S. E., ... & Kenworthy, M. D. (2014). Oyster reefs can outpace sea-level rise. *Nature climate change*, 4(6), 493-497.

- Saengsupavanich, C., Ariffin, E.H., Yun, L.S. and Pereira, D.A., 2022. Environmental impact of submerged and emerged breakwaters. *Heliyon*, p.e12626.
- Safak, I., Angelini, C., Norby, P. L., Dix, N., Roddenberry, A., Herbert, D., et al. (2020). Wave transmission through living shoreline breakwalls. *Cont. Shelf Res.* 211:104268. doi: 10.1016/j.csr.2020.104268
- Schoonees, T., Gijón Mancheño, A., Scheres, B., Bouma, T. J., Silva, R., Schlurmann, T., & Schüttrumpf, H. (2019). Hard structures for coastal protection, towards greener designs. *Estuaries and Coasts*, 42(7), 1709-1729.
- Schulte, D. M., Burke, R. P., & Lipcius, R. N. (2009). Unprecedented restoration of a native oyster metapopulation. *Science*, 325(5944), 1124-1128.
- Scott, T., M. Austin, G. Masselink, and P. Russell. 2016. Dynamics of rip currents associated with groynes — Field measurements, modelling and implications for beach safety. *Coastal Engineering* 107: 53–69. <https://doi.org/10.1016/j.coastaleng.2015.09.013>.
- Scyphers, S. B., Powers, S. P., Heck Jr, K. L., & Byron, D. (2011). Oyster reefs as natural breakwaters mitigate shoreline loss and facilitate fisheries. *PloS one*, 6(8), e22396.
- Scyphers, S.B., Powers, S.P. and Heck, K.L., 2015a. Ecological value of submerged breakwaters for habitat enhancement on a residential scale. *Environmental management*, 55, pp.383-391.
- Scyphers, S. B., Gouhier, T. C., Grabowski, J. H., Beck, M. W., Mareska, J., and Powers, S. P. (2015b). Natural shorelines promote the stability of fish communities in an urbanized coastal system. *PLoS One* 10:e0118580. doi: 10.1371/journal.pone.0118580
- Styles, R. (2015). Flow and turbulence over an oyster reef. *Journal of Coastal Research*, 31(4), 978-985.
- Suh, K., and R.A. Dalrymple. 1987. Offshore breakwaters in laboratory and field. *Journal of Waterway, Port, Coastal, and Ocean Engineering* 113 (2): 105–121. [https://doi.org/10.1061/\(ASCE\) 0733-950X\(1987\)113:2\(105\)](https://doi.org/10.1061/(ASCE) 0733-950X(1987)113:2(105)).
- Sutton-Grier, A. E., Wowk, K., and Bamford, H. (2015). Future of our coasts: the potential for natural and hybrid infrastructure to enhance the resilience of our coastal communities, economies and ecosystems. *Environ. Sci. Policy* 51, 137–148. doi: 10.1016/j.envsci.2015.04.006
- Sutton-Grier, A. E., Gittman, R. K., Arkema, K. K., Bennett, R. O., Benoit, J., Blicht, S., ... & Grabowski, J. H. (2018). Investing in natural and nature-based infrastructure: building better along our coasts. *Sustainability*, 10(2), 523.

- Temmerman, S., Meire, P., Bouma, T. J., Herman, P. M., Ysebaert, T., and De Vriend, H. J. (2013). Ecosystem-based coastal defence in the face of global change. *Nature* 504, 79–83. doi: 10.1038/nature12859
- Theuerkauf, S. J., Burke, R. P., & Lipcius, R. N. (2015). Settlement, growth, and survival of eastern oysters on alternative reef substrates. *Journal of Shellfish Research*, 34(2), 241-250.
- U.S. Army Corps of Engineers (USACE). 2002. Coastal engineering manual, 1110th-2nd–110th edn. Washington, D.C.: U.S. Army Corps of Engineers.
- Van Rijn, L. C. 2013. Design of hard coastal structures against erosion. Accessed online 22/10/2018. <https://www.leovanrijn-sediment.com/papers/Coastalstructures2013.pdf>. Accessed 22 Oct 2018.
- Vona, I., Gray, M. W., and Nardin, W. (2020). The impact of submerged breakwaters on sediment distribution along marsh boundaries. *Water* 12:1016. doi: 10.3390/w12041016
- Vona, I., Palinkas, C.M. and Nardin, W., 2022. Sediment Exchange Between the Created Saltmarshes of Living Shorelines and Adjacent Submersed Aquatic Vegetation in the Chesapeake Bay. *Coastal Wetlands Dynamics*.
- Weaver, R. J., Stehno, A., Bonanno, N., Sager, A., Kenny, A., Zehnder, J. A., ... & Allen, A. (2017). Scale model design of oyster reef structures as part of a showcase living shoreline project. *Shore & Beach*, 85(4), 41-54.
- White, M. E. & Wilson, E. A. In *The eastern oyster Crassostrea virginica* (eds. Kennedy, V. S., Newell, R. I. E. & Eble, A. F.) 559–580 (Maryland Sea Grant College, 1996).
- Wiberg, P.L.; Taube, S.R.; Ferguson, A.E.; Kremer, M.R.; Reidenbach, M. A. Wave attenuation by oyster reefs in shallow coastal bays. *Estuaries and coasts*, 2019, 42, pp. 331-347.
- Wilberg, M.J., M.E. Livings, J.S. Barkman, B.T. Morris, and J.M. Robinson. 2011. Overfishing, disease, habitat loss, and potential extirpation of oysters in upper Chesapeake Bay. *Marine Ecology Progress Series* 436: 131–144.
- Winslow, F. 1887. Deterioration of American oyster-beds. *The Popular Science Monthly* 20: 29–43.
- Winterwerp, J.C., P.L.A. Erfteemeijer, N. Suryadiputra, P. van Eijk, and L. Zhang. 2013. Defining eco-Morphodynamic requirements for rehabilitating eroding mangrove-mud coasts. *Wetlands*. 33 (3): 515–526. <https://doi.org/10.1007/s13157-013-0409-x>.

Wright LD., Gammischand RA., Byrne RJ, 1990. Hydraulic roughness and mobility of three oyster-bed artificial substrate materials. *Journal of Coastal Research*, 6(4), 867–878. Google Scholar

Zu Ermgassen, P. S., Spalding, M. D., Grizzle, R. E., & Brumbaugh, R. D. (2013). Quantifying the loss of a marine ecosystem service: filtration by the eastern oyster in US estuaries. *Estuaries and coasts*, 36(1), 36-43

## Chapter 2: The impact of submerged breakwaters on sediment distribution along marsh boundaries

### Abstract

Human encroachment and development on coastlines have led to greater amounts of armoring of shorelines. Breakwaters are a common feature along coastlines, which are used to dampen wave energy and protect shorelines from erosion. Their morphodynamic impact on the surrounding and subtidal environment have been extensively studied in the literature, but their impact on marsh geomorphology has not been frequently examined. To address this gap, our study quantifies the effects of breakwaters on sediment transport and marsh evolution under different wave regimes using Delft3D-SWAN, a geomorphodynamic numerical model. Model configurations used the same numerical domain, but scenarios had different sediments, waves, tides, basin slopes and breakwater distances from the shoreline to explore how waves and tidal currents shape coastal margins. Model results suggested breakwaters were responsible for an average wave damping between 10% - 50% proportional to the significant wave height across all modeled scenarios. Shear stress at the beginning of the marsh and the volume of sediment deposited at the end of the simulation (into the marsh behind the breakwater) increased on average between 20% - 40% proportional to the slope and distance of the breakwater from the shoreline. Sediment deposition in the marsh, within the area protected by the breakwater, was found to be lower than marsh deposition away from the structure, suggesting breakwaters reduce sediment supply for vegetated shorelines. Study results indicated breakwaters are good for wave breaking to protect shorelines from the wave's energy and reduce erosion. However, they might represent an obstacle for sediment transport and reduce sediment nourishment processes towards tidal wetlands, threatening long-term marsh survival. Identifying a balance between waves dampening and shoreline nourishment should be considered in the design and implementation of these structures.

**Keywords:** hydrodynamic; morphology; numerical modelling; breakwater

## 2.1 Introduction

Coastal regions are home to a large portion of the world's population. Environmental issues such as human development, habitat degradation, sea-level rise (SLR), and global warming seriously threaten coastal communities. Erosional control, pollutants filtration, food supply, are only some of the coastal ecosystem services that are likely to get lost over time due to a changing climate (Creel, 2003; Kay and Alder, 2005). The rapid population growth observed in many coastal areas also leads to increased stresses likely to degrade coastal and marine ecosystems. Half of the world's wetlands disappeared in the 20th century. For instance, Louisiana (USA) lost around 25% of its coastal wetlands since 1932 (Couvillion et al., 2017), while in the Chesapeake Bay, up to 94 km<sup>2</sup> of marsh was lost since the nineteenth century (Schieder et al., 2018).

To protect and maintain the boundaries of coastal regions, a common practice is to transform, alter, and armor shorelines with a variety of structures such as seawalls, breakwaters or bulkheads that reduce wave energy and shoreline erosion (Pilkey and Wright, 1988; Douglass and Pickel, 1999; Board, 2007). However, a full accounting of the ecological damage associated with these structures is rarely performed, considered, or even well understood prior to infrastructure construction but may be substantial once completed (Douglass and Pickel, 1999; Kennish, 2002; Board, 2007). For example, the construction of low crested coastal defense structures may results in seaward loss of soft-bottom habitats and associated assemblages of animals and plants (Airoldi, 2005). However, breakwater infrastructures have been also found to trap fine sediments, enhancing nearshore sedimentation patterns (Palinkas et al., 2016). Both wetland vegetation and engineered structures can protect coasts from wave energy, but it is important to understand the synergy between gray (any artificial/non-living solution for coastal defense) and green (any natural/living solution for coastal defense) solutions as their interaction may alter functionality of one or both defense methods.

Breakwaters, which were the object of this study, are offshore structures that break incoming waves to reduce their energy at the shoreline, able to trap sediments, and protect the coast from erosion (Board, 2007; Borsje et al., 2011; Sharifahmadian, 2015; Palinkas et al., 2016, 2018; [Klonaris](#) et al., 2018; Safari, 2018). Salt marsh vegetation is a natural barrier, dissipate waves energy, due to the drag created by plant stems and leaves (Allen and Pye, 1992; Broome et al., 2015), and reduce sediment re-suspension and promote deposition (Allen and Pye, 1992; Brooman et al., 1998). Saltmarshes are not only important for coastal defense but they also play key roles for nursery habitat, biological production, and nutrient cycling within coastal communities and ecosystems (Brooman, 1999).

Sediments and organic matter play a crucial role for salt marshes since grain deposition promote vertical accretion allowing marshes to keep up with sea level rise (Bricker-Urso et al., 1989; Schuerch et al., 2018); moreover, coastal wetland enhancement driven by sedimentation can have direct consequences for shoreline protection since the aboveground portion of vegetation can dampen waves and stabilize sediments (Hashim and Catherine, 2013). As a result, local ecology and ecosystem functions can benefit from this sedimentation since a healthy salt marsh also promotes feeding, roosting and nesting areas for a wide range of bird species (Cadwalladr et al., 1972; Burger et al., 1977; Kelleway et al., 2017; Himes-Cornell et al., 2018; Zedler et al., 2018; Friess et al., 2020) and nursery areas for many fish species (Daiber, 1977; Zedler et al., 2018; Friess et al., 2020).

The effect that breakwaters have on the sediment supply for saltmarshes remains poorly understood and not frequently examined. Previous studies in the literature were primarily concerned with analyzing the wave-field induced by these structures or the related morphological changes. Different studies in the literature address ecological aspects between breakwaters and submerged aquatic vegetation (SAV) feedbacks (Palinkas et al., 2010, 2016, 2018; Barth, 2011); however, fewer studies analyzed ecological features associated with breakwaters and saltmarshes.. The main works on breakwaters conducted with field, laboratory and numerical experiments are reported below.

### 2.1.1 Laboratory experiments on breakwaters

Laboratory experiments focused on hydrodynamic and morphodynamic changes associated with breakwaters. Experiments performed by Goda (1969) on wave-transmission coefficient ( $k_t$ ) showed  $k_t$  was mostly governed by the ratio of the depth of water above the breakwater crest to the incidence wave height. In his study, Goda only take into account vertical wall breakwaters and ignored the permeability of the structure. Similarly, Gourlay (1996) conducted 2D experiments on wave propagation over a reef, in order to evaluate the effect of wave height, wave period and submergence depth on the wave-induced current and setup. The experiments included impermeable reef (as well as Goda (1969)) and only regular waves were considered. Irregular waves were expected to behave differently with respect to wave setup. The effect of wave incidence angle and berm width on the resulting wave setup, overtopping and filtration flow was analyzed by Zanuttigh and Lamberti (2006). A “scale” model was performed in order to estimate filtration flux based on other available datasets; however, their approach failed for increased submergence depth. The most complete database regarding submerged breakwaters is the one given by van der Meer et al., 2005, which provided new empirical formulation based on 3D experiments conducted in a wave basin, in order to evaluate the effect of irregular waves on wave transmission, interaction of low-crested structures, reflection, and 3D effects. More recently, , wave transmission through artificial reef breakwaters was addressed by few more authors (Webb and Allen, 2017; Xuan et al., 2020).

Morphodynamic 3D experiments by Groenewoud et al. (1996) in a wave basin illustrated the effect of the gaps' length between submerged breakwaters on the shoreline response, similar to Turner et al. (2001) and Ranasinghe et al. (2006). An empirical formulation was proposed. Wave incidence angle, submergence depth and distance of breakwaters from the coastline resulted the key parameters in erosional and depositional processes. The above papers focused on the shoreline response following the presence of a reef. The full bathymetry evolution throughout the surf zone, however, was only quickly described, and remained poorly studied. Di Risio et al. (2010) performed laboratory measurements using a physical model. The bathymetry evolution of both unprotected and protected nourished beaches was tested

in a 45 m long and 1.5 m wide wave flume. It was observed that submerged breakwater switches erosive conditions to slightly accretive, at least within the tested experimental range (only cross-shore sediment transport was considered due to the two-dimensional experiment approach, and four different wave trains were simulated to distinguish between daily and storm conditions). More recently, Chen et al., 2016, and GT Klonaris et al., 2020, investigated tsunami-induced scouring and bed morphology evolution induced by offshore breakwaters, respectively.

The current research is missing laboratory tests regarding the impact of breakwaters on sediment supply for coastal vegetation.

#### 2.1.2 Numerical modeling of breakwaters

Numerical modeling has been widely used to study hydrodynamic and morphodynamic of breakwaters.

Van Gent (1994) investigated the hydrodynamic behavior of submerged breakwaters also considering the structure permeability. Similarly, Losada et al. (1996) studied breakwaters considering the effect of porous material and structure geometry, as well as Avgeris et al. (2004) who extended a low-order Boussinesq-type model (BTM) to account for wave propagation over permeable structures. Garcia et al. (2004) used a Reynolds Averaged Navier-Stokes (RANS) model to simulate the near-field processes around breakwaters. They accounted for nonlinear wave interactions and breaking-induced turbulence, by only considering regular wave attack. Lara et al. (2006) extended the same model but with irregular waves. More recently, Meringolo et al., 2015, used a Smoothed Particle Hydrodynamics (SPH) model to study interactions between waves and perforated breakwaters. Cannata et al., 2019, investigated the velocity field generated around submerged breakwaters, by using a 3D numerical model, while Pourteimouri et al., 2020, developed an integrated numerical model in order to simulate interaction between waves and permeable submerged breakwaters using extended Navier–Stokes equations.

Only a restricted number of studies involving numerical models simulated the bed morphology evolution. Van der Biezen et al. (1998) validated a two-horizontal dimensional (2DH) numerical model with field data on the morphological evolution behind an array of submerged breakwaters. Only regular wave incidence and impermeable structures were studied. Zyserman et al. (1999) analyzed the short and long term morphodynamic of a detached breakwater considering its geometry and orientation, validating their model with empirical formulae for the shoreline response, rather than field data. Lesser et al. (2003), highlighted how inappropriate breakwaters design may result to significant erosion at the shoreline, while Cáceres et al. (2005) studied the effect of structure freeboard and significant wave height on the bed evolution behind low-crested structures. More recently, Klouaris et al., 2020, conducted experimental and numerical investigations on bed morphology in the lee of submerged breakwaters, driven by regular and irregular waves. Nguyet-Minh Nguyen et al., 2022, combined a physical and CFD numerical model to investigate the suspended sediment trapping capacity in the Mekong Delta.

### 2.1.3 Field studies on breakwaters

None of the laboratory and numerical experiments listed above investigated ecological impacts of breakwaters on the surrounding environment. Previous field studies of breakwaters and natural reef, highlighted how they can efficiently enhance mudflat stability and shoreline mitigation, waves attenuation, and facilitate fisheries production (Scyphers et al., 2015; Chowdhury et al., 2019; Wiberg et al., 2019); however, the effect that breakwaters have on the sediment supply for saltmarshes remains poorly understood and not frequently examined. For example, Airoidi et al. (2005) and Moschella et al. (2005), estimated the ecological impact of breakwaters without considering their impact on sediment supply to saltmarshes. Moreover, we note Faraci et al. (2014), who investigated the bottom profile evolution of a perched nourished beach by physical and numerical models, while in 2018 (Faraci, 2018) investigated the morphodynamic and hydrodynamic response of a geocontainer submerged reef, focused on reflection and transmission through the structure;

similarly, Sumer et al. (2005) investigated the local scour at roundhead and along the trunk of low crested structures.

However, recent studies have analyzed the ecological impact of breakwaters. Scypers et al., 2014, studied ecological value of submerged breakwaters, finding that small scale breakwaters can act as habitat for filter-feeding bivalves, mobile invertebrates, and young fishes. Ido and Shimrit, 2015, highlighted how the ecological enhancement of concrete-based coastal infrastructures increased ecosystem services provided by the gray structures, making them more suitable and appropriate for a greener coastal defense. Palinkas et al., (2010, 2016, 2018), studied the influence of shoreline stabilization structures on the nearshore sedimentary environment focusing on SAV rather than saltmarshes. Mamo et al., 2021, studied the typology of rocks used for coastal defense, in order to evaluate consequent stresses on benthic communities. They found that ecological outcomes of coastal protection infrastructure could be improved by including native rocks of a range of different sizes in multiple patches and layers. Lastly, Martin et al., 2021, analyzed the effects of large-scale breakwaters on shoreline vegetation, pointing out that large-scale breakwaters could preserve marsh edge in high wave energy environments though their effectiveness into the future will require adaptive management in response to local sea-level rise.

In this study we sought to fill knowledge gaps on how breakwaters may influence marsh nourishment using the numerical model Delft3D coupled with SWAN (Simulating WAVes Nearshore). Breakwater effects on sediment supply to salt marsh were modelled under different scenarios of waves and tide conditions. This same numerical modelling approach has already been used to investigate the impact of waves on coastal morphology (Nardin and Fagherazzi, 2012; Nardin et al., 2013), estimate the effect of tides on the alternative deposition of mud and sand (Leonardi et al., 2014), examine the influence of vegetation on bars evolution (Lera et al., 2019), and simulate wave propagation in harbors (Cooper et al., 2016). The current chapter was conceived as an introduction to the carried-out research to preliminarily analyze hydrodynamic and morphodynamic effect of breakwaters, in order to evaluate the

best configuration to be adopted in field studies along the eroding shoreline in the Lake Cove (see Chapter three).

## 2.2 Material and Methods

### 2.2.1 Model description

We present modeling results on how breakwaters affect the resilience of salt marshes under different wave conditions in a rectangular basin with rectangular cells, whose long cell dimension is parallel to the coast. The different run configurations use the same domain but with different sediments, waves, tides, basin slopes and distances of the breakwater to the shoreline.

Delft3D (Roelvink and Van Banning, 1995; Lesser et al., 2004) is an open-source computational fluid dynamics package that simulates fluid flow, waves, sediment transport, and morphological changes at different timescales. An advantage of Delft3D is the full coupling of the hydrodynamic and morphodynamic modules so that the flow field adjusts in real-time as the bed topography changes. The equations of fluid motion, sediment transport, and deposition are discretized on a 3D curvilinear, finite-difference grid and solved by an alternating direction implicit scheme. For our model, we used the bi-dimensional formulation of the hydrodynamic and morphodynamic models implemented in Delft3D.

The generation and propagation of waves in shallow water is computed by SWAN, which is able to mimic random, short-crested waves in the open ocean and in shallow water regions. The key processes incorporated in SWAN are: wave-wave interactions, wave refraction, and wave dissipation, that includes bottom friction (Hasselmann et al., 1973) and wave breaking (Battjes et al., 1978).

Here we present the essential model equations, but further details can be found in Lesser et al. (2004). For notation, refer to Table 2. The mass-balance equation in Cartesian coordinates for an incompressible fluid with shallow water approximation, which is solved by Delft3D is:

$$\nabla \cdot \vec{V} = 0, \quad (1)$$

where  $\vec{V}$  is the velocity vector with component  $u$ ,  $v$ ,  $w$  along the  $x$ ,  $y$  and  $z$  direction.

The momentum equations for unsteady, incompressible and turbulent flow is:

$$\rho \frac{D\vec{V}}{Dt} = -\nabla p + \nabla \cdot \tau + \rho g, \quad (2)$$

where  $\frac{D\vec{V}}{Dt}$  is the material derivate,  $\rho$  is the fluid density,  $\vec{V}$  is the flow velocity,  $p$  is the pressure and  $\tau$  is the fluid shear stress tensor which has order two.

Due to the shallow water approximation, the vertical momentum equation is reduced to the hydrostatic pressure equation; the vertical and horizontal eddy viscosity instead are computed by the  $k$ - $\epsilon$  model (Rodi et al., 1984) and a large eddy simulation method (L  v  que et al., 2007) respectively.

The suspended sediment transport is calculated by solving the three-dimensional advection-diffusion equation:

$$\frac{\partial C}{\partial t} = D \nabla^2 C - \vec{V} \cdot \nabla C + R, \quad (3)$$

where  $C$  is the mass concentration,  $D$  the diffusion coefficient,  $\vec{V}$  the velocity field and  $R$  describes sources or sinks of the quantity  $C$ .

For cohesive sediments, the exchange between the water column and the bed in term of erosion and deposition are calculated with Partheniades-Krone formulations (Partheniades, 1965), while for non-cohesive sediments, the exchange is computed by the Van Rijn method (Van Rijn, 1993), in which the formulation depends on the diameter of the suspended sediment (see supplemental material).

Changes in bed bathymetry are computed from the gradients in sediment transport vectors as follow:

$$(1 - \epsilon_{por}) \frac{\partial z_b}{\partial t} = -\frac{\partial S_x}{\partial x} - \frac{\partial S_y}{\partial y} + T_d, \quad (4)$$

where  $\epsilon_{por}$  is the bed porosity,  $z_b$  is the bed level (positive up) (m),  $S_x$ ,  $S_y$  are the total sediment transport components per unit width in the  $x$  and  $y$  directions ( $m^2/s$ ), and  $T_d$  is the deposition or erosion rate of suspended sediment (m/s).

The evolution of the wave motion is instead described by SWAN solving the spectral action balance equation:

$$\frac{\partial}{\partial t} N + \frac{\partial}{\partial x} c_x N + \frac{\partial}{\partial y} c_y N + \frac{\partial}{\partial \sigma} c_\sigma N + \frac{\partial}{\partial \theta} c_\theta N = \frac{S}{\sigma}, \quad (5)$$

where the left-hand side is the kinematic part of the equation. The first term represents the local change rate of action density in time while the second and the third one describes propagation of action in geographical space (along the  $x$ - $y$  direction with velocity  $c_x$  and  $c_y$  respectively). The fourth term represents shifting of the relative frequency due to variations in depths and currents, the fifth is the depth-induced and current-induced refraction, and lastly the quantities  $c_\sigma$  and  $c_\theta$  are the propagation velocities in the spectral space. The right-hand side of the equation contains the source/sink term that represents all physical processes including generation, dissipation, or wave energy redistribution.

The impact of vegetation on hydrodynamics is modeled as an effect on the bed roughness and flow resistance. In Delft3D, this is accomplished by using Baptist's formulation (Baptist et al., 2005), which models vegetation as rigid cylinders characterized by stem diameter ( $D$ ), height ( $H_v$ ), drag coefficient ( $C_D$ ) and density ( $m$ ). The expression of the Chézy coefficient has been derived by Baptist et al. (2007), building on results of a 1DV  $k$ - $\varepsilon$  turbulence model developed by Uittenbogaard (2003), which solves a simplification of the 3D Navier-Stokes equation for horizontal flow conditions with additional assumptions to include the effect of vegetation in the  $k$ - $\varepsilon$  turbulence closure. The vertical flow velocity profile is assumed to be divided in two zones due to the presence of vegetation: constant ( $u_v$ ) inside the vegetated patch and logarithmic above.

In the case of fully submerged vegetation, the total shear stress  $\tau_t$  is given by the sum of the bed shear stress  $\tau_b$  and the component due to the vegetation  $\tau_v$ :

$$\tau_t = \rho g h i = \tau_b + \tau_v \quad (6)$$

$$\tau_b = \frac{\rho g}{C_b^2} u_v^2 \quad (7)$$

$$\tau_v = \frac{1}{2} \rho C_D m H_v u_v^2 \quad (8)$$

$$m = nD \quad (9)$$

where  $\rho$  is the water density,  $g$  is the gravitational acceleration,  $h$  is the water depth,  $i$  is the water surface slope,  $C_b$  is the drag coefficient of the vegetation,  $u_v$  is the uniform velocity component,  $C_D$  is the bottom Chézy coefficient,  $H_v$  is the vegetation height,  $n$  is the number of stems per unit area,  $D$  is the stem diameter, and  $u_v$  is the uniform velocity component defined as:

$$u_v = \sqrt{\frac{hi}{C_b^{-2} + (2g)^{-1}C_D m H_v}} \quad (10)$$

The vegetated bed bottom shear stress is given by:

$$\tau_{bv} = f_s \tau_t \quad (11)$$

defined as a function of the total shear stress and the reduction factor  $f_s$ , that is obtained by replacing Eq. 10 in Eq. 7:

$$f_s = \frac{1}{1 + \frac{C_D H_v C_b^2}{2g}} \quad (12)$$

By combining Eq. 6 and Eq. 11, the vegetated bed bottom shear stress becomes:

$$\tau_{bv} = f_s \frac{\rho g}{C_{rs}^2} \bar{u}^2 \quad (13)$$

where the Chézy friction  $C_{rs}$  value is given by:

$$C_{rs} = \sqrt{\frac{1}{C_b^{-2} + (2g)^{-1}C_D m H_v}} + \frac{\sqrt{g}}{k} \ln\left(\frac{h}{H_v}\right) \quad (14)$$

in which  $k$  is the Von Karman constant ( $k=0.41$ ). At the transition from submerged to emergent vegetation the second term of the equation becomes zero.

Baptist's equation has been largely evaluated through field data and laboratory experiments and the predicted results have been compared by several studies with experimental data, finding a good fit (Arboleda et al., 2010; Crosato and Saleh, 2011).

The model simulates the hydrodynamic and sediment transport processes involved in the morphological evolution of a salt marsh, in the presence of subtidal breakwater. The numerical domain is a square (2 km  $\times$  2 km) whose computational

grid is composed of 147 x 143 cells, in the  $x$  and  $y$  direction respectively, which is refined gradually from the eastern side (40 m x 40 m) to the western (5 m x 5 m) (Figure 2.1).

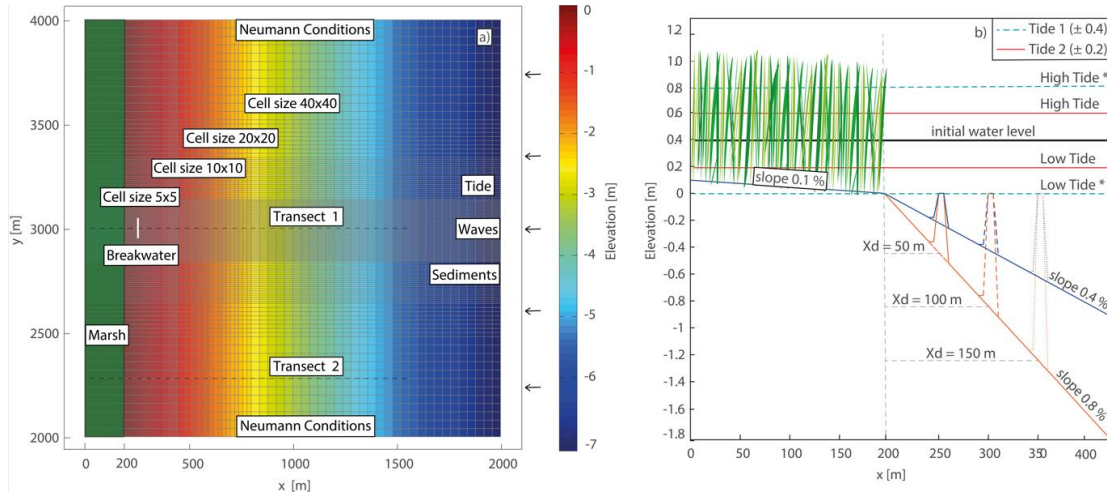


Figure 2.1. Domain configuration. Figure (a) planimetry of the model with cells dimension and boundary conditions on the North/South side (Neumann condition) and East side (waves, tide and sediment concentration). Transect 1 and 2 will be used later in the paper for making comparison on breakwater effect on sediment transport. Figure (b) longitudinal profile of the domain with the two different slopes used (blue line=0.4% and orange line=0.8%), with three different breakwater positions and two tide conditions (red continuous line= $\pm 0.2$ m and cyan dashed line= $\pm 0.4$ m).

The breakwater was imported into the model as an integral part of the bed level but with a non-eroding bottom, which made the structure waterproof (no flow through the breakwater). The height of the structure varied with  $x_d$  (Figure 2.1b), while length and width were fixed at 100m and 10m respectively. Breakwater dimensions were based on the computational domain cells' size (5 x 5 m locally). Twenty cells along the  $y$  direction (100 m) and two cells along the  $x$  direction (10 m) allowed breakwater hydrodynamic and morphodynamic in the simulations to be properly modelled. In the vertical direction, five-meter-deep layer of mixed cohesive and non-cohesive sediments (50 % of each) was originally accessible for erosion at the bottom of the domain. Neumann conditions were imposed on the North and South boundary, while on the East boundary different conditions were fixed: incoming waves, incoming sediment concentration and water level variation.

We wanted to simulate the most realistic and natural conditions possible found among coastal wetland environments in Chesapeake Bay. For this reason, we referred to and adopted values from Wiberg et al. (2019), who, in her experiment in Virginia Coastal Reserve (a similar environment as the Chesapeake Bay), measured waves between 0.03 and 0.52 m, and bathymetric slopes between 0.28 % and 1.05 %.

We set up our runs varying the basin slope (0.4 % and 0.8 %), the breakwater distance to the shoreline ( $x_d$ ) (50 m, 100 m, 150 m), wave's height (0.2 m, 0.3 m, 0.5 m, 0.7 m), tide ( $\pm 0.2$  m  $\pm 0.4$  m), sediment concentration (for both cohesive and non-cohesive sediments, 0.2 kg/m<sup>3</sup> 0.4 kg/m<sup>3</sup>) and the sand fraction diameter  $D_{50}$  (100  $\mu$ m 150  $\mu$ m). Non-cohesive sediments were characterized by a specific density of 2650 kg/m<sup>3</sup> and dry bed density of 1600 kg/m<sup>3</sup> while characteristics of the cohesive sediment were chosen in agreement with values provided by Berlamont et al., (1993). Specific density was 2,650 kg/m<sup>3</sup>, dry bed density was 500 kg/m<sup>3</sup> and setting velocity was 0.5 mm/s. Wave parameters ( $H_s$  and  $T_p$ ) were selected to simulate waves generated into the bay, so we analysed the previously mentioned  $H_s$  values with a period  $T_p$  of 5 s and a direction orthogonal to the shoreline. We imposed these values at the East boundary. Wave reflection was not accounted for in the wave model so that wave energy was dissipated at the coastline.

The bottom stress was modelled with Chézy's formulation. We used two different values of this parameter, one for the bed level of the domain ( $C_D=60$ ) and one for the breakwater roughness ( $C_D=20$ ). The initial condition of the models consisted of an initial water level fixed at 0.4 m. The suspended sediment eddy diffusivities were a function of the fluid eddy diffusivities and were calculated using horizontal large eddy simulation and grain settling velocity. The horizontal eddy diffusivity coefficient was defined as the combination of the subgrid-scale horizontal eddy viscosity, computed from a horizontal large eddy simulation, and the background horizontal viscosity, here set equal to 0.001 m<sup>2</sup>/s<sup>2</sup> (Edmonds and Slingerland, 2010; Nardin et al., 2016). To satisfy the numerical stability criteria of Courant Frederichs-Levy, we used a time step  $\Delta t = 3$  sec (Lesser et al., 2004). To decrease the simulation time a morphological scale factor of 50 was used in our models (a user device to multiply the deposition and erosion rate in each  $\Delta t$ ). A

sensitivity analysis showed that morphological factor of 50 was acceptable.

Combining the duration of the single simulation, 4 days, and the value of morphological factor, the model returned morphological changes for 200 days.

Combining all the variables for run combinations (Table 2.1), we obtained 192 different simulations to run from which the results were extracted. For notation, refer to Table 2.2.

Marsh characteristics were uniformly distributed along the shoreline, and aimed to replicate representative summer conditions for the Chesapeake Bay or similar estuarine environments (vegetation height = 1.0 m, stem diameter = 0.5 cm, and stem density = 400 shoots  $m^{-2}$ ) (Christiansen et al., 2000; Nardin et al., 2018; Sun et al., 2018; Zhu and Wiberg, 2022).

Table 2.1 Variables for run combinations

H <sub>s</sub> [m]				x <sub>d</sub> [m]			sl [%]	
0.2	0.3	0.5	0.7	50	100	150	0.4	0.8
D <sub>50</sub> [μm]				T [m]			C [Kg/m <sup>3</sup> ]	
100	150			± 0.2	± 0.4		0.2	0.4

Table 2.2 Coefficients from equations 1-5 and variables for run combinations

C	Mass concentration of sediment fraction kg/m <sup>3</sup>	θ	Wave direction
C <sub>x</sub>	Propagation velocity in the x-space m/s	S	Source/sink term for the action Balance equation
C <sub>y</sub>	Propagation velocity in the y-space m/s	S <sub>x</sub>	Total sediment transport in the x direction, m <sup>2</sup> /s
C <sub>σ</sub>	Propagation velocity in the σ-space m/s	S <sub>y</sub>	Total sediment transport in the y direction, m <sup>2</sup> /s
C <sub>θ</sub>	Propagation velocity in the θ-space m/s	sl	Basin slope, %
D	Diffusion coefficient	τ	Fluid shear stress tensor
D <sub>50</sub>	Median diameter, μm	t	Time, s
ε <sub>por</sub>	Bed porosity	T <sub>d</sub>	Deposition or erosion rate (m/s)
g	Gravity acceleration m/s <sup>2</sup>	T	Tidal conditions, m
H <sub>s</sub>	Wave height, m	V	Velocity field m/s
N	Density spectrum	x	Longitudinal direction, m

$p$	Fluid pressure, N/m <sup>2</sup>	$x_d$	Breakwater distance from the coast
$R$	Source/sink term for the advection-diffusion equation	$y$	Transversal direction, m
$\rho$	Fluid density kg/m <sup>3</sup>	$z$	Elevation m
$\sigma$	Frequency	$z_b$	Bed level, m

### 2.3 Results

Our focus was on Delft3D models for simulating hydrodynamics of flow and sediment transport coupled with SWAN wave analysis model. To understand how breakwaters impact salt marshes resilience, we first analyzed the wave damping and the hydrodynamic, followed by morphodynamics.

This modeling analysis revealed some key findings: breakwaters are efficient at breaking waves and reducing wave energy delivered the shoreline (Figure 2.2); the shear stress decreases with increasing breakwater distance to the shoreline and it also increases proportionally to wave heights (Figure 2.5). The slope also affects the shear stress. Slope was positively correlated with greater magnitude of shear stress, which directly impacted marsh scarp erosion since steeper sloped basin eroded to a greater extent (Figure 2.5). However, the higher basin slope allowed more sediment deposition into the marsh. Similarly, model scenarios with the closest distance of the breakwater from the shoreline and those with higher incoming waves also promoted deposition into the marsh (Figure 2.6). Last, we found that breakwater likely reduce sediment supply for tidal marshes, since deposition within the vegetation far from the breakwater was higher than behind the structure (into the marsh) (Figure 2.10).

Following, a detailed analysis of model results and coastal geomorphological implications is reported.

#### 2.3.1 Hydrodynamic results

Breakwater was found to efficiently dampen between 10% - 50% of the incoming wave heights under all configurations (Figure 2.2). The wave damping was

inversely proportional to  $x_d$  and proportional to  $H_s$  following a power law ( $R^2 = 0.51$ ), while the slope did not affect this specific process. Our results (Figure 2.2b) were markedly consistent with the wave damping results of Wiberg et al. (2019), who also observed a reduction between 10 % - 50 % of incoming waves in a similar coastal environment at Virginia Coastal Reserve (VCR).

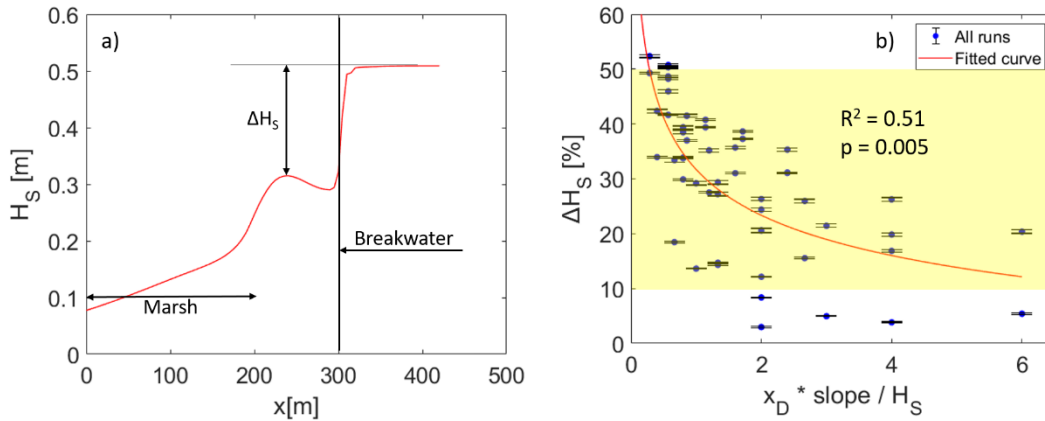


Figure 2.2. (a) Example of wave damping for the  $x_d=100$  m configuration. Type of line changes according to the wave height, the color is relative to slope and tide. Red continuous line represents ( $H_s=0.2$  sl=0.4 % T=0.4), blue continuous ( $H_s =0.2$  sl=0.8 % T=0.4), cyan dashed ( $H_s =0.5$  sl=0.8 % T=0.8) and so on. (b) Wave damping for all runs as function of the dimensionless variable  $x_d*\text{slope}/H_s$ . Bars represent the standard deviation. The yellow shaded area defines wave dampening measured in the VCR by Wiberg et al., 2019. Modeling wave attenuation is mostly within the measured range.

A clear increase in wave height ( $H_s$ ) immediately behind waves were dampened on breakwaters (Figure 2.2a) was created by the vorticity generated by the structure. A recirculation area made the  $u$  velocity component negative (toward the open sea) (Figure 2.3b), drawing water back toward the breakwater:

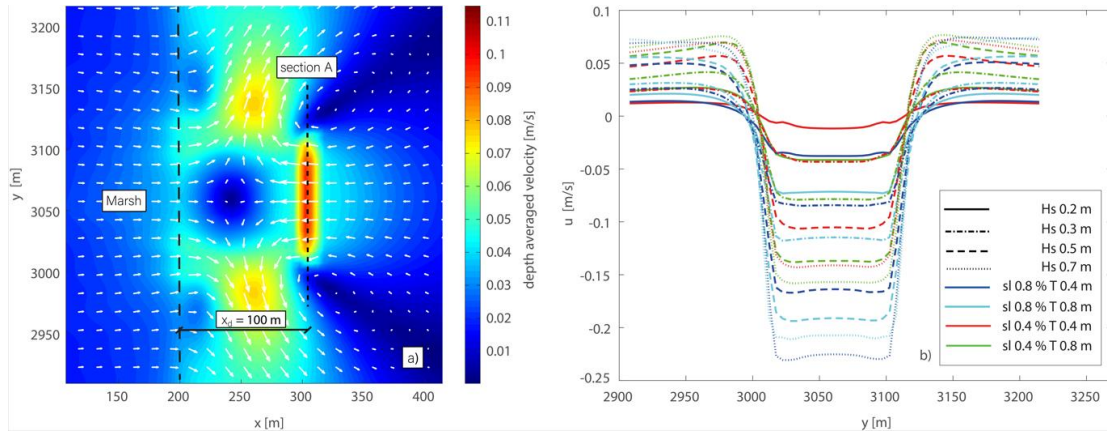


Figure 2.3. (a) Velocity field around the breakwater related to the configuration with  $x_d=100$  m,  $H_s=0.5$  m and  $\% = 0.008$  during the tidal flood. (b) U velocity component along section A related to all runs with  $x_d=100$  m (same reading key of Figure 2.2a)

The magnitude of the u velocity component was inversely proportional to  $H_s$  and slope and proportional to  $x_d$  following a power law (Figure 2.4;  $0.95 < R^2 < 0.98$ ), which described how increasing of waves and distance of the breakwater to the shoreline allowed these vortices to direct water behind the breakwater and raise the wave crests vertically (Figure 2.4).

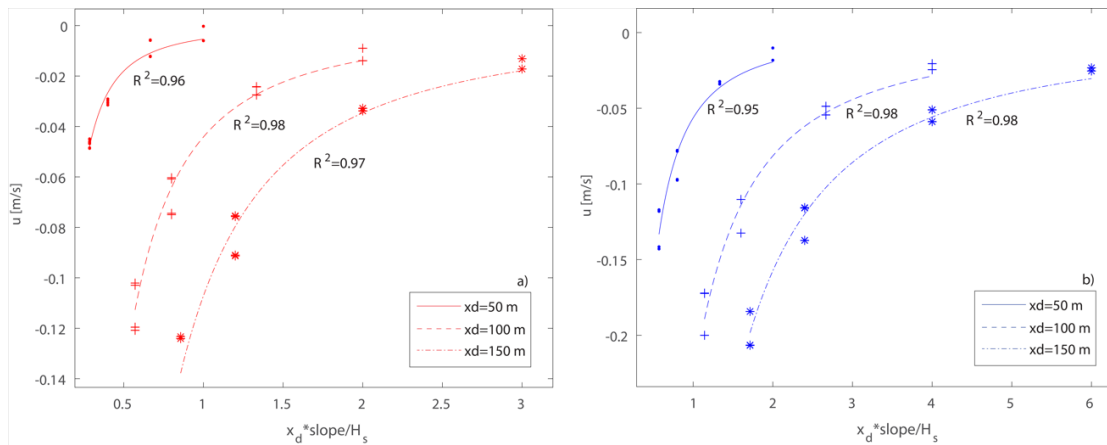


Figure 2.4. Mean u velocity during one tidal cycle measured at the centre of section A, as function of the dimensionless variable  $x_d * \text{slope} / H_s$  for all simulations with slope=0.4 % (a) and 0.8 % (b).

The shear stress peak due to the presence of the breakwater was clearly identified (Figure 2.5a), while the shear stress value into the marsh increased with

wave height, slope and tide (Figure 2.5b). The shear stress value at the marsh scarp ( $x=200$  m) for all runs, as function of  $x_d$ , tide and waves, revealed how the magnitude of the shear stress was proportional to  $H_s$  and inversely proportional to  $x_d$ , while the slope increasing effect augmented the erosion at the marsh edge (Figure 2.5c). The tide did not significantly impact the shear stress. Shear stress was correlated with the dimensionless variable for all distinct runs with slope 0.4% ( $R^2=0.70$ ) and 0.8% ( $R^2 = 0.67$ ). See appendix for correlations related to each single variable.

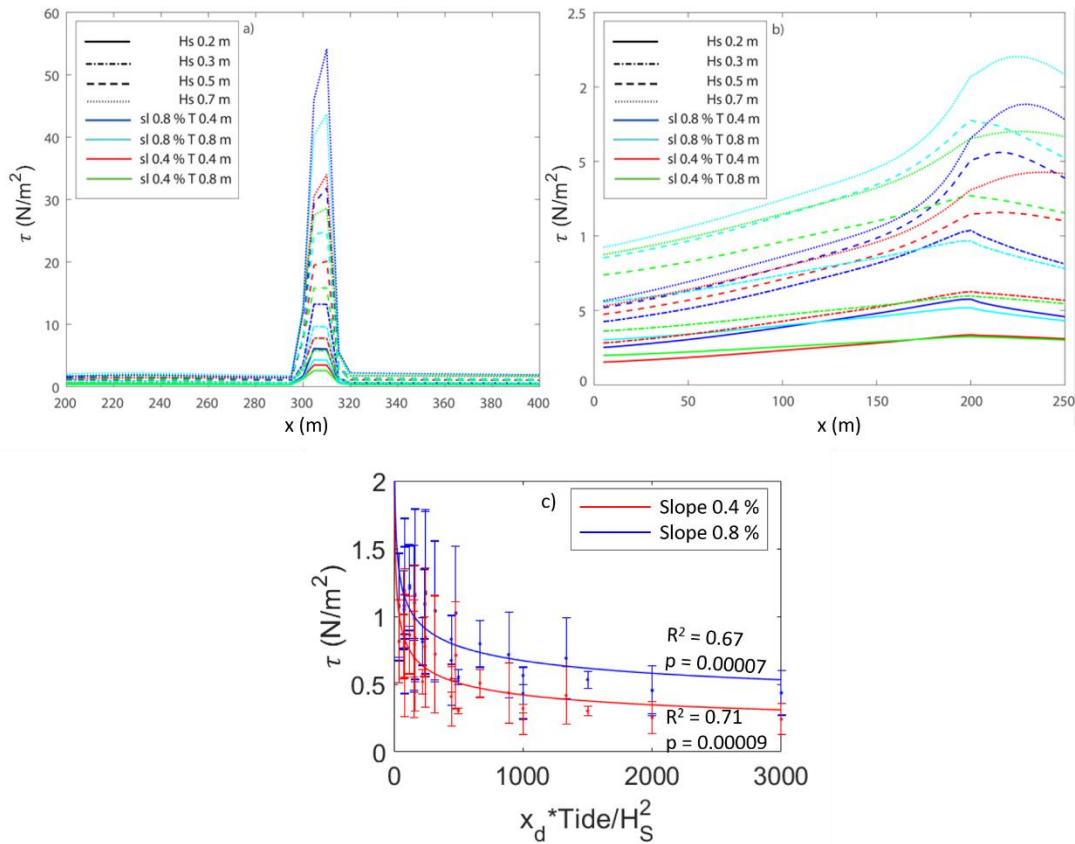


Figure 2.5 Shear stress as function of the  $x$  distance for the  $x_d=100$  m configuration. (a) Shear stress focus on the peak due to the presence of the breakwater (same reading key of Figure 2a). (b) Shear stress zoom on the marsh zone. (c) Shear stress value at the beginning of the marsh ( $x=200$  m) for the two different slopes as function of the dimensionless variable  $x_d * Tide / H_s^2$  (see appendix for correlations related to each single variable)

### 2.3.2 Morphodynamic results

Breakwaters impacted the shoreline damping waves and created a low energy zone behind the structure, allowing sedimentation. Our results demonstrated how sediment accumulation into the marsh at the end of the simulations was inversely proportional to the distance of the breakwater to the shoreline and proportional to  $H_s$ . The distance of the breakwater from the shoreline plays an important role on sediment transport. Sediment deposition into the marsh was negatively correlated with the breakwater distance to shoreline (Figure 2.6b). The volume deposited was proportional to  $H_s$  and inversely proportional to  $x_d$ , following a power law correlation ( $0.50 < R^2 < 0.52$ ), while the slope increasing increase the sediment accumulation into the marsh (Figure 2.6b). Figure 2.6a also shows how a greater distance of the breakwater from the shore leads to greater erosion of the marsh scarp, aspect that will be taken up later in Figure 2.8.

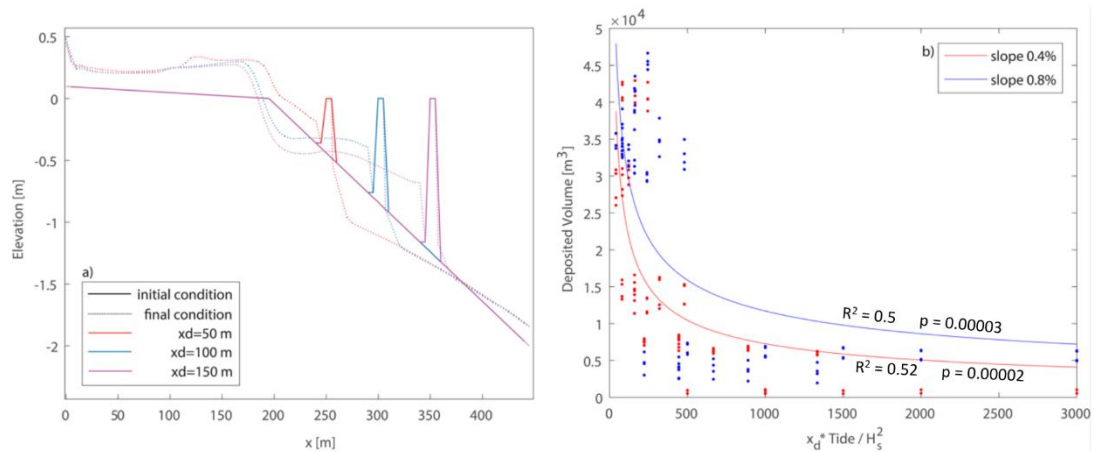


Figure 2.6. (a) Bed level profile after the end of the simulation compared to the initial condition, for the simulation with slope 0.8 %,  $H_s=0.5$  m, Tide= $\pm 0.2$  m,  $C_s=0.2$  kg/m<sup>3</sup> and  $D_{50}=100$   $\mu$ m. (b) Sediment deposition into the salt marsh behind the breakwater as function of breakwater distance from the shoreline, tide and wave height (see appendix for correlations related to each single variable).

We identified and quantified several important structural (e.g. breakwater position) and environmental characteristics (wave height bathymetric slope) on sediment deposition within marshes; we calculated the deposited volume as the

difference between the initial bed level and the bed level at the end of the simulation into the salt marsh behind the breakwater, and then multiplied by the area of the cells in order to obtain the total deposited volume. The estimation was therefore punctual made cell by cell. With regard the wave height abatement, on the other hand, an average wave damping was calculated during a tide cycle. However, the tide was found to play a dominant role in marsh erosion (Figure 2.7). This role was illustrated using the erosion ratio defined as the final  $x_d$  over the initial value of  $x_d$  as function of the tide for all the  $x_d$ , wave heights and for the two different values of concentration. We observed the tide to be strongly and positively correlated with the erosion at the marsh boundary. The erosion ratio for the 0.8 m tide condition, which reached the marsh platform at low tide, was greater than the 0.4 m tide condition as increasing both the breakwater distance to the coastline and the wave height was observed to increase shoreline erosion. Additionally, the lower suspended sediment concentrations lead to higher erosion. It is also possible to observe how wave height equal to 0.7 do not follow the same behaviour as the other wave heights, but only cause deposition in the marsh (Figure 2.7). This mismatch is due to the great energy that the model develops in the presence of such waves, in environments governed by a very low energy regime.

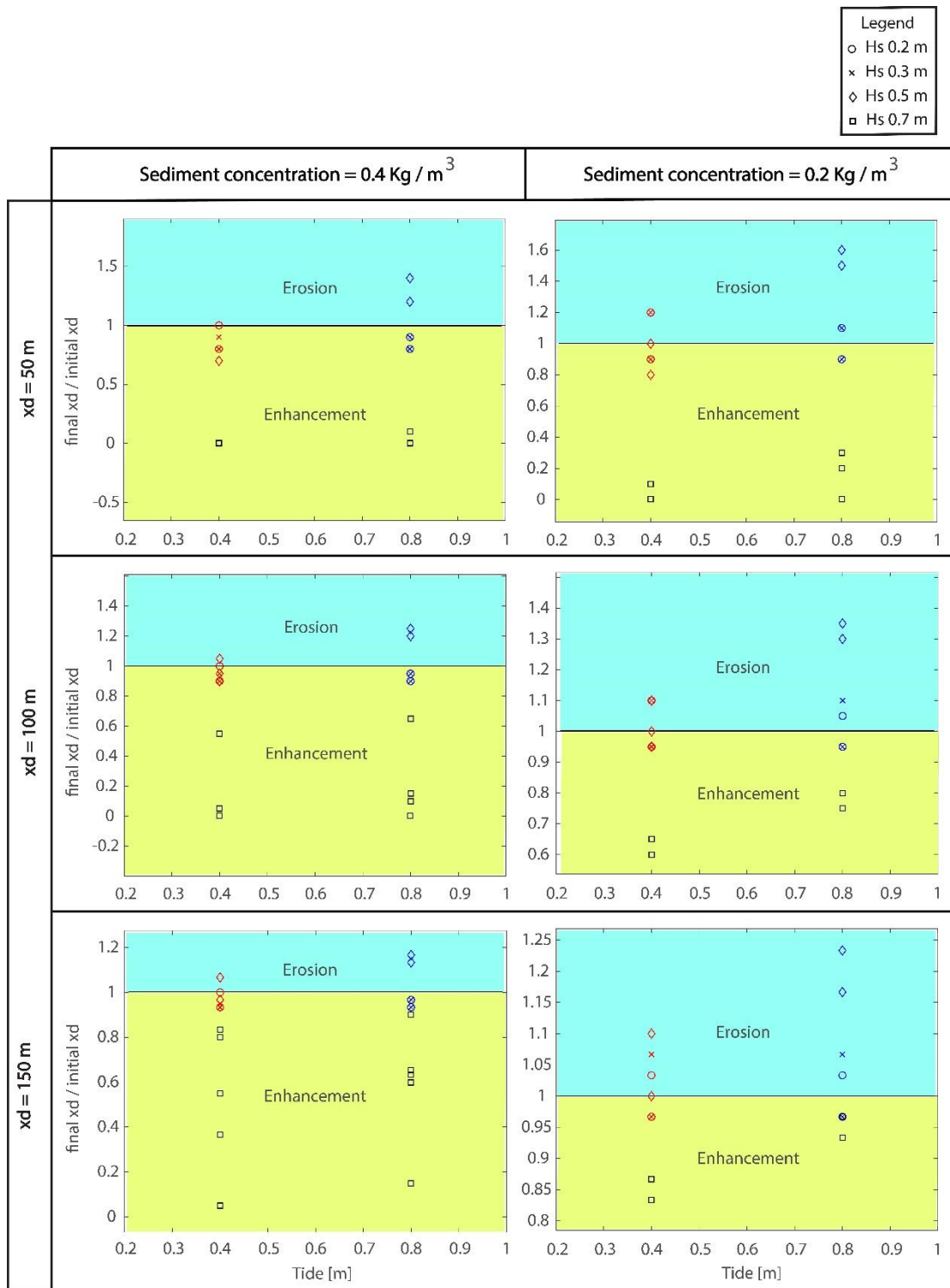


Figure 2.7 Ratio between the breakwater distance to the shoreline as function of the tide. The increasing of tide and breakwater distance to the coast increase the erosion at the marsh boundary, except for storm-related simulations (wave heights equal to 0.7 m), which mainly results in deposition into the marsh.

The eroded volume of the marsh scarp (the scarp of the marsh was defined as the computational space between the breakwater and the beginning of the marsh,  $x=200$  m) from model configurations found to cause erosion (see Figure 2.7), as function of the dimensionless variable  $x_d * \text{Tide} / H_s^2$ , for the two different slopes, is summarized in Figure 2.8. A linear correlation between the dimensionless variable and the eroded volume for both the basin slopes (Figure 2.8). Collectively, these relationships demonstrate how the erosion was proportional to the slope, tide, wave height and the breakwater distance to the shoreline (see appendix for correlations related to each single variable).

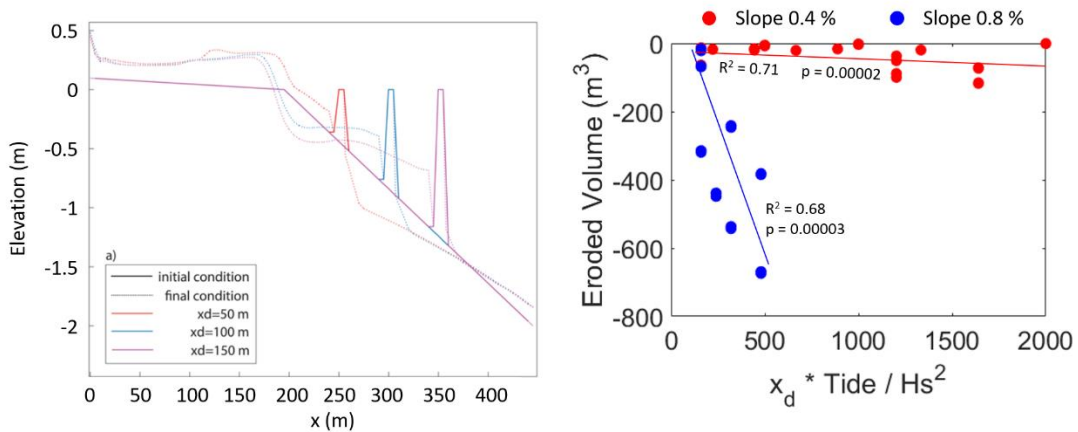


Figure 2.8. (a) Bed level profile after the end of the simulation compared to the initial condition, for the simulation with slope 0.8 %,  $H_s=0.5$  m,  $\text{Tide}=\pm 0.2$  m,  $C_s=0.2$   $kg/m^3$  and  $D_{50}=100$   $\mu m$ . (b) Eroded marsh volume for those configurations which cause erosion (see Figure 2.7) as function of the dimensionless variable  $x_d * \text{Tide} / H_s^2$  (see appendix for correlations related to each single variable).

We provided an example of cohesive sediment concentration distribution at the end of the simulation around the breakwater area, for the run with  $H_s=0.5$  m, slope=0.8%,  $\text{Tide}=\pm 0.4$  m and  $x_d=100$  m, for the two sediment concentrations a) 0.4  $kg/m^3$  and b) 0.2  $kg/m^3$  (Figure 2.9). The simulation demonstrated the higher sediment concentration (plot a) allows more sedimentation in the area protected by the breakwater and also into the marsh. Sandy sediments, on the other hand, were not

considerably distributed within the calculation domain, due to the low energy developed by the hydrodynamics of our model.

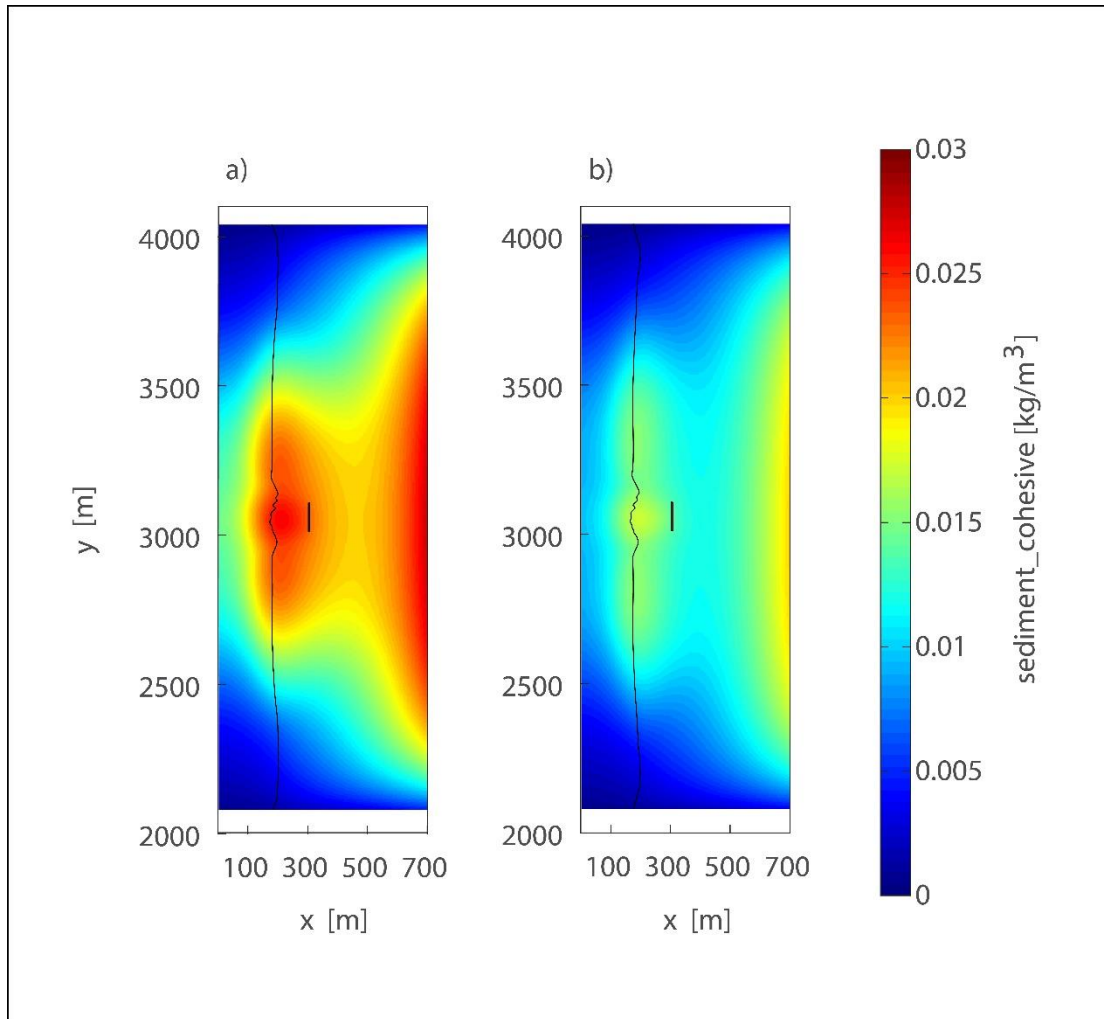


Figure 2.9. Sediment concentration plot for the run with  $H_s=0.5$  m, slope=0.8 %, Tide= $\pm 0.4$  m and  $x_d=100$  m. a) Sediment concentration =  $0.4 \text{ kg/m}^3$  and b) Sediment concentration =  $0.2 \text{ kg/m}^3$

An important aspect related to the sediment deposition into the saltmarsh appeared after comparing the volume accumulated behind the breakwater (into the marsh, from  $x=0$  to  $x=200$  m) and far away from it (into the marsh), revealing how

breakwaters block sediment transport and prevent nourishment of the marsh (Figure 2.10).

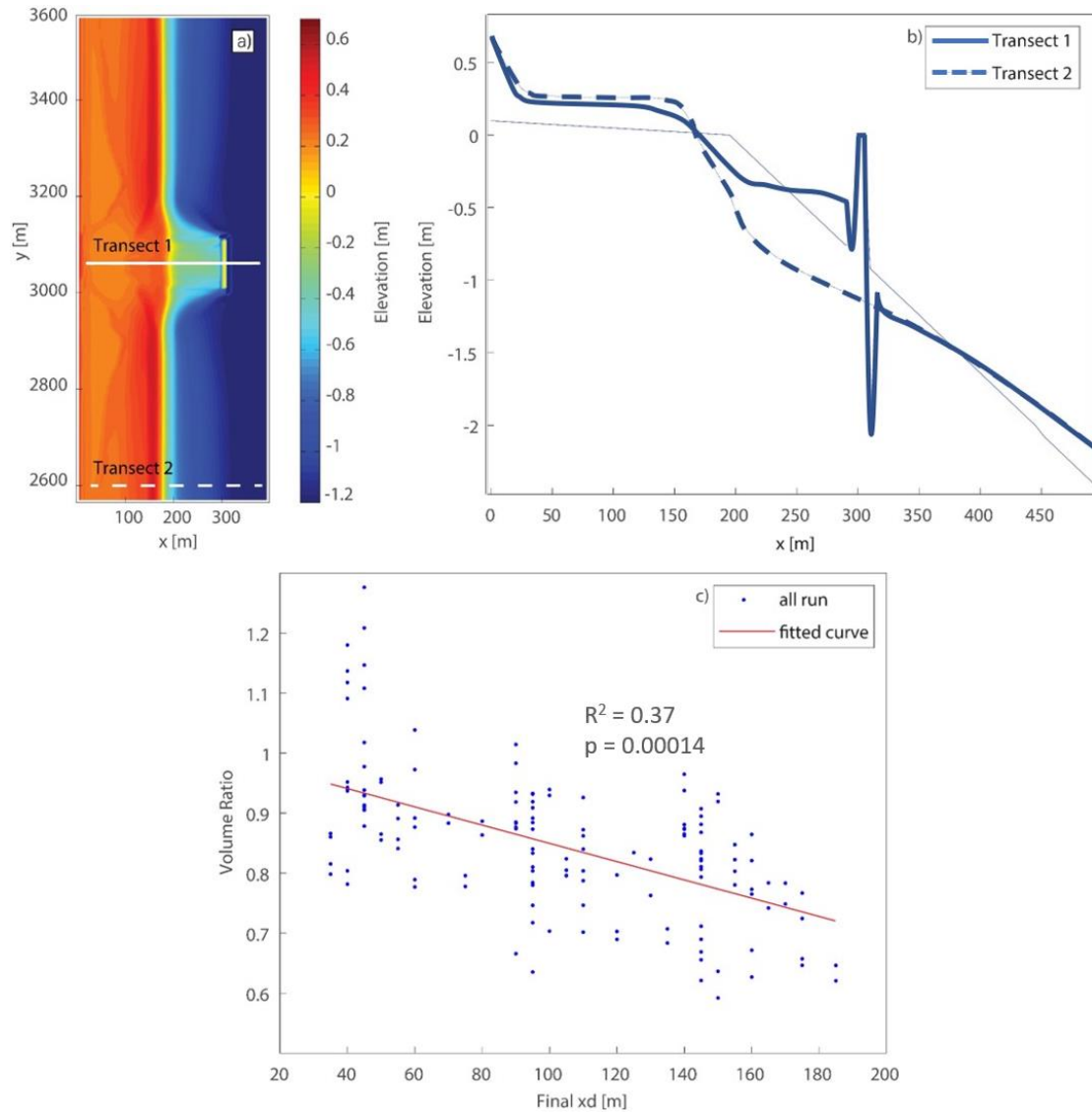


Figure 2.10. (a) 2D bed level at the end of the simulation with slope=0.8 % case,  $H_s=0.5$  m,  $x_d=100$  m and Tide= $\pm 0.4$  m. (b) Longitudinal profile of transect 1 and 2 for the same simulation. The continuous line represents the initial condition, the dash line the transect 1 final bed level condition and the point line transect 2 final bed level condition. (c) Ratio between the deposited volume on transect 1 and 2 for all runs.

We compared two 100x200 m check volumes centred on transect 1 and 2 into the saltmarsh (Figure 2.10a and 2.10b). In particular, we highlighted the ratio between the sediment accumulation behind and far away from the breakwater, into the marsh,

as function of the final breakwater distance to the shoreline (Figure 2.10c). Volume ratio was defined as the ratio between the deposited volume on transect 1 over the deposited volume on transect 2, into the salt marsh. For most of runs the volume ratio was lower than 1 (Figure 2.10c), meaning that sediments were blocked by the breakwater, while without breakwater more sediments were allowed to reach the marsh.

A typical morphodynamic response due to the presence of breakwater is the scouring effect happening at the tip of the structure, as is shown on our results on Figure 2.10b. This behaviour happens naturally with submerged structures and has commonly been observed in previous studies such as Sumer et al. (2000).

Runs with wave heights 0.7 m do not follow the trend of the others because of the great amount of energy that this configuration generated into the model and were excluded from the chart (but see discussion for more commentary on this scenario).

A long-term analysis of coastal dynamics has been also simulated to look at the effect that breakwaters can have on long-shore sediment transport (Figure 2.11). Our results show how through the time, breakwaters tend to create morphodynamic structures known as salient and tombolo, as is shown in many papers in the literature such as Hanson et al. (1991). These morphodynamic structures tend to be less accentuate with increasing of breakwater distance to the shoreline (Figure 2.11).

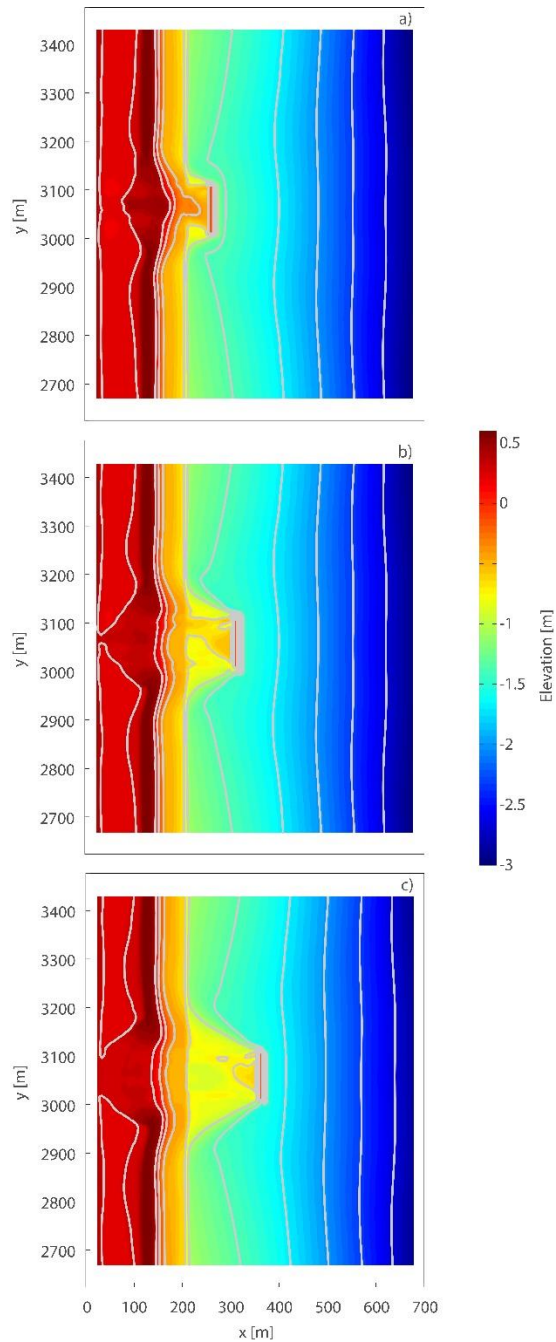


Figure 2.11. Long term simulation for (a)  $x_d=50$  m, (b)  $x_d=100$  m and (c)  $x_d=150$  m. The Figure shows how these morphodynamic structures tend to be less accentuate with increasing of breakwater distance to the shoreline.

A further analysis was carried out to investigate the wave transmission phenomenon over the breakwater under different structure characteristics (height and crest width) (see Appendix 1).

## 2.4 Discussion

Our numerical experiment that couples Delft3D-SWAN models generates plausible results about sediment transport around breakwaters and the influence of waves and tides in shallow coastal bays.

Simulation results demonstrate how breakwaters were responsible for an average wave dampening of 10 % - 50 % (Figure 2.2), similar to empirical studies by Wiberg et al., (2019), who measured the same range of wave dampening under similar coastal environment conditions at VCR. Other studies have shown wave attenuation provided by submerged artificial and/or natural reef-breakwaters, underlining the importance of incoming wave direction, orientation of the structure itself, and tidal inundation duration regarding the breaking process (Chauvin, 2018; Wiberg et al., 2019; Morris et al., 2021; Hogan and Reidenbach, 2022). Our runs kept the same incoming waves direction perpendicular to the breakwater, and the same structure position parallel to the shoreline. The inference of our study is limited to our specific study conditions; nevertheless, they provide insight on the fundamental physical forces and principals underlying sediment load transport and fate.

The distance of the breakwater to the shoreline also affected the hydrodynamics, reducing the shear stress value as the distance increased. Sediment deposition into the salt marsh was primarily driven by wave height and the distance of the breakwater to the shoreline. Greater wave heights were associated with greater sediment suspension and transport, while increasing breakwater distance to shore decreased the amount of deposition due to the lower transport energy of waves that were broken further offshore. This is in agreement to the study of Birben et al. (2005), which investigated the effect of breakwaters parameters on sediment accumulation. They found that the deposition in the area protected by the breakwater was inversely proportional to the breakwater distance to the shoreline and that the deposition and transport of sediments decreases with decreasing wave height (Vona et al., 2021). Our modeling approach and results can be used to help guide future breakwater design to promote salt marshes stability and longevity. Future breakwaters deployment should consider placing these structures in locations that allow marsh nourishment (closer to

the coastline), avoiding sediments accumulation offshore and reducing coastal erosion.

The erosion at the marsh boundary was mostly governed by the tide. When the water level reached the marsh platform, waves had more erosion power as they dissipated their energy directly on the marsh edge, while a higher water levels allowed the dissipation to happen through the marsh platform with less impacts on marsh boundary erosion. These results are also similar to Tonelli et al (2010) who observed the water level to play an essential role on the marsh boundary erosion. Such erosional behaviour was confirmed in our results (Figure 2.7), where the  $\pm 0.4$  m tidal condition, which reached the marsh platform at low tide, eroded more than the  $\pm 0.2$  m condition and was always higher than the platform level. Moreover, Figure 2.8 illustrates the effect of tide and slope on the erosion, demonstrating how increasing tide and basin slope increased the erosion of the marsh scarp.

Results regarding the influence of the tide on the functioning of breakwaters highlights how higher water levels inhibit the protective performance of breakwaters, suggesting they could be drowned by Sea Level Rise (SLR) and quickly become ineffective. Future modeling efforts may want to consider examining this scenario to better understand legacy infrastructure performance in the face of climate change.

The presence of the breakwater is also likely to trap sediments and create less deposition in the area protected by it compared to an area without obstacles (Figure 2.10). This fact shows an important aspect about breakwaters and their behaviour. They are efficient at breaking waves and reducing their energy, but on the other hand they can be an obstacle for sediments and consequently for saltmarshes survival. Moreover, the breakwater distance to the shoreline was significantly, inversely related to the amount of sediment transported and deposited into the marsh; therefore, the best structure configuration, with respect to marsh nourishment, would be the one with the closest distance to the shoreline (Figure 2.10). However, tradeoffs with other marine ecosystems such as SAV and/or fish have to be considered when implementing these kinds of infrastructures. The ecological damage that usually results from gray structures implementation can lead to habitat alteration and losses in the nearshore, threatening the sustainability of many ecosystem services (Chambers,

1991; Douglass and Pickel, 1999; Minton, 1999; Jackson et al., 2001; Kennish, 2002; NRC, 2007).

Our model shows how greater waves cause more erosion; however, this trend is not followed by the 0.7 m wave height, as it mainly causes deposition enriching in the marsh (Figure 2.7). The higher the wave, the greater the amount of deposition into the saltmarsh, while a flatter basin slope will lead to less deposition. Treating wave heights equal to 0.7 m as a storm-level (Wiberg et al., 2019), our results agree with Castagno et al. (2018) who demonstrated using Delft3D that extreme events are likely to enrich coastal wetlands with more sediments.

As our model points out, the water level and therefore the increase in sea level are crucial to consider for the long-term functioning of breakwaters, since they are likely to become less efficient with accelerating SLR. A recently advanced engineering concept to cope with the growing threat SLR is the use of hybrid infrastructures, which combines built and natural solution for coastal defence and is thought to exploit the benefits that accompany each approach. Hybrid infrastructure that can adapt to changing environmental conditions, such as coral or oyster reefs working in conjunction with grey structure to dampen incoming waves, is attractive alternative that can sustainably stabilize shoreline while also contributing immense ecological value (Sutton-Grier et al., 2015; Fleming et al., 2017). The advantage of integrating breakwaters and other in-water infrastructure with oysters is that the reefs these organisms form may grow with SLR (Rodriguez et al., 2014; Ridge et al., 2017), providing greater guarantees that these structures could provide protection to coastal environments long after the grey structure has been drowned.

However, accelerated SLR will likely affect many coastal regions susceptible to flooding, storm surge, erosion, and many others (Scyphers et al., 2011). SLR causes coastal wetlands to migrate landward, and further accelerations in SLR might threaten tidal marshes if they will not keep up with the increased rate of SLR. Estimations of vertical marshes accretion indicate these environments might get drowned if SLR accelerates (Scyphers et al., 2011). Study results suggested breakwaters may inhibit sediment supply for tidal marshes, and a combined increase in the rate of SLR can seriously threaten coastal wetlands. The transformation of

backbarrier marshes to open water due to SLR will likely enlarge tidal prisms (leading to erosion of shorelines bordering the tidal inlets) and increase the size of ebbtidal deltas (enhancing shoreline erosion away from inlets). Further hydro and morphodynamic studies are needed for different SLR scenarios to better understand the sustainability of high and low marshes. Understanding and forecasting the thresholds of coastal wetland stability in the face of climate changes and SLR are among the most important issues to be addressed and should be the focus of coastal research for decades to come (Scyphers et al., 2011).

In the view of a possible reuse of all the deposited material behind the breakwater for coastal zone management and protection, A. De Vincenzo et al. (2018) offers an important analysis on how material accumulated in reservoirs might be reused in nourishment works. They reported a study case of the Guardialfiera reservoir in Italy, but this application suggests how such approach can be tested, for instance, also in the restoration of coastal wetlands along the eastern shore of the United States.

## 2.5 Conclusions

Understanding sediment transport dynamic is a key aspect for the protection and the survival of saltmarshes. In this study we investigated breakwater effects on sediment supply and morphological changes for a vegetated shoreline. The presence of the breakwater certainly reduces the incoming waves by dissipating the energy and protecting the coast as clearly shown in Figure 2.11. However, the breakwater distance to the coast affects sediment transport and may inhibit marsh nourishment if not properly considered during planning and deployment activities. Greater distances are associated with less sediment deposition and more erosion of the marsh scarp. The slope, tide and wave heights play different roles in the sediment supply for the vegetation: (a) slope was positively correlated with greater amounts of deposition into the saltmarsh; (b) tide or water level at similar elevations to the marsh platform was

more likely to erode; (c) higher waves were observed to bring more sediments towards the marsh, but they also have more erosion power.

Our study, which highlights to conflicting effects of breakwater (coastal protection vs marsh malnourishment), is relevant and applicable for field studies and future coastal management in areas such as Chesapeake Bay. Study results also suggest that more research is needed to help find a balance between wave dampening and sediment supply during the design and implementation of breakwater infrastructures.

Based on study results, breakwaters in the Lake Cove are expected to promote sediment deposition and protect the marsh from wave energy, but also to reduce sediment nourishment toward the shore. Field studies presented in the next chapter further explore hydro and morphodynamic impact of intertidal breakwaters, under a wide variety of environmental conditions (wind, waves, tide).

## 2.6 References

- Airoldi, L. An ecological perspective on the deployment and design of low-crested and other hard coastal defence structures. *Coastal Engineering*, 2005, 52, pp. 1073-1087.
- Allen, J. R.; Pye, K. Saltmarshes: morphodynamics, conservation and engineering significance. Cambridge University Press. 1992.
- Arboleda AM, Crosato A, Middelkoop H. 2010. Reconstructing the early 19th-century Waal River by means of a 2D physics-based numerical model. *Hydrological Processes* 24: 3661–3675 <https://doi.org/10.1002/hyp.7804>.
- Baptist, M. J. (2005). Modelling floodplain biogeomorphology.
- Baptist MJ, Babovic V, Rodríguez Uthurburu J, Keijzer M, Uittenbogaard RE, Mynett A, Verwey A. 2007. On inducing equations for vegetation resistance. *Journal of Hydraulic Research* 45(4): 435–450.
- Barth, N., 2011. *Impact of breakwaters on sediment characteristics and submerged aquatic vegetation*. University of Maryland, College Park.
- Battjes, J.A.; Janssen, J.P.F.M. Energy loss and set-up due to breaking of random waves. *Coastal Engineering*, 1978, pp. 569-587.
- Berlamont, J.; Ockenden, M.; Toorman, E.; Winterwerp, J. The characterisation of cohesive sediment properties. *Coastal Engineering*, 1993, 21, pp. 105-128.
- Birben, A.R.; Özölçer, İ.H.; Karasu, S.; Kömürcü, M.İ. Investigation of the effects of offshore breakwater parameters on sediment accumulation. *Ocean Engineering*, 2007, 34, pp.284-302.
- Board, O.C.; National Research Council. Mitigating shore erosion along sheltered coasts; National Academic Press: 500 Fifth Street, N.W. Washington, DC 20001, USA, 2007.
- Boorman, L.A.; Garbutt, A.; Barratt, D. The role of vegetation in determining patterns of the accretion of salt marsh sediment. Geological Society, London, Special Publications, 1998, 139, pp. 389-399.
- Boorman, L.A. Salt marshes—present functioning and future change. *Mangroves and Salt Marshes*, 1999, 3, pp. 227-241.
- Borsje, B.W.; van Wesenbeeck, B. K.; Dekker, F.; Paalvast, P.; Bouma, T. J.; van Katwijk, M. M.; de Vries, M. B. How ecological engineering can serve in coastal protection. *Ecological Engineering*, 2011, 37, pp. 113-122.

- Bricker-Urso, S.; Nixon, S. W.; Cochran, J. K.; Hirschberg, D. J.; Hunt, C. Accretion rates and sediment accumulation in Rhode Island salt marshes. *Estuaries*, 1989, 12, pp. 300-317.
- Broome, S. W.; Rogers Jr, S. M.; Seneca, E. D. Shoreline erosion control using marsh vegetation and low-cost structures. 2015.
- Burger, J.; Howe, M.A.; Hahn, D.C.; Chase, J. Effects of tide cycles on habitat selection and habitat partitioning by migrating shorebirds. *The Auk*, 1977, 94, pp. 743-758.
- Cadwalladr, D.A.; Owen, M.; Morley, J.V.; Cook, R.S. Wigeon (*Anas penelope* L.) conservation and salting pasture management at Bridgwater Bay National Nature Reserve, Somerset. *Journal of Applied Ecology*, 1972, pp. 417-425.
- Castagno, K.A.; Jiménez-Robles, A.M.; Donnelly, J.P.; Wiberg, P.L.; Fenster, M.S.; Fagherazzi, S. Intense storms increase the stability of tidal bays. *Geophysical Research Letters*, 2018, 45, pp. 5491-5500.
- Chambers JR (1991) Coastal Degradation and Fish Population Losses. In: Stroud R, editor. *Stemming the Tide of Coastal Fish Habitat Loss: National Coalition for Marine Conservation*. pp. 45–51.
- Chowdhury, M.S.N.; Walles, B.; Sharifuzzaman, S.M.; Hossain, M.S.; Ysebaert, T.; Smaal, A.C. Oyster breakwater reefs promote adjacent mudflat stability and salt marsh growth in a monsoon dominated subtropical coast. *Scientific reports*, 2019, 9, p. 8549.
- Christiansen, T., Wiberg, P. L., & Milligan, T. G. (2000). Flow and sediment transport on a tidal salt marsh surface. *Estuarine, Coastal and Shelf Science*, **50**(3), 315– 331. <https://doi.org/10.1006/ECSS.2000.0548>
- Cooper, A.H.; Mulligan, R.P. Application of a spectral wave model to assess breakwater configurations at a small craft harbour on Lake Ontario. *Journal of Marine Science and Engineering*, 2016, 4, p. 46.
- Couvillion, B.R., Beck, H., Schoolmaster, D., Fischer, M., 2017. Land area change in coastal Louisiana (1932 to 2016) scientific investigations map 3381. U.S. Geological Survey Scientific Investigations Map 3381, p. 16 <https://doi.org/10.3133/SIM3381>.
- Crosato A, Saleh MS. 2011. Numerical study on the effects of floodplain vegetation on river planform style. *Earth Surface Processes and Landforms* 36: 711–720 <https://doi.org/10.1002/esp.2088>.
- Daiber, F.C. Salt marsh animals: Distributions related to tidal flooding, salinity and vegetation. *Ecosystems of the world*, 1977.

- De Vincenzo, A.; Covelli, C.; Molino, A.J.; Pannone, M.; Ciccaglione, M.; Molino, B. Long-Term Management Policies of Reservoirs: Possible Re-Use of Dredged Sediments for Coastal Nourishment. *Water*, 2019, 11(1), p.15.
- Douglass, S.L.; Pickel, B.H. The tide doesn't go out anymore - the effect of bulkheads on urban shorelines. *Shore and Beach*, 1999, 67, pp. 19-25.
- Edmonds, D.A.; Slingerland, R.L. Significant effect of sediment cohesion on delta morphology. *Nature Geoscience*, 2010, 3(2), pp.105-109.
- Faraci, C.; Scandura, P.; Foti, E. Bottom profile evolution of a perched nourished beach. *Journal of waterway, port, coastal, and ocean engineering*, 2014, 140(5), p. 04014021.
- Faraci, C. Experimental investigation of the hydro-morphodynamic performances of a geocontainer submerged reef. *Journal of Waterway, Port, Coastal, and Ocean Engineering*, 2018, 144(2), p.04017045.
- Fleming, C.S.; Dillard, M.K.; Regan, S.D.; Gorstein, M.; Messick, E.; Blair, A. A coastal community vulnerability assessment for the Choptank Habitat Focus Area. *NOAA Technical Memorandum NOS NCCOS 225*, 2017, pp. 92.
- Friess, D.A., Yando, E.S., Alemu, J.B., Wong, L.W., Soto, S.D. and Bhatia, N., 2020. Ecosystem services and disservices of mangrove forests and salt marshes. *Oceanography and marine biology*.
- Hanson, H.; Kraus, N.C. Shoreline response to a single transmissive detached breakwater. *Coastal Engineering*, 1991, pp. 2034-2046.
- Hashim, A.M.; Catherine, S.M.P. Effectiveness of mangrove forests in surface wave attenuation: a review. *Research journal of applied sciences, engineering and technology*, 2013, 5, pp. 4483-4488.
- Hasselmann, K.; Barnett, T.P.; Bouws, E.; Carlson, H.; Cartwright, D.E.; Enke, K.; Ewing, J.A.; Gienapp, H.; Hasselmann, D.E.; Kruseman, P.; Meerburg, A. Measurements of wind-wave growth and swell decay during the Joint North Sea Wave Project (JONSWAP). *Ergänzungsheft*, 1973, pp. 8-12.
- Himes-Cornell, A., Pendleton, L. and Atiyah, P., 2018. Valuing ecosystem services from blue forests: A systematic review of the valuation of salt marshes, sea grass beds and mangrove forests. *Ecosystem services*, 30, pp.36-48.
- Jackson JBC, Kirby MX, Berger WH, Bjorndal KA, Botsford LW, et al. (2001) Historical overfishing and the recent collapse of coastal ecosystems. *Science* 293: 629–638.
- Kay, R; Alder, J. Coastal Planning and Management, 2nd ed.; Taylor & Francis: 270 Madison Ave, New York, NY 10016, USA, 2005.

- Kelleway, J.J., Cavanaugh, K., Rogers, K., Feller, I.C., Ens, E., Doughty, C. and Saintilan, N., 2017. Review of the ecosystem service implications of mangrove encroachment into salt marshes. *Global Change Biology*, 23(10), pp.3967-3983.
- Kennish, M.J. Environmental threats and environmental future of estuaries. *Environmental Conservation*, 2002, 29, pp. 78–107.
- Klonaris, G.T., Metallinos, A.S., Memos, C.D. and Galani, K.A., 2020. Experimental and numerical investigation of bed morphology in the lee of porous submerged breakwaters. *Coastal Engineering*, 155, p.103591.
- Leonardi, N.; Sun, T.; Fagherazzi, S. Modeling tidal bedding in distributary-mouth bars. *Journal of Sedimentary Research*, 2014, 84, pp. 499-512.
- Lera, S.; Nardin, W.; Sanford, L.; Palinkas, C.; Guercio, R. The impact of submersed aquatic vegetation on the development of river mouth bars. *Earth Surface Processes and Landforms*, 2019, 44, pp. 1494-1506.
- Lesser, G.R.; Roelvink, J.V.; Van Kester, J.A.T.M.; Stelling, G.S. Development and validation of a three-dimensional morphological model. *Coastal engineering*, 2004, 51, pp. 883-915.
- Lévêque, E.; Toschi, F.; Shao, L.; Bertoglio, J.P. Shear-improved Smagorinsky model for large-eddy simulation of wall-bounded turbulent flows. *Journal of Fluid Mechanics*, 2007, 570, pp.491-502.
- Minton MD (1999) Coastal Wetland Restoration and Its Potential Impact on Fishery Resources in the Northeastern United States. American Fisheries Society Symposium 22: 405–420.
- Moschella, P.S.; Abbiati, M.; Åberg, P.; Airoidi, L.; Anderson, J. M.; Bacchiocchi, F.; Granhag, L. Low-crested coastal defence structures as artificial habitats for marine life: using ecological criteria in design. *Coastal Engineering*, 2005, 52, pp. 1053-1071.
- Nardin, W.; Fagherazzi, S. The effect of wind waves on the development of river mouth bars. *Geophysical Research Letters*, 2012, 39.
- Nardin, W.; Mariotti, G.; Edmonds, D.A.; Guercio, R.; Fagherazzi, S. Growth of river mouth bars in sheltered bays in the presence of frontal waves. *Journal of Geophysical Research: Earth Surface*, 2013, 118, pp. 872-886.
- Nardin, W.; Edmonds, D.A.; Fagherazzi, S. Influence of vegetation on spatial patterns of sediment deposition in deltaic islands during flood. *Advances in Water Resources*, 2016, 93, pp. 236-248.
- Nardin, W., Larsen, L., Fagherazzi, S., & Wiberg, P. (2018). Tradeoffs among hydrodynamics, sediment fluxes and vegetation community in the Virginia Coast

Reserve, USA. *Estuarine, Coastal and Shelf Science*, **210**, 98– 108. <https://doi.org/10.1016/j.ecss.2018.06.009>

NRC (2007) Mitigating shore erosion along sheltered coasts. In: Council NR, editor. Washington, D.C.: National Academies Press. 174 p.

Palinkas, C.M., Koch, E.W. and Barth, N., 2010, March. Sedimentation adjacent to naturally eroding and breakwater-protected shorelines in Chesapeake Bay. In *IOP Conference Series: Earth and Environmental Science* (Vol. 9, No. 1, p. 012012). IOP Publishing.

Palinkas, C.M.; Barth, N.; Koch, E.W.; Shafer, D.J. The influence of breakwaters on nearshore sedimentation patterns in Chesapeake Bay, USA. *Journal of Coastal Research*, 2016, 32, pp. 788-799.

Palinkas, C.M., Sanford, L.P. and Koch, E.W., 2018. Influence of shoreline stabilization structures on the nearshore sedimentary environment in mesohaline Chesapeake Bay. *Estuaries and Coasts*, **41**, pp.952-965.

Partheniades, E. Erosion and deposition of cohesive soils. *Journal of the Hydraulics Division*, 1965, 91, pp.105-139.

Pilkey, O.H.; Wright, W. Seawalls versus Beaches. *Journal of Coastal Research*, 1988, special issue n° 4, pp. 41-64.

Post, J.C.; Lundin, C.G. Guidelines for integrated coastal zone management; The World Bank: Headquarters, 1818 H Street, NW Washington, DC 20433, USA, 1996.

Ridge, J.T.; Rodriguez, A.B.; Fodrie, F.J. Evidence of exceptional oyster-reef resilience to fluctuations in sea level. *Ecology and evolution*, 2017, 7, pp. 10409-10420.

Rodi, W.; Scheuerer, G. Scrutinizing the k-epsilon-model under adverse pressure gradient conditions. *4th Symposium on Turbulent Shear Flows*, 1984, pp. 2-8.

Rodriguez, A.B.; Fodrie, F.J.; Ridge, J.T.; Lindquist, N.L.; Theuerkauf, E.J.; Coleman, S.E.; Grabowski, J.H.; Brodeur, M.C.; Gittman, R.K.; Keller, D.A.; Kenworthy, M.D. Oyster reefs can outpace sea-level rise. *Nature climate change*, 2014, 4, pp. 493-497.

Roelvink, J.A.; Van Banning, G.K.F.M. Design and development of DELFT3D and application to coastal morphodynamics. *Oceanographic Literature Review*, 1995, 11, p.925.

Safari, M.D., 2018. A short review of submerged breakwaters. In *MATEC Web of Conferences* (Vol. 203, p. 01005). EDP Sciences.

- Schieder, N.W., Walters, D.C. and Kirwan, M.L., 2018. Massive upland to wetland conversion compensated for historical marsh loss in Chesapeake Bay, USA. *Estuaries and coasts*, 41, pp.940-951.
- Schuerch, M.; Spencer, T.; Temmerman, S.; Kirwan, M.L.; Wolff, C.; Lincke, D.; McOwen, C.J.; Pickering, M.D.; Reef, R.; Vafeidis, A.T.; Hinkel, J. Future response of global coastal wetlands to sea-level rise. *Nature*, 2018, 561, pp. 231-234.
- Scyphers, S.B.; Powers, S.P.; Heck, K.L. Ecological value of submerged breakwaters for habitat enhancement on a residential scale. *Environmental management*, 2015, 55, pp. 383-391.
- Sharifahmadian, A., 2015. *Numerical models for submerged breakwaters: coastal hydrodynamics and morphodynamics*. Butterworth-Heinemann.
- Sumer, B.M.; Fredsøe, J. Experimental study of 2D scour and its protection at a rubble-mound breakwater. *Coastal Engineering*, 2000, 40(1), pp.59-87.
- Sumer, B.M.; Fredsøe, J.; Lamberti, A.; Zanuttigh, B.; Dixen, M.; Gislason, K.; Di Penta, A.F. Local scour at roundhead and along the trunk of low crested structures. *Coastal Engineering*, 2005, 52(10-11), pp.995-1025.
- Sun, C., Fagherazzi, S., & Liu, Y. (2018). Classification mapping of salt marsh vegetation by flexible monthly NDVI time-series using Landsat imagery. *Estuarine, Coastal and Shelf Science*, 213, 61– 80. <https://doi.org/10.1016/j.ecss.2018.08.007>
- Sutton-Grier, A.E.; Wowk, K.; Bamford, H. Future of our coasts: The potential for natural and hybrid infrastructure to enhance the resilience of our coastal communities, economies and ecosystems. *Environmental Science & Policy*, 2015, 51, pp. 137-148.
- Tonelli, M.; Fagherazzi, S.; Petti, M. Modeling wave impact on salt marsh boundaries. *Journal of geophysical research: Oceans*, 2010, 115(C9).
- Van Rijn, L.C. Principles of sediment transport in rivers, estuaries and coastal seas. (Vol. 1006, pp. 11-3). *Amsterdam: Aqua publications*, 1993, 1006, pp. 11-3.
- Vona, I., Palinkas, C.M. and Nardin, W., 2021. Sediment exchange between the created saltmarshes of living shorelines and adjacent submersed aquatic vegetation in the Chesapeake Bay. *Frontiers in Marine Science*, 8, p.727080.
- Wiberg, P.L.; Taube, S.R.; Ferguson, A.E.; Kremer, M.R.; Reidenbach, M. A. Wave attenuation by oyster reefs in shallow coastal bays. *Estuaries and coasts*, 2019, 42, pp. 331-347.

Zedler, J.B., Bonin, C.L., Larkin, D.J. and Varty, A., 2018. Salt marshes. In *Encyclopedia of ecology* (pp. 614-622). Elsevier.

Zhu, Q. and Wiberg, P.L., 2022. The importance of storm surge for sediment delivery to microtidal marshes. *Journal of Geophysical Research: Earth Surface*, 127(9), p.e2022JF006612.

## Chapter 3: Oysters' integration on submerged breakwaters: field and modeling simulations in the Choptank River (MD, US)

### Abstract

Sea level rise (SLR) and increasing storm frequency threaten coastal environments. Engineering solutions such as breakwaters will become ineffective for wave attenuation and erosion control due to SLR. As a natural alternative, oysters create three-dimensional, complex reef structures that attenuate wave energy and increase sedimentation rates. If coupled with breakwaters, oysters may maintain breakwaters' efficiency over time as they are expected to grow with SLR. Such coupling was therefore studied within two locations of the Choptank River, Lake Cove and Bill Burton State Park. We measured bathymetric changes over three years (via GPS) and wave dampening due to 4 man-made intertidal breakwaters within the Lake Cove, while high resolution bathymetric data was collected in the Bill Burton in order to perform numerical simulations. Then, we modeled the coupling of breakwaters and oysters through Delft3D-SWAN to evaluate the performances of such hybrid solutions on coastal protection, under future scenarios of SLR and climate changes. Modeling hydrodynamic results showed a gradual reduction of wave attenuation due to SLR. However, when oysters were included into the modeling, wave dampening and shoreline protection were better preserved over time in both the Lake Cove and Bill Burton. Morphodynamic results showed increasing net export of sediment from the coast due to SLR. Oyster addition provided shoreline protection and sediment retention also in 100 and 150 years compared to the use of breakwaters alone, thanks to oysters' capability to grow with SLR. The coupling between oysters and breakwaters may represent a valuable and effective methodology to protect our coast over a changing climate and a rising sea, where optimal conditions for oysters' survivability occur and are maintained over time.

**Keywords:** Nature based solutions, numerical modelling, oyster reef breakwaters, sea level rise, wave attenuation, morphodynamic

### 3.1 Introduction

Coastal environments are the most important and intensely used over the world, due to their immense ecological, social and economic benefits (Post and Lundin, 1996; Creel, 2003; Kay and Alder, 2005). Since the past several decades, concern has increased over the decline of coastal ecosystem services due to growing threats such as human development, habitat degradation, enhanced storm activities and SLR. A combination of these environmental factors and human activities also contributes to shoreline retreat that is happening in many coastal zones around the world (Post and Lundin, 1996; Creel, 2003; Zhang et al., 2004; Kay and Alder, 2005; Board, 2007; Williams et al., 2018).

To protect and maintain the boundaries of coastal regions, a common practice is to armor shorelines with a variety of artificial infrastructures (or gray structures, non-living solutions usually adopted for coastal defense), such as breakwaters, that reduce waves energy at the coast and shoreline erosion (Pilkey and Wright, 1988; Douglass and Pickel, 1999; Board, 2007). Breakwaters are structures designed according to the Hudson equation (Hudson et al., 1979) especially employed in high energy environments. In low energy environments, breakwaters refer to smaller defensive structures, which are not usually designed based on wave conditions (e.g. Hudson equation). In this paper, the term breakwater refers to structures located within a low energy environment. Breakwaters are built off-shore and parallel to the coast, usually made of concrete, rocks, sandbags or geotextiles. Part of the wave energy is dissipated by wave breaking or friction losses, part is reflected back to the sea, and part is transmitted through the structure or by overtopping (Pilarczyk ,2003). Changes in hydrodynamics induced by the presence of the structure (Mory and Hamm, 1997) alter gradients in sediment transport and thus cause morphological changes (Van Rijn, 2013a). Decreasing current along the coast on the landward side of breakwaters can induce sediment deposition, while increasing flow velocity as the current leaves the sheltered area can cause erosion downstream of the structure. Deposition is usually more pronounced in the middle of the structure (landward side) than on both sides, due to wave diffraction. Diffracted waves curve inwards in the

sheltered area of the structure and decrease in height (Hsu and Silvester 1990). Breakwater length ( $L_B$ ), the width of the surf zone ( $X_D$ ) and the gap ( $G_B$ ) between multiple breakwaters, also affect sediment trapping. Landward deposition increases with increasing  $L_B$ , decreasing  $X_D$  and  $G_B/L_B^2$  (Suh and Dalrymple, 1987; Birben et al., 2007; Vona et al., 2020). However, despite the benevolent aspects regarding shoreline defense, breakwaters (as well as other artificial solutions), do not take the ecological aspects of the coasts into account and they are vulnerable to climate changes and SLR (Temmerman et al., 2013). Higher water levels, with respect to the breakwater crest, inhibit the protective benefits of gray structures (i.e. less wave attenuation provided by breakwaters), and a combined increase in storminess would make coastal environments and communities more vulnerable to inundation and habitat loss if these defense structures will lose effectiveness.

Recent practice is to adopt natural solutions for coastal protection (such as vegetation or oyster reefs) instead of traditional engineering practices, in order to provide similar erosion-control functions of armored structures, while also maintaining the ecological benefits of nature-based solutions (Davis et al., 2015; Scyphers et al., 2015; Gittman et al., 2016a).

Oysters are a genus of bivalve mollusks found to live within the moderate salinity portion of coastal areas (5–30psu), where they seek refuge from predation, competition and disease, less tolerant and predominant in lower salinity areas (Chu et al., 1993; White et al., 1996; Fodrie et al., 2014; Johnson, 2014). Oysters are well recognized to provide a wide variety of ecosystem services useful for the environment (Coen et al., 2007), defined as the provided benefits for human and environmental health. Such benefits vary from shoreline protection, water filtration, carbon sequestration and many others (Coen et al., 2007; Grabowski and Peterson, 2007; Hogan and Reidenbach, 2021). From an engineering perspective, oysters are able to attenuate wave energy and increase sedimentation rates due to the three-dimensional structure they form once fully developed (Dame and Patten, 1981; Coen et al., 2007). In addition to physical interaction with overlying waters, unlike gray infrastructures, oyster reefs can self-repair after damage and respond to changing environmental conditions (Ferrario et al., 2014, Sutton-Grier et al., 2015). Furthermore, oyster reefs

are projected to accrete at a similar pace to sea-level rise (Ridge et al., 2017; Rodriguez et al., 2014) and it is a reasonable expectation that their ecosystem services, including shoreline stabilization, could also be sustainably maintained well into the future.

However, oyster reefs can only be established within environments that allow oyster sustainability. Specifically, site conditions must be suitable for oyster survival, growth and reproduction. An adequate level of larval supply and recruitment is key in order to support reef growth over time (Kennedy et al., 1996). The settlement of new populations naturally occurs over pre-existing oyster reefs or artificial hard substrates. Oyster larvae are able to change their position vertically along the water column, to then settle and get attached to the most suitable substrate. The horizontal transport, however, is mainly due to the flowing current (Wood and Hargis, 1971; North et al., 2008). Consequently, higher recruitment rates and reef formation are mostly allowed within low energy environments (estuarine and coastal bays), where hydrodynamic conditions allow the settlement and the establishment of new populations (Kennedy et al., 1996; Capelle et al., 2019; Fivash et al., 2021). Shorelines directly exposed to incoming wave heights, strong wind and longshore currents are definitely not suitable for oyster-based infrastructures.

Temperature influences oysters' physiology, life and survival as well. Adult oysters are very tolerant of extreme temperatures and can be found within water bodies with annual ranges between -2°C and 36°C (Butler, 1954; Gunter, 1954; Galtsoff, 1964; Kennedy et al., 1996). However, oysters can die if exposed to brief high temperatures or longer low temperatures (Fingerman and Fairbanks, 1957; Kennedy et al., 1996). Spawning is also regulated by temperature. It usually occurs with rising temperatures (Medcof, 1939; Kennedy et al., 1996), but a minimum threshold must be reached before it will occur. In general, oysters in southern regions exhibit longer spawning periods than northern oysters, which have more limited time during the year. Temperature also affects oysters' growth rate, lower during colder seasons (Lowe et al., 2017).

Recent research effort has mainly focused on studying the ability of these oyster-based infrastructures to reduce wave energy and mitigate shoreline erosion

(Steven et al., 2011; Chowdhury et al., 2019; Wiberg et al., 2019 ; Morris et al., 2021), on estimating the growth rate of these reefs compared to SLR (Rodriguez et al., 2014; Ridge et al., 2017), or analyzing the roughness of oyster beds in comparison with free bed case scenario (Wright et al., 1990; Style, 2015). Few studies, however (Hogan and Reidenbach, 2021), have investigated the coupling between oysters and artificial structures in order to create an effective hybrid solution capable of self-adapt without losing effectiveness in the face of climate changes and SLR. Natural and Nature-Based Features (NNBF) (USACE 2012) integration with existing gray infrastructure may enhance the current performance of the armoring (i.e. shoreline stabilization and soil accretion), extend its effectiveness into the future, and cost less to build and maintain, while also improving the ecological value of these artificial structures (Sutton-Grier et al., 2018). However, little information is available about how to ‘green the gray’ infrastructure with oysters or other NNBF. Moreover, the current research is missing projections on future scenarios of climate change and SLR.

The current study aimed therefore to provide more insights regarding oysters as a nature-based solution for coastal protection. In particular, the coupling between oysters and breakwaters was analyzed in order to immediately improve the effectiveness (higher roughness and wave dampening) and longevity of these gray structures in the face of SLR. Field and modeling approaches were adopted.

Within the Lake Cove, the fieldwork designed to measure wave attenuation and bathymetric changes following the installation of 4 man-made breakwaters, built to prevent or slow down the erosion of a retreating shoreline, within the University of Maryland Center for Environmental Science (UMCES) – Horn Point Laboratory (HPL). Breakwaters were built by coupling several oyster castles (OCs). OCs are modular cinder blocks (made of a mixture of concrete and oysters’ shells) that can interlock each other under different shapes and combinations, also used to enhance oyster population. They have been shown to promote recruitment, retainment, vertical accretion and horizontal expansion of oyster habitats (Theuerkauf et al. 2015; Hogan and Reidenbach, 2022). However, oysters did not develop over our structures and we were not able to study such coupling more deeply in the field. We found different

plausible reasons for such failure to occur and we will expose them later in the manuscript within the discussion section.

Field activities in the Bill Burton aimed at characterizing sedimentological grain size and the bathymetry of the study area.

Data collected in both study sites were then used to validate the numerical approach, performed through Delft3D-SWAN, aimed at evaluating the long-term functioning of these hybrid infrastructures under different scenarios of SLR and climate change. Delft3D has been extensively tested in several studies in the literature (Nardin et al., 2018; Vona et al., 2021; Zhu and Wiberg, 2022).

Given the little information available, more eco-engineering studies testing hybrid infrastructure, evaluating performances against SLR and climate change, and creating broad guidance for designs and siting of this technology have been repeatedly requested (e.g. Temmerman et al., 2013; Ferrario et al., 2014, Sutton-Grier et al., 2015; 2018). Without detailed studies and guidance, attempts at restoration efforts will probably be inefficient and lack full effectiveness for long-term coastal protection.

### 3.2 Study sites

Our study area is located on the Eastern Shore of Maryland (MD) where parts of Dorchester and Talbot Counties live within the boundaries of the Choptank River and represent some of MD's most climate vulnerable coasts (Maryland Sea Grant 2015). Shoreline armoring in MD is widespread within the Chesapeake Bay: eight Chesapeake Bay sub-estuaries are more than 50% armored and twenty-three other sub-estuaries are between 30% and 50% armored (Patrick et al., 2016). Local SLR predictions are 0.43m and 1.13m by 2050 and 2100, respectively, if emissions continue at the current pace, threatening many natural resources and local communities (Boesch et al., 2013; Boesch et al., 2018).

Following a more detailed description of the two study sites, Lake Cove and Bill Burton State Park.

### 3.2.1 Lake Cove

Within the Choptank River, the Lake Cove is a small creek part of the UMCES – HPL campus, that has been eroding over the past several decades (Figure 1). Historical images (Figure A1) showed the Cove mouth in 1939 consisted of two narrow channels connected to the Choptank River, with no sign of shoreline armoring. Nowadays, the Cove inlet is much wider, suggesting waves and longshore current being the primary source of erosion at the site. The severe occurring erosion has led to extensive armoring of the Cove shoreline along boundaries with the Choptank River (Figure 3.1). Although historical images clearly show erosion happening since the last century (Figure A1), the most damaged area in recent years is the eastern side, characterized by several trees fallen into the water following the collapse of a cliff and a retreating marsh. In order to reduce or slow down the erosion happening on the shore, we built in summer 2019 four man-made breakwaters (ten meters long each), by coupling several OCs. Breakwaters were designed in 3 rows (3x3 blocks as the base, 2x2 in the middle layer and one on the top layer) for a total height of 60 cm. They were submerged at high tide during summer conditions and slightly emerged at low tide. The site was monitored before (2018) and after construction for a 3-years period (2019–2022). The study area is also characterized by the presence of three dilapidated breakwaters at the cove inlet, always submersed and not really effective (Figure 3.1); shallow waters, less than 2m deep, predominant wind direction coming from N-W and intensities around 5 m/s (based on annual statistics of raw NOAA wind data).

Figure 3.2 shows the coastline evolution of the Lake Cove from 1994 to 2017.

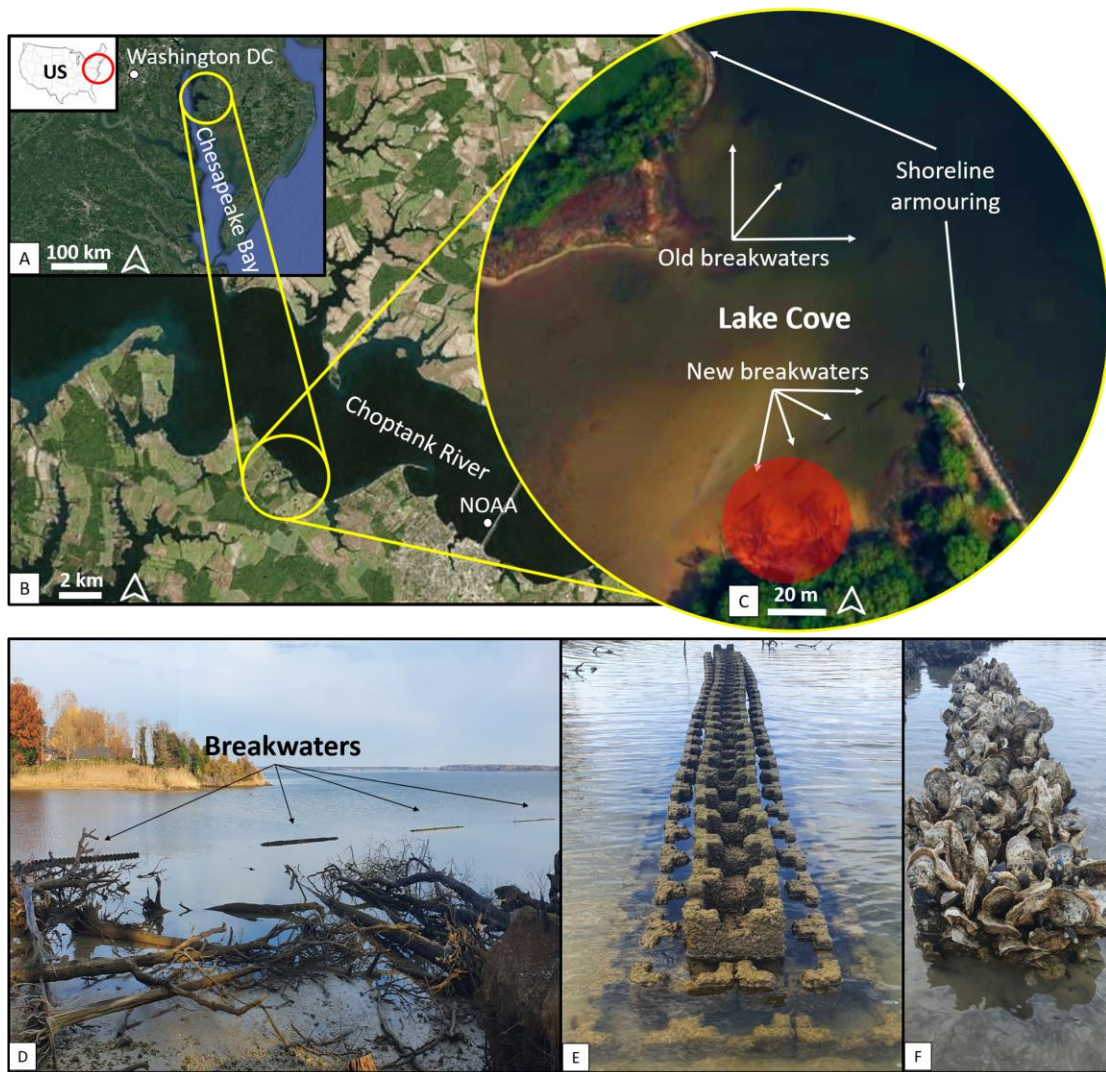


Figure 3.1. (A) Study area frame on the eastern shore of US, within the Choptank River in Chesapeake Bay. (B) Zoom on the Choptank River. (C) Zoom on the Lake Cove. The red circle indicates the area impacted by fallen trees. (D) Breakwaters view from the shoreline side, with detail of fallen trees into the water. (E) Detail of one breakwater within the Lake Cove. (F) Detail of two years old OCs colonized by oysters.

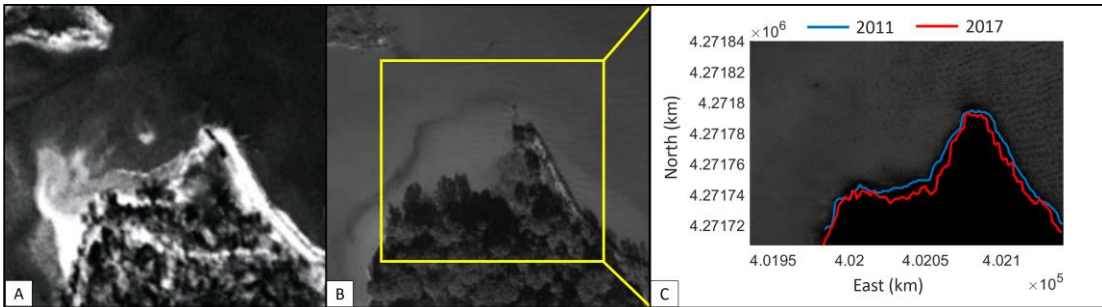


Figure 3.2. (A) Historical image showing the Lake Cove in 1994 (credit: Tom Fisher). (B) Lake Cove in 2016 (credits: Google Earth). (C) Shoreline evolution from 2011 (blue line) to 2017 (red line). Coastline changes have been evaluated by NDWI (negative on land and positive on water) extracted from Google Earth Engine through the National Agriculture Imagery Program (NAIP).

### 3.2.2 Bill Burton State Park

The Bill Burton State Park is located along the upper coastline of the Choptank River. The site is characterized by the presence of three big rocky breakwaters (usually emerged, about 35/40 m long) and two jetties (about 20 m long), dedicated to the protection of a small sandy shoreline (Figure 3.3). Water depth within the protected area on the landward side of the breakwaters is less than 2 m deep, while it becomes much deeper moving toward the open Choptank on the seaward side of breakwaters. Main wind direction, according to the Cambridge station just on the other side of the river, comes from N-W with intensity around 5 m/s (based on annual statistics by [www.windfinder.com/windstatistics/cambridge\\_choptank\\_river](http://www.windfinder.com/windstatistics/cambridge_choptank_river)).



Figure 3.3. (A) Study area frame on the eastern shore of US, within the Choptank River in Chesapeake Bay. (B) Zoom on the Choptank River. (C) Zoom on the Bill Burton State Park.

### 3.3 Material and Methods

#### 3.3.1 Lake Cove

##### 3.3.1.1 Field measurements

The main purpose of the fieldwork in the Lake Cove was to create hybrid infrastructures (breakwaters + oysters) by seeding OC with oyster larvae in the field once being installed, and then measure and quantify the protective improvements, especially regarding wave dampening. Challenges encountered in the field (see discussion) denied us to successfully obtain fully developed oyster reef breakwaters, and the comparison of wave attenuation between structures with and with no oysters was only done with partially oyster-covered breakwaters. Morphological changes have also been tracked in order to evaluate structures' impact on depositional and erosional patterns.

Field measurements were taken over the 4 breakwaters placed in front of the eroding shoreline. Bathymetric changes were tracked by using a Topcon Hiper Lite

Plus GPS GLONASS L1 L2 Base RTK that was georeferenced with the relative geoid and GPS base stationed at a GNSS benchmark located within the UMCES - HPL campus. Eight predefined transects along both sides of each breakwater have been monitored since the summer of 2019 (Figure 3.4). Wave data was recorded from 27<sup>th</sup> to 30<sup>th</sup> March 2022 by using one Spotter Buoy (SB) and one High-Resolution Acoustic Doppler Current Profiler (ADCP HR). Both instruments were placed over the closer breakwater to the Cove mouth as moving further into the cove, wave height gradually dissipated for bottom frictions and breaking.

The SB (<https://www.sofaroccean.com/products/spotter>), placed on the seaward side of the oyster castle about five meters distant, recorded wave data continuously at 2.5 Hz and returned wave characteristics (Significant wave height ( $H_s$ ), Peak period ( $T_P$ )) every 30 min. The ADCP HR, placed on the landward side about five meters distant, collected pressure data in dbar every 30 min for 17 min continuously at 4 Hz. In order to obtain wave parameters ( $H_s$  and  $T_P$ ), we processed the recorded ADCP HR pressure data with Oceanlyz, a Matlab application developed by Karimpour and Chen, 2017. The resulting wave characteristics were then compared to the SB data in order to estimate wave dampening ( $\Delta H_s$ ). A third instrument, a Low Resolution ADCP (ADCP LR), was placed at the Lake Cove mouth to collect pressure data every 30 min in order to register the water level.

Superficial sediment samples were also collected and analyzed in order to characterize the bed level composition around the OCs (Figure 3.4). Grain sizes were analyzed by wet-sieving samples through a 64- $\mu\text{m}$  mesh. The sand-sized fraction ( $>64 \mu\text{m}$ ) was dry-sieved from 64-100  $\mu\text{m}$  with a set of 3 sieves. Mud and sand data were then combined to estimate median sediment grain diameters  $D_{50}$ .  $D_{50}$  size and sorting for the non-cohesive and cohesive fraction were obtained using the geometric method of moments in GRADISTATv8 software (Blott and Pye, 2001; Nardin et al., 2016a). However, the limited set of sieves size might underestimate the  $D_{50}$ . Bed level strength at the same points as sediment samples, was measured through a shear vane (Chandler, 1988; Nardin et al., 2016a).

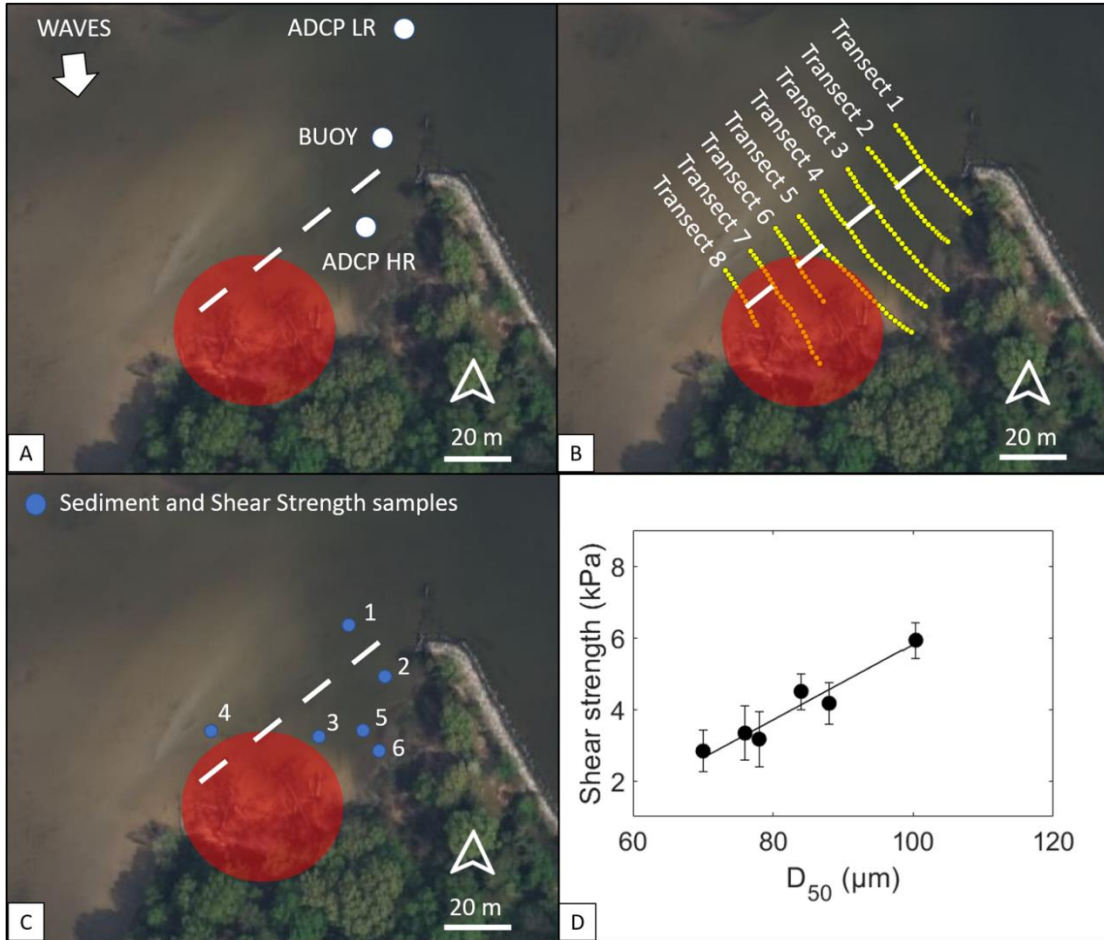


Figure 3.4. (A) Instrument deployment during March 27<sup>th</sup> to 30<sup>th</sup>, 2022. Red circle indicates area impacted by fallen trees (B) Monitored transects via GPS surveys along both sides of each breakwater. (C) Sediment sample locations. (D) Shear strength as function of  $D_{50}$ .

### 3.3.1.2 Numerical model

To predict how oyster castle additions to existing gray infrastructure influence coastal inundation and resiliency in Lake Cove under a changing climate, the proposed study used the Delft3D-SWAN modeling system. Lake Cove's modeling included extensive validation through field data of water level, wave data,  $\Delta H$ s and bathymetric changes. Delft3D (Roelvink and Van Banning, 1995; Lesser et al., 2004) is an open-source numerical model to study hydrodynamic flows, wave generation and propagation, sediment transport, and morphological changes. Hydrodynamic and morphodynamic modules are fully coupled so that changes in the bed topography

correspond to flow field adjustments in real time. The FLOW module in Delft3D performs hydrodynamic, sediment transport, and morphological changes on a 3D curvilinear finite-difference grid, solved by an alternating direction implicit scheme. In our study, the 2D formulation of the hydrodynamic and morphodynamic models was used.

Waves generation and propagation in shallow water are computed by SWAN, which includes processes such as wave–wave interaction, refraction and dissipation. Wave dissipation included bottom friction (Hasselmann et al., 1973) and wave breaking (Battjes and Janssen, 1978). Below, the essential governing equations for the model are discussed. Further details can be found in Lesser et al. (2004) and Vona et al. (2021).

Delft3D solves the mass-balance and momentum-balance equations in cartesian coordinates for an incompressible fluid with shallow water approximation. The suspended sediment transport is calculated by solving the three-dimensional Advection-Diffusion equation. Changes in bed bathymetry are computed from the gradients in sediment transport vectors, while the evolution of the wave motion is described by SWAN, which solves the spectral action balance equation.

### 3.3.1.3 Model set-up

A double nesting grid was used in order to better propagate wave motion and avoid numerical instabilities. The outer and coarser wave grid was composed of 169 and 109 cells in the x and y directions, respectively, refined from offshore (100 x 100 m) to the Cove (50 x 50 m). The flow domain (nested into the wave grid) was around 3 × 3 km. The computational grid was composed of 341 cells in the x-direction and 270 cells in the y-direction, and it was gradually refined from offshore (20 x 20 m) to the Cove (2 x 5 m; Figure 3.5). For the coarse part of the domain, bathymetry was obtained from the NOAA National Ocean Service (30-meter resolution Digital Elevation Model), while for the Cove, flights were carried out via Unmanned Aerial Vehicle (UAV) in Spring 2018 prior to construction, in order to provide high resolution bathymetric data, around 2x2 cm (Nardin et al., 2021; Taddia et al., 2021).

The UAV survey was carried out during an exceptional low tide occurred the 3<sup>rd</sup> of March, 2018, which made the Cove completely uncovered. Low tide peaked around -0.9 m (NAVD88) allowing the UAV to clearly survey the study area (Figure A3). Breakwaters were imported into the model as an integral part of the bed level with a non-eroding bottom, which made the structures waterproof (no flow through the breakwaters). Breakwater crests at the Cove mouth were at -0.30 m (NAVD88). In front of the eroding shoreline, breakwater crests were between -0.10 and 0 m (NAVD88), with less submergence found moving forward into the Cove, due to the shallower bathymetry (Figure 3.5). All breakwater crests were surveyed via GPS. In the vertical direction, five-meter-deep layer of mixed cohesive and non-cohesive sediments was originally accessible for erosion at the bottom of the domain.

Neumann conditions were imposed on the West and East boundary of the flow domain, while the North boundary was forced by water level variation. Wind was imposed on the WAVE domain in order to generate waves taken then by the FLOW domain (Figure 3.5). Wave reflection was not accounted for in the wave model, so wave energy was dissipated at the coastline.

Superficial sediment analysis revealed a mixed composition of very fine sand and mud with  $D_{50}$  between 70 and 100  $\mu\text{m}$ . Non-cohesive sediments were characterized by a specific density of  $2650 \text{ kg/m}^3$ , dry bed density of  $1600 \text{ kg/m}^3$  and  $D_{50}$  equal to 100  $\mu\text{m}$ . Characteristics of cohesive sediment were chosen in agreement with values provided by Berlamont et al. (1993); specific density was  $2650 \text{ kg/m}^3$ , dry bed density was  $500 \text{ kg/m}^3$  and setting velocity was 0.25 mm/s. In order to morphologically calibrate the model according to recorded bathymetric changes, we adopted cohesive critical shear stress for erosion equal to  $0.7 \text{ N/m}^2$  and cohesive erosion parameter equal to  $5 \cdot 10^{-6} \text{ kg/m}^2/\text{s}$ .

The bed level roughness was chosen equal  $65 \text{ m}^{1/2}/\text{s}$  according to Chézy's formulation (Mouret, 1921). The initial condition of the models was a fixed water level at 0.5 m. The suspended-sediment eddy diffusivities (function of the fluid eddy diffusivities) were calculated using a horizontal large eddy simulation and grain settling velocity. The horizontal eddy diffusivity coefficient was defined as a combination of the subgrid-scale horizontal eddy viscosity (computed from a

horizontal large eddy simulation) and the background horizontal viscosity, which was set equal to  $0.001 \text{ m}^2 / \text{s}^2$  (Edmonds and Slingerland, 2010; Nardin et al., 2016b). To satisfy the numerical stability criteria of Courant–Friedrichs–Lewy, we used a time step  $\Delta t = 1.2 \text{ s}$  (Lesser et al., 2004). A morphological scale factor (a user device to multiply the deposition and erosion rate in each  $\Delta t$ ) equal 50 was used in order to decrease computational time. Combining the duration of the single simulation, 4 days, and the value of morphological factor, the model returned morphological changes for 200 days. Sensitivity analysis showed the high morphological factor did not influenced water level and wave height (Figure A4).

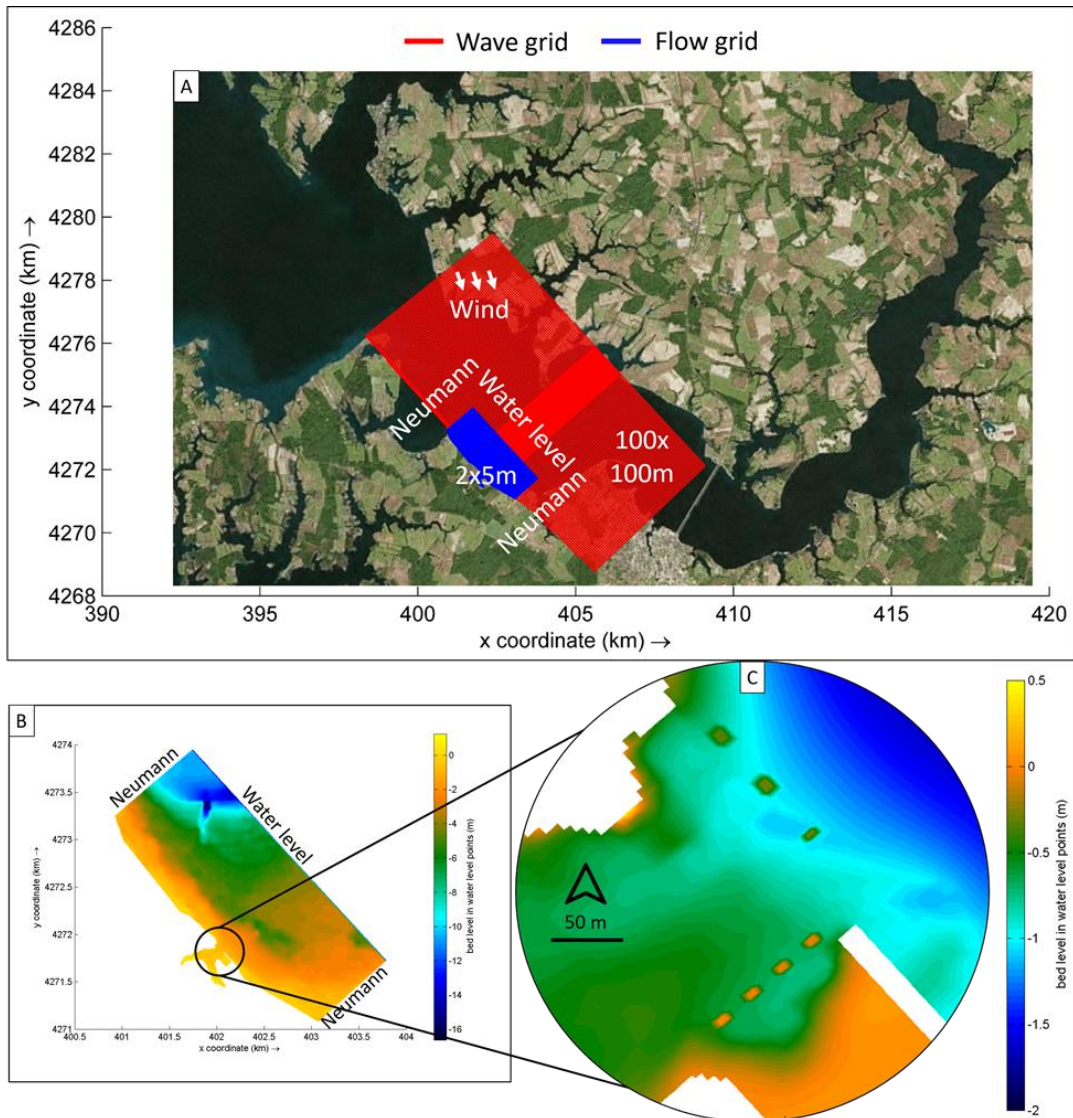


Figure 3.5. Model computational grid and bathymetry. (A) Computational grids used in the modeling. (B) Bathymetry of the FLOW domain and (C) zoom on the study area.

### 3.3.1.4 Modeling SLR and oysters' growth

We then set up our numerical experiments by exploring three case scenarios, no breakwaters (no BWs), gray breakwaters (BW), breakwaters and oysters (BW+O). We applied four different wind intensities coming from NW (5, 10, 15, 20 m/s) on the WAVE domain, and they were kept constant during simulations. We then varied the mean water level (MWL), by considering the actual MWL and its

projection in 20, 50 and 100 years, to evaluate OCs' behavior under increasing sea levels (Table 3.1).

The global rate of SLR ranges between 3-4 mm/yr, and it is projected to rise up to 10-20 mm/yr at the end of the century (Oppenheimer and Hinkel, 2018). In this study, we adopted as actual MWL the mean value recorded in the field during our deployment (-0.1 m NAVD88). Then, we added 3 mm/yr for 20 years in order to reproduce the actual rate of SLR; 6 mm/yr for the following 30 years in order to reproduce acceleration in SLR rate and, ultimately, 10 mm/yr for the last 50 years. The estimated MWL related to each SLR scenario (Table 3.2), was kept constant during the associated numerical experiment. We thus did not dynamically simulate the increasing MWL due to SLR in our simulations. Modeled tidal excursion was representative of real tidal oscillation in Lake Cove, around 60 cm (we adopted 60 cm) and was kept constant during all simulations.

Oysters were modeled by increasing breakwater height, in order to reproduce their vertical growth. Rodriguez et al., 2014, reported growth rates for oysters around 2.5 cm/yr, measured within an intertidal marsh environment in North Carolina, US. However, reef vertical accretion might have different rates, based on sea level conditions. When the reef crest reaches the upper limit of the tidal range (the “growth ceiling”) where oysters cannot grow due to aerial-exposure stresses, reef crest vertical accretion is reduced to the rate of SLR (Rodriguez et al., 2014). In our study, we approximated the growth ceiling with the MWL (Rodriguez et al., 2014). Thus, in order to simulate oysters' vertical growth, breakwater height was increased until the MWL associated to the considered SLR scenario and was kept constant during the simulation (Table 3.2). By doing so, reef vertical accretion was reduced to the rate of SLR:

$$h_{BW}(t) = h_0 + t \cdot slr(t) \quad (3.1)$$

$$t = \begin{cases} 0 \rightarrow \text{nowadays} \\ 20 \text{ years} \\ 50 \text{ years} \\ 100 \text{ years} \end{cases}$$

where  $h_0$  represents the initial breakwater crest height (m) ( $h_0$  is below MWL), “slr” is the rate of SLR (m/yr) and “t” the time (yr). We did not consider oysters' growth below the MWL, which may be even faster than SLR (around 10 cm/yr), as well as lateral expansion (Rodriguez et al., 2014).

Table 3.1. Run configurations

SLR scenario	wind (m/s)			
	5	10	15	20
present day	no BWs	no BWs	no BWs	no BWs
	BWs	BWs	BWs	BWs
	BWs+O	BWs+O	BWs+O	BWs+O
20 yr SLR	no BWs	no BWs	no BWs	no BWs
	BWs	BWs	BWs	BWs
	BWs+O	BWs+O	BWs+O	BWs+O
50 yr SLR	no BWs	no BWs	no BWs	no BWs
	BWs	BWs	BWs	BWs
	BWs+O	BWs+O	BWs+O	BWs+O
100 yr SLR	no BWs	no BWs	no BWs	no BWs
	BWs	BWs	BWs	BWs
	BWs+O	BWs+O	BWs+O	BWs+O

Table 3.2. SLR modeling scenarios

Scenario	MWL-NAVD88
Present day	-0.10 m
20 yrs SLR	-0.04 m
50 yrs SLR	0.14 m
100 yrs SLR	0.64 m

### 3.3.2 Bill Burton State Park

#### 3.3.2.1 Field measurements

Field measurements in the Bill Burton aimed at classifying grain size composition of the bed level  $D_{50}$  and collecting bathymetric data in order to develop extensive numerical experiments discussed in the next chapter. As well as the Lake Cove, bathymetry was surveyed by using a Topcon Hiper Lite Plus GPS GLONASS

L1 L2 Base RTK that was georeferenced with the relative geoid and GPS base stationed at a GNSS benchmark located within the Bill Burton State Park. Superficial sediment samples were analyzed in order to characterize the median diameter in the area protected by the breakwaters (Figure 3.6). Grain sizes were analyzed by wet-sieving samples through a 64- $\mu\text{m}$  mesh. The sand-sized fraction ( $>64\ \mu\text{m}$ ) was dry-sieved from 64-100  $\mu\text{m}$  with a set of 3 sieves. Mud and sand data were then combined to estimate median sediment grain diameters  $D_{50}$ . The mean grain size and sorting for the non-cohesive fraction were obtained using the geometric method of moments in GRADISTATv8 software (Blott and Pye, 2001; Nardin et al., 2016a).

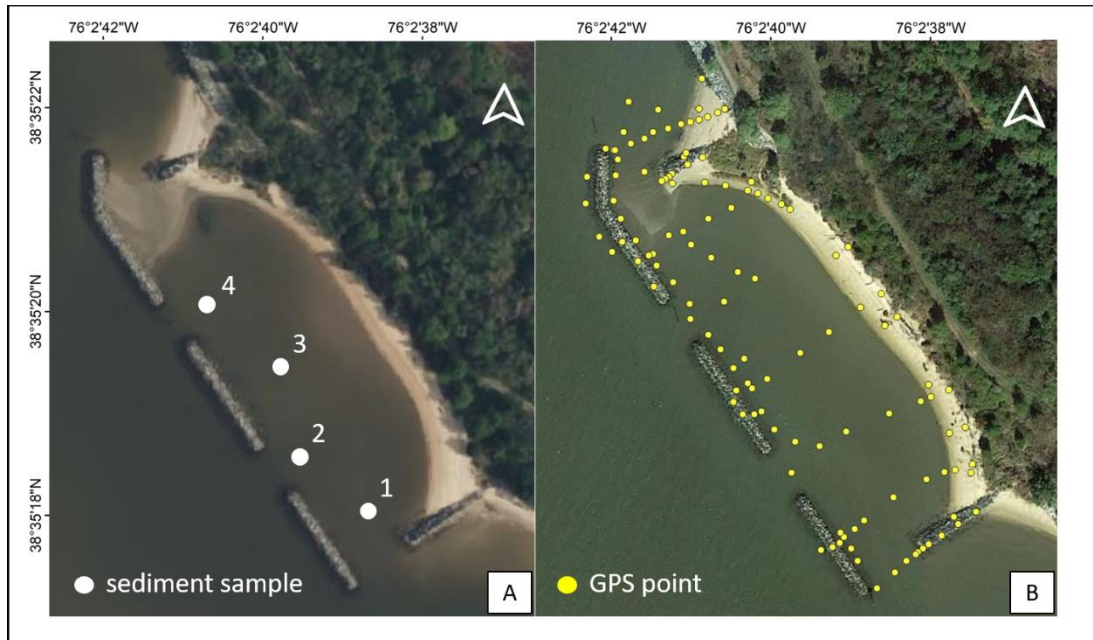


Figure 3.6. (A) Sediment sample locations for the Bill Burton and (B) GSP survey.

### 3.3.2.2 Numerical model

A double nesting grid was used for the Bill Burton in order to better propagate wave motion and avoid numerical instabilities, as well as for the Lake Cove. The outer and coarser wave grid was composed of 158 and 81 cells in the x and y directions, respectively, refined from offshore (100 x 100 m) to the shore (50 x 50 m).

The flow domain (nested into the wave grid) was around  $3 \times 3$  km. The computational grid was composed of 244 cells in the x-direction and 177 cells in the y-direction, and it was gradually refined from offshore (20 x 20 m) to the shore (5 x 5 m; Figure 3.7). For the coarse part of the domain, bathymetry was obtained from the NOAA National Ocean Service (30-meter resolution Digital Elevation Model), while for the finer part, high resolution bathymetric data (discussed in the previous section) were taken via GPS. Breakwaters were imported into the model as an integral part of the bed level with a non-eroding bottom, which made the structures waterproof. Breakwater crests were between -0.8 and -0.7 m (NAVD88). All breakwater crests were surveyed via GPS. In the vertical direction, five-meter-deep layer of mixed cohesive and non-cohesive sediments was originally accessible for erosion at the bottom of the domain.

Neumann conditions were imposed on the West and East boundary of the Flow domain, while the South boundary was forced by water level variation. Constant wind from S-W was imposed on the Wave domain in order to generate waves taken then by the Flow domain. Wave reflection was not accounted for in the wave model, so wave energy was dissipated at the coastline.

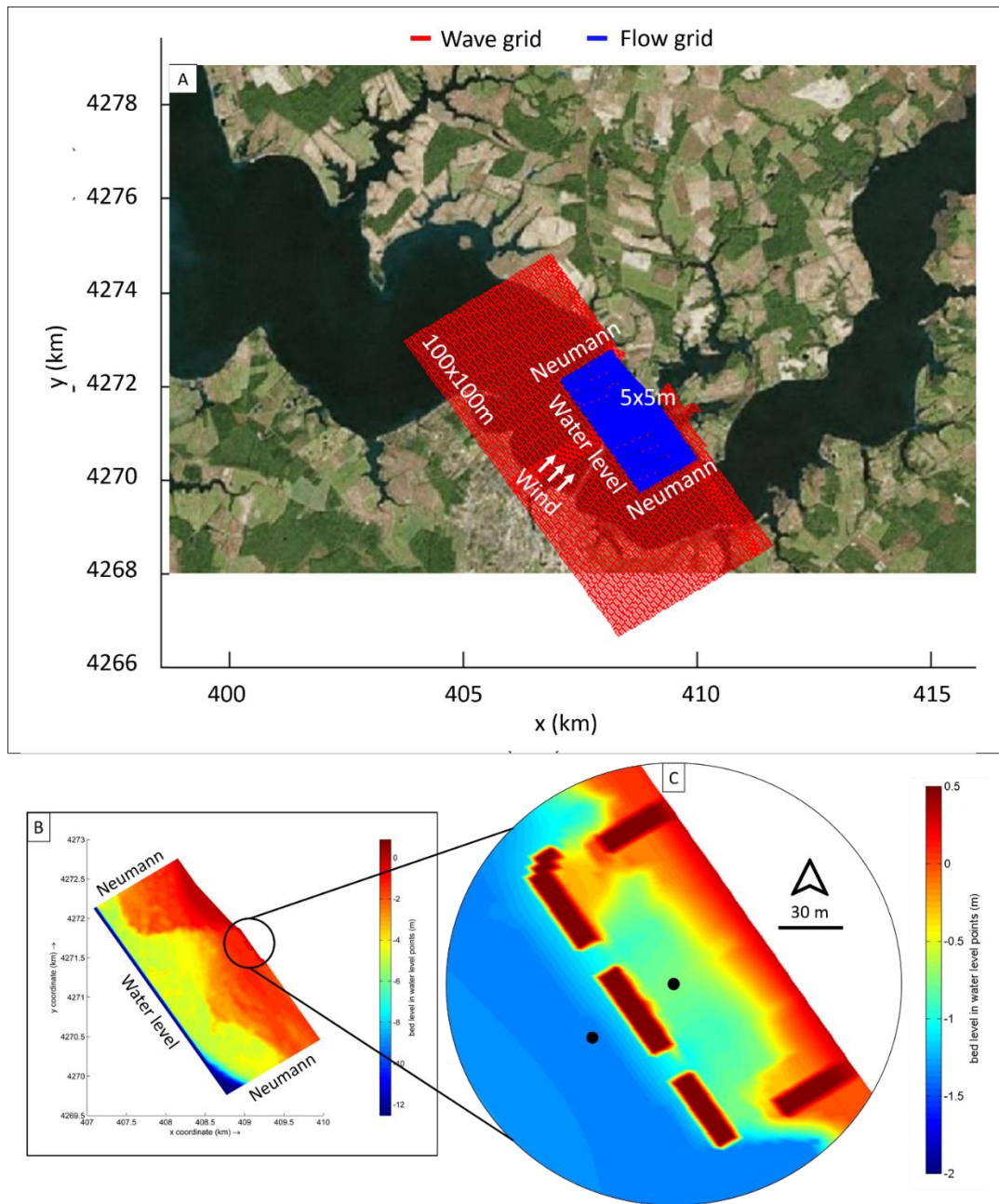


Figure 3.7. Model computational grid and bathymetry. (A) Computational grids used in the modeling. (B) Bathymetry of the FLOW domain and (C) zoom on the study area with location of observation points over the middle breakwaters.

We then set up our numerical experiments by varying wind intensities (5-10-15 m/s) and the mean water level (MWL). Four different SLR scenarios were considered, the actual MWL and its projection in 50, 100 and 150 years. Oysters were

only included into the 150 years SLR scenario, since the associated MWL was high enough to drown breakwaters and make them suitable for oyster colonization.

Modeling parameters were chosen in agreement with the Cove model, as well as SLR and modeling oyster growth assumptions.

### 3.4 Results

#### 3.4.1 Lake Cove – Field results

Insights of the activities carried out in the Lake Cove are reported below.

Sedimentological analyzes will be presented first, followed by wave attenuation results and bathymetric changes.

Analyzes aimed at characterizing the bed level composition revealed it was mainly made of very fine sand with low mud content. Higher mud content up to 47% was found along transect three, close to the shoreline (samples 5 and 6).  $D_{50}$  was between 70 and 100  $\mu\text{m}$ , coarser on the seaward side of breakwaters and decreased moving more internally into the cove (Table 3.3). Bed shear strength was positively correlated with the  $D_{50}$  (Figure 3.4 D).

Table 3.3. Sediment characteristics in the Lake Cove

Sample	Sand content (%)		Mud content (%)	$D_{50}$ ( $\mu\text{m}$ )
	Fine sand	Very fine sand		
1	35	64	1	110
2	9	89	2	84
3	1	91	8	78
4	82	14	4	88
5	0	79	21	76
6	0	53	47	70

During the period of our deployment (from 27<sup>th</sup> to 30<sup>th</sup> March 2022) to collect wave data in Lake Cove over the gray breakwaters, meteorological conditions recorded at the NOAA station in Cambridge (ID: 8571892) indicated a predominant

wind direction coming from N/W with speeds ranging from 5 and 15 m/s. This wind was capable of generating wave heights up to 40 cm (recorded by the SB at the seaward side of the breakwater), with associated wave periods between 4.5 and 2 seconds (Figure A2). The comparison between wave height recorded in front of (SB) and behind (ADCP HR) the breakwater revealed a good efficiency of the structure in breaking waves up to 45% at high tide and up to 95% at low tide (Figure 3.8). The water level recorded by the ADCP LR at the Cove mouth showed good agreement with the nearby NOAA station in Cambridge (MD, US).

During the period of our deployment (from 10<sup>th</sup> to 13<sup>th</sup> February 2023) to collect wave data in Lake Cove over the partially oyster-covered breakwaters, the NOAA station in Cambridge indicated a predominant wind direction coming from N/W with speeds ranging from 4 and 10 m/s. This wind was capable of generating wave heights up to 25 cm at high tide (recorded by the SB at the seaward side). The comparison between wave height recorded before (SB) and after (ADCP HR) the structure revealed a good efficiency of the partially oyster-covered breakwater in breaking waves up to 45% at high tide and up to 70% at low tide (Figure 3.9).

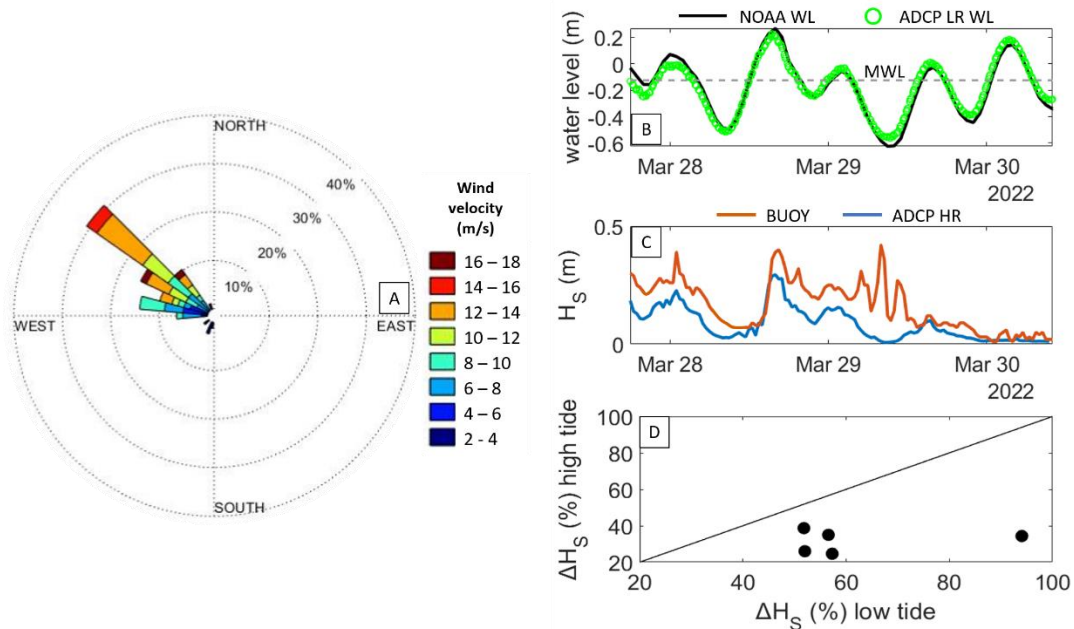


Figure 3.8. (A) Wind rose recorded at the NOAA station in Cambridge (ID: 8571892) during March 27<sup>th</sup> to 30<sup>th</sup>, 2022. (B) Water level recorded at the NOAA station in Cambridge during March 27<sup>th</sup> to 30<sup>th</sup>, 2022. (C) Wave data collected by the SB and the ADCP HR. (D) Wave damping at high tide vs low tide.

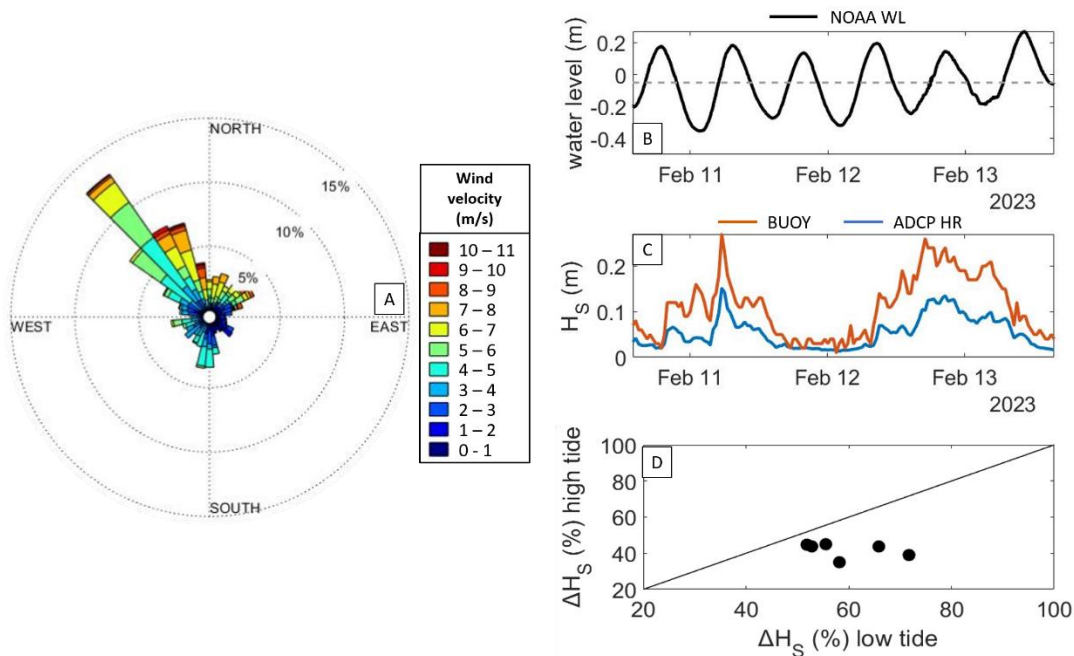


Figure 3.9. (A) Wind rose recorded at the NOAA station in Cambridge (ID: 8571892) during February 10<sup>th</sup> to 13<sup>th</sup>, 2023. (B) Water level recorded at the NOAA station in Cambridge during February 10<sup>th</sup> to 13<sup>th</sup>, 2023. (C) Wave data collected by the SB and the ADCP HR. (D) Wave damping at high tide vs low tide.

Wave damping comparison between datasets with and without oysters, resulted in similar  $\Delta H_s$ . Averaged  $\Delta H_s$  associated with partially oyster-covered breakwaters at high tide was slightly higher (40%) than gray breakwaters (30%), while at low tide the wave attenuation resulted similar for both cases (around 60%) (Figure 3.10). However, measurements collected in different periods of time, did not allow us to compare wave damping under the same tidal, wind and wave height conditions. Nevertheless, similarities emerged between the two datasets and comparison was then plausible. This aspect will be explored in more detail in the discussion.

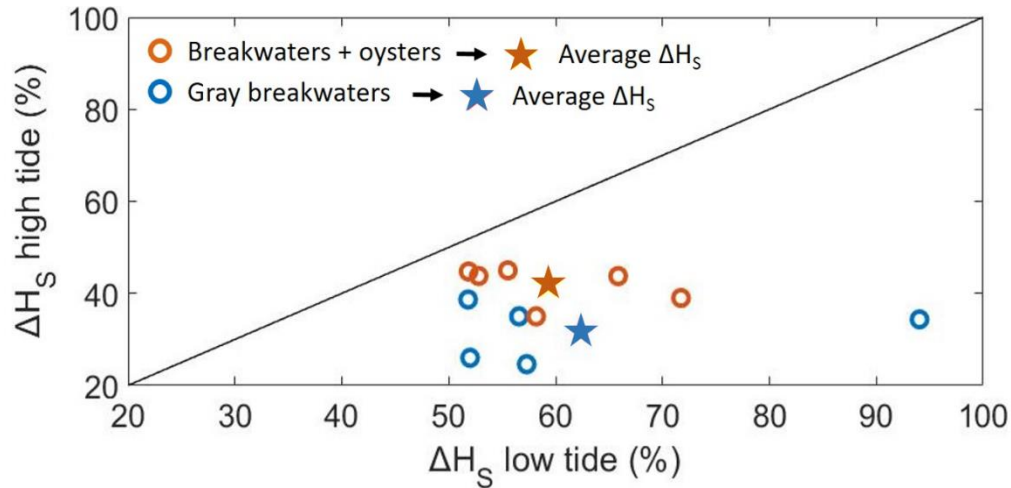


Figure 3.10. Comparison of wave dampening between breakwaters with and with no oysters. Stars mark average values.

Morphodynamic results about Lake Cove revealed breakwaters emulated the behavior of common structures in coastal water bodies. Transect 1 showed complete erosion as it was the most subject to longshore current and waves. Transect 3 showed complete erosion as well, despite the protection given by the first breakwater, likely due to differences in sediment characteristics along the transect revealed from our sediment analysis. Transects 2, and 4 showed the classic behavior of any kind of barrier immersed into a water body, erosion at the seaward side of the structure and deposition at the landward side (Figure 3.11).

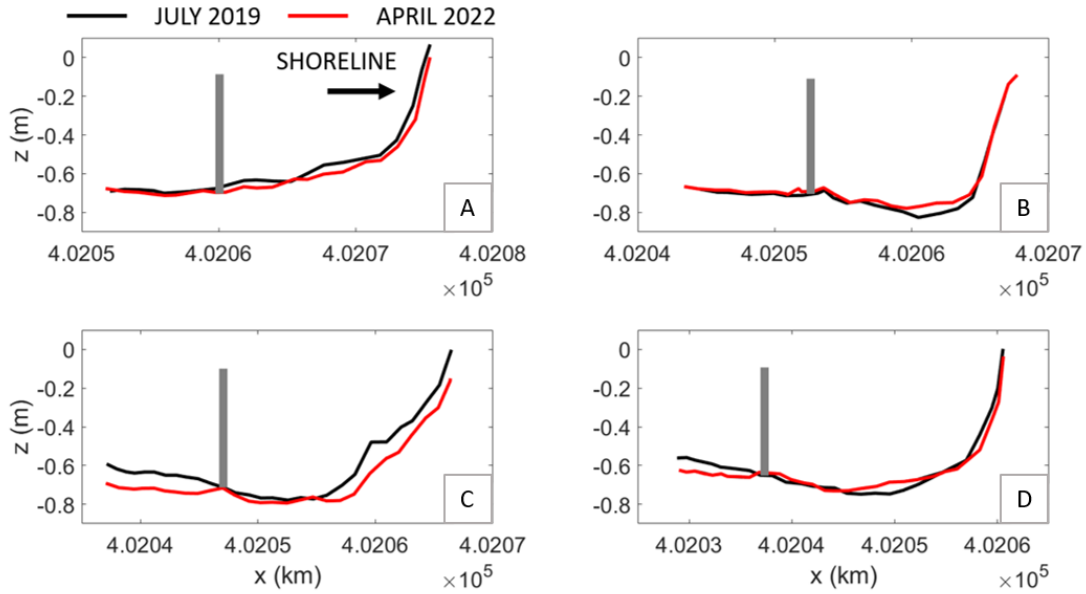


Figure 3.11. (A) Bathymetric changes from July 2019 to April 2022 along transect 1; (B) transect 2; (C) transect 3; (D) transect 4.

### 3.4.2 Lake Cove - Modeling results

#### 3.4.2.1 Lake Cove – Model validation

Hydrodynamic numerical validation was performed by forcing the model with both recorded water level and wind characteristics (velocity and direction) at the NOAA station in Cambridge during 27<sup>th</sup> to 30<sup>th</sup> March 2022 (station ID: 8571892). Wind time-series was applied on the WAVE domain, while water level time-series on the FLOW domain. Modeled water level, wave height and  $\Delta H_s$  were in good agreement with field measurements.

The water level was well predicted by the model at the observation point corresponding to the ADCP LR. The significant wave height recorded in the model at the SB (seaward side of breakwater 1) and the ADCP HR (landward side of breakwater 1), showed good agreement with measured values in the field. The wave spectrum in correspondence with the SB was well reproduced by the model. Simulated  $\Delta H_s$  was also found to be close to the measured one at high and low tide (Figure 3.12).

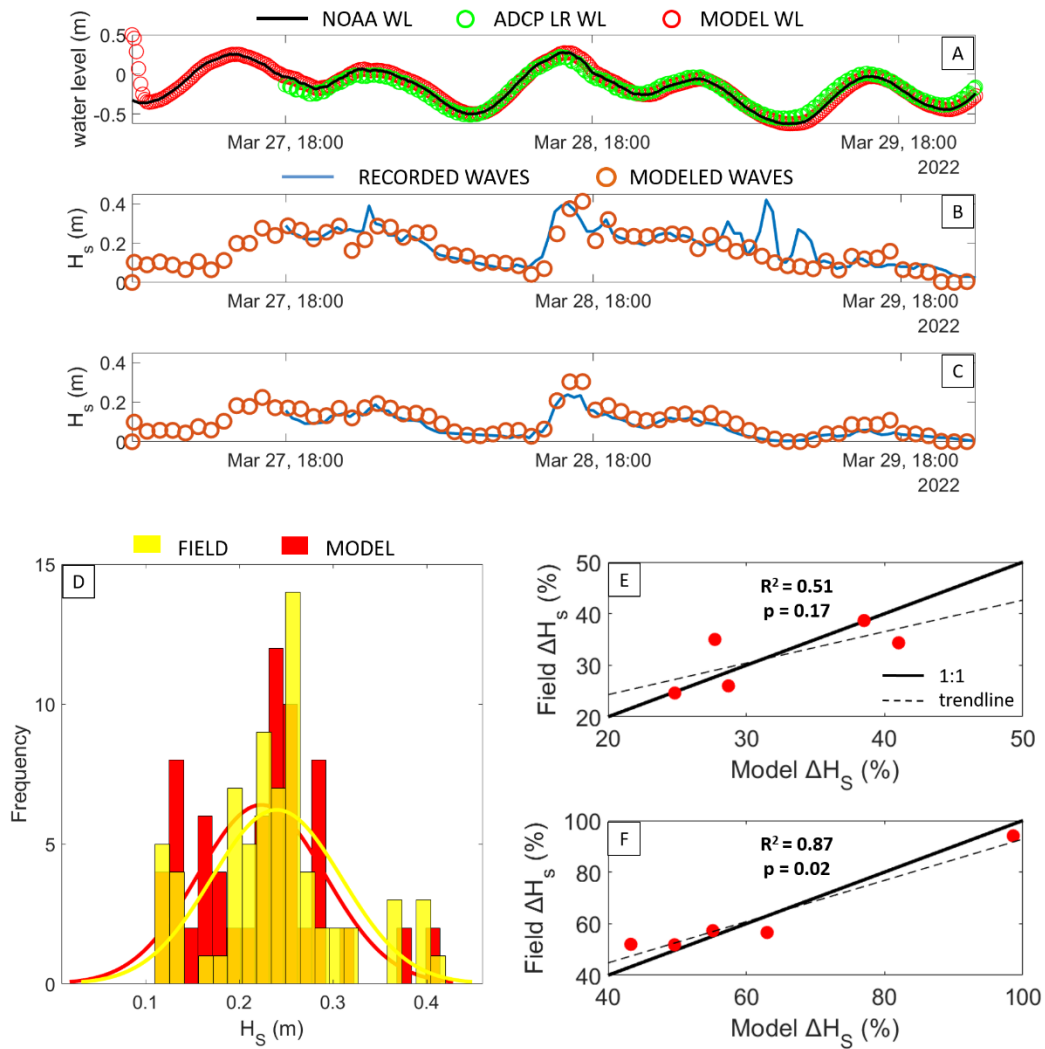


Figure 3.12. (A) Recorded tidal signal from the ADCP LR and corresponding modeled water level in Delft3D. (B) Significant wave height recorded by the Buoy (seaward side) and corresponding modeled waves in Delft3D. (C) Significant wave height extracted from the ADCP HR (landward side) and corresponding modeled waves in Delft3D. (D) Histograms of wave data recorded by the Buoy and corresponding modeled wave heights distribution. (E) Modeled and field  $\Delta H_s$  at high tide; (F) low tide.

Morphodynamic validation aimed instead to replicate the erosion/depositional transect behavior observed in almost three years. To reproduce observed values in the field within a reasonable computational time, three different scenarios forced by the same water level (the one recorded during instruments deployment) and three wind

intensities coming from N/W (5, 10, 15 m/s according to recorded wind) have been simulated in order to cover the most typical local weather conditions. The modeled erosion/deposition along each transect corresponded to the average of the 3 different simulations. Morphodynamic validation aimed to highlight the correct qualitative rather than quantitative transects behavior regarding deposition and erosion, given the challenges of replicating weather conditions that occurred in almost three years of observations and the need to keep shorter computational times. Due to the collapse of the cliff in the Cove with related fall of trees in front of transects five to eight, only the first two breakwaters (transects one to four) were used in the morphodynamic validation phase.

Morphodynamic results revealed good agreement of the model with GPS investigations carried out in the field. The qualitative behavior of transects regarding erosion and deposition was well reproduced by the model. We compared seaward erosion, landward deposition and scarp erosion measured in the field with values obtained from the model (Figure 3.13 A). Transect 1 resulted in erosion as observed in the field (Figure A5); transects 2 and 4 showed erosion at the seaward side of the structures and deposition landward in agreement with what was observed in the field (Figure A6). Transect 3 was the only one that did not match the measured values as it resulted in seaward erosion and landward deposition, in disagreement with the total erosion measured in the field (Figure A6). Bed level composition was uniform within the computational domain (50% sand, 50% mud), therefore the model could not capture the different behavior of transect 3 due to higher mud content, as shown by our sediment analysis. Moreover, bed shear strength varied within the Cove linearly with the  $D_{50}$ , while sediment characteristics were kept constant in space in the model. Overall, deposition/erosion values were close between the model and field, except for transect 3, where the greatest deviations occurred (Figure 3.13 B).

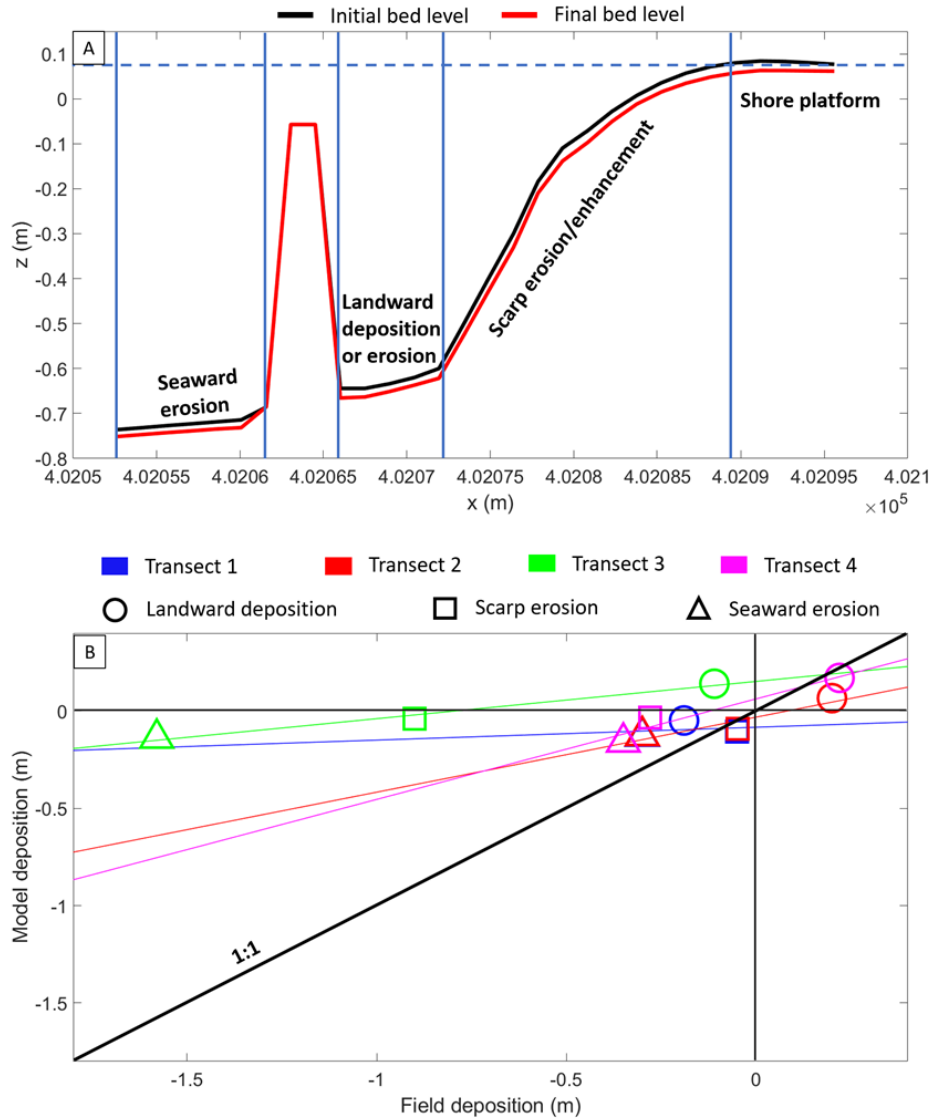


Figure 3.13. (A) Definition of seaward erosion, landward deposition and scarp erosion. The example along transect 1 is taken from simulation with actual MWL and wind = 10m/s. (B) Modeled and measured seaward erosion, landward deposition and scarp erosion along transects 1 to 4.

### 3.4.2.2 Lake Cove – hydro and morphodynamic modeling results

This section analyzes numerical results from modeling experiments performed with Delft3D-SWAN. Hydrodynamic and morphodynamic simulations aimed to highlight the impact of coupling oysters and submerged breakwaters regarding coastal defense, in the face of SLR and climate changes. Hydrodynamic is presented first,

followed by morphodynamic. An example of the wave field and morphodynamic evolution around our breakwaters is given in Figure 3.14.

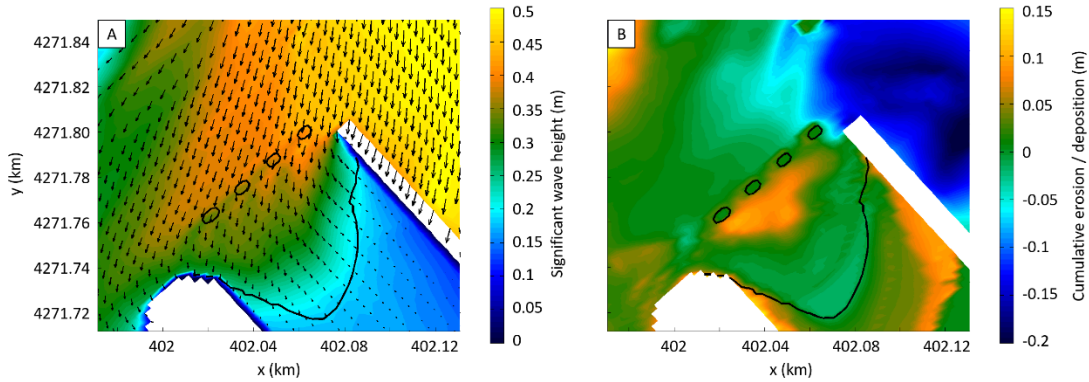


Figure 3.14 (A) Modeled wave field around gray breakwaters in the Lake Cove at high tide. Results are taken from simulation with actual MWL and wind intensity = 15 m/s. Black line defines the final bed level threshold at 0.05 m (NAVD88). (B) Cumulative erosion / deposition for the simulations with actual MWL and wind intensity = 15 m/s.

Hydrodynamic results emphasized changes in  $\Delta H_S$  over increasing sea levels.  $\Delta H_S$  was estimated by comparing modeled  $H_S$  at observation points in correspondence with the SB and the ADCP deployed in the field.  $\Delta H_S$  was then averaged ( $\overline{\Delta H_S}$ ) among high tide peaks and low tide troughs, respectively, in each simulation.

Modeling results showed  $\overline{\Delta H_S}$  to be proportional to the time-averaged  $H_S$  ( $\langle H_S \rangle$ ), measured in correspondence of the SB) and inversely proportional to time-averaged MWL ( $\langle MWL \rangle$ ), measured in correspondence of the SB), as expected.  $\overline{\Delta H_S}$  among all simulations gradually reduced over time due to SLR for both high (Figure 3.15 A) and low tide (Figure 3.15 B). Positive values of  $\overline{\Delta H_S}$  were also associated for the scenario with no BWs, up to 20% at high tide (Figure 3.15 C) and 40% at low tide (Figure 3.15 D) for the actual MWL scenario. The shallow bathymetry around our breakwaters naturally attenuated bigger incoming waves, due to bottom friction and breaking (Figure A7).  $\overline{\Delta H_S}$  in 100 yrs, however, was only 5% at both high and low tide (Figure 3.15 C,D). Results from the no BWs “present day” scenario represented

our base-case and insights about simulations with gray BWs and BWs+O were reported relative to the base-case.

The scenario with gray BWs returned  $\overline{\Delta H_S}$  up to 30% at high tide (Figure 3.15 C) and 60% at low tide (Figure 3.15 D) in the actual MWL scenario. However, in 100 yrs,  $\overline{\Delta H_S}$  became similar to the no BWs scenario, for both high and low tide (Figure 3.15 C,D). The case experiment with BW+O, on the other hand, resulted in greater  $\overline{\Delta H_S}$  compared to the previous two cases.  $\overline{\Delta H_S}$  was up to 40% at high tide (Figure 3.15 C) and 65% at low tide (Figure 3.15 D) in the actual MWL scenario.  $\overline{\Delta H_S}$  in 100 yrs was 30% at high tide and 35% at low tide (Figure 3.15 C,D).

To better highlights improvements over time provided by oysters in terms of  $\Delta H_S$ ,  $\overline{\Delta H_S}$  related to each configuration (no BWs, BWs, or BWs+O) was averaged ( $\overline{\overline{\Delta H_S}}$ ) among same SLR scenarios (Table 3.1). Results reported as function of  $\langle \text{MWL} \rangle$  showed BWs+O experiment definitely improved  $\overline{\overline{\Delta H_S}}$  at high tide (Figure 3.15 E) compared to no BWs and gray BWs scenarios, for all simulated MWL. At low tide, BWs+O resulted in  $\overline{\overline{\Delta H_S}}$  higher than gray BWs only in 100 yrs, while it was greater than no BWs for all SLR scenarios (Figure 3.15 F). Overall, results showed  $\Delta H_S$  was maintained over time by the presence of oysters.

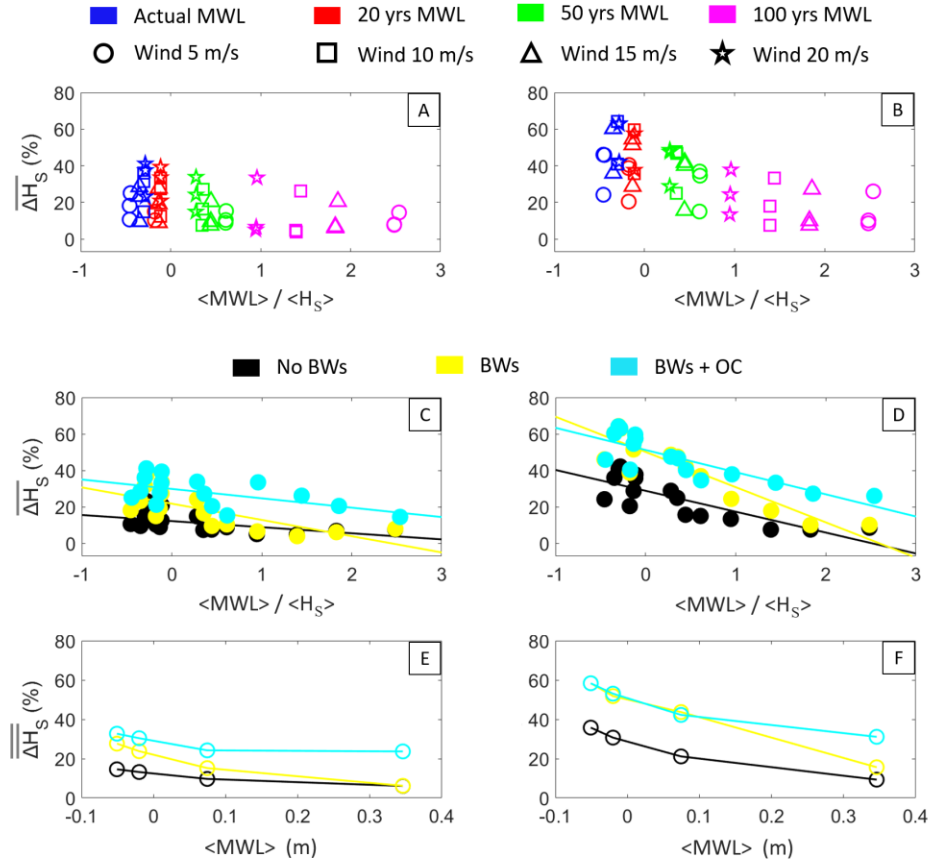


Figure 3.15. (A) Modeling  $\overline{\Delta H_S}$  over the first breakwater at high tide as function of the dimensionless variable  $\langle \text{MWL} \rangle / \langle H_S \rangle$ , for the four simulated MWL. (B) Modeling  $\overline{\Delta H_S}$  over the first breakwater at low tide as function of the dimensionless variable  $\langle \text{MWL} \rangle / \langle H_S \rangle$ , for the four simulated MWL. (C) Modeling  $\overline{\Delta H_S}$  over the first breakwater at high tide as function of the dimensionless variable  $\langle \text{MWL} \rangle / \langle H_S \rangle$ , for the three simulated scenarios (no BWs, BWs, BWs+C). (D) Modeling  $\overline{\Delta H_S}$  over the first breakwaters at low tide as function of the dimensionless variable  $\langle \text{MWL} \rangle / \langle H_S \rangle$ , for the three simulated scenarios. (E) Modeling  $\overline{\Delta H_S}$  over the first breakwaters at high tide as function of  $\langle \text{MWL} \rangle$ , for the three considered scenarios (no BWs, BWs, BWs+O). (F) Modeling  $\overline{\Delta H_S}$  over the first breakwaters at low tide as function of  $\langle \text{MWL} \rangle$ , for the three considered scenarios.

Time-averaged shear stress ( $\langle \tau \rangle$ ) on the landward ( $\langle \tau_L \rangle$ ) and seaward ( $\langle \tau_S \rangle$ ) side of breakwaters, measured at the SB and the ADCP HR deployed in the field, were found to be directly proportional to  $\langle H_S \rangle$  and inversely proportional to  $\langle \text{MWL} \rangle$  (Figure 3.16 A-E). The presence of breakwaters slightly reduced shear stress compared to the no BWs scenario, while a combination of BWs+O resulted in little further reduction of bottom stress compared to the previous two cases.

Averaged  $\langle H_s \rangle$  and  $\langle \tau \rangle$  across all simulations ( $\langle \langle H_s \rangle \rangle$  and  $\langle \langle \tau \rangle \rangle$ , respectively), were progressively reduced along each breakwater, from the first one, the closer to the Cove mouth, to the fourth one, the farther to the Cove mouth (Figure 3.16 F,G).  $\langle \langle H_s \rangle \rangle$  on the seaward side was reduced up to 15% on the fourth BW compared to the first one, and up to 20% on the landward side (Figure 3.16 F). Seaward  $\langle \langle \tau \rangle \rangle$  was reduced by up to 40% on the fourth BW compared to the first one; similarly, landward  $\langle \langle \tau \rangle \rangle$  decreased by up to 30% between the first and fourth BW (Figure 3.16 G).

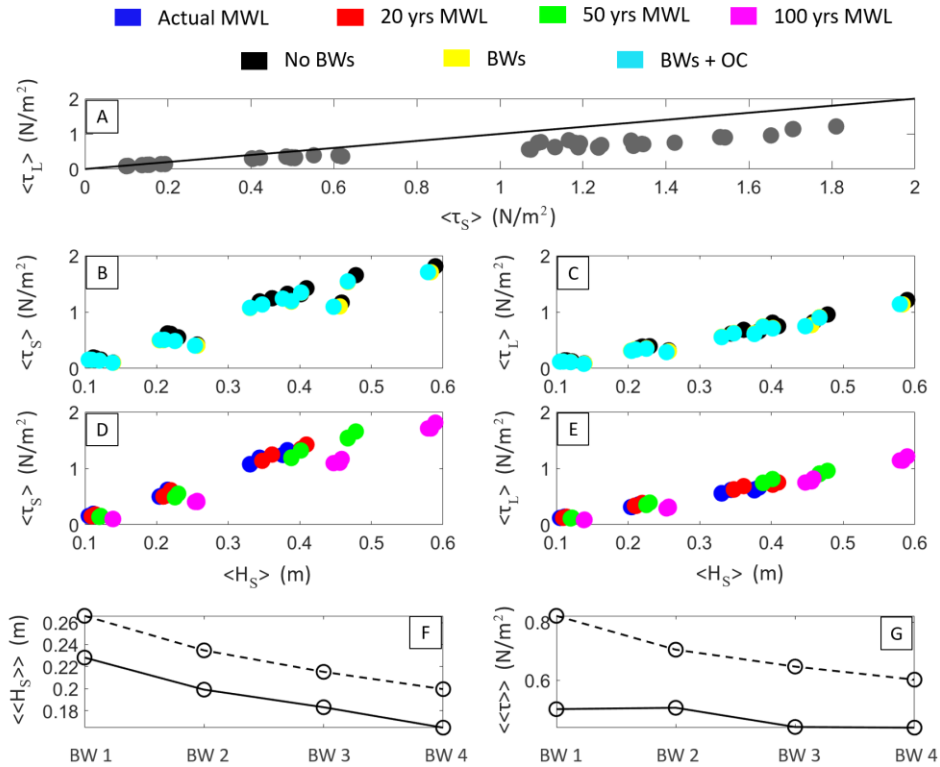


Figure 3.16 (A) Modeled  $\langle \tau_s \rangle$  (in correspondence with the Buoy) versus  $\langle \tau_L \rangle$  (in correspondence with the ADCP HR). (B) Modeling  $\langle \tau_s \rangle$  over the first breakwater as a function of  $\langle H_s \rangle$ , for the three considered scenarios (no BWs, BWs, BWs+O). (C) Modeling  $\langle \tau_L \rangle$  over the first breakwater as a function of  $\langle H_s \rangle$ , for the three considered scenarios. (D) Modeling  $\langle \tau_s \rangle$  over the first breakwater as a function of  $\langle H_s \rangle$ , for the four considered MWL. (E) Modeling  $\langle \tau_L \rangle$  over the first breakwater as function of  $\langle H_s \rangle$ , for the four considered MWL. (F) Seaward (dashed line) and landward (continuous line) modeled  $\langle \langle H_s \rangle \rangle$  along the four breakwaters. (G) Seaward (dashed line) and landward (continuous line) modeled  $\langle \langle \tau \rangle \rangle$  along the four breakwaters.

To underline morphological changes associated with different simulations, we estimated the deposition within the shore platform along each transect, as the cumulative deposition/erosion at the end of each numerical experiment. Results discussed below refer to the sum across all transects within the considered simulation. Likewise, we calculated deposition on the landward side of breakwaters and the scarp erosion/enhancement (e.g. see earlier Figure 3.13 A).

Morphodynamic results revealed deposition within the shore platform was proportional to  $\langle H_s \rangle$  and inversely proportional to the  $\langle MWL \rangle$  related to each SLR scenario. Higher  $\langle H_s \rangle$  in combination with lower  $\langle MWL \rangle$  were able to resuspend and transport higher amounts of sediments due to the greater induced shear stress. Increases in  $\langle MWL \rangle$  resulted in reduced shear stress, less resuspension and sediment transport. However, higher  $\langle MWL \rangle$  (associated with 100yrs SLR) allowed the generation of bigger  $\langle H_s \rangle$  which were still able to resuspend and transport high amounts of sediment. The deposition within the shore platform was higher in the scenario with no BWs, compared to simple BWs and BWs+O, a clear sign that coastal defense structures also reduce sediment replenishment toward the coast (Figure 3.17 A,D). Landward breakwater deposition was proportional to  $\langle H_s \rangle$  and inversely proportional to  $\langle MWL \rangle$  related to each SLR scenario. Erosion at the landward side of BWs was associated with the scenario with no BWs (due to the presence of no structure) for most of the simulations, greater for higher  $\langle MWL \rangle$  and  $\langle H_s \rangle$ . The scenario with simple BWs resulted in landward deposition (smaller for greater  $\langle MWL \rangle$ ) for the actual, 20 yrs and 50 yrs water level experiment compared to the no BWs. However, the highest  $\langle MWL \rangle$  simulated in 100 years inhibited protective benefits provided by BWs (reduced  $\Delta H_s$ ), and associated bigger  $\langle H_s \rangle$  were more able to induce landward erosion rather than deposition (as for the no BWs case scenario). The scenario with BWs+O, on the other hand, was able to maintain the deposition positive also in 100 years, thanks to oysters' capability to maintain the protective benefits ( $\Delta H_s$ ) of BWs over time (Figure 3.17 B,E). Scarp erosion/enhancement showed a similar trend to the landward deposition. It was negatively correlated to the  $\langle MWL \rangle$  and positively to  $\langle H_s \rangle$ . Scarp erosion for both cases with no BWs and gray BWs was associated with smaller  $\langle MWL \rangle$  (actual, 20

and 50 yrs) and  $\langle H_s \rangle$ , whereas the combination of higher  $\langle H_s \rangle$  with smaller  $\langle MWL \rangle$  (able to generate greater shear stress and thus sediment transport) allowed for deposition on the scarp (for both no BWs and gray BWs scenarios). However, the highest  $\langle MWL \rangle$  simulated in 100 years inhibited protective benefits provided by BWs (decreased  $\Delta H_s$ ), and associated bigger  $\langle H_s \rangle$  were more able to erode the scarp than promote deposition on it. The scenario with BWs+O was instead able to protect the scarp also in 100 years compared to the previous two cases, thanks to oysters' adaptability to SLR (Figure 3.17 C,F).

To look at the behavior of each different transect, the deposition within the shore platform, on the landward side of breakwaters and the scarp erosion/enhancement along each transect, was averaged within same case-scenarios (no BWs, BWs, BWs+O). Averaged shore deposition (*shore deposition*) was greater for the no BWs case, as mentioned earlier in the manuscript (Figure 3.17 G). It was higher on the first transect to then reduced until transect 5 and remain similar from transects six to eight. The average landward deposition (*landward deposition*) was greater for the case with BWs+O, slightly smaller for the BWs scenario and always negative for the no BWs scenario (Figure 3.17 H). *Landward deposition* increased with increasing distance to the Cove mouth from transect one to six, to then slightly decrease on transect seven and eight. Average scarp erosion/deposition (*scarp erosion/dep*) was close to zero for the BWs+O case scenario along each transect, while it was negative for both cases with no BWs and BWs, especially for transects three to eight. The greater distance to the Cove mouth resulted in greater average scarp erosion, except for the BWs+O case scenario (Figure 3.17 I).

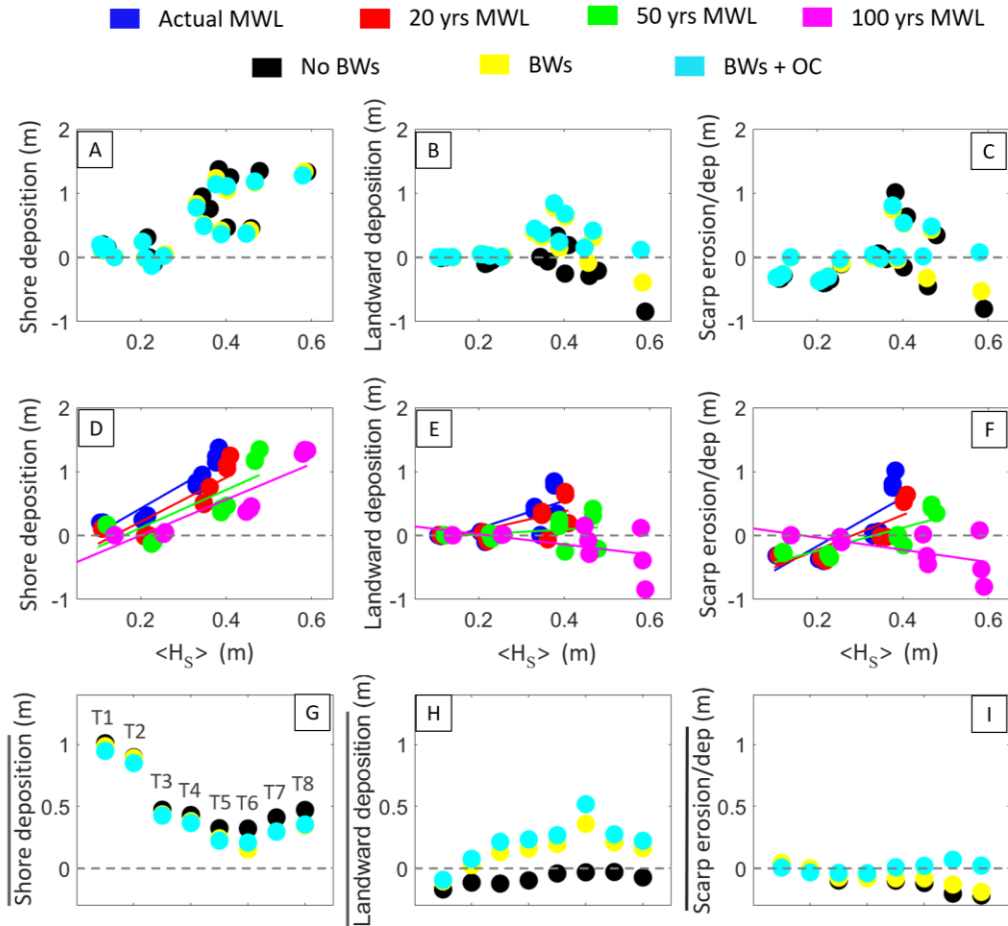


Figure 3.17 (A) Deposition within the shore platform as function of  $\langle H_s \rangle$ , for the three simulated scenarios. Deposition was equal to the cumulative value among all transects. (B) Deposition on the landward side of breakwaters as function of  $\langle H_s \rangle$ , for the three simulated scenarios. Landward deposition was equal to the cumulative value of all transects. (C) Scarp erosion/deposition as function of  $\langle H_s \rangle$ , for the three simulated scenarios. Scarp erosion/deposition was equal to the cumulative value of all transects. (D) Deposition within the shore platform as function of  $\langle H_s \rangle$ , for the four simulated MWL. Deposition was equal to the cumulative value of all transects. (E) Deposition on the landward side of breakwaters as function of  $\langle H_s \rangle$ , for the four simulated MWL. Landward deposition was equal to the cumulative value of all transects. (F) Scarp erosion/deposition as function of  $\langle H_s \rangle$ , for the four simulated MWL. Scarp erosion/deposition was equal to the cumulative value of all transects. (G) Deposition within the shore platform along each transect. Deposition was averaged over all simulations belonging to the same scenario (no BWs, BWs, BWs+O). (H) Deposition on the landward side of breakwaters along each transect. Landward deposition was averaged over all simulations belonging to the same scenario. (I) Scarp erosion/deposition along each transect. Scarp loss/enhancement was averaged over all simulations belonging to the same scenario.

To study the impact of the different configurations on the shoreline enhancement/loss, the net sedimentation rate (sediment budget) was estimated as the sum of erosion and deposition at the end of each simulation, within the internal domain shown in Figure 3.18 A. The sediment budget followed the same trend as landward BWs deposition. It was positively correlated to  $\langle H_s \rangle$  and negatively to  $\langle \text{MWL} \rangle$ . A negative, or close to zero, sediment budget was associated with smaller  $\langle H_s \rangle$  across all simulated  $\langle \text{MWL} \rangle$ , whereas higher  $\langle H_s \rangle$  allowed for shoreline enhancement. However, the highest  $\langle \text{MWL} \rangle$  simulated in 100 years inhibited protective benefits provided by BWs, and associated bigger  $\langle H_s \rangle$  were more able to produce negative values of sediment budget (net sediment loss for both cases with no BWs and gray BWs). The scenario with BWs+O was instead able to promote shoreline enhancement also in 100 years, thanks to oysters' capability to maintain the protective benefits of BWs over time (Figure 3.18 B,C). The sediment budget was better preserved over time when oysters were included in shoreline protective design.

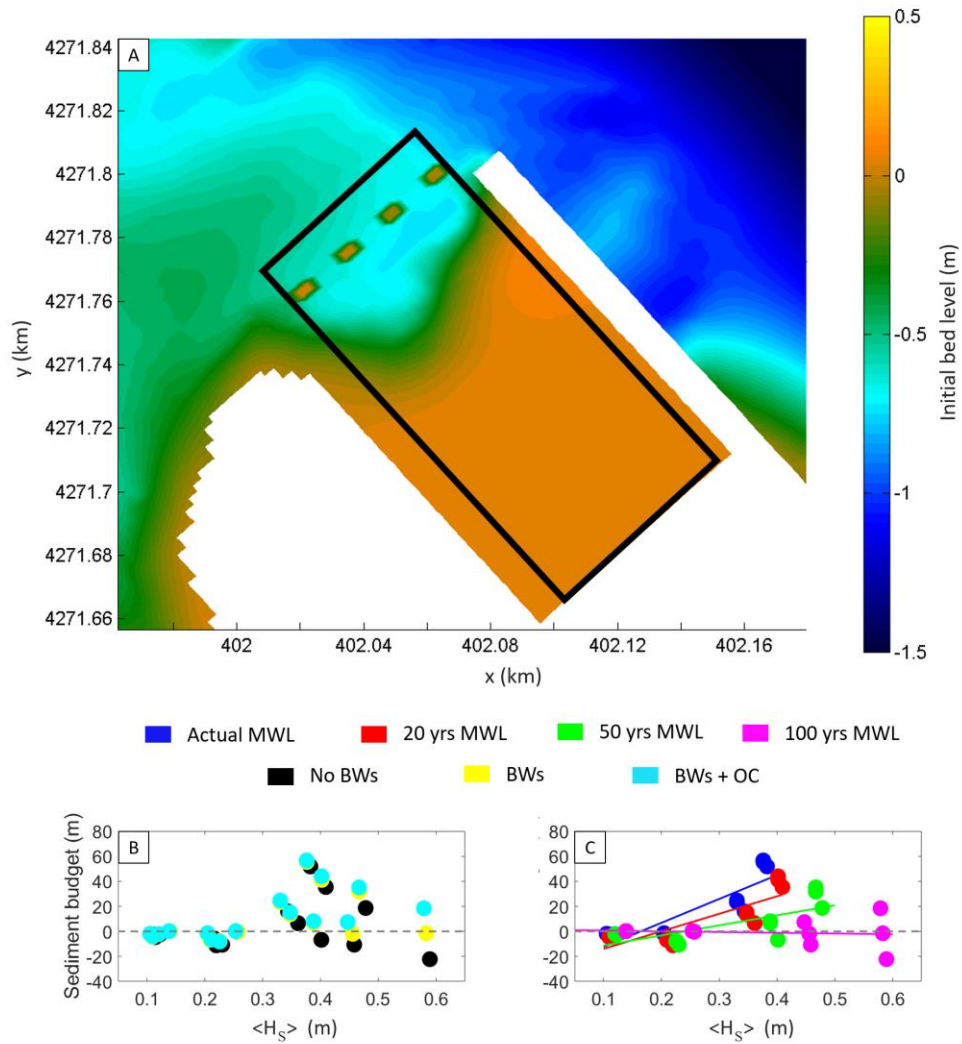


Figure 3.18 (A) Sub-domain (blue rectangular box) used to quantify the sediment budget of the shoreline. Sediment budget was defined as the cumulative value of erosion and deposition within the sub-domain. (B) Sediment budget as function of  $\langle H_s \rangle$ , for the three different scenarios (no BWs, BWs, BWs+O). (C) Sediment budget as function of  $\langle H_s \rangle$ , for the four investigated MWL.

### 3.4.3 Bill Burton State Park - Field results

The GPS survey allowed us to reconstruct the Digital Elevation Model (DEM) of the study area (Figure 3.19). Collected points were then interpolated in order to obtain a continuous map. Analysis results revealed shallow depths in the area sheltered by breakwaters (landward side of the breakwaters) and deeper waters towards the open Choptank (seaward side of the breakwaters).

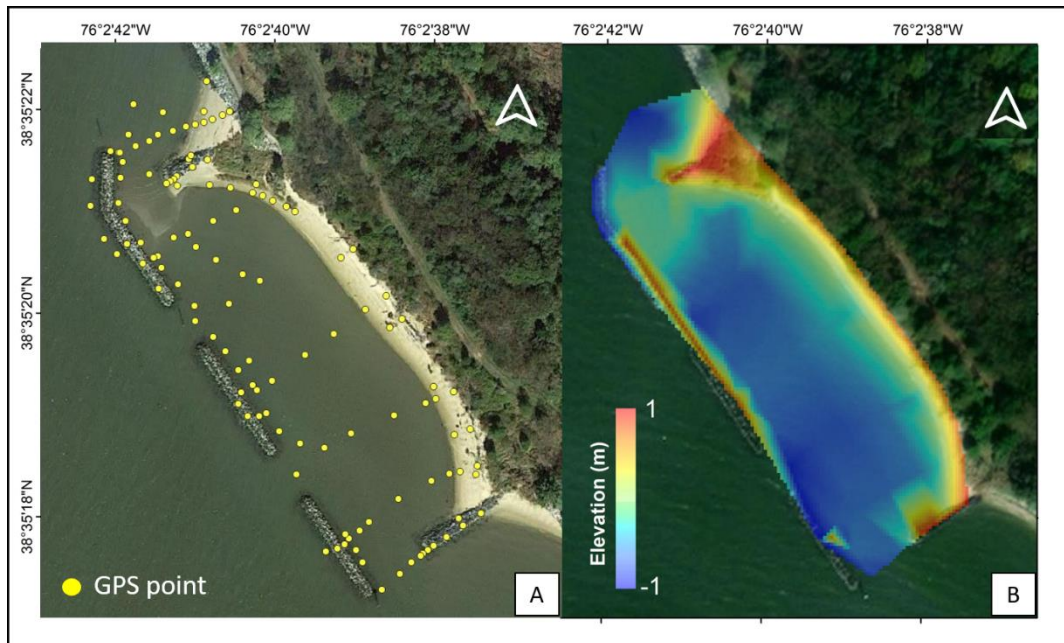


Figure 3.19 (A) Collected GSP points during our field-survey. (B) Bathymetry of the Bill Burton State Park.

Analyzes aimed at characterizing the sediment grain size in the Bill Burton State Park revealed the composition was purely composed of very fine sand with a  $D_{50}$  between 78 and 81  $\mu\text{m}$  (Table 3.4). This  $D_{50}$  value has been then entered into the model discussed in the next chapter, in order to characterize non-cohesive sediments.

Table 3.4. Sediment characteristics in the Bill Burton State Park

Sample	Sand content (%)		Mud content (%)	D <sub>50</sub> (μm)
	Fine sand	Very fine sand		
1	0	96	4	80
2	0	95	5	81
3	0	90	10	78
4	0	95	5	81

### 3.4.4 Bill Burton - Hydro and morphodynamic modeling results

The modeling performed in the Bill Burton State Park had similar purposes than the one involving the Lake Cove. Numerical simulations aimed to evaluate the long-term behavior of breakwaters to predict possible conservation plans and evaluate the use of oysters as a possible measure.

An example of the wave field and morphodynamic evolution around the breakwaters is given in Figure 3.20.

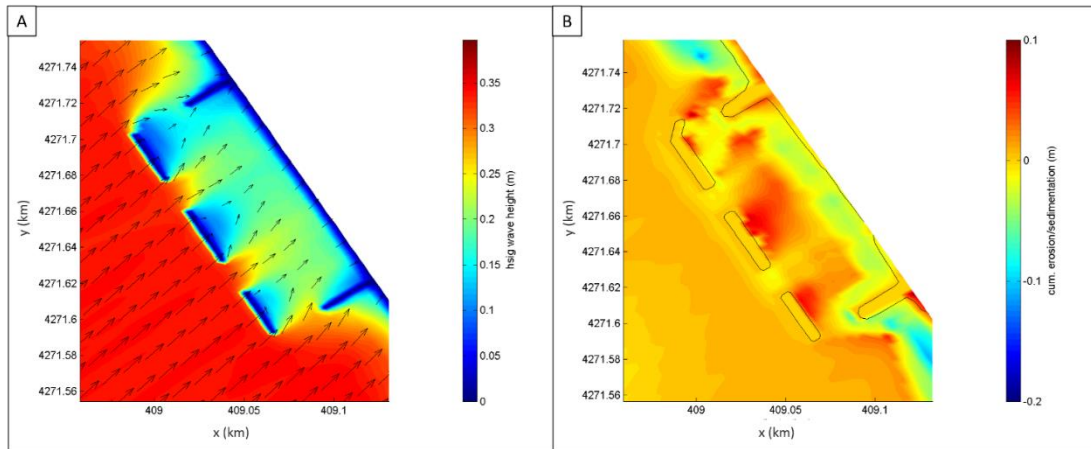


Figure 3.20. (A) Modeled wave field around breakwaters in the Bill Burton. Results are taken from simulation with actual MWL and wind intensity = 10 m/s. Black line defines bed level threshold at 0 m (NAVD88). (B) Cumulative erosion / deposition for the simulations with actual MWL and wind intensity = 10 m/s.

Hydrodynamic results showed  $\overline{\Delta H_s}$ , measured in correspondence of the middle breakwater, to be proportional to the time-averaged  $H_s$  ( $\langle H_s \rangle$ , measured at the seaward side of the middle breakwater) and inversely proportional to time-

averaged MWL ( $\langle \text{MWL} \rangle$ , measured at the seaward side of the middle breakwater), as expected. Wave dampening among all simulations gradually reduced over time due to SLR (Figure 3.21).

The coupling with oysters was only studied in simulations with MWL corresponding to 150-year SLR, capable of completely submerge breakwaters, making them suitable for oysters' incorporation. Modeling results suggested the efficiency of breakwaters was preserved also in 150 years, only when oysters were included into the breakwater design (Figure 3.21 A,B).

Time-averaged shear stress ( $\langle \tau \rangle$ ) on the landward ( $\langle \tau_L \rangle$ ) and seaward ( $\langle \tau_S \rangle$ ) side of the middle breakwater, were found to be directly proportional  $\langle H_S \rangle$  and inversely proportional to  $\langle \text{MWL} \rangle$  (Figure 3.21 C,D). Both the averaged  $\langle H_S \rangle$  and  $\langle \tau \rangle$  across all simulations ( $\langle \langle H_S \rangle \rangle$  and  $\langle \langle \tau \rangle \rangle$ , respectively) were similar along each breakwater. Landward values were reduced around 50% compared to the seaward side (Figure 3.21 E,F).

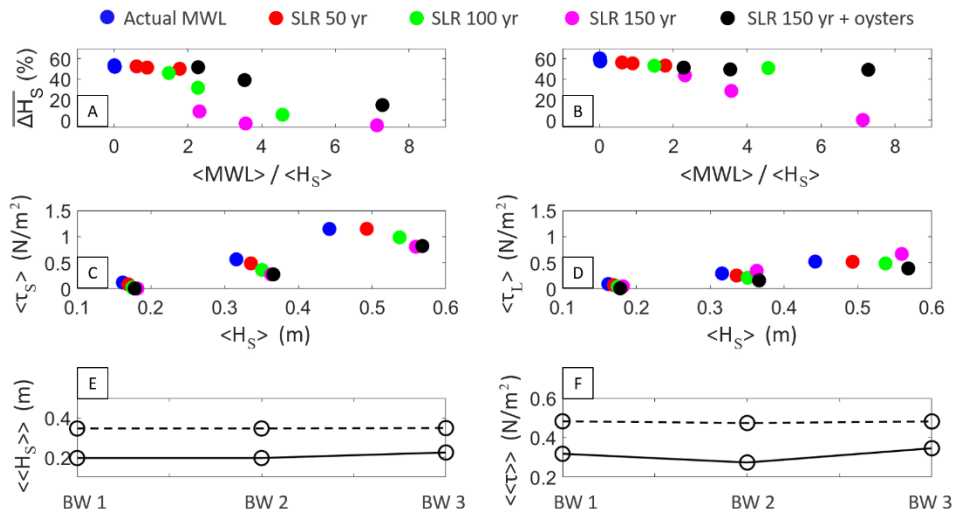


Figure 3.21 (A) Modeling  $\overline{\Delta H_S}$  over the middle breakwater at high tide as function of the dimensionless variable  $\langle \text{MWL} \rangle / \langle H_S \rangle$ . (B) Modeling  $\overline{\Delta H_S}$  over the middle breakwater at low tide as function of the dimensionless variable  $\langle \text{MWL} \rangle / \langle H_S \rangle$ . (C) Modeled  $\langle \tau_S \rangle$  over the middle breakwater as a function of  $\langle H_S \rangle$ . (D) Modeling  $\langle \tau_S \rangle$  over the middle breakwater as a function of  $\langle H_S \rangle$ . (E) Seaward (dashed line) and landward (continuous line) modeled  $\langle \langle H_S \rangle \rangle$  along the three breakwaters. (F) Seaward (dashed line) and landward (continuous line) modeled  $\langle \langle \tau \rangle \rangle$  along the three breakwaters.

To study the impact on the shoreline enhancement \ loss, a sediment budget was estimated as the sum of erosion and deposit at the end of each simulation within the internal domain shown in Figure 3.22 A. The sediment budget was positively correlated to  $\langle H_s \rangle$  and negatively to  $\langle MWL \rangle$ . It was gradually reduced over time due to SLR, and only by coupling oysters and breakwaters it was better preserved. Higher  $\langle H_s \rangle$  allowed for shoreline enhancement for the actual MWL, 50 and 100 yr SLR. However, the highest water level simulated in 150 years inhibited protective benefits provided by breakwaters, and associated bigger  $\langle H_s \rangle$  were more able to produce close to zero values of sediment budget. Oyster addition was instead able to promote shoreline enhancement also in 150 years, thanks to oysters' capability to maintain the protective benefits of breakwaters over time (Figure 3.22 B). The sediment budget was better preserved over time when oysters were included in shoreline protective designs.

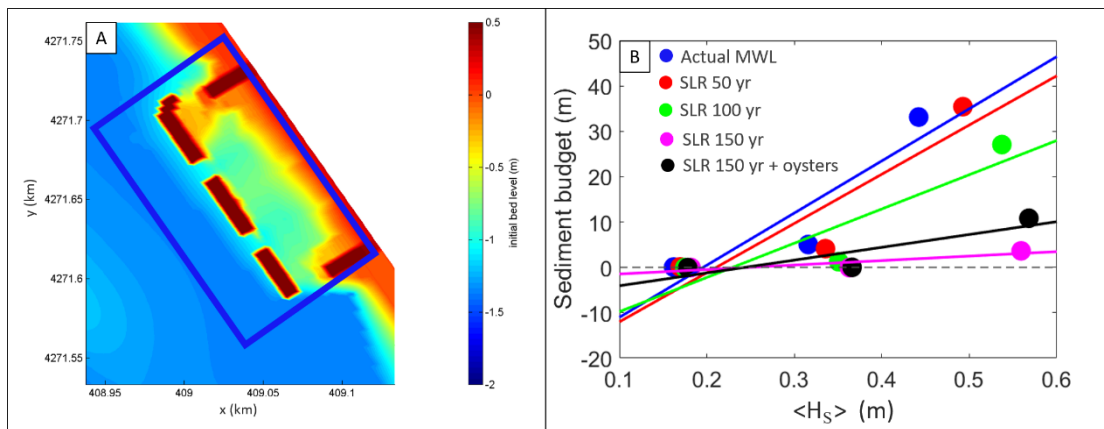


Figure 3.22 (A) Sub-domain (blue rectangular box) used to quantify the sediment budget of the shoreline. Sediment budget was defined as the cumulative value of erosion and deposition within the sub-domain. (B) Sediment budget as function of  $\langle H_s \rangle$ .

### 3.5 Discussion

#### 3.5.1 Field observations

Our study, which couple field and numerical disciplines, revealed the pivotal role of coupling oysters and submersed breakwaters in the face of SLR.

Field measurements of wave data recorded in the Lake Cove over the first BW (the closer to the Cove mouth), demonstrated the efficacy of such gray structure in absorbing wave motion, thereby reducing incoming wave height by up to 45% at high tide and 95% at low tide. Similarly, Wiberg et al. (2019), recorded wave damping by oyster reefs in the Virginia Coastal Reserve (VCR), up to 50% in water depths between 0.5 and 1 m, highlighting the importance of incoming wave direction and structure position and/or orientation regarding the breaking process. The most unfavorable wind conditions to the healthiness of the Cove's eastern side come from N/W, perpendicular to the coastline, where greater fetches lead to higher waves. Breakwaters are oriented parallel to the shore, in order to mitigate more damaging events coming from N/W. Wave data recording over the gray breakwaters, captured the most unfavorable weather conditions for coastal health (N/W wind), ideal, on the other hand, to highlight the protective benefits of breakwaters in terms of wave breaking. The MWL during our deployment was relatively low, -0.15m (NAVD88), so that at low tide breakwaters were almost fully exposed, hence the high  $\Delta H$ s. At high tide, although breakwater crests were covered by over 20 cm, results revealed  $\Delta H$ s up to 45%, underlining the protective benefits provided by our structures even when fully submerged.

Measurement of wave data collected over the partially oyster-covered breakwaters revealed an averaged increase in wave dampening at high tide compared to the case of gray breakwaters, up to 20% more, while there was no difference at low tide. However, the tidal, wind and wave heights conditions were slightly different between the two measurements, which made the comparison between wave attenuation less intuitive. Wind direction was equal in both records, NW, while gusts and mean velocities were lower for partially oyster-covered breakwaters. The slower

wind was then able to generate smaller waves, up to 25 cm, almost half of the maximum  $H_s$  associated with gray structures. The elevation of breakwater crest compared to the MWL is a crucial aspect in the behavior of these infrastructures. The data associated with gray structures (no oysters) had MWL (-0.15 m) approximately equal to breakwaters crest (approximately -0.1). The MWL associated with the partially oyster-covered breakwaters on the other hand, was higher, around -0.05 m (NAVD88). Nevertheless, the coupling with oysters increased breakwater crest of about 10 cm around 0.0 m NAVD88, closely to the recorded MWL. Wave dampening data acquired therefore more sense and clarity when compared. Even though only partially covered, our results showed breakwaters and wave attenuation have been improved by the coupling with oysters. However, our two measurements of wave data cannot fully represent differences in wave dampening between gray vs green breakwaters. Multiple records under different conditions of tide, wind and waves, would be necessary in order to fully characterize the dissipation processes due to structures with and without oysters. Future studies involving fully oyster covered breakwaters and continuous wave data recording will be necessary in order to better investigate improvements in wave attenuation. A recent study performed in the VCR by Hogan et al., 2022, supports and strengthens the use of oysters in coastal defense through coupling with OCs, confirming clear improvement in wave attenuation after OC being naturally colonized by oysters.

GPS surveys aimed to track bathymetric changes in the Lake Cove, revealed typical morphodynamic evolution of any kind of structure immersed into a water body, landward deposition and seaward scouring (Van Rijn, 2013b). The first transect showed erosion on both sides of the structure (seaward and landward), as it was the most exposed to waves and longshore currents (also it was not provided with any offshore defensive work). The second and fourth transects showed a common morphodynamic trend of submersed coastal structures, landward deposition and seaward scouring, thanks to the protection provided by the first breakwater. Transect 3 showed total erosion both in front and behind the structure as well as transect 1, likely due to the higher mud content revealed by our sediment analysis. Bed shear strength was also found to be positively correlated with the  $D_{50}$ , which supported the

onshore erosion along transect 3. Deposition on the landward side of breakwaters, however, is usually more pronounced in the middle of the structure than on both sides, due to wave diffraction. Diffracted waves curve inwards in the sheltered area of the structure and decrease in height inside it (Hsu and Silvester 1990). Flow contraction at the end or between the gap of multiple breakwaters leads to flow acceleration and scour at the tip (Lillycrop and Hughes, 1993). GPS surveys conducted in the field tracked bathymetric changes along both sides of each breakwater, where wave diffraction and flow acceleration phenomena were most pronounced. However, field results showed a progressive increase in landward deposition along each transect (except for transect 3). Erosive phenomena due to flow acceleration and wave diffraction on lateral sides of breakwaters in Lake Cove, slow down but do not prevent sediment deposition.

### 3.5.2 Numerical simulations

Numerical experiments aimed to simulate the coupling between oysters and submerged breakwaters, in order to empathize benevolent aspects related to coastal protection, under different modeling scenarios. As oysters are expected to grow with SLR (Rodriguez et al., 2014), it is reasonable to expect oyster-based infrastructures representing a valuable, greener and more resilient solution for coastal defense, in the face of climate change and SLR.

Modeling results showed gradual decay in the efficiency of simple gray breakwaters in breaking waves over time, due to SLR (in both study sites). Contrary, the coupling with oysters' resulted in overtime maintenance of protective performances of BWs, thanks to oysters ability to grow with the SLR (Rodriguez et al., 2014; Ridge et al., 2017). Similar results were also found regarding the sediment budget, defined as the cumulative sum of erosion and deposition at the end of each simulation. Higher water levels inhibited the protective action of simple breakwaters and resulted in a negative sediment budget (net loss of sediments), whereas it was kept positive when oysters were included in the modeling. Sediment concentration at

the boundaries of model domain was null. Therefore, sediment resuspension was the main mechanism that contributed to depositional and erosional processes. However, several studies in the literature addressed the issue of the sediment budget, supporting our findings. Vegetation and intense wave energy enhanced sediment retention and the stability of tidal bays (Castagno et al., 2018; Nardin et al., 2020; Vona et al., 2021). Extreme water levels due to storm-surge events also increase sediment flux toward the shore, strengthen the sediment budget (Zhu and Wiberg, 2022). SLR and increasing in storm frequencies are likely to positively contribute to shoreline resiliency if oysters will be included in future coastal restoration plans, by enhancing sediment delivery and retention within shallow coastal environments.

The case scenario with no BWs then revealed that sediment transport within the shoreline was more allowed without the presence of obstacles in front of the shore, as found by Vona et al., (2020; 2021). Modeling results showed the higher the structure, the lower sediment replenishment was allowed within the shore. However, a dynamic structure capable of growing and adapting to the SLR was able to allow more landward BW deposition and less scarp erosion over time, compared with no BWs and simple BWs scenarios (Figure 3.23).

Numerical simulation results proved the goodness of coupling oysters with gray infrastructures, in order to provide durable and self-sustainable coastal protection in the face of climate changes and SLR. However, in order for oysters to work properly as nature-based infrastructure, ideal conditions for their survival have to be found within the environment. To be most effective on a long-term basis, it is key that oyster reefs are in locations that promote oyster reef growth through regular recruitment (low energy environments such as estuaries or shallow coastal bays). Then reef habitats create positive feedback for growth, as oyster larvae can settle and actively recruit to the oyster shells, promoting reef accretion (Gutierrez et al., 2003; Scyphers et al., 2011). Recruitment and spawning rates are influenced by temperature. Warmer regions allow for longer oyster spawning periods than colder regions, resulting as more suitable and resilient environment for oyster reefs establishment through the time (Lowe et al., 2017). The elevation of the reef crest with respect to the MWL also plays an important role. Higher reefs would make

oysters spend less time submerged, thus decreasing threats from predation and sedimentation (Lenihan, 1999; Fodrie et al., 2014; Johnson and Smee, 2014). However, higher elevations would expose oysters to greater stresses due to low temperatures, desiccation, and reduced food supply which may impact oysters' survivability (Johnson and Smee, 2014; Byers et al., 2015). This is crucial when thinking of oysters as nature-based solutions because coastal defense needs higher structures that mitigate erosive waves. However, taller structures negatively impact sediment transport and, furthermore, field measurements showed that even fully submerged, breakwaters provided coastal defense by damping up to 45% of incoming waves. Furthermore, oyster growth is influenced by aerial exposure (emergence during the tidal cycle), with maximum growth rates found to occur between 20-40% of exposure (Ridge et al., 2015). Increasing in MWL due to SLR may result in additional subaqueous space for oyster vertical accretion (Rodriguez et al., 2014). MWL has also been shown to correlate with coastal erosion. When MWL is at the same level as the coastline shelf, waves dissipate directly on the shore edge, causing erosion and habitat loss, rather than gradually dissipate on the shore platform (Tonelli et al., 2010; Vona et al., 2020). Competition among species such as aquatic algae may also affect growth and benthic processes of oysters (Thomsen and McGlathery 2006; Volaric et al. 2019; Hogan and Reidenbach, 2022). Inadequate planning involving oysters that don't look at these key aspects will likely prove to be less or completely ineffective.

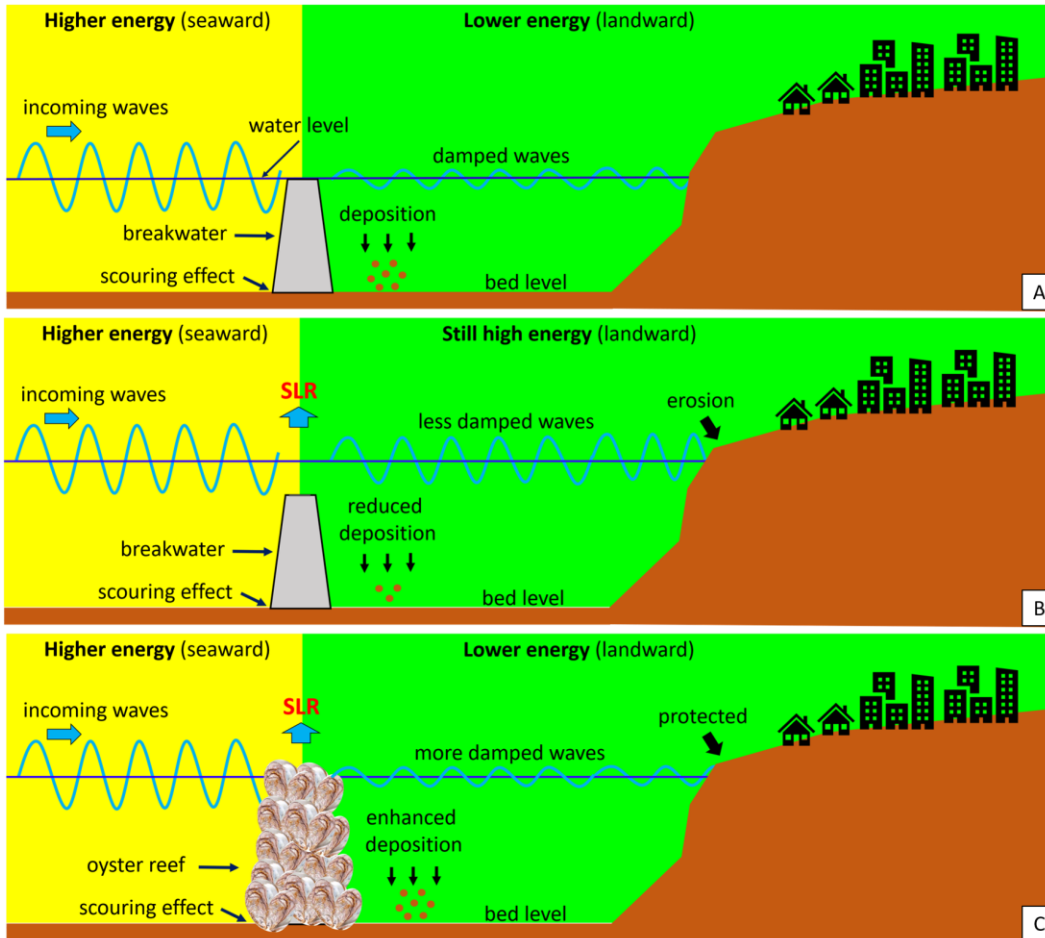


Figure 3.23. Simplified sketch of protective benefits provided by the coupling between oysters and submerged breakwaters, based on modeling results. (A) Gray breakwater only. (B) Gray breakwater with SLR. (C) Gray breakwater and oysters, capable of providing protective benefits over time.

### 3.5.3 Coastal management indications and study limitations

The primary objective of the current research was to create effective hybrid infrastructures by coupling BWs and oysters in the Lake Cove, to then measure protective benefits in terms of coastal defense. To fulfill this objective, two solutions were possible: seeding OCs with oyster larvae directly in the field (after building our castles) or taking advantage of the oyster hatchery within the HPL campus and seeding OCs into large tanks.

The seeding in the field proved to be inefficient due to multiple factors. Larvae dispersal was the first reason. Oyster larvae are recognized as good swimmers able to change their position along the water column, to then recognize the most suitable substrate to settle and grow. The transport over the space (x, y), on the other hand, is mainly due to the flowing current (Wood and Hargis, 1971; North et al., 2008). We, therefore, believe that part of the larvae has dispersed rather than remain confined around our breakwaters, resulting in low recruitment and colonization rates. Another key aspect was the water level. The MWL in Lake Cove is between 0 and 0.2m (NAVD88), just above the breakwater crests. However, variable weather conditions cause MWL to shift even below breakwater crests, exposing oysters to cold temperatures and lowering food supply, which affects their growth and survivability (Johnson and Smee, 2014; Byers et al., 2015). Another important aspect was dictated by the season during which seeding took place. Summer is characterized by high competitiveness among species (such as barnacles, aquatic vegetation and others) and this has reduced the success of settlement and colonization rate by oyster larvae over our breakwaters.

On the other hand, the seeding in the oyster hatchery proved to be very successful. Unlike the field, OCs in the hatchery was seeded individually, without building any castles. After 21 days (time needed for larvae to settle), OCs was moved into the Cove, in order to allow oysters to grow and develop within a natural environment. The large tanks avoided larvae dispersal, capable then of colonizing OCs with a higher success rate than the field. In addition, seeding in the tanks avoided the high competition between species that occurred during summer. The final result was great. After 2/3 years OCs were fully colonized by oysters, demonstrating the goodness of OC as a methodology to restore the oyster population (Theuerkauf et al., 2015; Hogan et al., 2022).

We tried to fill challenges encountered during fieldwork, through the numerical modeling Delft3D. Delft3D is well recognized for reproducing properly morphological and hydrodynamic patterns (Roelvink et al., 2015). However, oyster simulation as occurred in this study was pretty unique, but not fully replicable by the model. We only simulated vertical growth and not lateral reef expansion (Rodriguez

et al., 2014; Ridge et al., 2015), which may result in underestimated  $\Delta H$ s. Moreover, oyster vertical accretion was approximated at the same rate of SLR, similar to the reef crest, but slower than the growth rate occurring below the reef crest (Rodriguez et al., 2014; Byers et al., 2015; Ridge et al., 2015). Furthermore, increasing in mean sea level due to SLR was not dynamically simulated in our simulations. MWL associated with the considered SLR scenario was increased and kept constant during the simulation run. Consequently, oysters' growth also did not occur dynamically. Breakwater crest was increased until MWL (and kept constant) associated with the considered SLR scenario in each numerical experiment.

An oyster reef increases bed friction due to the rough and irregular three-dimensional structure it reaches once fully developed. Changes in the roughness also impact the drag force these reefs exert on flow hydrodynamic (Wright et al., 1990; Style, 2015; Kitsikoudis et al., 2020), thus on dissipative and protective features such as  $\Delta H$ s. However, the impact of frictional changes may be negligible when compared to reef elevation changes. Sensitivity analyses further showed that changing the roughness coefficient over our breakwaters did not particularly impact  $\Delta H$ s (Figure A8). Future investigations involving the full development of an oyster reef over time and space, as well as studies aimed at quantifying the impact of the roughness of an oyster reef on wave breaking, will be appropriate in order to fully evaluate the behavior of these nature-based infrastructures for coastal protection.

On the other hand, the high spatial resolution of the model provided reasonable outcomes regarding morphodynamic evolution of the Cove and Bill Burton over time. However, BWs were only represented by a few grid cells (in both models), resulting in lower resolution around the structures. Moreover, morphological analyses were based on short-duration simulations and did not include effects of long-term post-depositional change (e.g., subsidence, and long-term compaction). Therefore, our estimate may overpredict morphological changes over time within Lake Cove and Bill Burton, as shown by the high sediment budget associated with lower mean sea levels and bigger waves. Furthermore, changes in the water level associated with spring-neap tidal cycle were not considered due to computational reasons; the tide was kept constant in all simulations.

However, our model was still able to provide fundamental insights on the coupling between oysters and submersed breakwaters, showing  $\Delta H$ s and sediment budget may be preserved over time thanks to oysters' capability to self-adapt and grow with climate changes and SLR.

### 3.6 Conclusions

Our study analyzed hydrodynamic and morphodynamic aspects of gray structures for coastal defense, such as breakwaters, and aimed to enhance the use of oysters in coastal safety, in order to deal with future SLR and climate change scenarios. Extensive field data was collected in the Lake Cove, where four man-made breakwaters, built by coupling several OCs (also to promote oyster establishment, were investigated to measure protective benefits in terms of shoreline defense, such as  $\Delta H$ s and morphological changes. Delft3D-SWAN was then used to model the coupling between oysters and submerged breakwaters to simulate future scenarios of SLR and climate change, for the Lake Cove and the Bill Burton State Park.

Field studies showed gray breakwaters in the Lake Cove able to provide shoreline protection by attenuating incoming wave energy and promoting sediment deposition. The longshore current induced erosion at the Cove mouth which also affects part of the first breakwater along transect 1. Deposition is higher within the sheltered area except for transect 3 due to higher mud content revealed from sediment analysis. The model well replicated observed  $\Delta H$ s and morphological changes (except for transect 3).

Modeling results have shown a loss of protective benefits over time by gray breakwaters due to increase in sea level for both the Lake Cove and Bill Burton, except when coupled with oysters, capable of self-adapting and growing with SLR.  $\Delta H$ s drastically decreased over time, but remained significant only when oysters were included. The sediment budget of the shoreline shifted towards negative values (net loss of sediments) as well as the water level increased. However, oysters allowed the balance to be maintained positive also in 100 years.

Challenges encountered in the field (Lake Cove) did not allow oysters' establishment over our OC breakwaters, underlining the importance of environmental and biogeochemical conditions for reefs' establishment, growth and survivability. Water level and aerial exposure, as well as geographical location, temperature and salinity are key factors to consider when involving oysters in coastal protection. Future restoration plans involving oysters in coastal defense should definitely take these crucial aspects into account, in order to properly protect the coast in the face of climate changes and SLR, while also providing many other useful ecosystem services for the environment.

The next and last chapter gets deeper into the roughness of breakwaters. Field and numerical studies described in this chapter could not describe the effect of different roughness (with and without oysters) on flow hydrodynamics, as the spatial scale of the phenomenon was too small to be captured by our instruments. Therefore, a laboratory approach was adopted in order to deal with such a research topic.

### 3.7 Nomenclature

ADCP HR	Acoustic Doppler Current Profiler – High Resolution
ADCP LR	Acoustic Doppler Current Profiler – Low Resolution
BWs	Breakwaters
BWs+O	Breakwaters with oysters
$\Delta H_s$	Wave dampening
$\overline{\Delta H_s}$	Averaged $\Delta H_s$ among high tide peaks and low tide troughs
$\overline{\overline{\Delta H_s}}$	Averaged $\overline{\Delta H_s}$ across all simulations
$H_s$	Significant wave height
$\langle H_s \rangle$	Time averaged $H_s$
$\langle\langle H_s \rangle\rangle$	Averaged $\langle H_s \rangle$ across all simulations
HPL - UMCES	Horn Point Laboratory – University of Maryland Center for Environmental Science
<i>Landward deposition</i>	Deposition on the landward side of breakwaters averaged across same case scenarios (no BWs, BWs, BWs+O)
MWL	Mean water level
$\langle \text{MWL} \rangle$	Time averaged MWL
NNBFs	Natural and Nature-Based Features
OCs	Oyster castles
SB	Spotter Buoy
<i>Scarp erosion/deposition</i>	Scarp erosion/enhancement averaged across same case scenarios (no BWs, BWs, BWs+O)
<i>Shore deposition</i>	Deposition within the shore platform averaged across same case scenarios (no BWs, BWs, BWs+O)
$\tau$	Shear stress
$\tau_L$	Shear stress at the landward side of breakwaters
$\tau_S$	Shear stress at the seaward side of breakwaters
$\langle \tau \rangle$	Time averaged $\tau$
$\langle \tau_L \rangle$	Time averaged $\tau_L$

$\langle \tau_s \rangle$	Time averaged $\tau_s$
$\langle \langle \tau \rangle \rangle$	Averaged $\langle \tau \rangle$ across all simulations
$\langle \langle \tau_L \rangle \rangle$	Averaged $\langle \tau_L \rangle$ across all simulations
$\langle \langle \tau_s \rangle \rangle$	Averaged $\langle \tau_s \rangle$ across all simulations

### 3.8 References

- Battjes, J. A., and Janssen, J. P. F. M. (1978). “Energy loss and set-up due to breaking of random waves,” in *Coastal Engineering*, 569–587.
- Berlamont, J., Ockenden, M., Toorman, E., and Winterwerp, J. (1993). The characterisation of cohesive sediment properties. *Coast. Eng.* 21, 105–128. doi: 10.1016/0378-3839(93)90047-C
- Birben, A.R.; Özölçer, İ.H.; Karasu, S.; Kömürçü, M.İ. Investigation of the effects of offshore breakwater parameters on sediment accumulation. *Ocean Engineering*, **2007**, 34, pp.284-302.
- Blott, S. J., & Pye, K. (2001). GRADISTAT: a grain size distribution and statistics package for the analysis of unconsolidated sediments. *Earth surface processes and Landforms*, 26(11), 1237-1248.
- Board, O.C.; National Research Council. Mitigating shore erosion along sheltered coasts; National Academic Press: 500 Fifth Street, N.W. Washington, DC 20001, USA, 2007.
- Boesch, D. F., Atkinson, L. P., Boicourt, W. C., Boon, J. D., Cahoon, D. R., Dalrymple, R. A., ... & Sommerfield, C. K. (2013). Updating Maryland's sea-level rise projections.
- Boesch, D. F., Boicourt, W. C., Cullather, R. I., Ezer, T., Galloway Jr, G. E., Johnson, Z. P., ... & Sweet, W. V. (2018). *Sea-level rise: projections for Maryland 2018* (No. GSFC-E-DAA-TN64580).
- Butler, P.A., 1954. Summary of our knowledge of the oyster in the Gulf of Mexico.
- Byers, J. E., Grabowski, J. H., Piehler, M. F., Hughes, A. R., Weiskel, H. W., Malek, J. C., & Kimbro, D. L. (2015). Geographic variation in intertidal oyster reef properties and the influence of tidal prism. *Limnology and Oceanography*, 60(3), 1051-1063.
- Capelle, J.J., Leuchter, L., de Wit, M., Hartog, E. and Bouma, T.J., 2019. Creating a window of opportunity for establishing ecosystem engineers by adding substratum: a case study on mussels. *Ecosphere*, 10(4), p.e02688.
- Castagno, K.A., Jiménez-Robles, A.M., Donnelly, J.P., Wiberg, P.L., Fenster, M.S. and Fagherazzi, S., 2018. Intense storms increase the stability of tidal bays. *Geophysical Research Letters*, 45(11), pp.5491-5500.
- Chandler, R.J., 1988. The in-situ measurement of the undrained shear strength of clays using the field vane (pp. 13-44). West Conshohocken, PA, USA: ASTM International.

- Chowdhury, M. S. N., Walles, B., Sharifuzzaman, S. M., Shahadat Hossain, M., Ysebaert, T., & Smaal, A. C. (2019). Oyster breakwater reefs promote adjacent mudflat stability and salt marsh growth in a monsoon dominated subtropical coast. *Scientific reports*, 9(1), 1-12.
- Chu, F.-L. E., La Peyre, J. F. & Burreson, C. S. Perkinsus marinus infection and potential defense-related activities in Eastern Oysters, Crassostrea virginica: salinity effects. *J. Invertebr. Pathol.* 62, 226–232 (1993).
- Coen, L. D., Brumbaugh, R. D., Bushek, D., Grizzle, R., Luckenbach, M. W., Posey, M. H., ... & Tolley, S. G. (2007). Ecosystem services related to oyster restoration. *Marine Ecology Progress Series*, 341, 303-307
- Creel, L. Ripple effects: Population and coastal regions; Population Reference Bureau: 1875 Connecticut Ave., NW, Suite 520, Washington, DC 20009, USA, 2003; pp. 1-7.
- Dame, R. F., & Patten, B. C. (1981). Analysis of energy flows in an intertidal oyster reef. *Marine Ecology Progress Series*, 5(2), 115-124.
- Davis, J. L., Currin, C. A., O'Brien, C., Raffenburg, C., and Davis, A. (2015). Living shorelines: coastal resilience with a blue carbon benefit. *PLoS One* 10:e0142595. doi: 10.1371/journal.pone.0142595
- Douglass, S.L.; Pickel, B.H. The tide doesn't go out anymore - the effect of bulkheads on urban shorelines. *Shore and Beach*, 1999, 67, pp. 19-25.
- Edmonds, D. A., and Slingerland, R. L. (2010). Significant effect of sediment cohesion on delta morphology. *Nat. Geosci.* 3, 105–109. doi: 10.1038/ngeo730
- Ferrario, F., Beck, M. W., Storlazzi, C. D., Micheli, F., Shepard, C. C., & Airoidi, L. (2014). The effectiveness of coral reefs for coastal hazard risk reduction and adaptation. *Nature communications*, 5(1), 1-9
- Fingerman, M.I.L.T.O.N. and Fairbanks, L.D., 1957. Heat death and associated weight loss of the oyster *Crassostrea virginica*. *Tulane Stud. Zool*, 5(4), pp.55-68.
- Fivash, G.S., Stüben, D., Bachmann, M., Walles, B., van Belzen, J., Didderen, K., Temmink, R.J., Lengkeek, W., van der Heide, T. and Bouma, T.J., 2021. Can we enhance ecosystem-based coastal defense by connecting oysters to marsh edges? Analyzing the limits of oyster reef establishment. *Ecological Engineering*, 165, p.106221.
- Fodrie, F. J. et al. Classic paradigms in a novel environment: inserting food web and productivity lessons from rocky shores and saltmarshes into biogenic reef restoration. *J. Appl. Ecol.* 51, 1314–1325 (2014).
- Galtsoff, P.S., 1964. The American oyster, *Crassostrea virginica* gmelin (Vol. 64). US Government Printing Office.

Gittman, R. K., Peterson, C. H., Currin, C. A., Fodrie, F. J., Piehler, M. F., and Bruno, J. F. (2016a). Living shorelines can enhance the nursery role of threatened estuarine habitats. *Ecol. Appl.* 26, 249–263 doi: 10.1890/14-0716

Goda, Y. (2000). Random Seas and Design of Maritime Structures, Adv. Ser. *Ocean Eng*, 15, 443.

Grabowski, J. H. & Peterson, C. H. Restoring oyster reefs to recover ecosystem services in *Ecosystem Engineers: Concepts, Theory and Applications*. (eds. Cuddington, K., Byers, J. E., Wilson, W. G. & Hastings, A.) Elsevier/Academic Press, Netherlands. *Ecosystem Engineers: Concepts, Theory and Application*. Netherlands, Elsevier/Academic Press. pp. 281–298 (2007).

Gunter, G., 1954. The problem in oyster taxonomy. *Systematic Zoology*, 3(3), pp.134-137.

Gutiérrez, J. L., Jones, C. G., Strayer, D. L., & Iribarne, O. O. (2003). Mollusks as ecosystem engineers: the role of shell production in aquatic habitats. *Oikos*, 101(1), 79-90.

Hasselmann, K. F., Barnett, T. P., Bouws, E., Carlson, H., Cartwright, D. E., Eake, K., et al. (1973). Measurements of Wind-Wave Growth and Swell Decay During the Joint North Sea Wave Project (JONSWAP). *Ergänzungsheft zur Deutschen Hydrographischen Zeitschrift, Reihe A*.

Hogan, S., & Reidenbach, M. A. (2022). Quantifying Tradeoffs in Ecosystem Services Under Various Oyster Reef Restoration Designs. *Estuaries and Coasts*, 45(3), 677-690.

Hsu, J.R.C., and R. Silvester. 1990. Accretion behind single offshore breakwater. *Journal of Waterway, Port, Coastal, and Ocean Engineering* 116 (3): 362–380. [https://doi.org/10.1061/\(ASCE\) 0733-950X\(1990\)116:3\(362\)](https://doi.org/10.1061/(ASCE) 0733-950X(1990)116:3(362)).

Hudson, R.Y., Herrmann, F.A. and Sager, R.A., 1979. *Coastal hydraulic models* (No. SR-5)

Johnson, K. D. & Smee, D. L. Predators influence the tidal distribution of oysters (*Crassostrea virginica*). *Mar. Biol.* 161, 1557–1564 (2014).

Karimpour, A. and Chen, Q., 2017. Wind wave analysis in depth limited water using OCEANLYZ, A MATLAB toolbox. *Computers & Geosciences*, 106, pp.181-189.

Kay, R; Alder, J. *Coastal Planning and Management*, 2nd ed.; Taylor & Francis: 270 Madison Ave, New York, NY 10016, USA, 2005.

Kennedy, V.S., Newell, R.I. and Shumway, S., 1996. Natural environmental factors. The eastern oyster *Crassostrea virginica*. Maryland Sea Grant: College Park, 467, p.513.

- Lenihan, H.S. 1999. Physical-biological coupling on oyster reefs: How habitat structure influences individual performance. *Ecological Monographs* 69: 251–275.
- Lesser, G. R., Roelvink, J. A., van Kester, J. A. T. M., and Stelling, G. S. (2004). Development and validation of a three-dimensional morphological model. *Coast. Engl.* 51, 883–915. doi: 10.1016/j.coastaleng.2004.07.014
- Lévêque, E.; Toschi, F.; Shao, L.; Bertoglio, J.P. Shear-improved Smagorinsky model for large-eddy simulation of wall-bounded turbulent flows. *Journal of Fluid Mechanics*, 2007, 570, pp.491-502
- Lilycrop, W.J., and S.A. Hughes. 1993. Scour hole problems experienced by the Corps of Engineers; Data Presentation and Summary. CERC-93-2
- Lowe, M.R., Sehlinger, T., Soniat, T.M. and La Peyre, M.K., 2017. Interactive effects of water temperature and salinity on growth and mortality of eastern oysters, *Crassostrea virginica*: a meta-analysis using 40 years of monitoring data. *Journal of Shellfish Research*, 36(3), pp.683-697.
- Medcof, J.C., 1939. Larval life of the oyster (*Ostrea virginica*) in Bideford River. *Journal of the Fisheries Board of Canada*, 4(4), pp.287-301.
- Morris, R. L., La Peyre, M. K., Webb, B. M., Marshall, D. A., Bilkovic, D. M., Cebrian, J., ... & Swearer, S. E. (2021). Large-scale variation in wave attenuation of oyster reef living shorelines and the influence of inundation duration. *Ecological Applications*, 31(6), e02382.
- Mory, M., and L. Hamm. 1997. Wave height, setup and currents around a detached breakwater submitted to regular or random wave forcing. *Coastal Engineering* 31 (1-4): 77–96. [https://doi.org/10.1016/S0378-3839\(96\)00053-1](https://doi.org/10.1016/S0378-3839(96)00053-1).
- Mouret G (1921). Antoine Chézy: histoire d'une formule d'hydraulique. *Annales des Ponts et Chaussées* 61 165-259
- Nardin, W., & Fagherazzi, S. (2012). The effect of wind waves on the development of river mouth bars. *Geophysical research letters*, 39(12).
- Nardin, W., Woodcock, C. E., & Fagherazzi, S. (2016a). Bottom sediments affect *Sonneratia* mangrove forests in the prograding Mekong delta, Vietnam. *Estuarine, Coastal and Shelf Science*, 177, 60-70.
- Nardin, W., Edmonds, D. A., and Fagherazzi, S. (2016b). Influence of vegetation on spatial patterns of sediment deposition in deltaic islands during flood. *Adv. Water Resour.* 93, 236–248. doi: 10.1016/j.advwatres.2016.01.001
- Nardin, W., Lera, S. and Nienhuis, J., 2020. Effect of offshore waves and vegetation on the sediment budget in the Virginia Coast Reserve (VA). *Earth Surface Processes and Landforms*, 45(12), pp.3055-3068.

- Nardin, W., Taddia, Y., Quitadamo, M., Vona, I., Corbau, C., Franchi, G., ... & Pellegrinelli, A. (2021). Seasonality and Characterization Mapping of Restored Tidal Marsh by NDVI Imageries Coupling UAVs and Multispectral Camera. *Remote Sensing*, *13*(21), 4207.
- North, E. W., Schlag, Z., Hood, R. R., Li, M., Zhong, L., Gross, T., & Kennedy, V. S. (2008). Vertical swimming behavior influences the dispersal of simulated oyster larvae in a coupled particle-tracking and hydrodynamic model of Chesapeake Bay. *Marine Ecology Progress Series*, *359*, 99-115.
- Oppenheimer, M., & Hinkel, J. (2018). Sea Level Rise and Implications for Low Lying Islands, Coasts and Communities. *Notes*, *23*.
- Palinkas, C. M., & Russ, E. (2019). Spatial and temporal patterns of sedimentation in an infilling reservoir. *Catena*, *180*, 120-131.
- Partheniades, E. Erosion and deposition of cohesive soils. *Journal of the Hydraulics Division*, **1965**, 91, pp.105-139.
- Patrick, C. J., Weller, D. E., & Ryder, M. (2016). The relationship between shoreline armoring and adjacent submerged aquatic vegetation in Chesapeake Bay and nearby Atlantic coastal bays. *Estuaries and Coasts*, *39*(1), 158-170.
- Pilarczyk, K.W. 2003. Design of low-crested (submerged) structures – An overview –. In 6th international conference on coastal and port engineering in developing countries, Colombo, Sri Lanka.
- Pilkey, O.H.; Wright, W. Seawalls versus Beaches. *Journal of Coastal Research*, 1988, special issue n° 4, pp. 41-64.
- Post, J.C.; Lundin, C.G. Guidelines for integrated coastal zone management; The World Bank: Headquarters, 1818 H Street, NW Washington, DC 20433, USA, 1996.
- Ridge, J. T., Rodriguez, A. B., and Fodrie, F. J. (2017). Evidence of exceptional oyster-reef resilience to fluctuations in sea level. *Ecol. Evol.* *7*, 10409–10420. doi: 10.1002/ece3.3473
- Rodi, W.; Scheuerer, G. Scrutinizing the k-epsilon-model under adverse pressure gradient conditions. 4th Symposium on Turbulent Shear Flows, 1984, pp. 2-8.
- Rodriguez, A. B., Fodrie, F. J., Ridge, J. T., Lindquist, N. L., Theuerkauf, E. J., Coleman, S. E., ... & Kenworthy, M. D. (2014). Oyster reefs can outpace sea-level rise. *Nature climate change*, *4*(6), 493-497.
- Roelvink, J. A., & Van Banning, G. K. F. M. (1995). Design and development of DELFT3D and application to coastal morphodynamics. *Oceanographic Literature Review*, *11*(42), 925.

- Russ, E. R., & Palinkas, C. M. (2018). Seasonal-scale and decadal-scale sediment-vegetation interactions on the subaqueous Susquehanna River delta, upper Chesapeake Bay. *Estuaries and Coasts*, 41(7), 2092-2104.
- Sanford, L. P. (1994). Wave-forced resuspension of upper Chesapeake Bay muds. *Estuaries*, 17(1), 148-165.
- Scyphers, S. B., Powers, S. P., Heck Jr, K. L., & Byron, D. (2011). Oyster reefs as natural breakwaters mitigate shoreline loss and facilitate fisheries. *PloS one*, 6(8), e22396.
- Scyphers, S. B., Gouhier, T. C., Grabowski, J. H., Beck, M. W., Mareska, J., and Powers, S. P. (2015). Natural shorelines promote the stability of fish communities in an urbanized coastal system. *PLoS One* 10:e0118580. doi: 10.1371/journal.pone.0118580
- Styles, R. (2015). Flow and turbulence over an oyster reef. *Journal of Coastal Research*, 31(4), 978-985.
- Suh, K., and R.A. Dalrymple. 1987. Offshore breakwaters in laboratory and field. *Journal of Waterway, Port, Coastal, and Ocean Engineering* 113 (2): 105–121. [https://doi.org/10.1061/\(ASCE\) 0733-950X\(1987\)113:2\(105\)](https://doi.org/10.1061/(ASCE) 0733-950X(1987)113:2(105)).
- Sutton-Grier, A. E., Wowk, K., and Bamford, H. (2015). Future of our coasts: the potential for natural and hybrid infrastructure to enhance the resilience of our coastal communities, economies and ecosystems. *Environ. Sci. Policy* 51, 137–148. doi: 10.1016/j.envsci.2015.04.006
- Sutton-Grier, A. E., Gittman, R. K., Arkema, K. K., Bennett, R. O., Benoit, J., Blicht, S., ... & Grabowski, J. H. (2018). Investing in natural and nature-based infrastructure: building better along our coasts. *Sustainability*, 10(2), 523.
- Taddia, Y., Pellegrinelli, A., Corbau, C., Franchi, G., Staver, L. W., Stevenson, J. C., & Nardin, W. (2021). High-resolution monitoring of tidal systems using UAV: A case study on Poplar Island, MD (USA). *Remote Sensing*, 13(7), 1364.
- Temmerman, S., Meire, P., Bouma, T. J., Herman, P. M., Ysebaert, T., and De Vriend, H. J. (2013). Ecosystem-based coastal defence in the face of global change. *Nature* 504, 79–83. doi: 10.1038/nature12859
- Theuerkauf, S. J., Burke, R. P., & Lipcius, R. N. (2015). Settlement, growth, and survival of eastern oysters on alternative reef substrates. *Journal of Shellfish Research*, 34(2), 241-250.
- Thomsen, M.S., and K. McGlathery. 2006. Effects of accumulations of sediments and drift algae on recruitment of sessile organisms associated with oyster reefs. *Journal of Experimental Marine Biology and Ecology* 328: 22–34.

- Tonelli, M.; Fagherazzi, S.; Petti, M. Modeling wave impact on salt marsh boundaries. *Journal of geophysical research: Oceans*, **2010**, 115(C9).
- U.S. Army Corps of Engineers (USACE). 2012. *Engineering with nature fact sheet*. [https://ewn.el.erdc.dren.mil/pub/EWNFactSheet\\_Final.pdf](https://ewn.el.erdc.dren.mil/pub/EWNFactSheet_Final.pdf).
- Van Rijn, L.C. Principles of sediment transport in rivers, estuaries and coastal seas. (Vol. 1006, pp. 11-3). *Amsterdam: Aqua publications*, **1993**, 1006, pp. 11-3.
- Van Rijn, L. C. 2013a. Design of hard coastal structures against erosion. Accessed online 22/10/2018. <https://www.leovanrijn-sediment.com/papers/Coastalstructures2013.pdf>. Accessed 22 Oct 2018.
- Van Rijn, L. C. (2013b). Local scour near structures. *Taken from: www.leovanrijnsediment.com*.
- Volaric, M.P., P. Berg, and M.A. Reidenbach. 2019. An invasive macroalga alters ecosystem metabolism and hydrodynamics on a tidal flat. *Marine Ecology Progress Series* 628: 1–16.
- Vona, I., Gray, M. W., and Nardin, W. (2020). The impact of submerged breakwaters on sediment distribution along marsh boundaries. *Water* 12:1016. doi: 10.3390/w12041016
- Vona, I., Palinkas, C.M. and Nardin, W., 2022. Sediment Exchange Between the Created Saltmarshes of Living Shorelines and Adjacent Submersed Aquatic Vegetation in the Chesapeake Bay. *Coastal Wetlands Dynamics*.
- White, M. E. & Wilson, E. A. In *The eastern oyster Crassostrea virginica* (eds. Kennedy, V. S., Newell, R. I. E. & Eble, A. F.) 559–580 (Maryland Sea Grant College, 1996)
- Wiberg, P.L.; Taube, S.R.; Ferguson, A.E.; Kremer, M.R.; Reidenbach, M. A. Wave attenuation by oyster reefs in shallow coastal bays. *Estuaries and coasts*, 2019, 42, pp. 331-347
- Williams, A. T., Rangel-Buitrago, N., Pranzini, E., & Anfuso, G. (2018). The management of coastal erosion. *Ocean & Coastal Management*, 156, 4-20.
- Wood, L. H., & Hargis, W. J. (1971). *Transport of bivalve larvae in a tidal estuary* (pp. 29-44). Cambridge University Press.
- Wright LD., Gammischand RA., Byrne RJ, 1990. Hydraulic roughness and mobility of three oyster-bed artificial substrate materials. *Journal of Coastal Research*, 6(4), 867–878. [Google Scholar](#)
- Zhang, K., Douglas, B. C., & Leatherman, S. P. (2004). Global warming and coastal erosion. *Climatic change*, 64(1), 41-58.

Zhu, Q., & Wiberg, P. L. (2022). The importance of storm surge for sediment delivery to microtidal marshes. *Journal of Geophysical Research: Earth Surface*, 127(9), e2022JF006612.

## Chapter 4: Oysters' integration on submerged breakwaters: a laboratory and numerical experiment with scaled-down oyster castles

### Abstract

Oyster populations within the Chesapeake Bay have been drastically reduced over the past few decades mainly due to overharvesting and diseases. Regulations and restoration efforts have focused on restoring oyster populations while also considering their ability to provide ecosystem services, such as coastal protection, and water quality improvement, among others. To promote oyster growth and the settlement of new populations, a recent technique used along the east coast of the US is the use of Oyster Castles (OCs). However, hydrodynamic differences between gray and oyster-covered OCs have not been investigated and remain poorly understood. We quantified hydrodynamic differences that occur around these OCs during their early stage (i.e. castles without oysters), and with fully developed oysters covering the surface of the castles through a series of laboratory experiments. The experiments were conducted in a recirculating Odell-Kovaszny type channel at the Ecohydraulics and Ecomorphodynamics Laboratory (EEL) at the University of Illinois. OCs (both with and without oysters) were 3D printed at 1:7 scale to fit the canal, and Particle Image Velocimetry (PIV) was used for 2D flow characterization. Data showed noticeable differences in flow acceleration atop the castles when covered with oysters, as well as an increase in the generation and distribution of turbulent kinetic energy atop and around the oyster-covered castles. Magnitudes and spatial distribution of dissipation rates were also affected by the presence of oysters in both submerged and near-emergent conditions. The estimation of the drag coefficient, based on a 1D momentum balance, showed the presence of oysters increased the drag up to 50% in the emergent case, compared to the no-oyster scenario, while in the submerged case, the drag resulted in negative values due to increases in downstream momentum. Laboratory results were also supported by computational fluid dynamics (CFD) numerical simulations. Further research, in both unidirectional and oscillatory

flow conditions, will allow us to provide relevant guidelines on the design and use of oyster-populated breakwaters as a viable nature-based solution for coastal protection.

#### 4.1 Introduction

Oysters are a genus of bivalve mollusks found to live within coastal waterbodies with moderated salinity (5–30) (Chu et al., 1993; White et al., 1996; Fodrie et al., 2014; Johnson, 2014), well recognized to provide a wide variety of ecosystem services useful for the environment, such as shoreline protection, water filtration, carbon sequestration and many others (Coen et al., 2007; Grabowski and Peterson, 2007; Hogan and Reidenbach, 2022). Oysters form complex three-dimensional structures once fully developed, with rough surface elements, much larger than roughness height related to mud or sand substrates (Stiner and Walters, 2008; Styles, 2015). The greater roughness provided by oyster reefs (Wright, Gammisch, and Byrne, 1990) increases flow turbulence, shear stress and eddies generation, which in turn affect mixing and transport processes (Dame, 1996; Gutierrez et al., 2003; Style, 2015; Colden et al., 2016). Oysters also attenuate wave energy and increase sedimentation rates, which help stabilize shorelines vulnerable to erosion (Coen et al., 2007; Grabowski and Peterson, 2007; Hogan and Reidenbach, 2022).

In the last few decades, overharvesting and diseases globally reduced oyster population by 85% (Beck et al., 2011), with peaks reaching 99% in the upper Chesapeake Bay (Wilberg et al., 2011), resulting in the loss of many coastal ecosystem services. Regulations and restoration efforts have therefore focused on recovering oysters across coastal world areas (Cerco and Noel, 2007; Coen et al., 2007; Mann and Powell, 2007). The establishment of new populations naturally occurs over hard substrates (usually other oyster shells), where oyster larvae can settle, get attached and grow, after being transported and dispersed by coastal hydrodynamic stresses (Wood and Hargis, 1971; North et al., 2008). To enhance oysters' growth and the settlement of new populations while also providing coastal protection, a recent technique along the east coast of the US uses oyster castles (OCs). OCs are a mixture of concrete and oyster shell blocks, about 30 x 30 x 20 cm, which can interlock together in different shapes and combinations. They have proven effective in recruiting and retaining oysters and promoting both vertical growth and

horizontal expansion of oyster habitat (Theuerkauf et al., 2015; Hogan and Reidenbach, 2022).

Several studies in the literature have shown oysters' capability to reduce wave energy and mitigate shoreline erosion (Steven et al., 2011; Chowdhury et al., 2019; Wiberg et al., 2019; Morris et al., 2021), to grow at similar rates of SLR (Rodriguez et al., 2014; Ridge et al., 2017) and to restore other valuable ecosystem services (Grabowski and Peterson, 2007) supporting and promoting the use of oysters-based infrastructures in coastal protection. Wright et al., (1990), Styles (2015) and Vasileios Kitsikoudis et al., (2019), studied flow and turbulence over oyster reefs, finding greater turbulent kinetic energy, drag coefficient, and hydraulic roughness for healthy oysters-covered beds compared to degraded reefs and free sandy bars. Similarly, Reidenbach et al., (2007), and Cannon et al., (2022), investigated turbulence characteristics within coral and oyster reef canopies. Only a few field studies have investigated and quantified protective benefits of the coupling between oysters and OCs (Hogan and Reidenbach, 2022); however, this basin-scale study, was not able to capture micro hydrodynamic features such as the increased drag of OCs due to oysters.

Our study aimed therefore to quantify hydrodynamic differences that occur around these OCs during their early stage (i.e. castles without oysters), and with fully developed mollusks covering the surface of the castles. We aimed to highlight dissipative flow features for the oysters vs no-oysters configurations. Laboratory experiments were conducted in a recirculating Odell-Kovaszny type channel at the Ecohydraulics and Ecomorphodynamics Laboratory (EEL) at the University of Illinois, with a 2 m long straight test section, 0.15 m wide and 0.6 m deep. We analyzed 5 different scenarios (with and without oysters), varying the configuration of the OC, the flow velocity, and the water level (emergent and submerged conditions). OCs (both with and without oysters) were 3D printed at 1: 7 scale in order to fit the canal, and Particle Image Velocimetry (PIV) was used for 2D flow characterization. A computational fluid dynamic (CFD) software, Flow 3D (Flow Science, Inc., 2007), validated with laboratory velocity measurements, was then employed in order to support lab results. Flow-3D has been employed to solve the fluid motion equations

of a wide variety of fluid-mechanic problems, largely tested by many authors in the literature (Bayon et al., 2015; Ramezani and Sefidkoohi, 2016; Jafari et al., 2017; Ghasemi and Gerdefaramarzi, 2017).

More eco-engineering studies testing the performance of hybrid infrastructures under SLR and climate change scenarios have been requested by many authors in the literature, in order to create guidelines for the proper implementation of oysters as a nature-based solution for coastal protection (e.g. Temmerman et al., 2013; Ferrario et al. al., 2014, Sutton-Grier et al., 2015; 2018). Without detailed studies, restoration efforts are likely to be partially or completely inefficient for long-term shoreline defense. This last chapter studied therefore the impact of different breakwater roughness (with and without oysters) on flow hydrodynamics. The laboratory approach was needed in order to catch the smallest hydrodynamic features (important to fully describe the phenomenon), as we could not do in the previous chapters, since the spatial resolution of our field and modeling approaches was too coarse.

## 4.2 Material and Methods

### 4.2.1 Laboratory experiments

To study the impact of OCs, with and with no oysters, on flow hydrodynamics, PIV was used. PIV is an optical technique of flow visualization largely used in education and research. It is used to obtain instantaneous velocity measurements and related properties in fluids. The experiments were conducted in an Odell-Kovaszny type recirculating flume (Odell and Kovaszny, 1971), with a straight test section 2 m long, 0.15 m wide, and 0.6 m deep (Figure 4.1). A vertical axis disk-pump with uniformly distributed disks drives the flow to produce a uniform velocity profile with minimal vertical disturbance. A 5 W continuous-wave laser system was used to generate a vertical planar light sheet for PIV measurement with a thickness of 1 mm at the centerline of the flume. The same setup was used to generate a horizontal light sheet 2 cm below the surface to investigate the horizontal flow structure and validate the 2D vertical-plane approach of the study in our thin flume,

where wall effects can be ignored, even for the sparse and bare-bed cases. A 1-Megapixel camera, Edgertronic SC2+ high-speed camera, was used to capture 8-bit grayscale images at 60 Hz for 1 min (3,600 images) in each run. Raw images were processed in PIVlab (Thielicke and Stamhuis, 2014), a Matlab application in which consecutive sub-windows (arbitrarily overlapped) were used to obtain higher resolution results during flow field estimation. Three and four consecutive sub-windows, according to the considered scenario, 50% size passes with 50% overlapped interrogation areas, were chosen to obtain higher resolution results during cross-correlation calculation.

We analyzed 4 different scenarios (with oysters and no-oysters), varying the flow velocity (0.1 m/s and 0.3 m/s) and the water level (same height and twice the height of the structure) (Figure 4.2). The OCs used in the experiments (both with and without oysters) were 3D printed at 1: 7 scale in order to fit the laboratory flume.

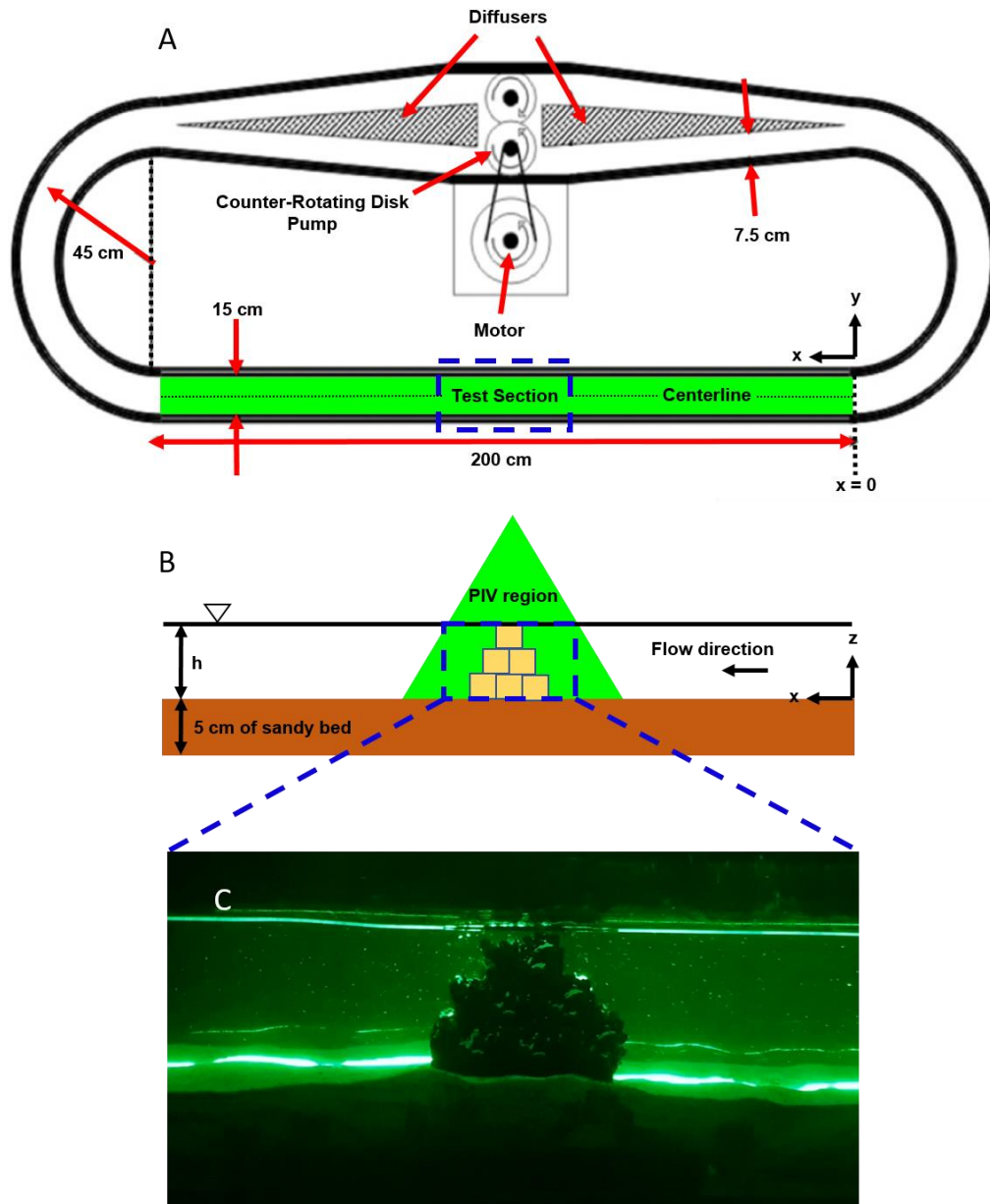


Figure 4.1. (A) Top-view and (B) side-view sketch of the flume setup for the emergent Case A (not to scale), where the water depth,  $h = 7.5$  cm, and the thickness of the sediment bed is equal to 5 cm. The blue-dashed rectangular area indicates the observation region for PIV measurement, also shown in plot (C)

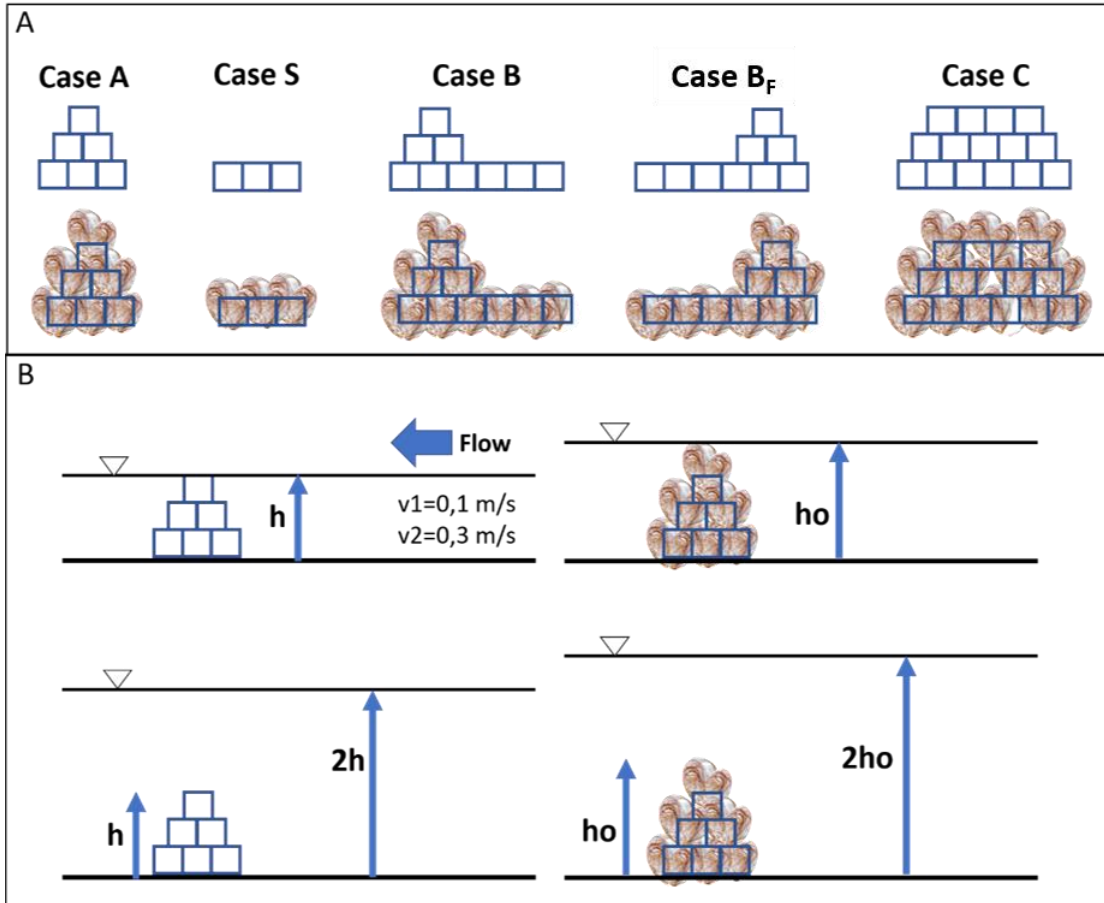


Figure 4.2. Set up of the different experiments. (A) Different analyzed geometries. (B) Water level and velocity configurations for the experimental set up.

#### 4.2.2 Flow 3D model

Once PIV analyses were completed, a CFD model created in Flow3D was used in order to support the 2D PIV experimental results.

FLOW-3D is a commercial software package developed by FlowScience, Inc (Flow Science, Inc., 2007), which uses the Volume of Fluid (VOF) to solve the nonlinear 3D Navier-Stokes equations, while the Fractional Area/Volume Obstacle Representation (FAVOR) method is used to compute the complex boundaries of the model domain. Different turbulence closure schemes, such as simple eddy viscosity, one-dimensional Prandtl mixing length, two-equation k-e, large-eddy, and four-equation ReNormalized Group (RNG), are implemented in Flow-3D (see appendix for modeling governing equations). The computational domain implemented in Flow-

3D represented the Odell-Kovaszny flume used for PIV experiments, 0.15 m wide, 0.6 m deep, while we doubled the length (4 m) in order to prevent numerical instabilities. OCs (both with and with no oysters) were imported as .stl file (the same used for 3D printing the scaled blocks employed in PIV experiments) and placed at the center of the numerical flume. A mesh block of 316260 cells (8 mm each) was fitted to the model geometry. To increase the model accuracy, a refined mesh (735840 cells, size of 2 mm) was defined around OCs in order to obtain higher spatial resolution. Boundary conditions were x-velocity rate at the inlet, continuity at the outlet, wall on the right, left and bottom sides, and pressure (P) equal zero on the top boundary (Figure 4.3). The turbulent model adopted in our simulations was the RNG, as it better agrees with experimental observations (Ramezani and Babagoli Sefidkoohi, 2016). Surface tension and wall friction were neglected.

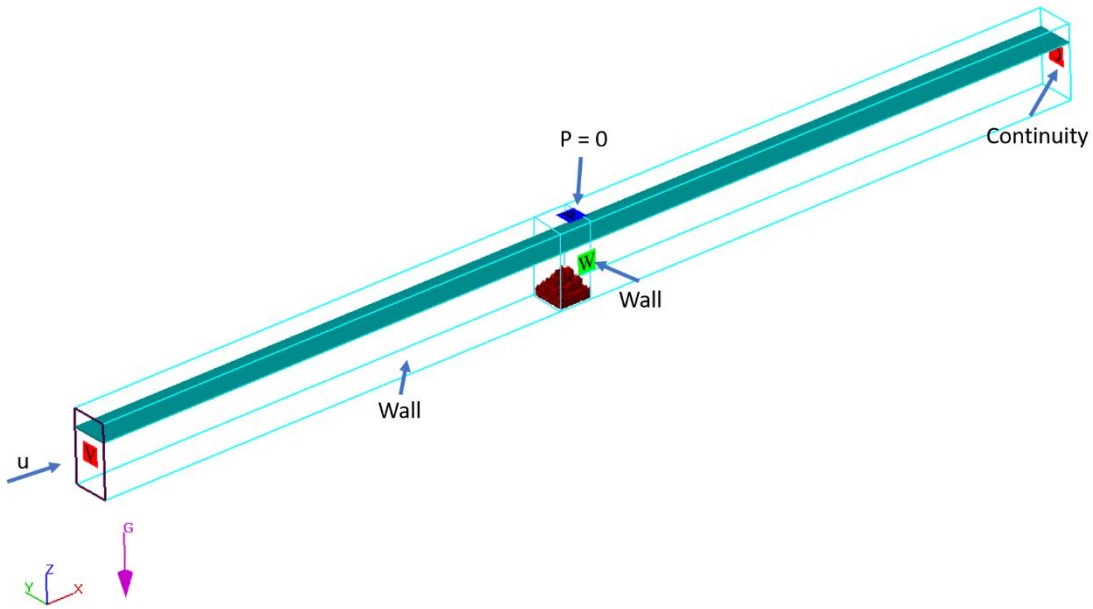


Figure 4.3. Flow 3D numerical domain

We only simulated submerged case A (faster flow), with and without oysters. Simulations were forced by x-velocity at the inlet of 0.13 m/s. We used the Flow-3D solver version 22.2.1.01 with four processors of a 64-bit desktop operating system.

Simulation runs were performed until model convergence, and validated according to the time-averaged 2D velocity field estimated in PIV.

### 4.3 Results

#### 4.3.1 PIV results

Laboratory experiment results are reported below. All quantities are time-averaged ( $\langle \rangle$ ) across the 1 min recorded video by the camera, to obtain the 2D time-averaged field. An example of the normalized velocity ( $\langle u \rangle / U$ , where  $U$  denotes the space-averaged 2D  $\langle u \rangle$ ), normalized vorticity ( $\langle \omega \rangle * h / U$ , where  $h$  denotes the water level depth), normalized Turbulent Kinetic Energy ( $\langle TKE \rangle / U^2$ ), normalized Turbulent Dissipation ( $\langle \epsilon \rangle * h / U^3$ ) and normalized Reynolds stresses ( $\langle u'v' \rangle / U^2$ ) is reported in Figure 4.4 and Figure 4.5, for the submerged Case A (faster flow) with and without oysters.

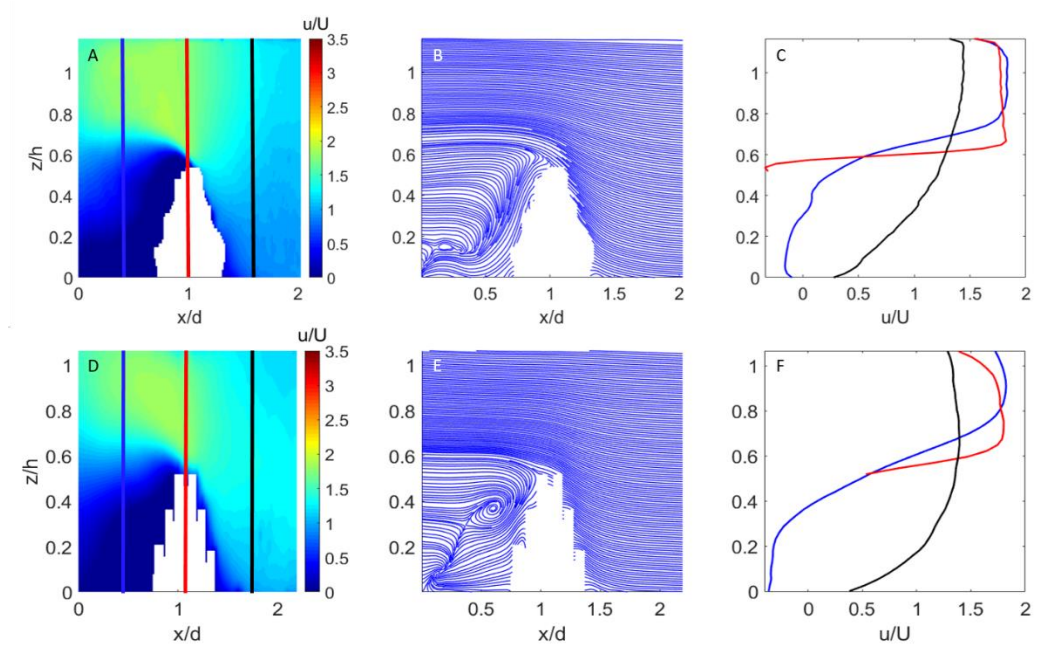


Figure 4.4. PIV results for the submerged Case A forced by the faster flow. (A) Normalized 2D velocity for oyster-covered OCs and (D) gray OCs. (B) Velocity streamlines for oyster-covered OCs and (E) gray OCs. (C) Upstream, middle and downstream velocity profiles for oyster-covered OCs and (F) gray OCs.

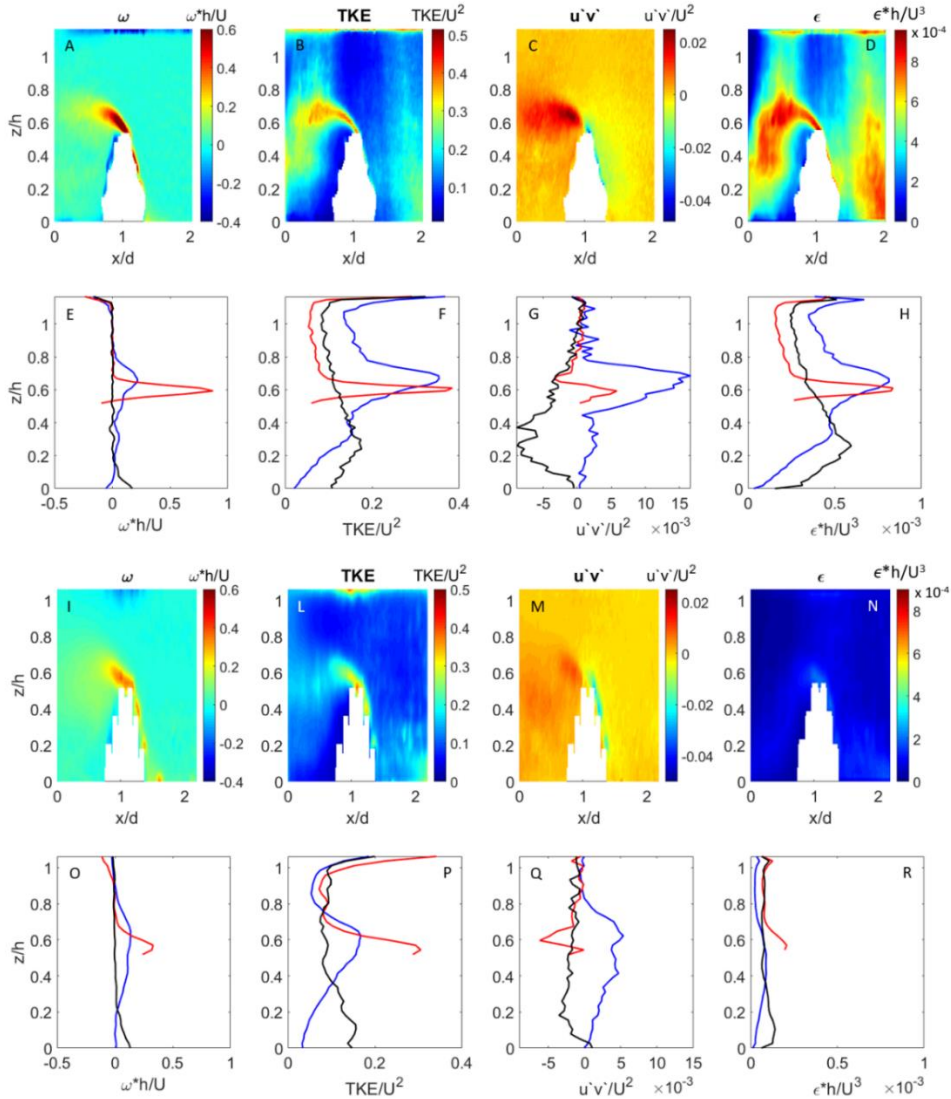


Figure 4.5. PIV output results. (A) Normalized 2D vorticity for the scenario with oysters and (E) vertical upstream, middle and downstream normalized vorticity profiles. (B) Normalized 2D TKE for the scenario with oysters and (F) vertical upstream, middle and downstream normalized TKE profiles. (C) Normalized 2D Reynold stresses for the scenario with oysters and (G) vertical upstream, middle and downstream normalized Reynold stresses profiles. (D) Normalized 2D Turbulent dissipation for the scenario with oysters and (E) vertical upstream, middle and downstream normalized Turbulent dissipation profiles. (I) Normalized 2D vorticity for the scenario without oysters and (O) vertical upstream, middle and downstream normalized vorticity profiles. (L) Normalized 2D TKE for the scenario without oysters and (P) vertical upstream, middle and downstream normalized TKE profiles. (M) Normalized 2D Reynold stresses for the scenario without oysters and (Q) vertical upstream, middle and downstream normalized Reynold stresses profiles. (N) Normalized 2D Turbulent dissipation for the scenario without oysters and (R) vertical upstream, middle and downstream normalized Turbulent dissipation profiles.

The next sections provide insights into the difference between oysters vs no oysters, on the impact of the different geometries and water levels. Then, drag coefficient ( $C_D$ ) results based on 1-D moment balance (black box approach) are presented, followed by near bed  $\langle TKE \rangle$  and near bed  $\langle u'v' \rangle$ . Results are divided by "regions", upstream, middle, and downstream of the structure, as shown in Figure 4.6. Quantities are space averaged within the regions.

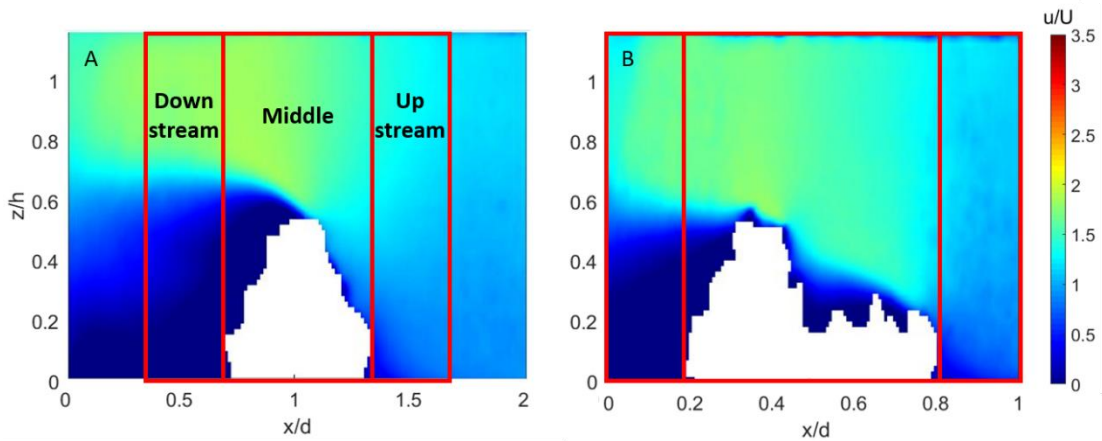


Figure 4.6. Subdivision of the observation domain in the upstream, middle, and downstream regions for (A) Case A (same for Case S) and (B) Case B (same for Case B<sub>F</sub> and Case C).

#### 4.3.1.1 Oyster-covered OCs vs gray OCs

Results regarding the velocity field around our structures showed  $\langle u \rangle / U$  decreased in both emergent and submerged cases, from the upstream to the downstream region (Figure 4.7 A-F). In the emergent case,  $\langle u \rangle / U$  decreased with increasing Re numbers for both oysters and no oysters scenarios in the upstream region (slightly higher for no oyster scenario) (Figure 4.7 A). The central region showed  $\langle u \rangle$  to be comparable with U, resulting in  $\langle u \rangle / U$  close to 1 for both cases (Figure 4.7 B), while in the downstream region (Figure 4.7 C)  $\langle u \rangle / U$  was positively correlated with Re numbers (slightly higher for the oyster scenario). The submerged case showed decreasing in  $\langle u \rangle / U$  from the upstream to the downstream region as well as the emergent case (Figure 4.7 D-F).  $\langle u \rangle / U$  increased with Re numbers in the

upstream region for both oysters and no oysters scenarios (higher for no oyster scenario) (Figure 4.7 D). The central region showed values of  $\langle u \rangle / U$  around 1 for both cases (Figure 4.7 E), while in the downstream region (Figure 4.7 F)  $\langle u \rangle / U$  was negatively correlated with Re numbers for the no oyster scenario and almost constant around 1 for the oyster scenario. Submerged cases were also associated with higher Re numbers compared to emergent cases. The higher water level (submerged OCs scenario) showed less variability around  $\langle u \rangle / U = 1$  compared to the emergent case between the upstream and the downstream regions.

Normalized Reynold stresses ( $\langle u'v' \rangle / U^2$ ) increased in magnitude from the upstream to the downstream region for both emergent and submerged cases (Figure 4.7 G-N). Negative  $\langle u'v' \rangle / U^2$  within the upstream region increased with Re numbers, in the emergent case (Figure 4.7 G). The middle region showed negative (gray OCs) and positive (oyster-covered OCs) Reynolds stresses (emergent case, Figure 4.7 H). In the upstream emergent region, positive  $\langle u'v' \rangle / U^2$  (higher for the oyster scenario) decreased for higher Re numbers (Figure 4.7 I). The submerged scenario showed less variability around  $\langle u'v' \rangle / U^2 = 0$  compared to the emergent study case, between the upstream and downstream regions (Figure 4.7 J,K). Negative  $\langle u'v' \rangle / U^2$  were found within the upstream and the middle regions, comparable for both gray and oyster-covered OCs ( $\langle u'v' \rangle / U^2$  increased with Re numbers) (Figure 4.7 J,K), whereas in the upstream region,  $\langle u'v' \rangle / U^2$  were almost constant with Re numbers (slightly higher for the oyster scenario) (Figure 4.7 L).

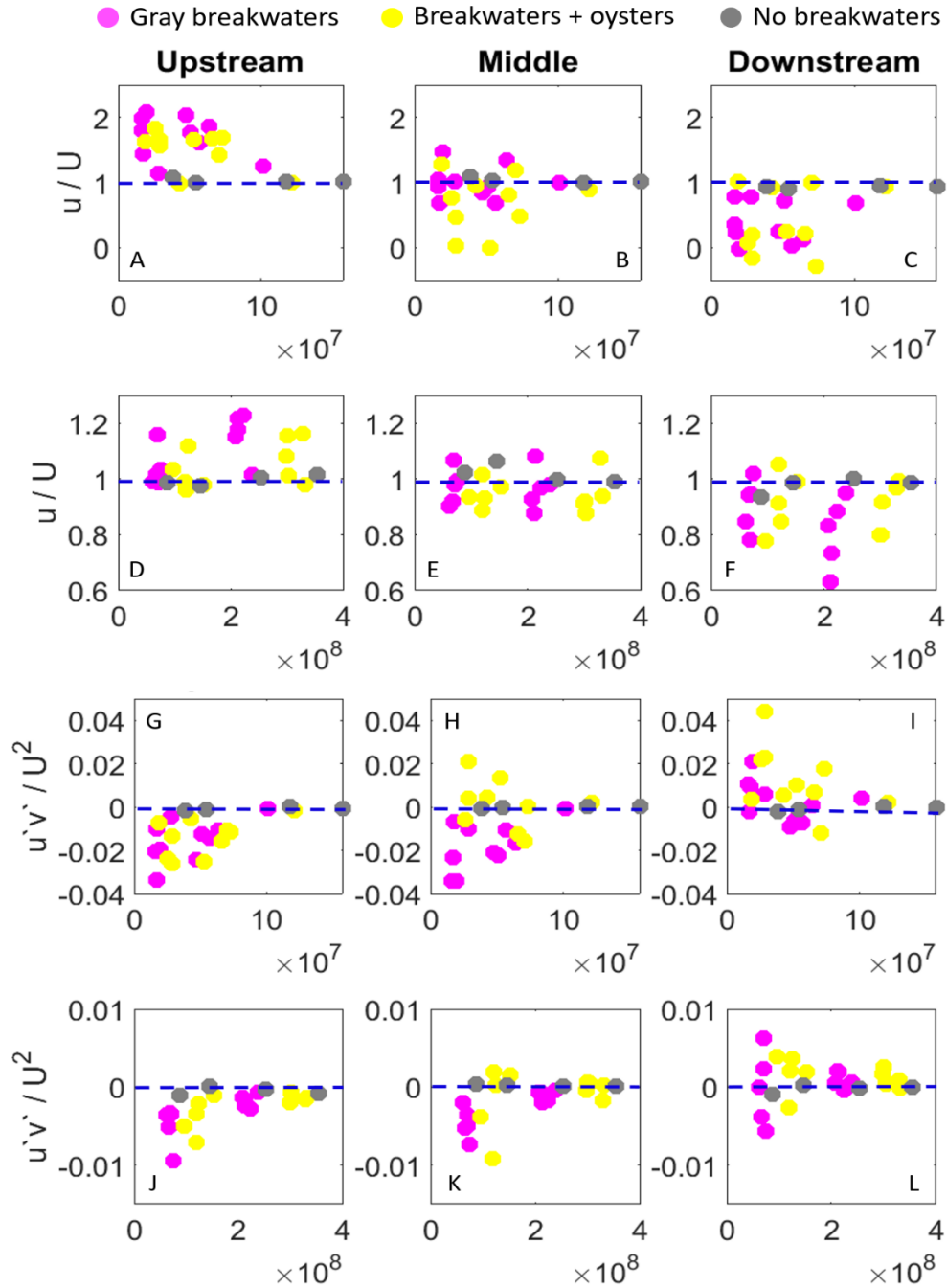


Figure 4.7. Normalized velocity for the emergent cases in the (A) upstream, (B) middle and (C) downstream regions. Normalized velocity for the submerged cases in the (D) upstream, (E) middle and (F) downstream regions. Normalized Reynolds stresses for the emergent cases in the (G) upstream, (H) middle and (I) downstream regions. Normalized Reynolds stresses for the submerged cases in the (J) upstream, (K) middle and (L) downstream regions.

Normalized vorticity ( $\omega h / U$ ) increased in the downstream region compared to the upstream for both oyster-covered and gray OCs, and for both emergent and submerged scenarios. Moreover, normalized vorticity was similar in magnitude between the scenario with and without oysters, for both emergent and submerged conditions. No statistically significant trend was found between Re numbers and normalized vorticity (Figure 4.8).

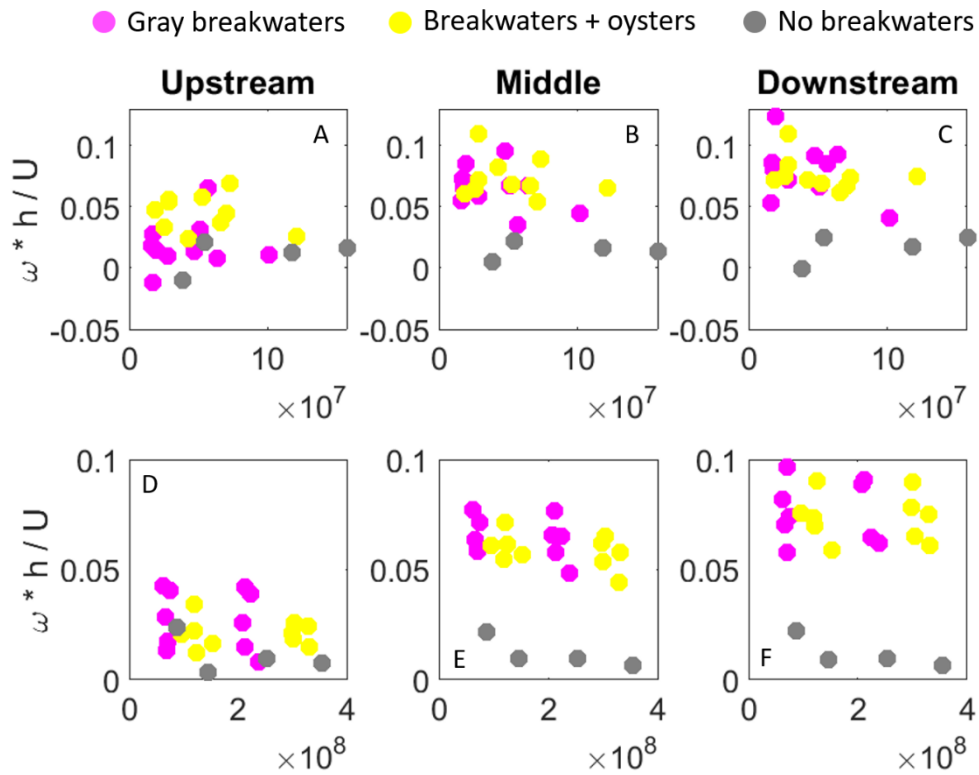


Figure 4.8. Normalized vorticity for the emergent cases in the (A) upstream, (B) middle and (C) downstream regions. Normalized vorticity for the submerged cases in the (D) upstream, (E) middle and (F) downstream regions.

Normalized TKE ( $TKE/U^2$ ) was better approximated by a power law, negatively correlated with Re numbers (Figure 4.9 A-F). It showed no significant difference between the upstream and downstream regions for both the emergent (Figure 4.9 A-C) and submerged (Figure 4.9 D-F) cases. However, the emergent case

showed  $TKE/U^2$  up to one order of magnitude greater than the submerged case. Oyster-covered and gray OCs scenarios were similar to each other (Figure 4.9 A-F).

Normalized turbulent dissipation ( $\varepsilon h / U^3$ ) was also better approximated by a power law. As well as normalized TKE, it showed no significant difference between the upstream and downstream regions for both the emergent (Figure 4.9 G-I) and submerged (Figure 4.9 J-L) cases. However, the emergent case showed  $\varepsilon h / U^3$  up to one order of magnitude greater than the submerged case. Oyster-covered and gray OCs scenarios were similar to each other (Figure 4.9 J-L).

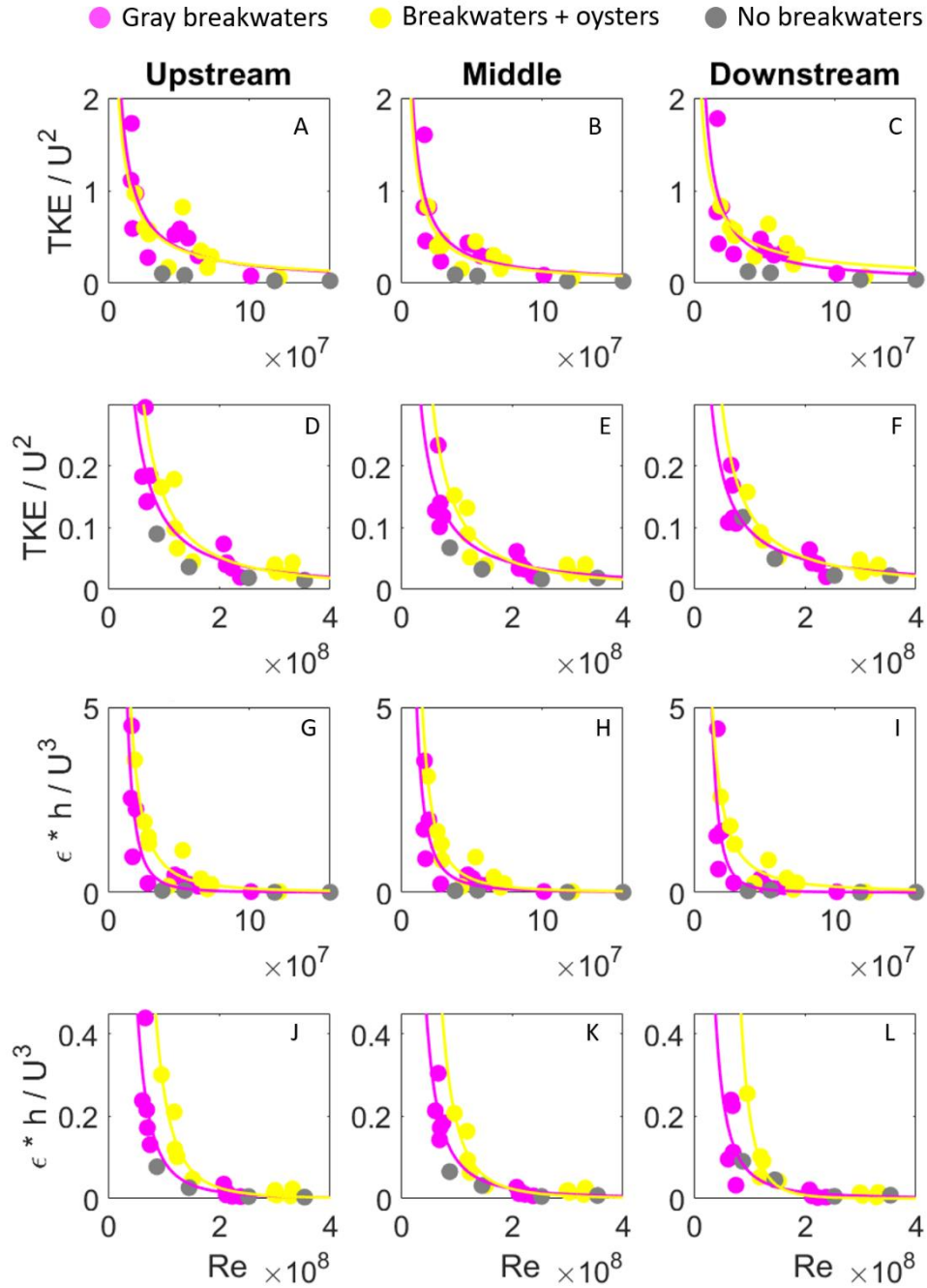


Figure 4.9. Normalized TKE for the emergent cases in the (A) upstream, (B) middle and (C) downstream regions. Normalized TKE for the submerged cases in the (D) upstream, (E) middle and (F) downstream regions. Normalized Turbulent dissipation for the emergent cases in the (G) upstream, (H) middle and (I) downstream regions. Normalized Turbulent dissipation for the submerged cases in the (J) upstream, (K) middle and (L) downstream regions.

#### 4.3.1.2 The impact of different OCs geometries on flow hydrodynamic

In our experiments, we analyzed how different breakwater geometries might impact flow hydrodynamics over the gray and oyster-covered structures. Normalized velocity decreased from upstream to downstream for both emergent (Figure 4.10 A-C) and submerged (Figure 4.10 D-F) OCs conditions. Case S was always submerged (also in the emergent cases), which resulted in  $\langle u \rangle / U$  being almost constantly equal to 1 from the upstream to the downstream region (Figure 4.10 A-C). In the emergent case, cases A and C produced the highest upstream velocities, while in the middle region, all cases were closer to 1 (Figure 4.10 A,B). Emergent case B produced the lower downstream velocities. In contrast, downstream  $\langle u \rangle / U$  for the emergent case B<sub>F</sub> was close to 1. Emergent case C and A produced normalized downstream velocities comparable with case B (Figure 4.10 C).

The submerged case (Figure 4.10 D-F) showed smaller variations of  $\langle u \rangle / U$  around  $\langle u \rangle / U = 1$  compared to the emergent case. Case S always resulted in  $\langle u \rangle / U$  close to 1 upstream and downstream. Case A produced the highest upstream normalized velocity, followed by cases B<sub>F</sub>, B and C. In the middle region, all cases showed  $\langle u \rangle / U$  close to 1. Case B showed the lowest downstream  $\langle u \rangle / U$ , followed by case A and C. Cases S and B<sub>F</sub> showed  $\langle u \rangle / U$  close to 1 (Figure 4.10 D-F).

Normalized Reynolds stresses  $\langle u'v' \rangle / U^2$  shifted towards positive values from upstream to downstream, in both emergent (Figure 4.10 G-I) and submerged (Figure 4.10 L-N) conditions. Case S was close to 0 in the emergent scenario, upstream, in the middle section, and downstream the structure. Emergent case C produced the largest negatives  $\langle u'v' \rangle / U^2$  in the upstream region while emergent cases A, B and B<sub>F</sub> (all similar) were slightly smaller (Figure 4.10 G). The median region slightly increased Re stresses compared to the upstream region (Figure 4.10 H). Emergent case B in the downstream region showed the highest (positive)  $\langle u'v' \rangle / U^2$ , followed by case A, C and B<sub>F</sub> (Figure 4.10 I).

The submerged case showed more limited variations of  $\langle u'v' \rangle / U^2$  around  $\langle u'v' \rangle / U^2 = 0$  compared to the emergent case. Normalized Reynold stresses for Case S

were always around 0 upstream, in the center and downstream. Case B<sub>F</sub> showed greater negative  $\langle u'v' \rangle / U^2$  in the upstream, middle and downstream regions. In the downstream region, case A, B and S were associate with  $\langle u'v' \rangle / U^2$  slightly positive, while case C and B<sub>F</sub> were associated with negative (no oysters) and positive (yes oysters)  $\langle u'v' \rangle / U^2$  (Figure 4.10 J-L).

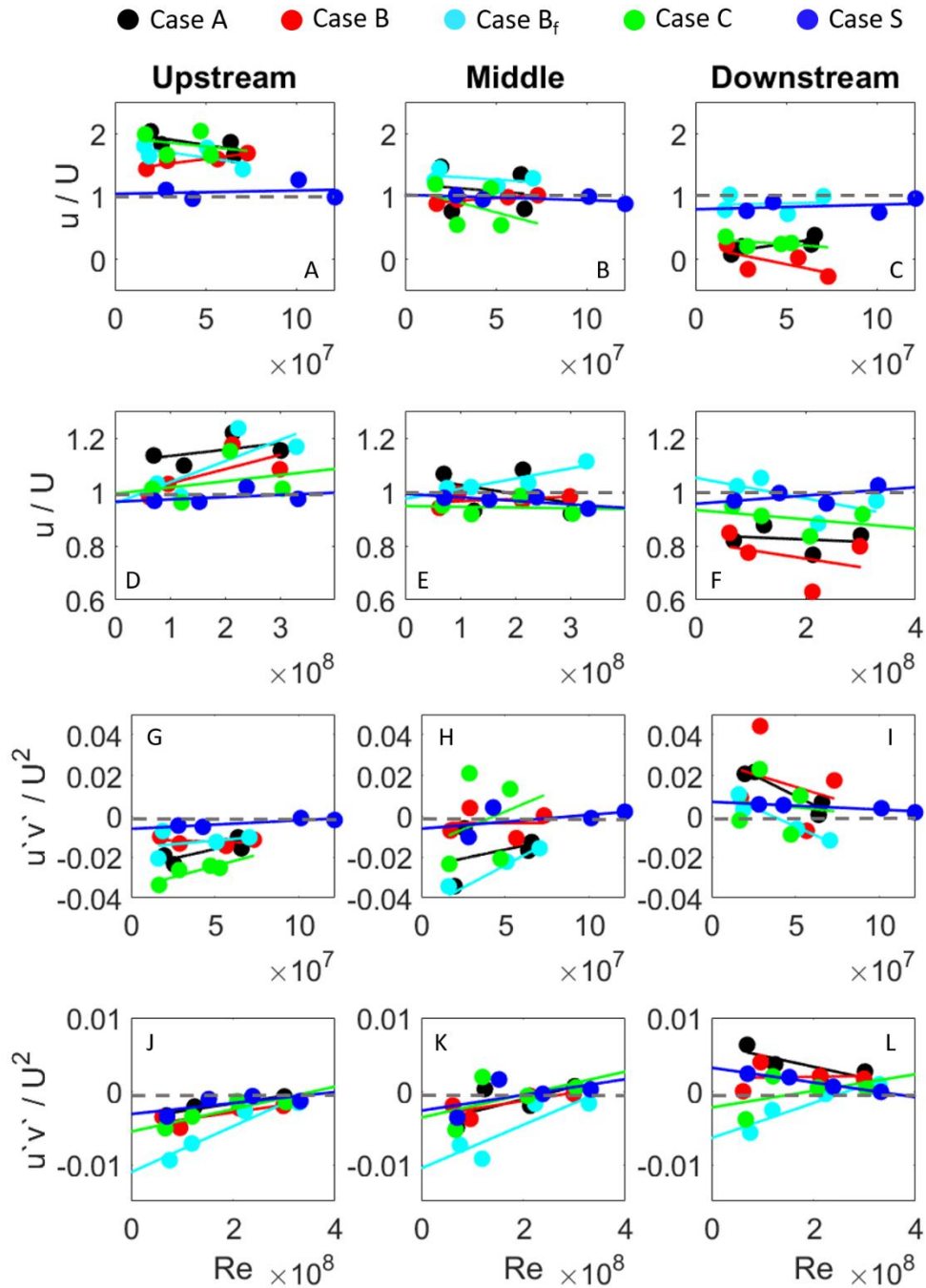


Figure 4.10. Normalized velocity for the emergent cases in the (A) upstream, (B) middle and (C) downstream regions. Normalized velocity for the submerged cases in the (D) upstream, (E) middle and (F) downstream regions. Normalized Reynolds stresses for the emergent cases in the (G) upstream, (H) middle and (I) downstream regions. Normalized Reynolds stresses for the submerged cases in the (J) upstream, (K) middle and (L) downstream regions.

Normalized vorticity in the emergent case (Figure 4.11 A-C) was positively correlated with Re numbers in the upstream region and negatively correlated downstream. Normalized vorticity increased in magnitude in the downstream region compared to the upstream. Case S showed smaller upstream and downstream eddies. Case B produced the highest vorticity in the upstream and downstream regions; case A and C also generated downstream vorticity comparable with case B. In the middle region there was not significant difference among all case scenarios (Figure 4.11 A-C).

The submerged case (Figure 4.11 D-F) showed normalized vorticity comparable to the emergent case. However, the linear correlations remained nearly constant with Re numbers in the three regions. Case S showed the lowest vorticity in the upstream and downstream regions. Case A showed  $\omega h / U$  almost zero in the upstream region, as well as Case S, while Case B, B<sub>F</sub> and C were slightly greater and close to each other. The middle region showed no significant difference among all cases. Case A and B showed highest  $\omega h / U$  downstream, while case B<sub>F</sub> and C were slightly lower (Figure 4.11 D-F).

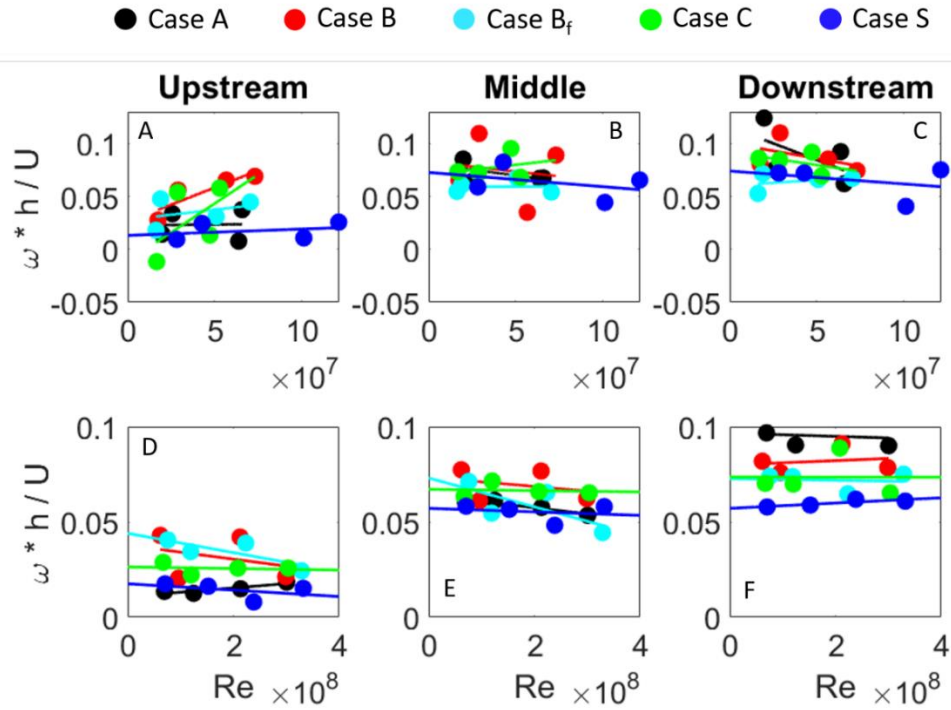


Figure 4.11. Normalized vorticity for the emergent cases in the (A) upstream, (B) middle and (C) downstream regions. Normalized vorticity for the submerged cases in the (D) upstream, (E) middle and (F) downstream regions.

In the emergent condition (Figure 4.12 A-C), normalized TKE showed a linear trend (decreasing as a function of  $Re$ ) from upstream to downstream. Case C produced highest  $TKE/U^2$  in all regions, followed by case  $B_f$ , A, B and lastly case S (Figure 4.12 A-C). The submerged case (Figure 4.12 D-F) showed a similar trend to the emergent scenario, but up to 1 order of magnitude smaller. Case C produced the highest  $TKE/U^2$  and case S the lowest (Figure 4.12 D-F).

Normalized dissipation rate had a similar trend  $TKE/U^2$ . Case C produced the greatest dissipation rates in the emergent case, followed by case  $B_f$ , case A, case B and lastly Case S (Figure 4.12 G-I). The linear trend, decreasing with  $Re$  numbers, was also repeated in the submerged case (one order of magnitude smaller than the emergent condition) (Figure 4.12 J-L). Case C produced the highest dissipation rates in all regions, slightly higher downstream than upstream.

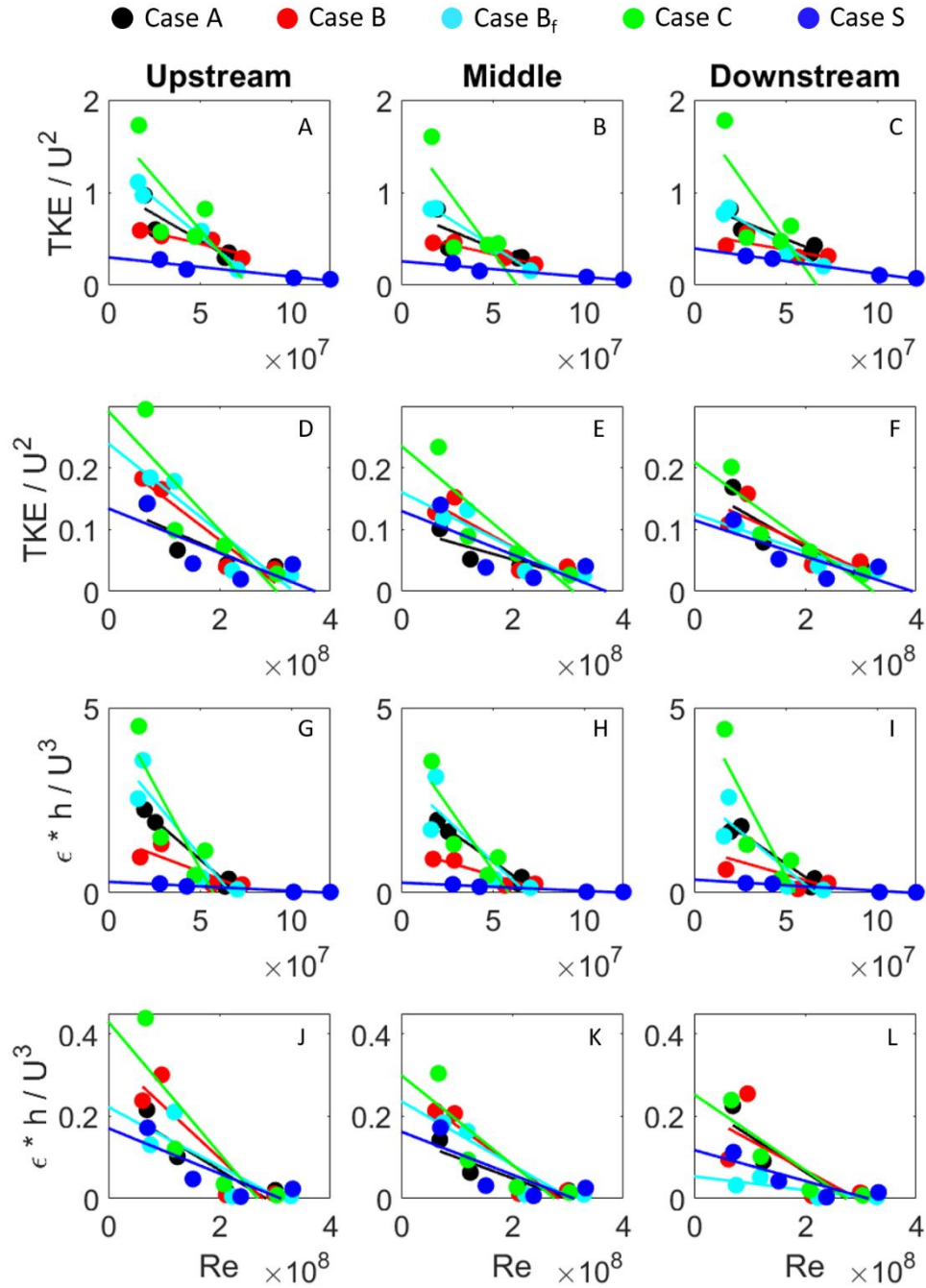


Figure 4.12. Normalized TKE for the emergent cases in the (A) upstream, (B) middle and (C) downstream regions. Normalized TKE for the submerged cases in the (D) upstream, (E) middle and (F) downstream regions. Normalized Turbulent dissipation for the emergent cases in the (G) upstream, (H) middle and (I) downstream regions. Normalized Turbulent dissipation for the submerged cases in the (J) upstream, (K) middle and (L) downstream regions.

#### 4.3.1.3 Drag coefficient estimation based on the 1D momentum balance

To analyze the effect of oysters regarding the drag produced by our OCs, we applied the 1-D momentum balance (black box approach based on the upstream and downstream momentum) along the x direction, as changes in fluid momentum (M) equalized the applied force to the system (Nevin et al., 1983). Therefore, we first quantified the drag force ( $F_D$ ), and then estimated the drag coefficient ( $C_D$ ), as follow:

$$\begin{aligned}M &= A U^2 \\F_D &= A_1 U_1^2 - A_2 U_2^2 \\C_D &= F_D / U_1^2\end{aligned}$$

where A indicates pixel/cell area. Subscripts 1 and 2 denote upstream ( $x/d=0$ ) and downstream ( $x/d=1,2$ ) regions, respectively

Oyster-covered OCs increased the drag coefficient in the emergent case up to 50%, compared to gray OCs (Figure 4.13 A,C). The submerged case, on the other hand, showed negative  $C_D$  for oyster-covered OCs, denoting an increase in downstream flow momentum along the centerline (Figure 4.13 B,D). Case B, B<sub>F</sub>, and C resulted in negative  $C_D$  also for gray OCs when forced by the slower flow. Oyster-covered case S (always submerged) resulted in negative  $C_D$  also in the emergent case, supporting the fact that higher water levels increased downstream flow momentum along the centerline. Higher flow velocity did not influence  $C_D$  in the emergent case, while a faster flow increased  $C_D$  in the submerged case (decreased downstream momentum) (Figure 4.13).

- Gray breakwaters – slower flow
- Gray breakwaters – faster flow
- ★ Breakwaters + oysters – slower flow
- ★ Breakwaters + oysters – faster flow
- ★ No structure

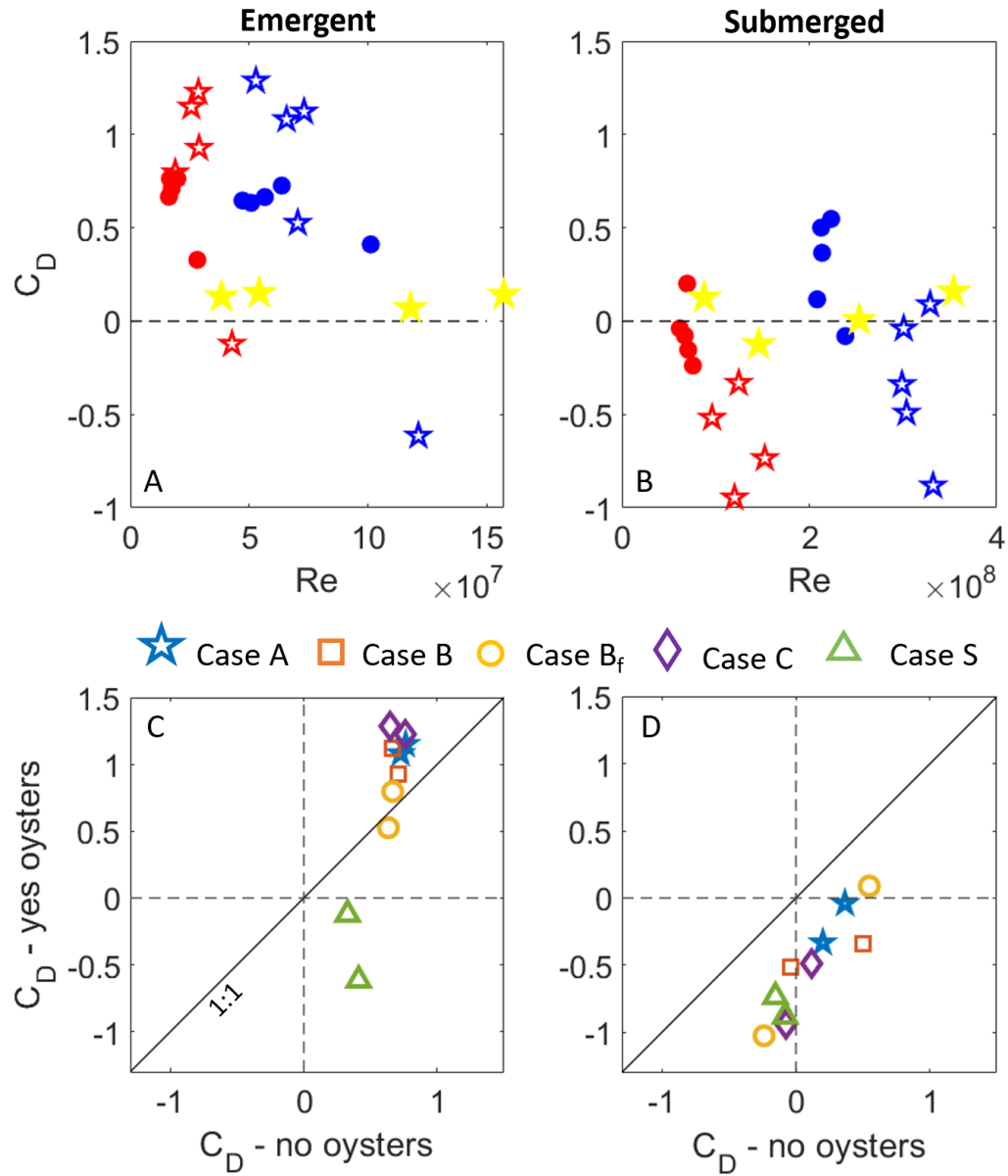


Figure 4.13. Drag coefficient as a function of Reynolds numbers for the (A) emergent and (B) submerged cases. Comparison of the drag coefficient between oyster vs no oyster scenarios in the (C) emergent and (D) submerged cases

#### 4.3.1.4 Near bed TKE and Reynold stresses

In order to link hydrodynamic features with sediment dynamics, we analyzed near bed  $TKE/U^2$  and near bed  $u'v'/U^2$  in the upstream and downstream regions. Near bed  $u'v'/U^2$  decreased linearly with near bed  $TKE/U^2$  in the upstream region, for both emergent and submerged cases. Both the emergent and submerged cases showed negative near bed  $u'v'/U^2$  upstream, while emergent near bed  $TKE/U^2$  was around twice than compared to the submerged scenario (Figure 4.14 A). In the downstream region, near bed  $u'v'/U^2$  slightly increased with increasing near bed  $TKE/U^2$  for the emergent case, while near bed  $u'v'/U^2$  decreased linearly with near bed  $TKE/U^2$  for the submerged case (Figure 4.14 B). Normalized near bed Reynold stresses and TKE were higher for gray OCs in the upstream region (Figure 4.14 C); downstream the structure, near bed  $u'v'/U^2$  remained nearly constant with near bed  $TKE/U^2$  for oyster-covered OCs, while it slightly increased for gray OCs (Figure 4.14 D). Overall, the emergent case showed near bed  $u'v'/U^2$  and  $TKE/U^2$  to be around twice bigger than the submerged case, whereas oyster-covered and gray OCs slightly differed from each other.

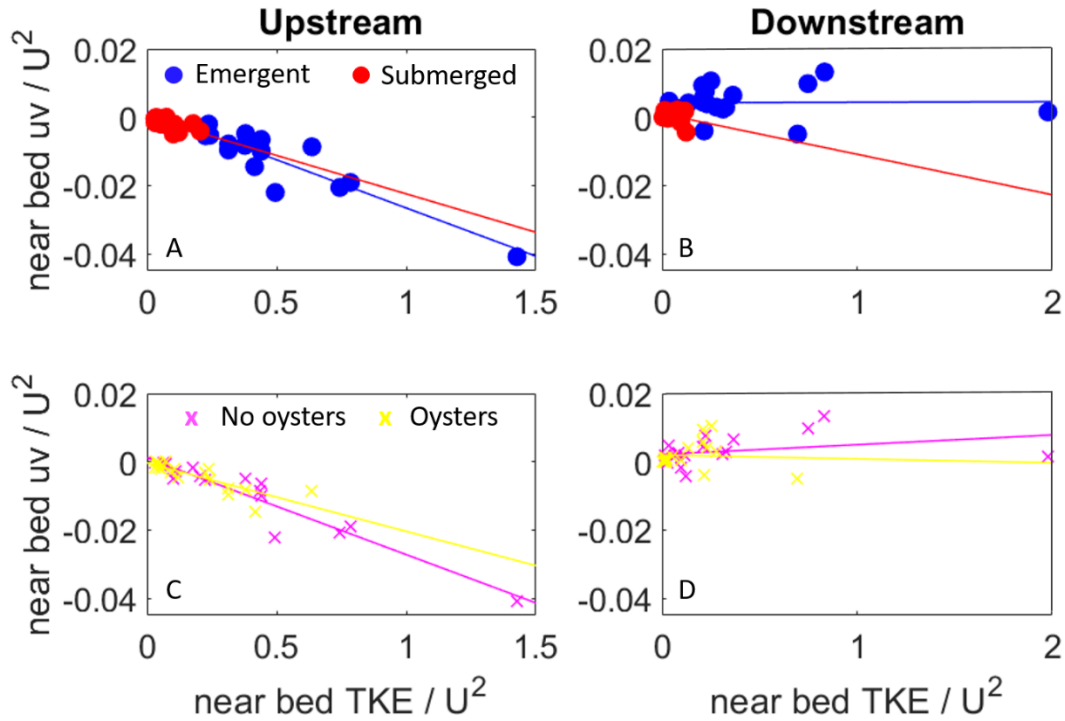


Figure 4.14. Normalized near bed Reynolds stresses vs normalized near bed TKE in the (A,C) upstream and (B,D) downstream regions.

#### 4.3.2 Flow 3D results

CFD numerical modeling aimed to compare PIV insights regarding  $C_D$ , in order to support and strengthen study results. Model validation showed good agreement with PIV velocity data measured at the flume centerline (Figure 4.15). The 1D momentum balance was used as it was used in PIV to estimate  $C_D$ . Results showed the same trend as found in laboratory experiments, negative  $C_D$  for oyster-covered OCs and positive  $C_D$  for gray OCs (Figure 4.16). Flow 3D overestimated the increase in downstream momentum balance compared to PIV, resulting in a greater negative  $C_D$  for oyster-covered OCs. However, moving the downstream section further forward, towards the end of the domain (section 2 and 3 in Figure 4.16 A), we found a decrease in downstream momentum along the centerline, which made  $C_D$  more comparable with PIV results (Figure 4.16 C).

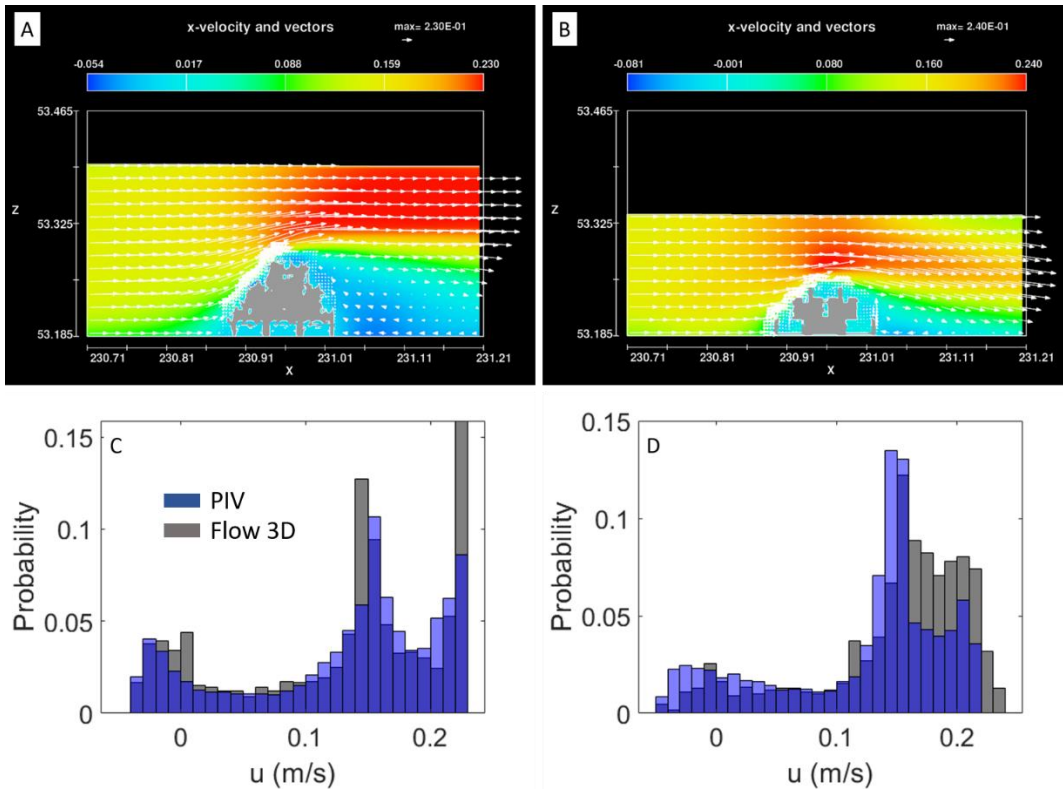


Figure 4.15. Flow 3D velocity field for the submerged Case A over (A) oyster-covered OCs and (B) gray OCs. (C) PIV and Flow 3D velocity histograms for oyster-covered OCs and (D) gray OCs.

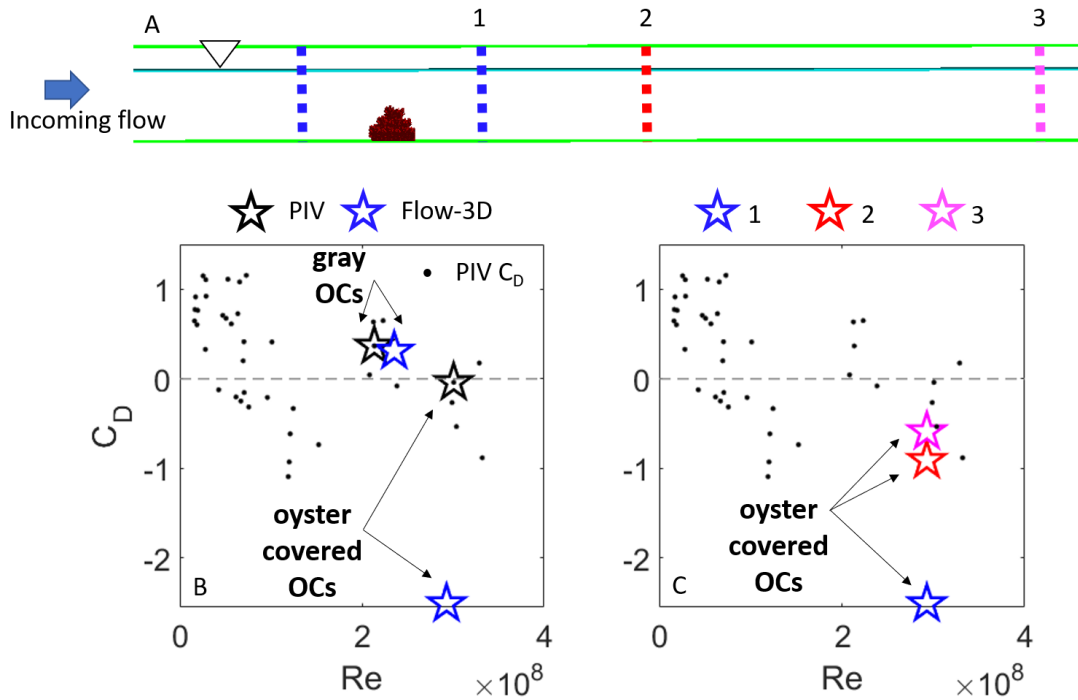


Figure 4.16. Drag coefficient comparison between PIV and Flow 3D. (A) Downstream sections used in Flow 3D to estimate  $C_D$ . The blue cross sections refer to the same window size used in PIV. (B) PIV and Flow 3D estimated  $C_D$  for gray and oyster-covered OCs. (C) Estimated  $C_D$  in Flow 3D by varying the downstream cross sections for oyster-covered OCs.

Given the unclear estimation of the drag coefficient based on the 1D momentum balance, we also calculated (in Flow 3D) the downstream  $C_D$  through a formulation from Poggi et al., (2004), in which the  $C_D$  is function of the Reynold stresses, the longitudinal pressure gradient and  $u$ :

$$C_D = - \left( \frac{\partial \langle \overline{u'w'} \rangle}{\partial z} + \frac{\partial p}{\partial x} \right) (a u^2)^{-1}$$

Results are shown in Figure 4.17. The formulation provided by Poggi et al., (2004) revealed positive  $C_D$ , slightly higher for the oyster-covered OCs.

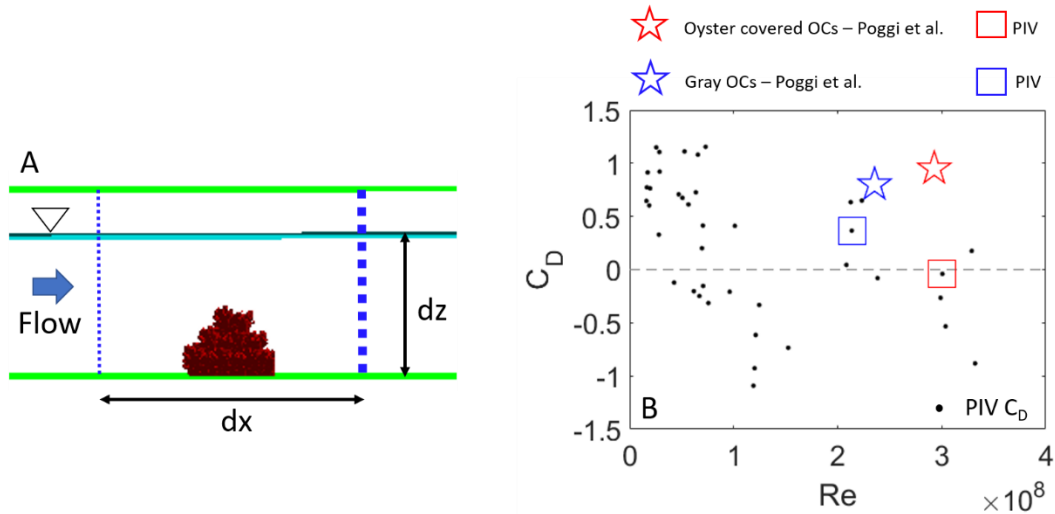


Figure 4.17 (A) Domain for the calculation of the downstream  $C_D$  based on Poggi et al., (2004). (B)  $C_D$  comparison between PIV and formulation by Poggi et al., (2004)

#### 4.4 Discussion

##### 4.4.1 Oyster-covered OCs vs gray OCs

Laboratory experiments aimed to investigate the hydrodynamic differences between gray and oyster-covered OCs. Results demonstrated a drop in velocity in the downstream region (for both water levels), due to the presence of the structure (both with and without oysters), which was also associated with the formation of vortex motions that changed the magnitude and direction of downstream velocity. Results from other studies revealed that rigid structures such as buildings or trees, reduced flow velocities and vertical shear, but enhanced turbulence production (Stoll, 1988).

Reynolds stresses shifted from negative to positive from the upstream to the downstream region, showing a downstream transfer of momentum. The case with oysters showed normalized  $u'v'$  being higher than no oyster scenario in the emergent case (middle and downstream regions), while in the submerged case, normalized  $u'v'$  were very similar for both oyster and no oyster scenarios (slightly higher for the oyster scenario). The higher water level reduced differences between oyster vs no oyster scenarios.

Turbulence characteristics observed in our experiments agree with previous studies regarding flow amenities over oyster reefs. Observed turbulent kinetic energy dissipation rates ( $\epsilon$ ) and turbulent energy (TKE) in the lab were on the order of  $10^{-4}$ , in agreement with Style (2015) and Kitsikoudis et al., 2020. Other studies in the literature, regarding above-canopy turbulent measurements, showed similar rates of dissipation and turbulent energy over coral reefs (e.g. Reidenbach et al., 2006;  $\epsilon : 10^{-5} \text{ m}^2 / \text{s}^3$  ; TKE:  $10^{-4} \text{ m}^2 / \text{s}^2$  ), red mangrove prop roots (e.g. Kibler et al., 2019;  $\epsilon : 10^{-6} \text{ m}^2 / \text{s}^3$  ; TKE:  $10^{-3} \text{ m}^2 / \text{s}^2$  ), and submerged seagrass canopies (e.g. Hansen and Reidenbach, 2017;  $\epsilon : 10^{-5} \text{ m}^2 / \text{s}^3$  ; TKE:  $10^{-3} \text{ m}^2 / \text{s}^2$  ). TKE and Turbulent dissipation were similar for oyster vs no oysters. However, in the emergent case, TKE and dissipation rates were up to one order of magnitude greater than submerged case, denoting higher water levels drastically reduce TKE and dissipation rates.

#### 4.4.2 The impact of different OCs geometries on flow hydrodynamic

The different analyzed OCs geometries revealed case C produced the highest TKE in the emergent case (upstream, middle and downstream regions). In the submerged case, the highest TKE also generated by the C case was closer to the other geometry scenarios. Turbulent dissipation rates had a similar trend of TKE. Case C produced the highest dissipation rates, both in the emergent and submerged cases. Results showed that larger structures (case C), likely block hydrodynamic flow, resulting in high TKE and dissipation rates. Case S, on the other hand, represented the smaller structure and resulted in low TKE and turbulent dissipation. Negative Reynolds stresses were produced by all cases in the upstream region (both emergent and submerged conditions). The downstream region, on the other hand, showed positive Re stresses, denoting increasing transport of downstream momentum along the centerline. Structure geometries also affected velocity distribution. Cases S and B<sub>F</sub> smoothed downstream velocity in both emergent and submerged conditions, while cases A, B, and C slowed down the downstream velocity more, compared to the other case scenarios (both emergent and submerged). The submerged case, however, showed less variability in flow velocity between the upstream and downstream regions, denoting higher water depth has less impact on flow alteration over OCs.

#### 4.4.3 Drag coefficient

The drag coefficient estimation based on the 1D momentum balance revealed a  $C_D$  for the case with oysters almost twice bigger than the no oyster, in the emergent case. However, the submerged case showed negative  $C_D$  for the oyster scenario and mixed (negative and positive)  $C_D$  for the no oyster scenario. The S case was always submerged, resulting in always negative  $C_D$ .  $C_D$  was mostly affected by OCs geometry and flow velocity, especially in the submerged case. The cases with bulkier structures (cases C, B<sub>F</sub> and B) forced by the slower flow, resulted in negative  $C_D$  also for gray OCs, denoting as bigger structures and slower velocities enhanced downstream momentum along the centerline. Numerical simulations through Flow 3D supported negative  $C_D$  values (estimated using 1D momentum balance as well as

for PIV data) for the submerged case A with oyster-covered OCs, and positive  $C_D$  for gray OCs. However, moving the downstream section further forward (towards the end of the domain), downstream momentum along the centerline gradually reduced (but still higher than upstream). The presence of oysters lengthened the turbulent region downstream of the breakwater along the centerline, and associated dissipative phenomena involved more computational space along the x-direction.

The estimation of the drag coefficient based on the formulation provided by Poggi et al., (2004) revealed positive  $C_D$ , in disagreement with PIV results. However, Poggi et al., (2004) developed the drag formulation for vegetation canopies, which cannot be fully representative of our study case.

Other studies in the literature reported  $C_D$  for oyster reefs ranging between 0.03 and 0.15 (Reidenbach et al., 2006; Styles, 2015; Cannon et al., 2022). The drag coefficient estimation based on the 1D momentum balance overestimates the  $C_D$  compared to the above cited studies, but still offers good insights regarding the difference between gray and oyster-covered OCs. The observed moment increase in the upstream region in the submerged case was likely due to non-equilibrium turbulence budgets above and within the oyster canopy, typically associated to enhanced production in the shear layer at the canopy-flow interface (Reidenbach et al., 2007; Cannon et al., 2022). Previous studies of flow above submerged canopies reported a non-equilibrium turbulent budget for oyster reefs (Kitsikoudis et al., 2020), coral reefs (Reidenbach et al., 2007), and plant canopies (Finnigan, 2000). However, momentum increase did not correspond in the emergent case. Furthermore, downstream momentum enhancement may not correspond if the whole three-dimensionality of the flow will be considered. Future 3D studies are needed in order to better characterize the drag coefficient and flow amenities over and around gray and oyster-covered OCs.

#### 4.4.4 Implication for oyster restoration and coastal defense

Results of our study highlighted the water level represents a key element associated with the hydrodynamics around oyster-covered and gray OCs. Higher water levels induce turbulence production which translates into increased downstream momentum along the centerline. Conversely, lower sea levels reveal oysters-covered OCs being able to provide more drag compared to gray OCs, thus dissipating more flow momentum along the centerline. The water level, however, plays a key role in oyster survivability. Lower sea levels would make oysters spend less time submerged, decreasing threats from predation and sedimentation. However, emergent reefs would expose oysters to threats such as desiccation, freezing, lower food supply, and others (Johnson and Smee 2014; Byers et al. 2015). Recruitment rates, essential for supporting oyster reef life over time, are also affected by water level (Rodriguez et al., 2014; Ridge et al., 2015). This is key to consider in relation to the OCs geometry. Our study reveals that larger structures, such as case C, increase TKE and dissipation rates, slow down the flow, and produce higher drag values in the emergent case. However, emergent structures may compromise oyster sustainability because of the higher stresses due to the lower sea levels, while submerged structures (such as case S) are more suitable for oysters' establishment but produce the least alteration in flow and also negative drags, resulting in increasing downstream momentum along the centerline. However, the increase in downstream momentum may be negligible in the presence of wave dissipation phenomena. Wave attenuation is mainly a function of the water level with respect to the reef crest, incoming wave height and period, wave angle attack, and bed level morphology (Galvin, 1972; Madson et al., 1988). Dissipation of wave energy occurs due to the impact of the whole breakwater, rather than its smaller rough features such as oysters. The increase in downstream momentum along the centerline could be orders of magnitude smaller than wave energy attenuation, thus being negligible. However, increased downstream turbulence could re-suspend and transport a higher amount of sediment, rather than promoting deposition, altering bed morphology.

A recent study from Palinkas et al., (2022) highlighted the importance of addressing uncertainties in the performance and long-term sustainability of oyster-reef breakwaters, through detailed experiments, computational and physical

modeling. While protecting the shore, oyster-covered breakwaters can also increase biodiversity, shoreline recreational opportunities, and raise awareness of coastal health. By combining different multi-approaches (Palinkas et al., 2022), it may be possible to fill the gap between restoration projects' implementation and expected outcomes.

#### 4.4.5 Study limitation

Our study was based on laboratory experiments through PIV. PIV is a valuable laboratory technique, used to study a wide variety of hydrodynamic problems (Raffel et al., 1998). However, 2D PIV better performs when flow characteristics measured at the flume centerline are representative of the entire flow. The OCs employed in our study (with and with no oysters) induced a lot of three-dimensionality in the flow, due to their different geometries; thus, flow characteristics measured at the centerline could not be representative of the whole flow around gray and oyster-covered OCs. This factor contributed to the uncertainties in the estimation of the drag coefficient based on the 1D momentum balance. The increase in downstream momentum may not correspond if the whole flow three-dimensionality will be considered. Furthermore, scaled-down experiments (1:7) may also reduce the accuracy of our results.

Numerical modeling through Flow3D supported laboratory results. However, Flow3D overestimated the downstream increase in flow momentum, resulting in more negative  $C_D$  (for the oyster-covered OCs scenario) compared to PIV. The difference between lab and numerical experiments may be due to the higher velocity field developed downstream of the oyster-covered structure in Flow3D (see Figures 4.15 A and 4.15 C). The faster velocity likely raised the downstream flow momentum compared to PIV, leading to more negative  $C_D$ .

Future 3D studies are needed in order to better analyze flow characteristics over and around gray and oyster-covered OCs.

#### 4.5. Conclusions

Our study, performed through laboratory and numerical experiments, aimed to show the differences between gray and oyster-covered OCs. The research revealed a higher drag coefficient (based on the 1D momentum balance) associated with emergent oyster-covered OCs, denoting a greater efficiency of OCs in reducing downstream flow momentum. However, fully submerged OCs showed a downstream momentum increase when covered by oysters, in both laboratory and numerical experiments. The different geometries analyzed in our study revealed larger structures exert greater TKE and dissipation rates in both emergent and submerged conditions. Bulky OCs configurations, such as case C, increased the drag coefficient in the emergent case, while it enhanced downstream momentum along the centerline when fully submerged. Flow three-dimensionality is a key aspect that we have not considered, and could have affected momentum balance estimation. However, studies in the literature found non-equilibrium in the turbulent budget over oyster and coral reefs, as well as plant canopies, which may support our study results.

Further research, in both unidirectional and oscillatory flow conditions, will allow us to clarify and provide relevant guidelines on the design and use of oyster-populated breakwaters as a viable nature-based solution for coastal protection.

#### 4.6 References

- Bayon, A., Valero, D., García-Bartual, R. and López-Jiménez, P.A., 2016. Performance assessment of OpenFOAM and FLOW-3D in the numerical modeling of a low Reynolds number hydraulic jump. *Environmental modelling & software*, 80, pp.322-335.
- Beck, M.W., Brumbaugh, R.D., Airolidi, L., Carranza, A., Coen, L.D., Crawford, C., Defeo, O., Edgar, G.J., Hancock, B., Kay, M.C. and Lenihan, H.S., 2011. Oyster reefs at risk and recommendations for conservation, restoration, and management. *Bioscience*, 61(2), pp.107-116.
- Byers, J. E., Grabowski, J. H., Piehler, M. F., Hughes, A. R., Weiskel, H. W., Malek, J. C., & Kimbro, D. L. (2015). Geographic variation in intertidal oyster reef properties and the influence of tidal prism. *Limnology and Oceanography*, 60(3), 1051-1063
- Cannon, D., Kibler, K.M., Kitsikoudis, V., Medeiros, S.C. and Walters, L.J., 2022. Variation of mean flow and turbulence characteristics within canopies of restored intertidal oyster reefs as a function of restoration age. *Ecological engineering*, 180, p.106678.
- Cerco, C.F. and Noel, M.R., 2007. Can oyster restoration reverse cultural eutrophication in Chesapeake Bay?. *Estuaries and Coasts*, 30, pp.331-343.
- Chowdhury, M. S. N., Walles, B., Sharifuzzaman, S. M., Shahadat Hossain, M., Ysebaert, T., & Smaal, A. C. (2019). Oyster breakwater reefs promote adjacent mudflat stability and salt marsh growth in a monsoon dominated subtropical coast. *Scientific reports*, 9(1), 1-12
- Chu, F.-L. E., La Peyre, J. F. & Burreson, C. S. Perkinsus marinus infection and potential defense-related activities in Eastern Oysters, Crassostrea virginica: salinity effects. *J. Invertebr. Pathol.* 62, 226–232 (1993).
- Coen, L. D., Brumbaugh, R. D., Bushek, D., Grizzle, R., Luckenbach, M. W., Posey, M. H., ... & Tolley, S. G. (2007). Ecosystem services related to oyster restoration. *Marine Ecology Progress Series*, 341, 303-307
- Colden, A.M., Fall, K.A., Cartwright, G.M. and Friedrichs, C.T., 2016. Sediment suspension and deposition across restored oyster reefs of varying orientation to flow: implications for restoration. *Estuaries and Coasts*, 39, pp.1435-1448.
- Ferrario, F., Beck, M. W., Storlazzi, C. D., Micheli, F., Shepard, C. C., & Airolidi, L. (2014). The effectiveness of coral reefs for coastal hazard risk reduction and adaptation. *Nature communications*, 5(1), 1-9

- Finnigan, J., 2000. Turbulence in plant canopies. *Annual review of fluid mechanics*, 32(1), pp.519-571.
- Flow Science, 2018. Flow-3D User Manual v11. 2.
- Fodrie, F. J. et al. Classic paradigms in a novel environment: inserting food web and productivity lessons from rocky shores and saltmarshes into biogenic reef restoration. *J. Appl. Ecol.* 51, 1314–1325 (2014).
- Galvin, C.J., 1972. Wave breaking in shallow water. *Waves on beaches and resulting sediment transport*, pp.413-456.
- Ghasemi, M. and Soltani-Gerdefaramarzi, S., 2017. The scour bridge simulation around a cylindrical pier using Flow-3D. *Journal of Hydrosociences and Environment*, 1(2), pp.46-54.
- Grabowski, J.H. and Peterson, C.H., 2007. Restoring oyster reefs to recover ecosystem services. *Ecosystem engineers: plants to protists*, 4, pp.281-298.
- Gracia, A., Rangel-Buitrago, N., Oakley, J.A. and Williams, A.T., 2018. Use of ecosystems in coastal erosion management. *Ocean & coastal management*, 156, pp.277-289.
- Gutiérrez, J. L., Jones, C. G., Strayer, D. L., & Iribarne, O. O. (2003). Mollusks as ecosystem engineers: the role of shell production in aquatic habitats. *Oikos*, 101(1), 79-90
- Hansen, J.C. and Reidenbach, M.A., 2017. Turbulent mixing and fluid transport within Florida Bay seagrass meadows. *Advances in Water Resources*, 108, pp.205-215.
- Hogan, S., & Reidenbach, M. A. (2022). Quantifying Tradeoffs in Ecosystem Services Under Various Oyster Reef Restoration Designs. *Estuaries and Coasts*, 45(3), 677-690
- Jafari, M., Babajani, A., Hafezisefat, P., Mirhosseini, M., Rezaia, A. and Rosendahl, L., 2018. Numerical simulation of a novel ocean wave energy converter. *Energy Procedia*, 147, pp.474-481.
- Johnson, K. D. & Smee, D. L. Predators influence the tidal distribution of oysters (*Crassostrea virginica*). *Mar. Biol.* 161, 1557–1564 (2014).
- Kibler, K.M., Kitsikoudis, V., Donnelly, M., Spiering, D.W. and Walters, L., 2019. Flow–vegetation interaction in a living shoreline restoration and potential effect to mangrove recruitment. *Sustainability*, 11(11), p.3215.

- Kitsikoudis, V., Kibler, K.M. and Walters, L.J., 2020. In-situ measurements of turbulent flow over intertidal natural and degraded oyster reefs in an estuarine lagoon. *Ecological Engineering*, 143, p.105688.
- Madsen, O.S., Poon, Y.K. and Graber, H.C., 1988. Spectral wave attenuation by bottom friction: Theory. In *Coastal engineering 1988* (pp. 492-504).
- Mann, R. and Powell, E.N., 2007. Why oyster restoration goals in the Chesapeake Bay are not and probably cannot be achieved. *Journal of Shellfish Research*, 26(4), pp.905-917.
- Meyer, D.L., Townsend, E.C. and Thayer, G.W., 1997. Stabilization and erosion control value of oyster cultch for intertidal marsh. *Restoration Ecology*, 5(1), pp.93-99.
- Morris, R. L., La Peyre, M. K., Webb, B. M., Marshall, D. A., Bilkovic, D. M., Cebrian, J., ... & Swearer, S. E. (2021). Large-scale variation in wave attenuation of oyster reef living shorelines and the influence of inundation duration. *Ecological Applications*, 31(6), e02382.
- Nevin, J. A., Mandell, C., & Atak, J. R. (1983). The analysis of behavioral momentum. *Journal of the Experimental analysis of behavior*, 39(1), 49-59.
- North, E. W., Schlag, Z., Hood, R. R., Li, M., Zhong, L., Gross, T., & Kennedy, V. S. (2008). Vertical swimming behavior influences the dispersal of simulated oyster larvae in a coupled particle-tracking and hydrodynamic model of Chesapeake Bay. *Marine Ecology Progress Series*, 359, 99-115.
- Odell, G.M. and Kovasznay, L.S., 1971. A new type of water channel with density stratification. *Journal of Fluid Mechanics*, 50(3), pp.535-543.
- Palinkas, C.M., Orton, P., Hummel, M.A., Nardin, W., Sutton-Grier, A.E., Harris, L., Gray, M., Li, M., Ball, D., Burks-Copes, K. and Davlasheridze, M., 2022. Innovations in coastline management with natural and nature-based features (NNBF): lessons learned from three case studies. *Frontiers in Built Environment*, p.62.
- Poggi, D., Katul, G.G. and Albertson, J.D., 2004. Momentum transfer and turbulent kinetic energy budgets within a dense model canopy. *Boundary-Layer Meteorology*, 111, pp.589-614.
- Raffel, M., Willert, C.E. and Kompenhans, J., 1998. *Particle image velocimetry: a practical guide* (Vol. 2, p. 218). Berlin: Springer.
- Ramezani, Y., Babagoli Sefidkoochi, R. 2016. Comparison of Turbulence Models for Estimation of Bed Shear Stress Around Bridge Abutment in Compound Channel, *Water and soil science*, 26(2): 95- 109

Reidenbach, M.A., Monismith, S.G., Koseff, J.R., Yahel, G. and Genin, A., 2006. Boundary layer turbulence and flow structure over a fringing coral reef. *Limnology and oceanography*, 51(5), pp.1956-1968.

Reidenbach, M.A., Koseff, J.R. and Monismith, S.G., 2007. Laboratory experiments of fine-scale mixing and mass transport within a coral canopy. *Physics of Fluids*, 19(7), p.075107.

Ridge, J. T., Rodriguez, A. B., and Fodrie, F. J. (2017). Evidence of exceptional oyster-reef resilience to fluctuations in sea level. *Ecol. Evol.* 7, 10409–10420. doi: 10.1002/ece3.3473

Rodriguez, A. B., Fodrie, F. J., Ridge, J. T., Lindquist, N. L., Theuerkauf, E. J., Coleman, S. E., ... & Kenworthy, M. D. (2014). Oyster reefs can outpace sea-level rise. *Nature climate change*, 4(6), 493-497.

Stoll, R.B., 1988. *An Introduction to Boundary Layer Meteorology*. Dordrecht, The Netherlands: Kluwer Academic, 666p

Styles, R. (2015). Flow and turbulence over an oyster reef. *Journal of Coastal Research*, 31(4), 978-985

Sutton-Grier, A. E., Wowk, K., and Bamford, H. (2015). Future of our coasts: the potential for natural and hybrid infrastructure to enhance the resilience of our coastal communities, economies and ecosystems. *Environ. Sci. Policy* 51, 137–148. doi: 10.1016/j.envsci.2015.04.006

Sutton-Grier, A. E., Gittman, R. K., Arkema, K. K., Bennett, R. O., Benoit, J., Blich, S., ... & Grabowski, J. H. (2018). Investing in natural and nature-based infrastructure: building better along our coasts. *Sustainability*, 10(2), 523.

Temmerman, S., Meire, P., Bouma, T. J., Herman, P. M., Ysebaert, T., and De Vriend, H. J. (2013). Ecosystem-based coastal defense in the face of global change. *Nature* 504, 79–83. doi: 10.1038/nature12859

Theuerkauf, S. J., Burke, R. P., & Lipcius, R. N. (2015). Settlement, growth, and survival of eastern oysters on alternative reef substrates. *Journal of Shellfish Research*, 34(2), 241-250

Thielicke, W. and Stamhuis, E., 2014. PIVlab—towards user-friendly, affordable and accurate digital particle image velocimetry in MATLAB. *Journal of open research software*, 2(1).

White, M. E. & Wilson, E. A. In *The eastern oyster Crassostrea virginica* (eds. Kennedy, V. S., Newell, R. I. E. & Eble, A. F.) 559–580 (Maryland Sea Grant College, 1996)

Wiberg, P.L.; Taube, S.R.; Ferguson, A.E.; Kremer, M.R.; Reidenbach, M. A. Wave attenuation by oyster reefs in shallow coastal bays. *Estuaries and coasts*, 2019, 42, pp. 331-347

Wilberg, M.J., Livings, M.E., Barkman, J.S., Morris, B.T. and Robinson, J.M., 2011. Overfishing, disease, habitat loss, and potential extirpation of oysters in upper Chesapeake Bay. *Marine Ecology Progress Series*, 436, pp.131-144.

Wood, L. H., & Hargis, W. J. (1971). *Transport of bivalve larvae in a tidal estuary* (pp. 29-44). Cambridge University Press

## Chapter 5: Conclusions

The carried out research has brought significant insights into the coupling between natural (oysters) and built (breakwaters) solutions for coastal protection.

Outcomes from Chapter 2 revealed breakwaters are important solutions for coastal defense, being able to reduce wave energy and protect the shoreline from erosion. However, they negatively impact the sediment supply for coastal vegetation. To improve coastal resilience, these gray structures should be placed closer to the shore, as greater distances were associated with less sediment deposition and greater erosion of the marsh edge. Nevertheless, higher wave heights (associated with storm events) combined with steeper basin slopes enhanced sediment replenishment for coastal wetlands.

Field studies from Chapter 3 showed gray breakwaters being able to provide shoreline protection by attenuating incoming wave energy and promoting sediment deposition in the Lake Cove, supporting modeling results of Chapter 2. However, challenges encountered in the field did not allow us to study the coupling of breakwaters and oysters more deeply within the Lake Cove, underlining the importance of environmental and biogeochemical conditions for reefs' establishment, growth and survivability. Water level and aerial exposure, as well as geographical location, temperature and salinity are key factors to consider when involving oysters in coastal protection. The Lake Cove modeling simulations, on the other hand, have shown a loss of protective benefits over time by gray breakwaters due to increase in sea level, except when coupled with oysters, capable of self-adapt and grow with SLR.  $\Delta H$ s drastically decreased over time, but remained significant only when oysters were included. The sediment budget of the shoreline shifted towards negative values (net loss of sediments) as well, as the water level increased. However, oysters allowed the balance to be maintained positive also in 100 years.

Laboratory experiments aimed to show hydrodynamic differences between gray and oyster-covered breakwaters. The research revealed a higher drag coefficient (based on the 1D momentum balance) associated with emergent oyster-covered

breakwaters, denoting a greater efficiency in reducing downstream flow momentum. However, fully submerged breakwaters showed a downstream momentum increase when covered by oysters, in both laboratory and CFD experiments. Flow three-dimensionality is a key aspect that we have not considered, and could have affected our results. However, studies in the literature found non-equilibrium in the turbulent budget over oyster and coral reefs, as well as plant canopies, which may support study results. Further research, in both unidirectional and oscillatory flow conditions, will allow to clarify and provide relevant guidelines on the design and use of oyster-populated breakwaters as a viable nature-based solution for coastal protection.

Principals established in this study are highly applicable for the design of fully-integrated hybrid infrastructures wishing to use oysters and other reef-forming species. Overall, the current dissertation highlights oysters' integration into coastal defense can offer new adaptive shoreline protection in the face of climate changes and SLR, where optimal conditions for oysters' survivability occur and are maintained over time. Estuaries and coastal bays are the most suitable environments for the development of oyster-based infrastructures, where hydrodynamic stresses allow the settlement and establishment of new oyster generations. Locations supported by higher larvae recruitment rates represent coastal areas where oyster-based infrastructures have the highest probability of success, and this research supported these NNBFs for improving shoreline resilience over a changing climate and a rising sea.



Wave parameters,  $H_s$  and  $T_s$  recorded by the SB and the ADCP HR are shown in Figure A2.

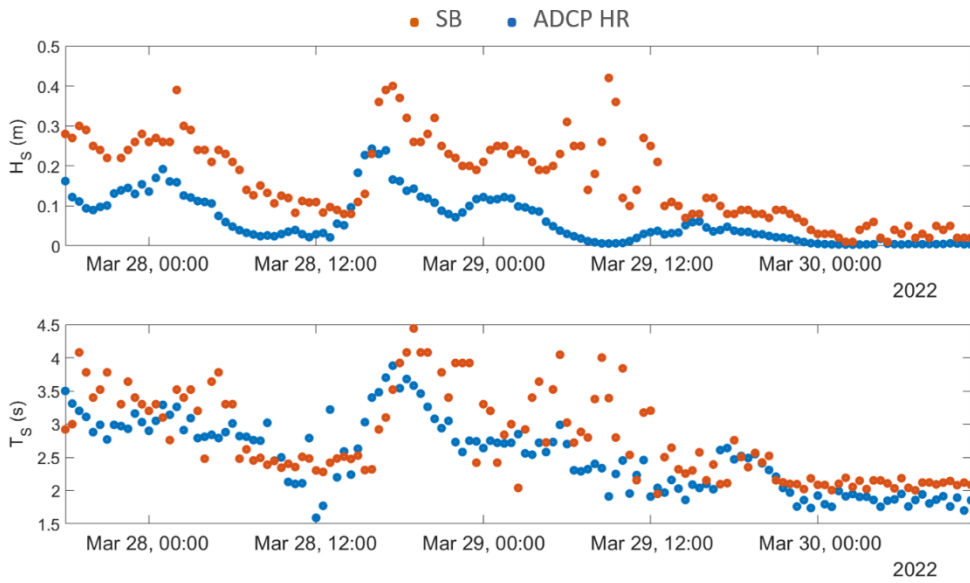


Figure A2. Significant wave heights and wave periods recorded by the SB and the ADCP HR.

The exceptional low tide during which the UAV survey aimed to collect bathymetric data of the Lake Cove and the Digital Elevation Model (DEM) obtained after post imagery processing are shown in Figure A3. References to the methodology used can be found in Nardin et al., 2021 and Taddia et al., 2021.

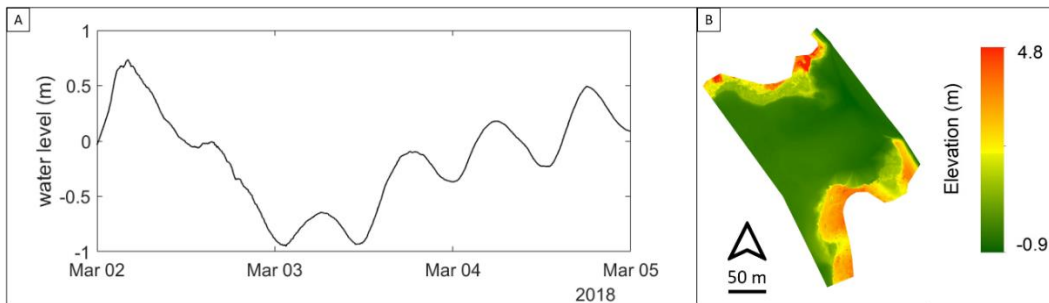


Figure A3. (A) Tidal signal recorded at the NOAA station in Cambridge (MD) from the 2<sup>nd</sup> to the 5<sup>th</sup> of March, 2018. (B) Digital elevation model of the Lake Cove obtained from UAV images post processing.

Sensitivity analysis showed the high morphological factor (50) used in the modeling did not influence water level and wave height recorded at the SB (Figure A4).

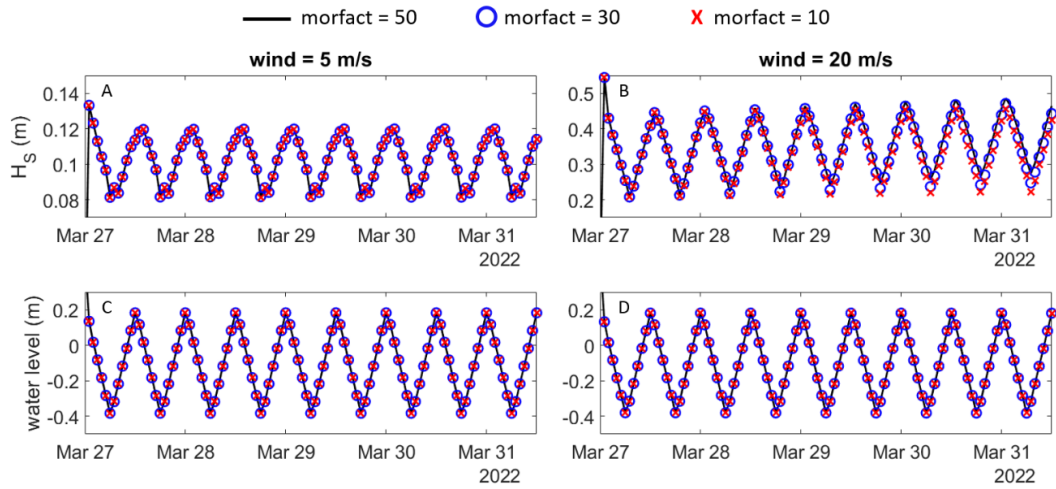


Figure A4. Sensitivity analysis regarding the impact of the morphological scale factor on  $H_s$  and water level.

The initial and final modeled bed levels along transects 1 and 2 are shown in Figure A5.

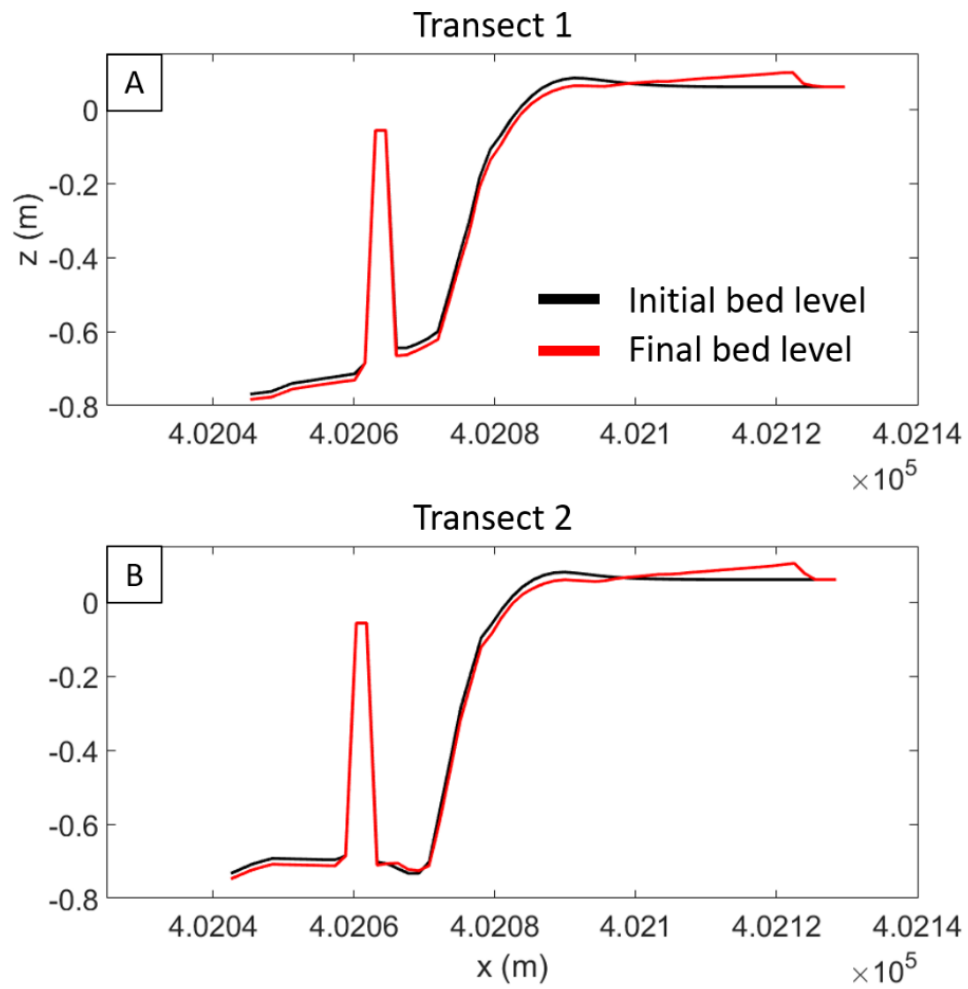


Figure A5. (A) Model final and initial bed level along transect 1 and (B) transect 2

The initial and final modeled bed levels along transects 3 and 4 are shown in Figure A6.

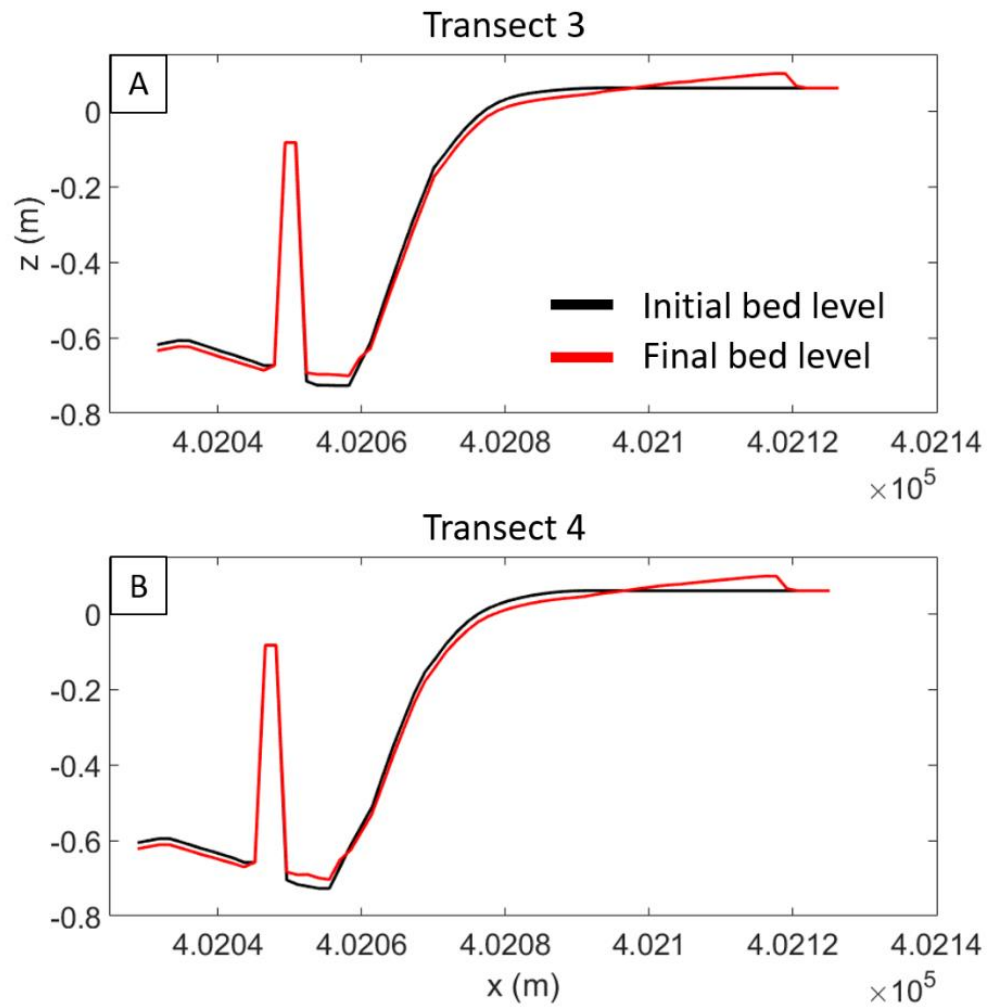


Figure A6. (A) Model final and initial bed level along transect 3 and (B) transect 4

Wave attenuation without and with gray breakwaters is shown in Figure A7

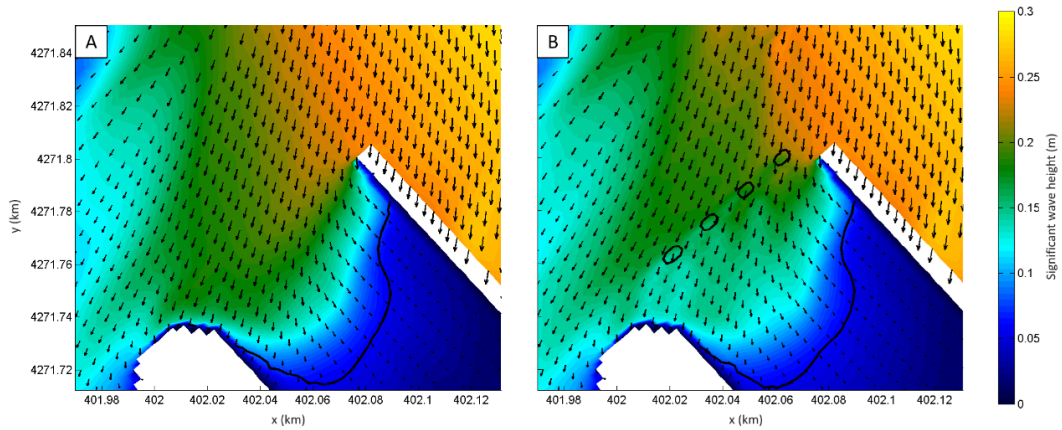


Figure A7. Modeled wave field in the Lake Cove at high tide for the scenario with (A) no breakwaters and (B) gray breakwaters. Results are taken from simulation with actual MWL and wind intensity = 15 m/s. Black line defines the final bed level threshold at 0.05 m (NAVD88).

Sensitivity analysis showed the model did not reveal any difference in wave attenuation by varying breakwater roughness (Figure A8).

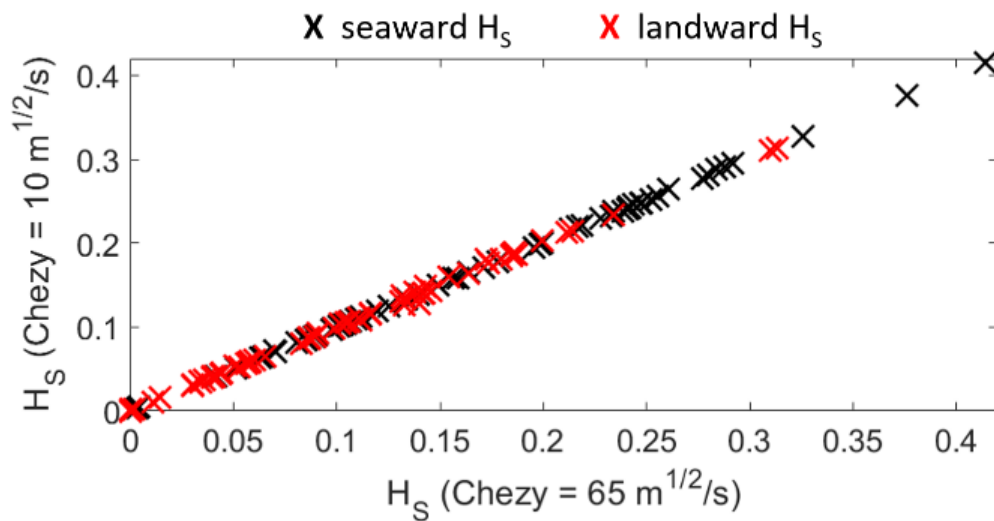


Figure A8. Sensitivity analysis regarding the impact of breakwater roughness on wave attenuation.

## *A.2 Lessons learned from modeling experiments – Sediment exchange between saltmarshes and SAV*

Modeling experiments have been performed in order to explore different scenarios than those analyzed in the current research. In particular, the sediment budget of a vegetated living shoreline (made by marsh only and marsh & rip-rap) and adjacent SAV bed was analyzed. Living shorelines are often designed by incorporating rip-rap rather than breakwaters, which provide similar erosion-control functions. The aim of this study was therefore to study how structures different from breakwaters affect the sediment budget of a vegetated shoreline, with the aim of promoting and encouraging the coupling of oysters also with other types of gray solutions. To better study these aspects, three different scenarios were simulated, (1) marsh only on the shore, (2) marsh and SAV bed within the shoreline, and (3) marsh, SAV, and rip-rap, varying the wave height, wave period and basin slope.

The study in question was carried out through Delft3D and more information and insights can be found in Vona et al., (2021).

Simulation results demonstrated the efficacy of the vegetated shoreline in absorbing wave motion, thereby reducing incoming wave height by up to 80%, similarly to a study by Manis et al. (2015). Shear stress was greatly reduced within the SAV bed, which favored higher deposition and lower erosion rates, and was positively correlated with slope, wave height, and period following a power law. Results about the sediment balance (defined as deposition - erosion) occurring between marsh and SAV among all simulated scenarios, revealed it was negative for the configuration that only included the marsh on the shore, indicating a net loss of sediment. The scenario with both vegetation communities drastically reduced sediment loss for low-energy and slope scenarios but still had a higher amount of sediment loss for higher energy and slope scenarios. The configuration with marsh, SAV, and rip-rap resulted in a higher sediment retainment for all wave conditions. The sediment budget was slightly positive under the action of ordinary external forcing, while for higher wave heights, which caused the greatest loss of sediments in

the other two configurations, the sediment balance was strongly positive. The increase in the basin slope increased sediment loss.

The delicate balance between the supply and loss of sediments is crucial in coastal wetland restoration plans. Artificial structures make it possible to avoid greater damage in extreme events, which also has a significant economic impact. Living shorelines certainly offer a valid and green solution to coastal protection, which, if coupled with man-made or natural structures, such as oyster reefs rather than rip-rap, can strengthen the resilience and the vitality of the coast.

### A.3 Flow 3D governing equations

The differential equations to be solved are written in terms of Cartesian coordinates (x, y, z). For cylindrical coordinates (r,  $\theta$ , z) the x-coordinate is interpreted as the radial direction, the y-coordinate is transformed to the azimuthal coordinate,  $\theta$ , and z is the axial coordinate. For cylindrical geometry, additional terms must be added to the Cartesian equations of motion. These terms are included with a coefficient  $\xi$ , such that  $\xi=0$  corresponds to Cartesian geometry, while  $\xi=1$  corresponds to cylindrical geometry.

All equations are formulated with area and volume porosity functions. This formulation, called FAVOR (Fractional Area/Volume Obstacle Representation Method) is used to model complex geometric regions. For example, zero-volume porosity regions are used to define obstacles, while area porosities may be used to model thin porous baffles. Porosity functions also introduce some simplifications in the specification of free- surface and wall boundary conditions. Generally, in FLOW-3D, area and volume fractions are time independent. However, these quantities may vary with time when the moving obstacle model is employed. Flow3D can work and analyze fluid dynamic phenomenon at the microscale providing a really high spatial and temporal resolution.

The general mass continuity equation is:

$$\begin{aligned} V_f \frac{\partial \rho}{\partial t} + \frac{\partial}{\partial x} (\rho u A_x) + R \frac{\partial}{\partial y} (\rho v A_y) + \frac{\partial}{\partial z} (\rho w A_z) + \xi \frac{\rho u A_x}{x} \\ = R_{DIF} + R_{SOR} \end{aligned} \quad (A.3.1)$$

where  $V_f$  is the fractional volume open to flow,  $\rho$  is the fluid density,  $R_{DIF}$  is a turbulent diffusion term, and  $R_{SOR}$  is a mass source. The velocity components (u, v, w) are in the coordinate directions (x, y, z) or (r,  $\theta$ , z).  $A_x$  is the fractional area open to flow in the x-direction,  $A_y$  and  $A_z$  are similar area fractions for flow in the y and z directions, respectively. The coefficient R depends on the choice of coordinate system in the following way. When cylindrical coordinates are used, y derivatives must be converted to azimuthal derivatives,

$$\frac{\partial}{\partial y} \rightarrow \frac{1}{r} \frac{\partial}{\partial \theta} \quad (\text{A.3.2})$$

This transformation is accomplished by using the equivalent form

$$\frac{1}{r} \frac{\partial}{\partial \theta} = \frac{r_m}{r} \frac{\partial}{\partial y} \quad (\text{A.3.3})$$

where  $y = r_m \theta$  and  $r_m$  is a fixed reference radius. The transformation given by Equation (3.3) is particularly convenient because its implementation only requires the multiplier  $R = r_m / r$  on each  $y$  derivative in the original Cartesian coordinate equations. When Cartesian coordinates are to be used,  $R$  is set to unity and  $\xi$  is set to zero.

The first term on the right side of Equation (3.1), is a turbulent diffusion term,

$$R_{\text{DIF}} = \frac{\partial}{\partial x} \left( v_\rho A_x \frac{\partial \rho}{\partial x} \right) + R \frac{\partial}{\partial y} \left( v_\rho A_y R \frac{\partial \rho}{\partial y} \right) + \frac{\partial}{\partial z} \left( v_\rho A_z \frac{\partial \rho}{\partial z} \right) + \xi \frac{\rho v_\rho A_x}{x} \quad (\text{A.3.4})$$

where the coefficient  $v_p$  is equal to  $cp\mu/\rho$ , in which  $\mu$  is the coefficient of momentum diffusion (i.e., the viscosity) and  $cp$  is a constant whose reciprocal is usually referred to as the turbulent Schmidt number. This type of mass diffusion only makes sense for turbulent mixing processes in fluids having a non-uniform density.

The last term,  $R_{\text{SOR}}$ , on the right side of Equation (3.1) is a density source term that can be used, for example, to model mass injection through porous obstacle surfaces.

Compressible flow problems require solution of the full density transport equation as stated in Equation (3.1). For incompressible fluids,  $\rho$  is a constant and Equation (3.1) reduces to the incompressibility condition:

$$\frac{\partial}{\partial x} (uA_x) + R \frac{\partial}{\partial y} (vA_y) + \frac{\partial}{\partial z} (wA_z) + \xi \frac{uA_x}{x} = \frac{R_{\text{SOR}}}{\rho} \quad (\text{A.3.5})$$

For problems in which the propagation of acoustic pressure waves is important, but the fluid may otherwise be treated as incompressible, the density time derivative is approximated by:

$$\frac{\partial \rho}{\partial t} \approx \frac{1}{c^2} \frac{\partial p}{\partial t} \quad (\text{A.3.6})$$

where  $c^2$  is the square of the sound speed and  $p$  is the pressure. This approximation is valid in the range:

$$\left| \frac{\delta \rho}{\rho} \right| < 0.1 \quad (\text{A.3.7})$$

With this approximation the modified continuity equation then becomes:

$$\frac{V_F}{\rho c^2} \frac{\partial p}{\partial t} + \frac{\partial}{\partial x} (uA_x) + R \frac{\partial}{\partial y} (vA_y) + \frac{\partial}{\partial z} (wA_z) + \xi \frac{uA_x}{x} = \frac{R_{SOR}}{\rho} \quad (\text{A.3.8})$$

The equations of motion for the fluid velocity components ( $u$ ,  $v$ ,  $w$ ) in the three coordinate directions are the Navier-Stokes equations with some additional terms,

$$\begin{aligned} \frac{\partial u}{\partial t} + \frac{1}{V_F} \left\{ uA_x \frac{\partial u}{\partial x} + vA_y R \frac{\partial u}{\partial y} + wA_z \frac{\partial u}{\partial z} \right\} - \xi \frac{A_y v^2}{x V_F} \\ = -\frac{1}{\rho} \frac{\partial p}{\partial x} + G_x + f_x - b_x - \frac{R_{SOR}}{\rho V_F} (u - u_w - \delta u_s) \end{aligned} \quad (\text{A.3.9})$$

$$\begin{aligned} \frac{\partial v}{\partial t} + \frac{1}{V_F} \left\{ uA_x \frac{\partial v}{\partial x} + vA_y R \frac{\partial v}{\partial y} + wA_z \frac{\partial v}{\partial z} \right\} + \xi \frac{A_y u v}{x V_F} \\ = -\frac{1}{\rho} \left( R \frac{\partial p}{\partial y} \right) + G_y + f_y - b_y - \frac{R_{SOR}}{\rho V_F} (v - v_w \\ - \delta v_s) \end{aligned} \quad (\text{A.3.10})$$

$$\begin{aligned} \frac{\partial w}{\partial t} + \frac{1}{V_F} \left\{ uA_x \frac{\partial w}{\partial x} + vA_y R \frac{\partial w}{\partial y} + wA_z \frac{\partial w}{\partial z} \right\} \\ = -\frac{1}{\rho} \frac{\partial p}{\partial z} + G_z + f_z - b_z - \frac{R_{SOR}}{\rho V_F} (w - w_w - \delta w_s) \end{aligned} \quad (\text{A.3.11})$$

In these equations,  $(G_x, G_y, G_z)$  are body accelerations,  $(f_x, f_y, f_z)$  are viscous accelerations,  $(b_x, b_y, b_z)$  are flow losses in porous media or across porous baffle plates, and the final terms account for the injection of mass at a source represented by a geometry component.

## A.4 Linear wave theory

### A.4.1 Problem formulation

In fluid dynamics, a linearized description of the propagation of gravity waves on the surface of a homogeneous fluid layer is given by the airy wave theory (often referred to as linear wave theory).

The free surface elevation  $\eta(x,t)$  of one wave component is sinusoidal, as a function of horizontal position  $x$  and time  $t$ :

$$\eta(x, t) = a \cos(kx - \omega t) \quad (\text{A.4.1})$$

where

- $a$  is the wave amplitude in meter,
- $\cos$  is the cosine function,
- $k$  is the angular wavenumber in radians per meter, related to the wavelength  $\lambda$  by  $k = 2\pi/\lambda$ ,
- $\omega$  is the angular frequency in radians per second, related to the period  $T$  and frequency  $f$  by  $\omega = 2\pi/T = 2\pi f$ .

The waves propagate along the water surface with the phase speed  $c_p$ :

$$c_p = \frac{\omega}{k} = \frac{\lambda}{T} \quad (\text{A.4.2})$$

The angular wavenumber  $k$  and frequency  $\omega$  are not independent parameters (and thus also wavelength  $\lambda$  and period  $T$  are not independent) but are coupled. Surface gravity waves on a fluid are dispersive waves (exhibiting frequency dispersion), meaning that each wavenumber has its own frequency and phase speed.

Waves propagate in the horizontal direction, with coordinate  $x$ , and a fluid domain bound above by a free surface at  $z = \eta(x,t)$ , with  $z$  the vertical coordinate (positive in the upward direction) and  $t$  being time. The level  $z = 0$  corresponds to the mean surface elevation. The impermeable bed underneath the fluid layer is at  $z = -h$ .

Further, the flow is assumed to be incompressible ( $\nabla \cdot \mathbf{u} = 0$ ) and irrotational ( $\nabla \times \mathbf{u} = 0$ ), a good approximation of the flow in the fluid interior for waves on a liquid surface, and potential theory can be used to describe the flow. The velocity

potential  $\Phi(x,z,t)$  is related to the flow velocity components  $u_x$  and  $u_z$  in the horizontal (x) and vertical (z) directions by:

$$u_x = \frac{\partial \Phi}{\partial x} \quad \text{and} \quad u_z = \frac{\partial \Phi}{\partial z} \quad (\text{A.4.3})$$

Then, due to the continuity equation for an incompressible flow, the potential  $\Phi$  has to satisfy the Laplace equation:

$$\frac{\partial^2 \Phi}{\partial x^2} + \frac{\partial^2 \Phi}{\partial z^2} = 0 \quad (\text{A.4.4})$$

Boundary conditions are needed at the bed and the free surface in order to close the system of equations. For their formulation within the framework of linear theory, it is necessary to specify what the base state (or zeroth-order solution) of the flow is. Here, we assume the base state is rest, implying the mean flow velocities are zero.

The bed being impermeable, leads to the kinematic bed boundary-condition:

$$\frac{\partial \Phi}{\partial z} = 0 \quad \text{at} \quad z = -h \quad (\text{A.4.5})$$

In case of deep water (by which is meant infinite water depth, from a mathematical point of view) the flow velocities have to go to zero in the limit as the vertical coordinate goes to minus infinity:  $z \rightarrow -\infty$ .

At the free surface, for infinitesimal waves, the vertical motion of the flow has to be equal to the vertical velocity of the free surface. This leads to the kinematic free-surface boundary-condition:

$$\frac{\partial \eta}{\partial t} = \frac{\partial \Phi}{\partial z} \quad \text{at} \quad z = \eta(x, t) \quad (\text{A.4.6})$$

If the free surface elevation  $\eta(x,t)$  was a known function, this would be enough to solve the flow problem. However, the surface elevation is an extra unknown, for which an additional boundary condition is needed. This is provided by Bernoulli's equation for an unsteady potential flow. The pressure above the free surface is

assumed to be constant. This constant pressure is taken equal to zero, without loss of generality, since the level of such a constant pressure does not alter the flow. After linearization, this gives the dynamic free-surface boundary condition:

$$\frac{\partial \Phi}{\partial t} + g\eta = 0 \quad \text{at} \quad z = \eta(x, t) \quad (\text{A.4.7})$$

Because this is a linear theory, in both free-surface boundary conditions (the kinematic and the dynamic one, equations) the value of  $\Phi$  and  $\partial\Phi/\partial z$  at the fixed mean level  $z = 0$  is used.

#### A.4.2 Solution for monochromatic waves

For a propagating wave of a single frequency (a monochromatic wave) the surface elevation is of the form:

$$\eta = a \cos(kx - \omega t) \quad (\text{A.4.8})$$

The associated velocity potential, satisfying the Laplace equation (A.4.4) in the fluid interior, as well as the kinematic boundary conditions at the free surface (A.4.5), and bed (A.4.6), is:

$$\Phi = \frac{\omega}{k} \frac{\cosh k(z+h)}{\sinh kh} \sin(kx - \omega t) \quad (\text{A.4.9})$$

with  $\sinh$  and  $\cosh$  the hyperbolic sine and hyperbolic cosine function, respectively. But  $\eta$  and  $\Phi$  also have to satisfy the dynamic boundary condition, which results in non-trivial (non-zero) values for the wave amplitude  $a$  only if the linear dispersion relation is satisfied:

$$\omega^2 = gk \tanh kh \quad (\text{A.4.10})$$

with  $\tanh$  the hyperbolic tangent. So angular frequency  $\omega$  and wavenumber  $k$  (or equivalently period  $T$  and wavelength  $\lambda$ ) cannot be chosen independently but are related. This means that wave propagation at a fluid surface is an eigenproblem. When  $\omega$  and  $k$  satisfy the dispersion relation, the wave amplitude  $a$  can be chosen freely (but small enough for Airy wave theory to be a valid approximation).

### A.5 Sediment transport in open channels

An overview on unobstructed sediment transport is presented and it is suggested to read van Rijn (1993) for more details. This appendix does not discuss in detail and only serves to show general practices and nomenclature.

#### A.5.1 Sediment properties

Sediments have many descriptive properties such as genetic origin, texture, organic content, etc. However, only the properties important for mathematical modelling of sediment transport are presented here.

#### **Density and Porosity**

Density of coastal and estuarine sediments is often between 2500 kg/m<sup>3</sup> to 2650 kg/m<sup>3</sup> and is denoted by  $\rho_s$ . The relative density with water ( $s$ ) is defined as:

$$s = \frac{\rho_{sediment}}{\rho_{water}} \quad (A.5.1)$$

Porosity of the sediment is amount of void space in the packed sediment and is related how the sediment is packed. It is written as either a decimal fraction between 0 and 1 or as a percentage.

#### **Shape, Size, and Angle of repose**

Sediment particles are rarely spherical and have highly irregular shapes. Due to this irregularity, sediment sizes are often described with the following diameters:

**Nominal diameter ( $d_v$ )** The diameter of a sphere with the same volume as the particle

**Sieve diameter ( $d_s$ )** The diameter equal to the length of sieve square which the particle passes through

Further, the sediment size distribution is created by doing a sieve analysis. The distribution is represented using the following parameters:

**D<sub>50</sub>** 50% of sediment have a smaller diameter than D<sub>50</sub> and is often the characteristic sediment size

**D<sub>90</sub>** 90% of sediment have a smaller diameter than D<sub>90</sub>

$$\text{Sorting coefficient (S}_r\text{)} \quad S_r = \sqrt{D_{90}/D_{50}} \quad (\text{A.5.2})$$

Angle of repose ( $\Phi$ ) is the maximum slope at which unconsolidated sediment can accumulate in a conical mound and remain stable.

### Settling velocity

Settling velocity ( $w_s$ ) of a particle is velocity at which a particle free-falling in still water stops accelerating i.e weight, buoyancy, and drag forces are balanced.

$$w_s = \sqrt{\frac{4gD_{50}(s - 1)}{3CD}} \quad (\text{A.5.3})$$

Where,  $g$  is acceleration due to gravity,  $s$  is the relative density, and  $CD$  is the drag coefficient of the particle dependent on the particle Reynolds number ( $Re_p = \frac{w_s D_{50}}{\nu}$ ).

### Relative inertia of particles

When  $s \leq 1$  (lighter than water), the particle is passive the flow and follows the fluid motion.

When  $s \gg 1$  (heavy particles), the sediment actively interacts with the flow and modifies the flow.

Furthermore, the particle size relative to the eddy size dictates the path of the particle. Stoker number ( $S_t$ ) a dimensionless number is defined to relate to the behavior of suspended particles in a fluid flow:

$$S_t = \frac{w_s}{u_*} \quad (\text{A.5.4})$$

Where,  $u_*^2 = -u'w'$  represents a characteristic velocity of the flow interacting with the sediment.

$S_t \gg 1$  The particle will detach from the flow and is often the characteristic sediment size

$S_t \ll 1$  The particle will closely follow the fluid streamlines

#### A.5.2 Initiation of motion and Suspension

Initiation of motion happens when the fluid flows provides sufficient bed-shear stress ( $\tau_b$ ) to dislodge the sediment particle from the bed. This stress is known as the critical bed-shear stress ( $\tau_c$ ). The generally accepted way of identifying initiation of sediment transport in currents is using the non-dimensional Shield's parameter denoted by  $\theta$  (Shields, 1936). This can also be called as mobility parameter. Many experiments are undertaken to determine the critical Shield's parameter ( $\theta_{cr}$ ) as a function of critical Reynolds number ( $Re_* = u_* \frac{D_{50}}{\nu}$ ).

Figure A.5.1 demonstrates the transport of particles for different distributions of bed-shear stress and critical bed-shear stresses. The effect of oscillatory flow on initiation of motion is largely unknown. The presence of cohesive sediment in the bed might increase the resistance against erosion drastically.

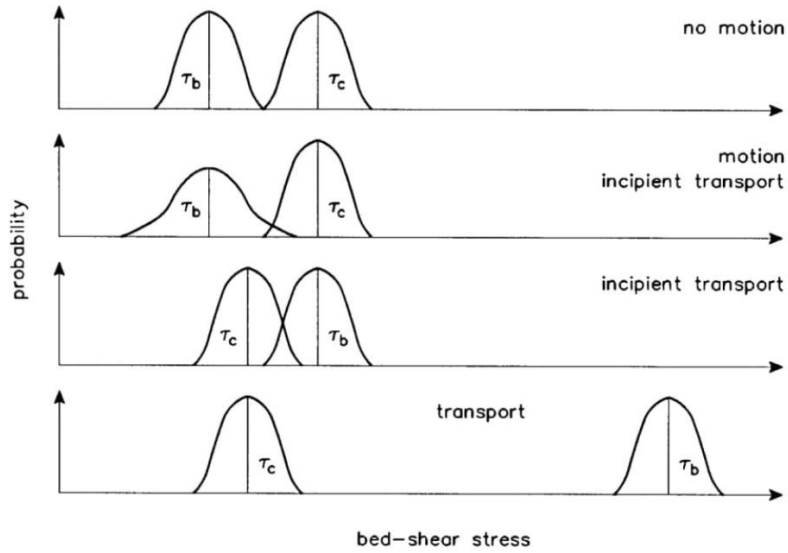


Figure A.5.1: Initiation of motion for a current over a plane bed according to stochastic approach. Image adopted from van Rijn (1993)

Parameters are defined as follows:

$$\theta = \frac{u_*^2}{(s-1)gd} = \frac{\tau_b}{\rho(s-1)gd} \quad (\text{A.5.5})$$

$$\begin{aligned} \theta_{cr} &= \frac{u_{*,cr}^2}{(s-1)gd} = \frac{\tau_{cr}}{\rho(s-1)gd} \\ &= f(Re_*, \phi, \text{Particle geometry}, \dots \text{etc}) \end{aligned} \quad (\text{A.5.6})$$

## Suspension

The suspension of particles happens when the sediment is picked up from the bed and then gets entrained in the flow. Therefore, the first condition for suspension is  $\theta > \theta_{cr}$  and the second condition is  $u_* \geq w_s$ .

### A.5.3 Types of sediment transport and their quantification

We can distinguish two main types of sediment motion:

- Bed load: sliding and rolling along bed (includes saltation)

- Suspended load: turbulent mixing supports sediment grains within flow

There is no clear distinction between bed-load and suspended load sediment transport. Therefore, a reference height is identified and bed-load is considered as the sediment transport in the layer of below the reference height (Figure A.5.2).

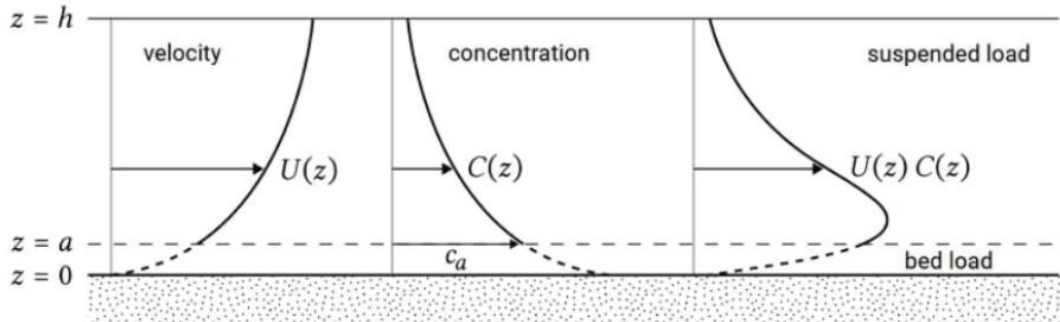


Figure A.5.2: Identifying bed-load and suspended-load in a flow. Image adopted from Bosboom and Stive (2021)

### Bed load

The bed-load sediment transport rate is defined as:

$$q_b = \int_0^a U(z)C(z)dz \quad (\text{A.5.7})$$

Where,  $U(z)$  is the velocity profile and  $C(z)$  is the sediment concentration profile.

Sediment concentration is defined as the volume or mass ratio of sediment to sediment and water mixture. However, in general the sediment transport models predict the non-dimensional sediment transport rate  $\Phi_b$ :

$$\Phi_b = \frac{q_b}{\sqrt{(s-1)gd_{50}^3}} \quad (\text{A.5.8})$$

Many experiments are conducted to determine these models and Bagnold (1956) was one of the earliest models. Further, Ribberink (1998) performed a high-quality set of experiments and proposed an empirical formulation.

- Bagnold (1956):

$$\Phi_b \approx (\theta - \theta_{cr}) \sqrt{\theta} \quad (\text{A.5.9})$$

• Ribberink (1998):

$$\Phi_b = m(\theta - \theta_{cr})^n \quad \theta \geq \theta_{cr} \quad (\text{A.5.10})$$

$$\Phi_b = 0 \quad \theta < \theta_{cr} \quad (\text{A.5.11})$$

$$m = 10.4, n = 1.67$$

• Meyer-Peter and Müller (1948) (Meyer-Peter–Müller (MPM) formula):

$$\Phi_b = 8 (\theta - \theta_{cr}) \quad (\text{A.5.12})$$

## Suspended load

The time averaged sediment concentration for suspended load is often given by a Rouse profile. This profile is derived from the advection-diffusion equation and the gradient diffusion theory (read Bosboom and Stive (2021) for derivation).

$$C(z) = C_a \left( \frac{a h - z}{z h + z} \right)^b \quad (\text{A.5.13})$$

Where, b is the Rouse number which is defined as:

$$b = \frac{w_s}{\kappa u_*} \quad (\text{A.5.14})$$

where,  $\kappa$  is the von Karman constant.

Wash load is a subset of suspended sediment consisting of very fine sediments that never deposit and are suspended in the flow throughout. Due to this nature the wash load never interacts with the bed sediment leaving no trace in the channel or extract any momentum from the flow.

A.6 Chapter 2 supplementary information

The impact of each individual variable on morphological parameters (shear stress, deposition and erosion), is reported in the following Figures. The wave height was positively correlated with the magnitude of the shear stress at the beginning of the marsh, while the tide did not significantly impact the shear stress. Greater breakwater distance from the shoreline resulted in slightly increased shear stress at the beginning of the marsh (Figure A.6.1).

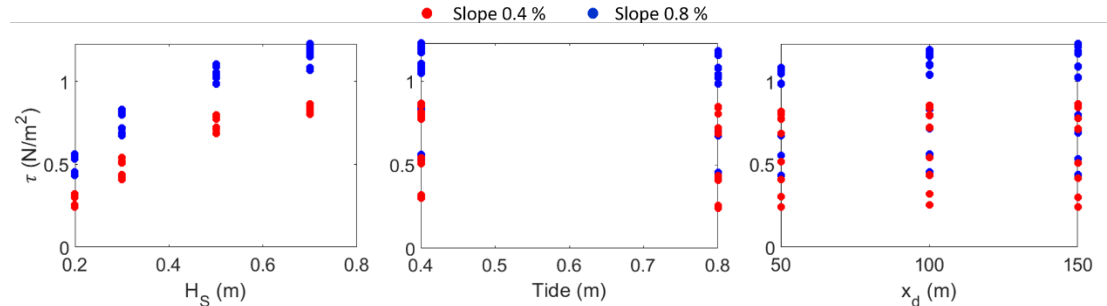


Figure A.6.1. Correlations between shear stress at the beginning of the marsh and (left plot)  $H_s$ , (middle plot) Tide, and (right plot)  $x_d$

The wave height was also positively correlated with the amount of deposition within the marsh platform, as well as the tide. The greater breakwater distance from the shore reduced sediment deposition in the marsh (Figure A.6.2).

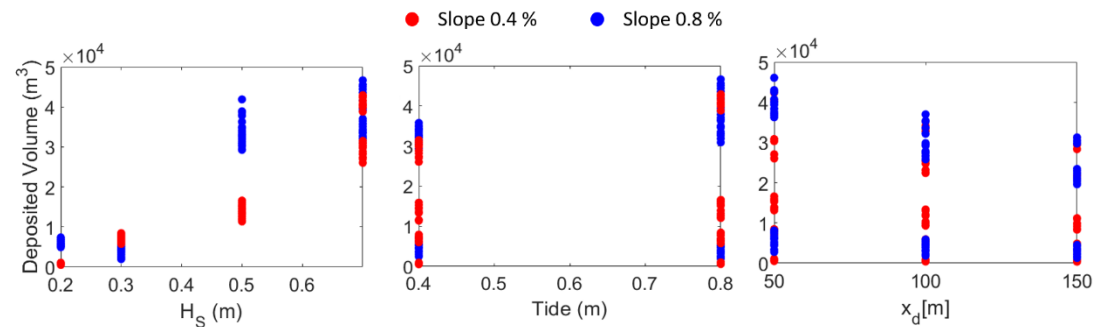


Figure A.6.2. Correlations between sediment deposition within the marsh and (left plot)  $H_s$ , (middle plot) Tide, and (right plot)  $x_d$

The erosion of the marsh scarp was positively correlated with the wave height, the tide, and the breakwater distance from the shore (Figure A.6.3).

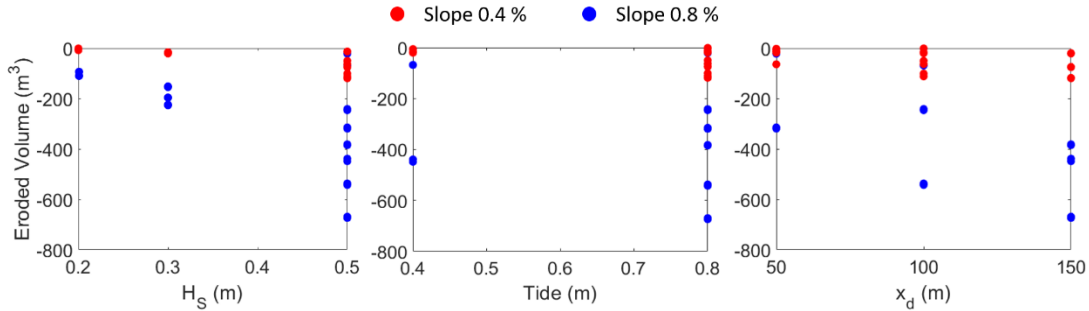


Figure A.6.3. Correlations between scarp erosion and (left plot)  $H_s$ , (middle plot) Tide, and (right plot)  $x_d$

A further analysis was carried out to investigate the wave transmission phenomenon over the breakwater. In general, transmissivity strongly depends on structure characteristics (height and crest width, roughness, permeability) and wave parameters (period, height, angle of attack). Furthermore, transmissivity can vary over time according to the tide, which, of course, greatly influences the exposure of the structure to many of these different factors (Buccino et al., 2007). As a case study, we developed a unique model scenario, under which the slope=0.8%, wave height=0.5 m, tide= $\pm 0.8$  m,  $x_d=100$  m, sediment concentration= $0.4 \text{ kg/m}^3$  and  $D_{50} = 150 \text{ }\mu\text{m}$ . Three different wave periods and breakwater geometries were examined. The first breakwater geometry was equal to the standard breakwater reported in the main body of the paper. The second one was twice as wide. The third consists of a standard breakwater but 30 cm higher (Figure A.6.4). To look at the effect that wave period and breakwater geometry have on wave transmission, we compared the wave period with the average transmitted wave height at the marsh boundary ( $x=200$  m) within a tidal cycle (Figure A.6.4). Our results, in agreement with Van Oosten et al., (2007), showed wave transmission to be proportional to the wave period, and higher structures to reduce wave height more (Figure A.6.4). The impact that geometric characteristics and wave period have on the sediment supply for salt marshes remains unexamined, but what transpires is that a higher structure reduces wave energy more, while longer periods transfer more energy over the breakwater. However, a taller structure is also likely to trap more sediments, whereas longer periods should be able to carry more sediments out. Study results suggested more research is needed to help

find a balance between waves' energy reduction and sediment supply during the design and implementation of breakwater infrastructures.

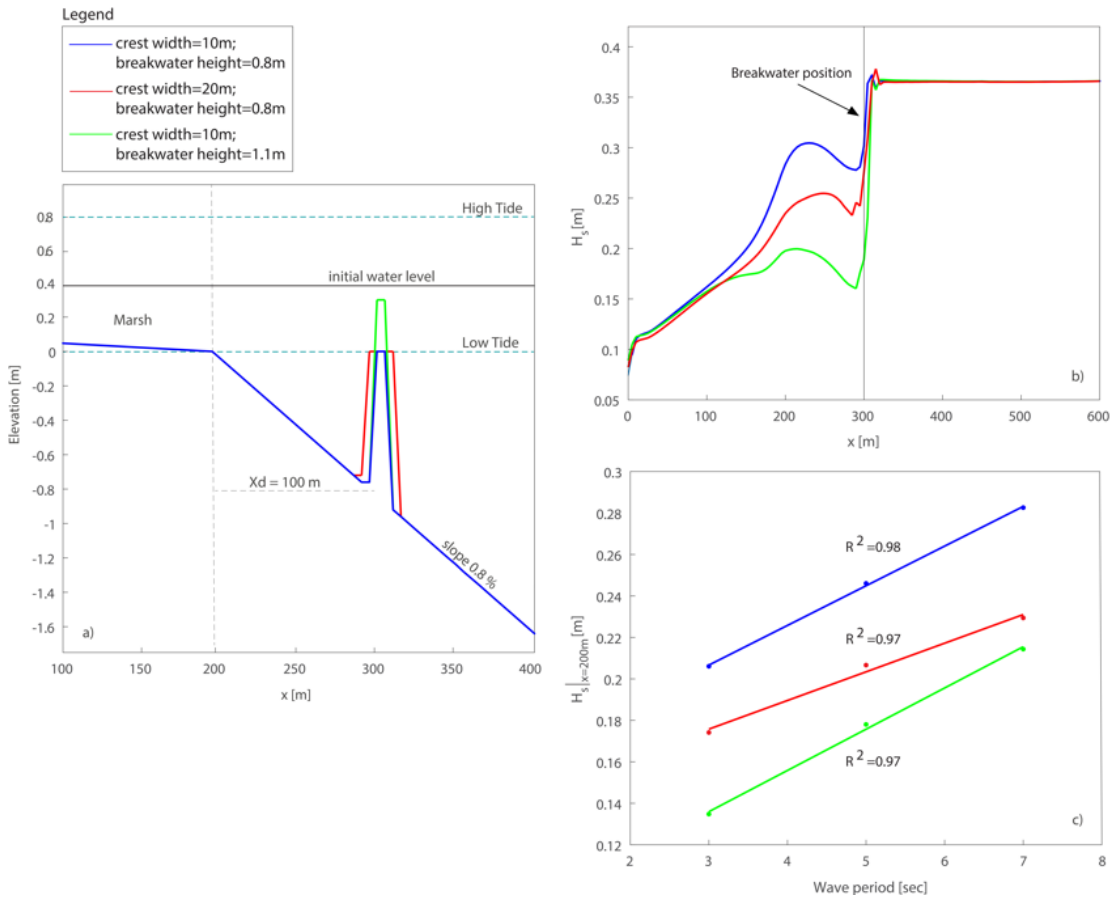


Figure A.6.4. Figure (a) the longitudinal profile of the domain used in this analysis, highlighting the three different breakwater configurations. (b) An example of wave damping for the case with wave period = 5 s, and (c) linear correlations between wave period and wave height measured at the marsh boundary ( $x=200$  m) for the three breakwater configurations.

## References

- Bagnold, R.A., 1956. The flow of cohesionless grains in fluids. *Philosophical Transactions of the Royal Society of London. Series A, Mathematical and Physical Sciences*, 249(964), pp.235-297.
- Bosboom, J. and Stive, M.J., 2021. Coastal dynamics.
- Meyer-Peter, E. and Müller, R., 1948. Formulas for bed-load transport. In *IAHSR 2nd meeting, Stockholm, appendix 2*. IAHR.
- Buccino, M.; Calabrese, M. Conceptual approach for prediction of wave transmission at low-crested breakwaters. *Journal of waterway, port, coastal, and ocean engineering*, **2007**, 133, 213–224.
- Ribberink, J.S., 1998. Bed-load transport for steady flows and unsteady oscillatory flows. *Coastal Engineering*, 34(1-2), pp.59-82.
- Shields, A., 1936. Application of similarity principles and turbulence research to bed-load movement.
- Van Oosten, R.P.; Marco, J.P.; Van der Meer, J.W.; Van Gent, M.R.A.; Verhagen, H.J. Wave transmission at low-crested structures using neural networks. *Coastal Engineering 2006*, **2007**, 5, 4932–4944.
- Vona, I., Palinkas, C.M. and Nardin, W., 2021. Sediment Exchange Between the Created Saltmarshes of Living Shorelines and Adjacent Submersed Aquatic Vegetation in the Chesapeake Bay. *Frontiers in Marine Science*, 8, p.727080.

